Modified Metal Oxide Gas Sensors for the Detection of Clandestine Chemistry Locations

David Christopher Pugh

Thesis submitted in partial fulfilment of the requirements of the degree of Doctor of Philosophy

University College London

2017

I, David Pugh confirm that the work presented in this thesis is my own. Where information has been derived from other sources, I confirm that this has been indicated in the thesis.

_____

David Pugh
10th June 2017

Abstract

Clandestine laboratories are locations where chemistry is carried out in secret, often with the intent to produce illegal drugs or other controlled substances. These laboratories are unregulated and not maintained to a good laboratory standard, presenting a risk to first responders, bystanders and the environment. Electronic noses based on metal oxide semiconducting (MOS) gas sensors present a potential technology to create devices for the detection of clandestine activity.

A range of sensors based on zinc oxide, chromium titanate and vanadium pentoxide have been manufactured and modified using zeolite material and metal ion doping. Sensor fabrication took place using a commercially available screen printer, a 3 x 3 mm alumina substrate containing interdigitated electrodes and a platinum heater track. All materials were modified with the protonated forms of zeolite beta, Y, mordenite and ZSM5, by incorporating these materials into the metal oxide to make up 30 % of the total ink. Zinc oxide was also modified by indium doping; doping levels were set at 0.2, 0.5, 1 and 3-mol % indium. These materials were synthesised using a co-precipitation method.

Sensors were exposed to a range of gases at operating temperatures between 250 and 500°C and concentrations between 50 ppb and 80 ppm. All tests were conducted on an in house testing rig, consisting of a 12-port sensing chamber, four mass flow controllers, six solenoid vales and supplies of compressed air and analyte gas.

Modification of sensors was found to improve their responsiveness, compared to the control sensors, in almost all cases. This is due to a combination of surface area enhancements, increased adsorption of material and a more accessible microstructure.

Machine learning techniques were applied to the sensor data to correctly classify the class of gas observed and to assess the overall sensor performance of each material. A high level of accuracy was achieved in determining the class of gas observed.

Contents

List of Figures

List of Tables

Abbreviations

CTO	Chromium Titanate
EDX	Energy Dispersive X-Ray Spectroscopy
MOS	Metal Oxide Semiconductor
MS	Mass Spectrometer
SEM	Scanning Electron Microscope
STP	Standard Temperature & Pressure
SVM	Support Vector Machine
T_{res}	Response Time
T_{rec}	Recovery Time
VOC	Volatile Organic Compound
XRD	X-Ray Diffraction
ZnO	Zinc Oxide

Acknowledgements

The completion of this thesis would not have been possible, were it not for the support of many excellent people. Firstly, thanks to my primary supervisor, Professor Ivan Parkin, for giving me the opportunity to undertake this research, and for the support and opportunities that I have received over the last four years.

Thanks to Professor Steve Hailes for his knowledge of machine learning and for assistance in several matters related to this project.

I would like to thank Professor David Williams and Dr Vandna Luthra, of the University of Auckland, New Zealand and Delhi University, India, for their hospitality and for the welcome and the opportunities I received at their host institutions.

The support of technical staff at the college has been invaluable to my work, and so I would like to thank Dr Kevin Reeves, Dr Tom Gregory, Dr Steve Firth and Martin Vickers. Special thanks should go to Tony Bernard, without whom, our lab equipment would not be running today.

I am eternally grateful for the support of the gas sensor research group, Dr Anu Naik and Dr Emma Newton, for initial training on all aspects of gas sensor fabrication and testing, to Paula Tarttelin and Gwyn Evans who I am proud to have shared the last four years with, and to Lauren Horsfall, Simon Coplowe and Valerie Reis, who are the future of gas sensing.

To Mr Steven Watson, my high school chemistry teacher, who sparked my interest in the subject and encouraged me to pursue it, without whom, I would not be where I am today.

Finally, I would like to thank my family for their support and encouragement over the last 26 years and Amy for always believing in me.

1. Introduction

Clandestine methamphetamine laboratories, sites of illegal methamphetamine production, pose a grave risk to members of the public, emergency service workers and the environment. In addition to producing illegal and dangerous substances, these laboratories are a fire and explosion hazard. The aim of this project is to develop an analytical tool for the detection of such environments. This chapter will introduce the concept of clandestine chemistry and will examine various methods of detecting such activities, focussing on metal oxide gas sensors whilst discussing potential modifications that can be made to enhance the sensitivity, selectivity and stability of these sensors.

1.1. Methamphetamine

Methamphetamine is a psychostimulant phenylamine compound. It exists as two enantiomers, in dextro and levro form. Dextromethamphetamine possesses psychostimulant effects, making it a potent synthetic psychotropic drug. Methamphetamine has some limited therapeutic use[1,2] but is much more widely used recreationally for its euphoric and stimulatory properties and is the most commonly used psychotropic drug in North America[3].

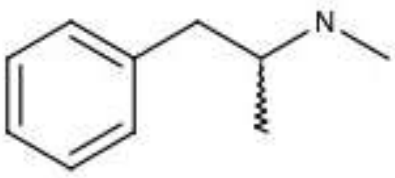

Figure 1.1. Skeletal structure of methamphetamine.

Methamphetamine is a colourless volatile oil, which is insoluble in water. Illicit forms of methamphetamine include powders, crystals, and tablets; the most common salt is the hydrochloride form, a white crystalline powder [4]. These products may be ingested, snorted, injected, or smoked.

Methamphetamine is a class A substance under the Misuse of Drugs Act (1971)[5], making it illegal in all forms and carrying a maximum penalty of life imprisonment for possession with intent to supply.

1.1.1. Methamphetamine Synthesis

Methamphetamine can be synthesised using any one of three relatively simple, readily available methods. Marketable quantities of the compound can therefore be produced using little equipment or knowledge of synthetic organic chemistry.

The P2P Method

The P2P method uses phenyl-2-propanone (P2P), a chemical similar in structure to methamphetamine as a starting material. P2P is obtained from phenylacetic acid and acetic anhydride[6]; reductive ammination of P2P with methylamine over an aluminium or mercury catalyst produces methamphetamine (Figure 1.2).

In a clandestine setting, very little equipment is required to perform methamphetamine syntheses using this method, a hotplate and several Pyrex dishes are often used as a heat source and reaction vessels respectively[6]. Both acetic anhydride and phenylacetic acid are flammable and for highly explosive mixtures with air. The absence of suitable equipment in clandestine laboratories (fume hoods, glassware, and a reliable heat source) makes this method of production dangerous both to the clandestine chemists and to the public in the surrounding area[7].

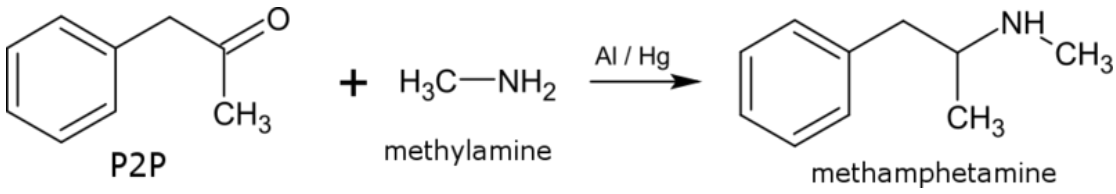

Figure 1.2. P2P method of methamphetamine synthesis.

In comparison to other syntheses methods (see below), methamphetamine production using the P2P method produces a lower quality product, with less addictive properties[8]. The P2P method of methamphetamine synthesis has therefore become less widely utilised over the last 20 years, this decline is in part due to restrictions being placed on reactants and precursors of the synthesis[9].

The Birch Reduction Method

The Birch reduction method uses ephedrine as a starting reagent; ephedrine is the active ingredient of the over the counter medicine Sudafed and is therefore readily available[10].

The Birch reduction method requires the use of large amounts of anhydrous ammonia, which is often stolen from or even sold by unscrupulous farmers, as well as the use of a palladium catalyst which is easily obtainable from commercially available jewellery. Thionyl chloride is obtained from batteries, while palladium is a common metal used in consumer electronics components. Consequently, the Birch reduction method of methamphetamine synthesis has become widespread within rural communities in the last decade[11].

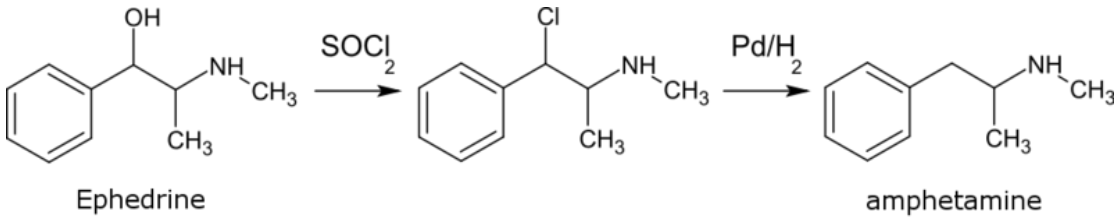

Figure 1.3. Synthesis of methamphetamine using the Birch reduction method.

In this reaction ephedrine is reduced to chloroephedrine, which subsequently undergoes catalytic hydrogenation to methamphetamine (Figure 1.3). A number of by-products, reactants and solvent vapours are present during this reaction, including ethanol, hydrocarbons and hydrogen chloride gas[12], which possess flammable, explosive and corrosive properties.

The success of the reaction is dependent on the extraction of ephedrine from over the counter medicines. Pharmaceutical companies have added filters to their products to interfere with the extraction of ephedrine.

The Red Phosphorus Method

Similarly, to the Birch reduction method, the red phosphorus method also uses ephedrine as a precursor for the production of methamphetamine, however many clandestine laboratory operators prefer this method, as it is relatively simple to perform.

Upon heating, the ephedrine precursor is rapidly iodinated, via hydrogen iodide , leading to the substitution of the hydroxyl group with iodide. In the second step of the reaction, red phosphorus consumes the iodine to form phosphorus triiodide (PI_3) and methamphetamine (Figure 1.4). In water, PI_3 decomposes to phosphorus acid (H_3PO_3), regenerating hydrogen iodide.

Red phosphorus is usually obtained from either the strike pads of matchboxes[13] or as phosphorus flakes from agricultural fertilisers[11].

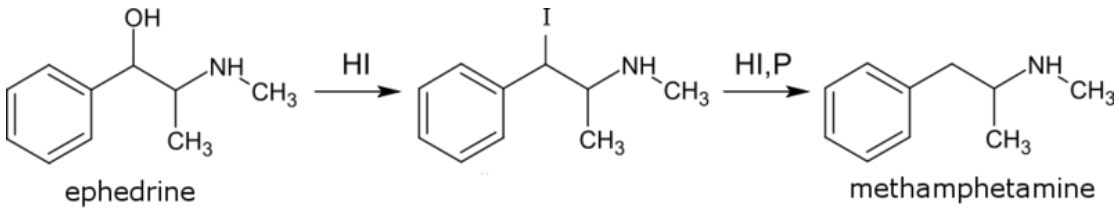

Figure 1.4. Reduction of ephedrine using hydrogen iodide in the presence of red phosphorus.

1.2. Clandestine Methamphetamine Laboratories

The relative ease of production of methamphetamine crystals means that large quantities of illicit drugs can be produced illegally for sale and recreational use in clandestine laboratories.

In North America, clandestine methamphetamine laboratories account for more than 50% of the total illegal laboratory seizures[14]. With a continually growing trade of methamphetamine in Europe[15] the prevalence of clandestine laboratories is set to increase further across the globe.

Such laboratories are found in a broad range of settings, including: rental properties, motel rooms, vehicles, motor homes, storage units and high-end hotel rooms[16]. As illustrated above the materials used and by-products produced in the production of methamphetamine, present a real danger of fire[17], explosion[11], as well as damage to the human nervous system[18]. Poisonous solvents used and produced in the synthesis of methamphetamine can saturate walls; carpets and ceilings, producing an unsafe environment for neighbours as well as adding increased risk to real estate[19]. The atmosphere in and around a site of clandestine methamphetamine production is a complex environment of harmful gases (see Table 1.1).

Table 1.1. Target airborne chemicals found in clandestine production environments, grouped by production route.

	Methamphetamine Synthesis		
	Birch Reduction	**P2P**	**Red P**
Acetone	✓	✓	✓
Ammonia	✓		
Cyclohexane	✓		
Ethanol	✓	✓	✓
Formic acid		✓	
Heptane	✓		
Hexane	✓		
Hydrogen iodide			✓
Iodine			✓
Methylamine		✓	
N-methylformamide		✓	
Phenyl acetone		✓	
Phosphine			✓
Tetrahydrofuran	✓		
Toluene	✓	✓	✓

Several large-scale explosions have occurred in recent years as a result of methamphetamine production. In November 2012, a large explosion in southern Indianapolis, USA, in the basement of a residential house caused two deaths and damage to twenty-six properties in the surrounding area[20] (Fig 1.5). Illegal use and manufacture of methamphetamine costs the United States government $180 million annually[21].

Figure 1.5. The aftermath of a methamphetamine lab explosion in Indianapolis in November 2012. Five homes were destroyed and further twenty-six were damaged. Two people were killed and seven people suffered major injuries requiring hospital treatment[19].

Ammonia, one of the key chemicals used in the Birch reduction method of methamphetamine production is of major concern[8]. Many large-scale explosions have occurred as a result of the presence of ammonia-based materials, most recently in April 2013, where there was a large-scale explosion at a fertiliser plant in Waco, Texas, USA[22]. The explosion was the result of a ruptured tank containing anhydrous ammonia[23]; the explosion killed 15 people, injured 180 and destroyed buildings in a five-block radius, illustrating the real dangers posed by mishandling such substances.

A lack of suitable sensing technology means that clandestine laboratories are often only discovered through unintentional means, for example when police are called to a scene to investigate an unrelated incident, such as a domestic disturbance.

The dangers posed by clandestine laboratories highlight the requirement for suitable sensing technologies to identify such sites prior to any dangerous incidents. Gas sensors may provide a solution to this problem.

1.3. Gas Sensing

There are many different technologies with the potential for sensing the effluent gases of drug production and approaches must be evaluated from a technical, economic and legal standpoint. A number of methods are discussed below, along with their advantages and disadvantages.

1.3.1. Sniffer Dogs

The gold standard for gas sensing has long been the use of sniffer dogs, whose highly trained noses can detect odours at part-per-trillion (ppt) concentrations[24].

Sniffer dogs are most widely utilised for drug detection at ports of entry, sports events and music festivals, however, canines have been trained for a number of other applications, including the detection of cancerous tumours[25], endangered insect species[26] and hypoglycaemia emergencies in diabetic patients[27](Figure 1.6).

Although trained canines offer a very efficient means of drug detection, they cannot comment on the vapour they are detecting, or give detailed information about concentration. In addition to this, the use of dogs in clandestine laboratory locations has other ethical implications; it is morally dubious to utilise live animals in potentially harmful chemical environments where their lives may be put at risk. In addition to these concerns, training a sniffer canine costs around $6000, and specially trained dogs cost around $2000 per annum to maintain. Therefore, the use of non-canine chemical sensors that can be easily and cost effectively produced and implemented in many different and potentially hazardous environments is of great interest to law enforcement agencies.

Figure 1.6. Police sniffer dog on patrol, assessing luggage for the presence of a controlled substance[28].

1.3.2. Ionisation Sensors

Ionisation sensors can be divided into two different technologies, ion mobility spectrometry (IMS) and photoionisation detection (PID). IMS is a highly sensitive technique that uses either a chemical or radioactive ionisation source[29] to analyse the composition of gas mixtures. Ionisation sensors are able to detect a wide range of gases at low concentrations; however, challenges include competitive ion/molecule reactions with matrix molecules, and problems with low temperature operation[30]. Sensing units are very expensive ($10,000-$50,000)[31]. Despite this high cost, IMS is well suited to detecting relative concentrations of target gases in stationary detection units.

The greatest strength of IMS analysis is the speed of response, which is typically in the order of milliseconds. The speed of response, combined with its high sensitivity, compact design and ease of use has led to IMS instruments use in airports for detection of explosives[32], weapons[33] and drugs[34].

Photoionisation detection (PID) uses UV light to ionize a gas between two electrodes. When gases are ionised, free electrons are collected at the devices electrodes, resulting in a change in current flow proportional to the concentration of the gas. PID devices have been known to detect volatile species at sub part per billion (ppb) level[35]. The

ionisation source and the detector are selected so that they do not ionize the main components in air (O_2 & N_2). PID is generally non-selective, however selective detection has been demonstrated using chemically selective filter materials[36].

Portable PID devices are available commercially for a number of applications, including: industrial hygiene[37], arson investigation[38], air quality monitoring[39] and cleanroom maintenance[40]. Such devices can cost between $500 and $6000, depending on the application, mobility and hardware used in the device.

1.3.3. Optical Sensors

Optical sensors are detectors that convert a change in light intensity into an electrical signal. As optical sensors can operate in gaseous or liquid phases, they have been utilised in a variety of technologies, including chemiluminescent, colourimetric and fluorescence sensors. Optical sensors have therefore been implemented in a wide range of applications, including environmental[41], medical[42] and pharmaceutical[43] analysis. The wide availability of miniature photo-detectors and light sources and the broad usage of optical fibres make optical chemical sensors very attractive for applications requiring portable and compact sensing solutions[44].

Optical sensors have excellent selectivity and are often able to identify multiple components of a chemical mixture in one measurement. Optical sensors rely on a specific chemical reaction to induce an optical change; as a result, sensors are selective to one type or class of analytes. Colorimetric response is, however, binary, with the ability to tell only the presence or absence of a compound[45]. Further disadvantages of optical sensors include a limited lifetime and interfering stray light[46].

1.3.4. Conductance-Based Sensors

Electrical conductance-based sensors have been implemented in multiple different environments, with a variety of functions. Examples of conductance-based sensors include chemically-sensitive field effect transistors (chemFETs)[47,48], thermal sensors[49,50] and semiconducting metal oxide sensors[51,52]. Sensing in these materials is based on

alterations in the space charge region (SCR) that are induced by an interacting target gas[53]. Determination of concentration and classification of the interacting gas is often possible and conductance based sensors are often cheap due to the simple and low-cost materials required[54].

Conductance-based sensors can detect a large number of target gases to a sub-ppb level in a reasonable amount of time (less than two minutes); disadvantages of this type of sensor include; susceptibility to catalyst poisoning[55] and sensor inhibitors (such as halogens)[56]. One class of conductance based sensors; metal oxide semiconductor gas sensors will be discussed in more detail below (Section 1.4).

1.4. Semiconducting Metal Oxides as Gas Sensors

The gas sensing properties of metal oxide semiconductors (MOS) were first illustrated by Taguchi *et.al.*[57], who demonstrated the gas sensitivity of sintered SnO_2. Since then, semiconducting metal oxide gas-sensor technology has been implemented across a much larger technological market, with many commercially available devices for security[58], safety and environmental[59] purposes. MOS gas sensors have certain specific advantages over other conductance based sensors, such as: higher robustness, up to 10 years of life, less sensitivity to environmental moisture and temperature, simple interface electronics as well as faster response and recovery times[60].

Metal oxide gas sensors operate on the principle of the absorbed gas altering the number of charge carriers, and therefore the conductivity of the semiconducting material from which the sensor is made. The change in conductivity is converted into a response the can indicate the presence and concentration of a target gas.

Semiconducting materials are defined as a substance with an electrical conductivity that *increases* with increasing temperature[61]. Semiconducting materials contain a valence and a conduction band, separated by a “band gap”. The existence of these bands is due to the overlap of a large number of molecular orbitals that are closely spaced in energy, forming an almost continuous band of energy levels. For conduction in such material to

occur, electrons must be excited from the filled valence band to the empty conduction band, where they can act as charge carriers (Fig 1.7).

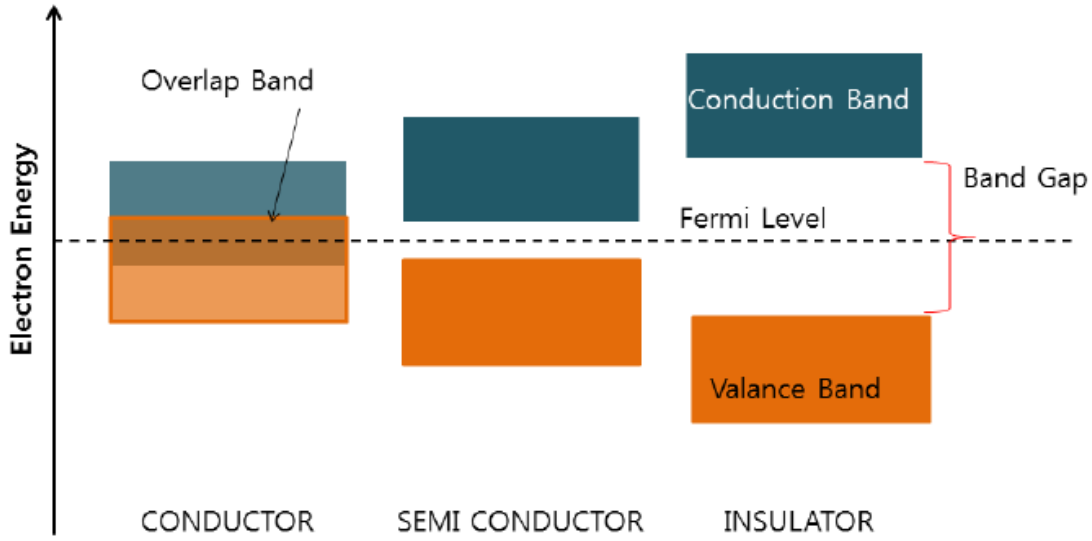

Figure 1.7. Schematic of a conductor, semi conductor and insulator, demonstrating differences in band gap. Figure adapted from Matato *et.al.*[62].

Semiconductor devices possess a range of interesting electronic properties, including variable resistance and sensitivity to heat and light. These properties can be altered by doping and the application of heat or light, semiconductors can therefore be used as switches, amplifiers and for energy conservation. Semiconductors are used in manufacturing, both in simple devices, such as light emitting diodes (LED), and in integrated circuits, which consist of many transistors (anywhere from two to many billions), which are connected in a network to produce devices such as televisions, oscilloscope screens as well as microchips used in computers and smartphones. Semiconductor technology underpins the basis of modern electronics and the industry is estimated to be worth over $300 billion[63].

Two types of semiconductor exist, intrinsic and extrinsic semiconductors. Intrinsic semiconductors (for example silicon and germanium) are pure materials without any significant dopant species present. At absolute zero (0 K), the probability of the conduction band being occupied is zero and the valence band being occupied is one[64]. Any conduction that takes place in the material above 0 K is a result of valence band

electrons with appropriate energy promoted to the conduction band. As a result of the ideal nature of the semiconductor, every electron in the conduction band leaves a hole in the valence band, and so the Fermi level is placed at the centre of the semiconductor.

Extrinsic semiconductors, on the other hand, are materials that contain a significant dopant species and therefore have varying electron and hole concentrations. The conductivity in these materials is controlled by the introduction of these donor and acceptor impurities within the material lattice.

Extrinsic semiconductors can be further split into n-type and p-type semiconductors based on the donor species (Fig 1.8), n-type semiconductors, such as arsenic doped gallium or phosphorus doped silicon, have an introduced donor impurity, containing donor electrons, in a donor state. Donor electrons require very little energy to enter the conduction band due to their small binding energies; as a result, their donor level is situated just below the conduction band. Electrons from this band enter the conduction band and act as charge carriers within the material. The electron distribution in an n-type semiconductor is different depending on extremes, at absolute zero, all electron states below the donor band are occupied, with the lowest vacant state being the conduction band. At higher temperatures, the number of intrinsic charge carriers is comparable to the number of donor electrons, and the material is able to act as an intrinsic semiconductor.

P-type semiconductors, such as silicon boride, have an introduced acceptor impurity. This introduces a narrow acceptor band; which lies just above the full valence band. As the temperature increases, electrons are thermally excited from the valence band into the acceptor band, in doing so, the valence band is left with holes, h^+, allowing the remaining electrons to be mobile and act as charge carriers in the valence band. Electrons need little energy to become excited from the valence band to the acceptor band due to low binding energies of the acceptor state. As with n-type semiconductors, electron distribution is dependant on the temperature of the semiconductor. At absolute zero, the valence band is full, and the lowest available states exist in the acceptor band.

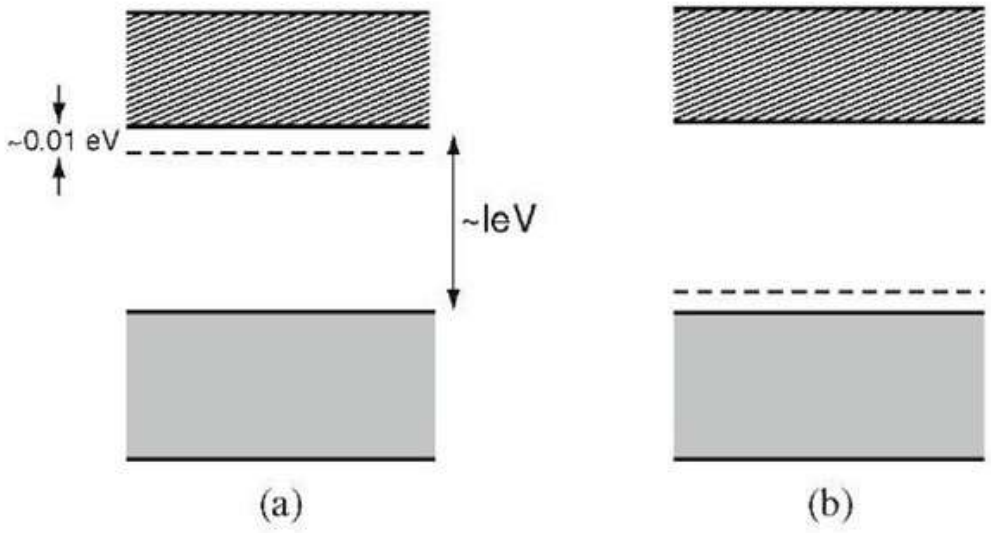

Figure 1.8. (a) Donor and (b) acceptor levels in extrinsic semiconductors. The dotted line shows the Fermi level of the material. In n-type material (a) there are electron energy levels near the top of the band gap so that they can be easily excited into the conduction band. In p-type material (b), extra holes in the band gap allow excitation of valence band electrons, leaving mobile holes in the valence band[65].

1.5. Gas Sensing Mechanism

Reactions between target gases and the MOS surface are complex, and there are many different ways in which an incoming target gas can alter the number of charge carriers. The principal mechanisms being adsorption, reaction and desorption of gas species on the surface[66].

In atmospheric air (~21% O_2), a MOS surface can be populated by several, different oxygen species, these being O^-, O^{2-} and O_2^-. These species, at the surface of the metal oxide, attract and immobilise electrons from the bulk of the material. This immobilisation of electrons at the surface of the material, along with the granular nature of the semiconductor, leads to the creation of an electron depletion layer, in n-type semiconductors and a hole accumulation layer in p-type materials.

In an n-type semiconductor, the electron depletion region is a high resistance area of the grain compared to the lower resistance bulk material. The opposite is true of p-type material; the hole accumulation layer is low resistance, compared to the higher

resistance bulk material.

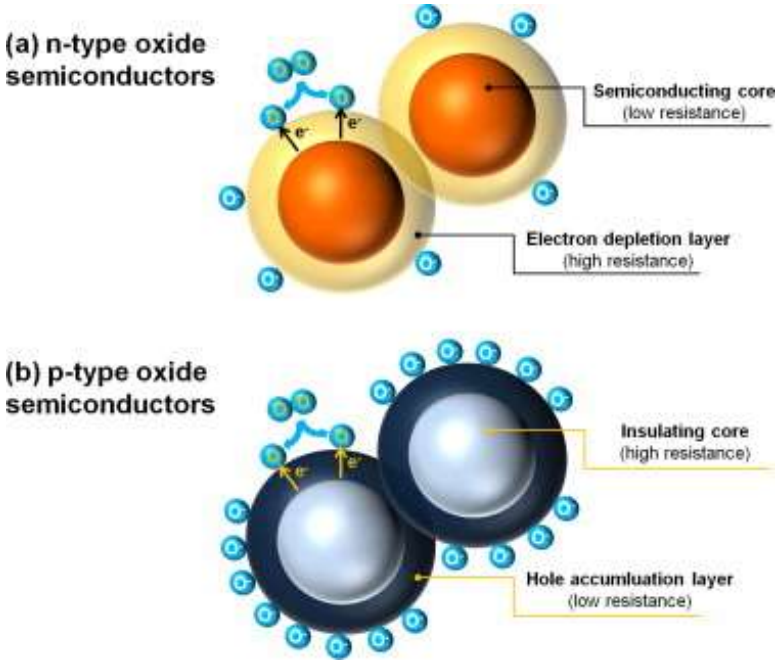

Figure 1.9. Schematic demonstrating the adsorption and breakdown of oxygen molecules on a semiconductor surface in which an electron depletion layer is formed in an n-type semiconductor (a) or a hole accumulation layer develops on a p-type semiconductor. Semiconductor grains of both n- and p-type materials, with adsorbed oxygen ions on them contain regions of high and low resistance through which the percolation of charge carriers must occur for a current to be observed[67].

These depletion and accumulation regions formed in a stable atmosphere produce a baseline resistance. On interaction with an analyte gas, oxygen ions are removed from the surface of the sensor, liberating electrons held at the surface according to the following equation, where R is a reducing gas and O^- is oxygen adsorbed at the sensor surface.

$$R_{(g)} + O^-_{(ads)} \rightarrow RO_{(g)} + e^-$$

In n-type sensors, the reintroduction of electrons into the material increases the charge carrier concentration, reducing the width of the high resistance electron depletion layer. When oxygen ions are removed from the sensor of a p-type material, electrons are reintroduced into the sensor material, reducing the hole density. This decreases the width of the hole accumulation layer, increasing the resistance in the grain. Oxidising gases have the opposite effect of the sensor response, as summarised in Table 1.2.

Table 1.2. Changes in resistance in n-type and p-type gas sensors based on the redox properties of the interacting gas, and the associated response calculation.

Material Type	Oxidising Test Gas	Reducing Test Gas
n-type	Resistance increases (R/R_0)	Resistance decreases (R_0/R)
p-type	Resistance decreases (R_0/R)	Resistance increases (R/R_0)

1.6. Interpretation of Results

The response of a metal oxide semiconductor gas sensor is displayed as a function of its baseline resistance, R_0. The response calculation varies based on the type of gas (oxidising or reducing) and the sensor material properties (n-type or p-type). For a sensor in air, in the absence of any target gas, R_0/R or R/R_0 is equal to one. On the introduction of a volatile analyte gas, the response increases until it reaches equilibrium between the sensor surface and the environment. In the absence of a test gas, the sensor response returns to one.

The kinetic data (response and recovery of the sensor) can be quantified based on two properties of the sensor. The response time (T_{res}) as defined by Yamazoe[68] and others, is the time taken for the sensor response to reach 90% of its maximum value, while the recovery time (T_{rec}) is the time taken for the sensor to return to within 10% of its baseline value following exposure to a target gas.

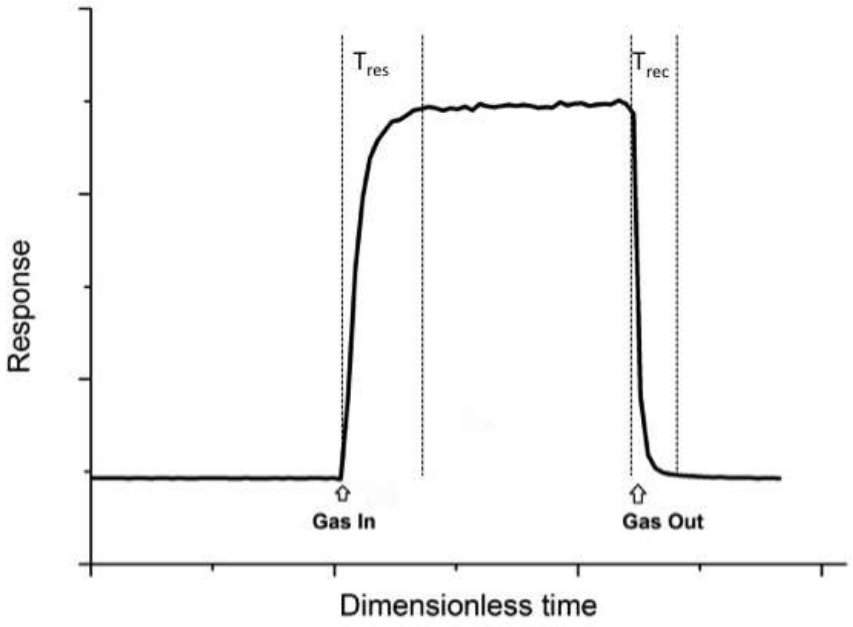

Figure 1.10. Typical response of MOS sensors on exposure to a target gas. T_{res} refers to the response time of the sensor, the time taken to reach 90% of the maximum value. T_{rec} refers to the recover time of the sensor, the time taken to reach within 10% of the original baseline resistance. Response refers to either R_0/R or R_0/R, dependent on the type of sensor and redox properties of the gas. This is calculated such that in air, the response is 1.

1.7. Production of Sensors

1.7.1. Thick Film Gas Sensors

Thick film sensors exist as thick (30-150 µm) layers of metal oxide, deposited by one of a number of techniques. The most common of these is screen-printing homogenous metal oxide inks. Metal oxide inks are produced by mixing gas sensitive materials with a binder, usually water or a hydrocarbon mixture, to produce a suspension (see section 2.2). This material is printed onto a substrate and electrodes (usually made of platinum, gold or silver). Printing of sensors is usually done with commercially available screen-printing tiles consisting of more than 200 individual substrates. This process ensures a controlled deposition of materials and limits the batch-to-batch variability of sensor samples.

Drop coating of sensors is another method of deposition, this involves dropping an amount of a solution containing MOS materials onto a sensor substrate and allowing the solvent to evaporate. Each sensor tile must be deposited individually, leading to variability in the amount of sensor material deposited on each sensor tile. This method is also less suitable for mass production due to the time required to deposit material on a large number of sensors.

Flame spray pyrolysis is a one step process in which a liquid feed – a metal precursor dissolved in a solvent – is sprayed with an oxidising gas into a flame zone. The spray is combusted and the precursor(s) are converted into nano sized metal or metal oxide particles, depending on the metal and the operating conditions. The technique is flexible and allows the use of a wide range of precursors, solvents and process conditions, thus providing control over particle size and composition[69].

1.7.2. Thin Film Gas Sensors

Thin film gas sensors consist of a thin (low µm-nm thickness), dense film of metal oxide material. Fabrication of the sensor is based on more complex deposition methods such as, chemical vapour deposition (CVD)[70,71] or physical vapour deposition (PVD)[72,73].

Chemical vapour deposition techniques involve the formation of a vapour from a volatile precursor material, followed by a chemical reaction of this phase, on a heated surface to form the desired product. Physical vapour deposition involves the evaporation or sputtering of a solid or liquid source to form a vapour, which is subsequently deposited onto a surface, both methods are commonly used in the semiconductor industry.

Thin film sensors potentially provide greater control of the gas sensor materials, due to the availability of different microstructures and morphologies. Vapour deposition techniques are conducive to a more automated production process than thick film production techniques. However thin films generally suffer from reduced sensing performance compared to their thick film counterpart's due to their dense thin film. Thick film gas sensors provide greater surface area and porosity, this increase in

available surface area leads to an increase in reaction sites, which in turn leads to an increase in sensor response.

The electron depletion and hole accumulation regions of thick and thin film sensors are arranged differently. In a thick film sensor, accumulation and depletion layers form around the edge of individual grains, forming areas of high and low resistance in the material. In a thin film material, in the absence of metal oxide grains, the accumulation/depletion regions form along the top of the sensor, with the bulk occupying the lower portion of the sensor.

The conductivity through thick and thin film materials also varies significantly, due to the porous and compact structures of the materials. For compact layers, the bulk of the material is not accessible to target gases and interaction can only take place at the geometric surface (the depletion layer, as shown in Fig 1.11). In the porous material, the gas can penetrate the entire film, and so each individual grain can be affected by the presence of an analyte gas, the response is therefore affected by the contribution of all grains, as opposed to a limited geometric surface.

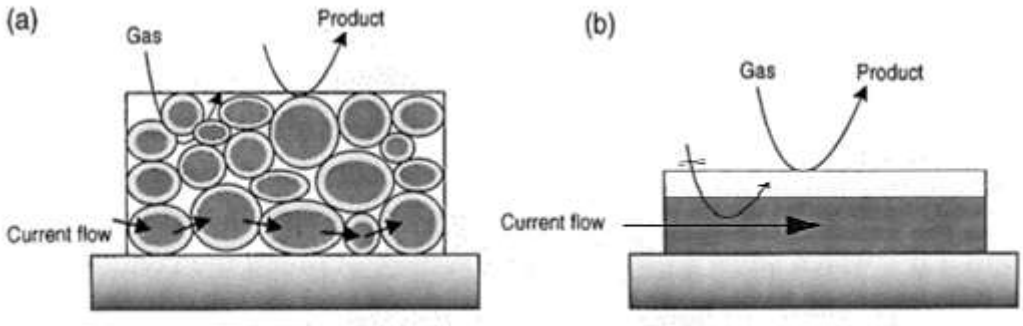

Figure 1.11. Schematic demonstrating the difference in current flow and gas interaction between thick film (a) and thin film (b) sensors. Gases can penetrate and interact with all sensor particles in a thick film device, while in thin film sensors the gas only interacts with the geometric sample. Figure not to scale. Figure adapted from Barsan *et.al.*[74].

Studies have been undertaken to compare the gas sensing properties of both thick and thin film sensors. Lee *et.al.*[75] examined the properties of thick and thin film tin oxide. The thick film sensor consisted of loosely connected grains, with boundaries in all

directions, while the thin film sensor, fabricated by metal oxide chemical vapour deposition (MOCVD) consisted of a dense columnar structure. In this study, thick film sensors were found to demonstrate a considerably larger magnitude of response than thin film sensors when exposed to gases under the same experimental conditions, in some cases up to an order of magnitude larger in response. The strong enhancement in the responsiveness of the thick film sensor, compared to the thin film sensors is attributed to the high surface area and surface sites of the thick film material, as opposed to the limited surface area of the thin film device.

1.8. Device Fabrication

Metal oxides gas sensing devices can be fabricated in a number of different ways. Fabrication methods should ensure that the crystallite size of the MOS material is as small as possible, any auxiliary elements should be dispersed uniformly and that the thickness and porosity of the sensing layer should be optimised to improve stability and durability.

Metal oxide powders can be produced using several wet chemistry methods; in general powders are milled with either water or an organic vehicle to produce a smooth homogenous suspension.

Metal oxide suspensions are then deposited over the electrodes. This usually involves either sintering the MOS material with coiled electrodes (usually gold or platinum) inserted into the material, or with MOS material printed onto a substrate. The sensor material is usually heated to its operating temperature using platinum or gold wire. A selection of deposition methods is shown in Fig 1.12.

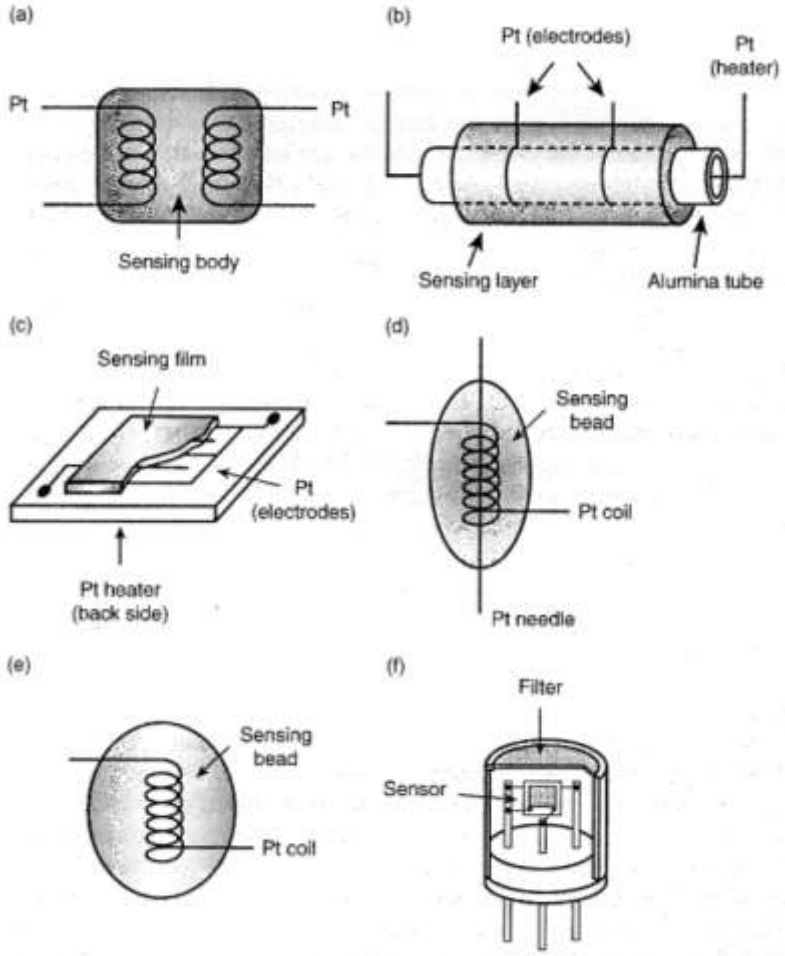

Figure 1.12. Schematic demonstrating the structure of substrate and device structures used in MOS sensor development. (a) Sintered block, (b) thin aluminum tube-coated layer, (c) screen printed thick film, (d) small bead inserted with a coil and heating needle, (e) small bead inserted with a coil, (f) complete sensor device consisting of sensor tile, metal cap and filter, bonded onto brass pins. Figure adapted from images by Lee (2013)[76].

1.9. Microstructural Effects in Gas Sensing

Thick film sensors are polycrystalline, meaning many grains are fused together to form a continuous layer of metal oxide sensing material. When these grains fuse together and oxygen ions adsorb at the sensor surface, Schottky barriers form at the space charge regions between grains.

In dry air, atmospheric oxygen interacts with the surface of the metal oxide and electrons from the conduction band of the metal oxide become trapped by the adsorbate, forming molecular or atomic oxygen ions adsorbed at the surface. As a result,

a depletion layer forms, in n-type materials, on the surface of grains; in an energy band representation (Fig 1.13), electrons require more energy to reach the surface (against the electric field of the negatively charged surface).

The space charge region does not usually extend across the whole grain, so there can be considered two separate regions in the sensor grain, the bulk region, not impacted by exposure to target gases and the space charge layer which is altered based dependent on adsorbents on the surface, both regions have significantly different conductivities.

Interactions between adsorbed oxygen and test gases alter the thickness of the space charge layer, and hence change the resistivity of the material. Liberated electrons reoccupy levels in the conduction band that were unavailable when oxygen was adsorbed at the surface; therefore the change in resistance in a MOS material varies based on the oxide and the type of gas involved in the sensing.

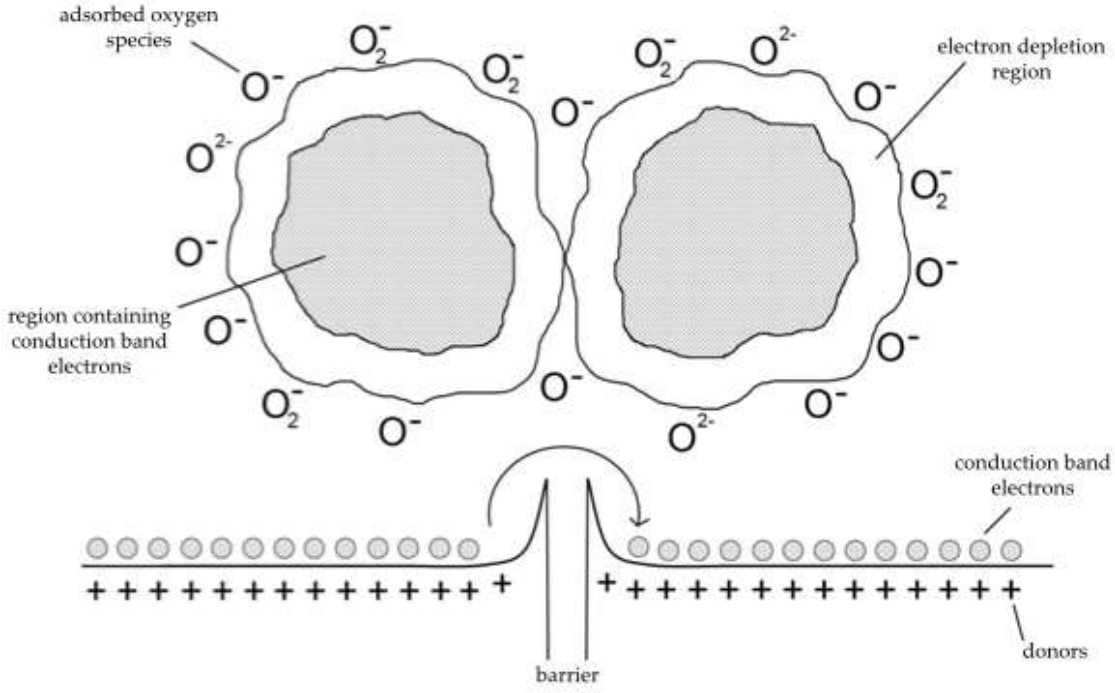

Figure 1.13. Schematic showing absorbed oxygen species on MOS grains, creating a Shottky barrier. Figure adapted from images by Afonja (2012)[77].

Williams *et.al.*[78] first proposed an equivalent circuit model for gas sensors, where the sensor material can be thought of as a simple circuit consisting of three resistors. The model assumes that only the accessible surface experiences a change in resistance on interaction with a target gas. A porous, gas sensitive material can be broken down into three regions, the surface region, equal to the Debye length (also known as the electron depletion region or space charge layer), which is altered based on the interaction of the gas, the bulk region, which consists of the rest of the grain and in unaffected by interaction with an analyte gas and therefore independent of the gas concentration and the particle boundary. The surface and bulk regions are in parallel to each other, while the particle boundary is in series to both.

The contribution of the particle boundary region is dependant on the extent of sintering that the sensing material has undergone: for materials where there is a large degree of sintering, the particle boundary region is similar in resistance to the bulk, as electrons will not need to cross the space charge region. For samples that have less contact between them, the boundary can be considered to be gas sensitive and Schottky barriers may exist between particles[71].

The equivalent circuit model considers that the surface and neck regions (areas connecting adjacent grains) are the same, this is true if:

- There is moderate particle overlap between individual grains.
- Target gas access to the neck is unrestricted.
- The neck exhibits surface trap limited, rather than Schottky barrier behaviour.
- The neck region is chemically equivalent to the circuit.

The size of the grains also has an impact on the sensing response because of the inter-grain connections formed; these connections can be broadly classified into three groups, known as grain control, boundary control and neck control.

Xu *et.al*.[79] have suggested that when the diameter of the crystallite (D) is more than twice the Debye length (L_D) the grain boundaries contribute the highest resistance

within the sensor material and the system is grain boundary controlled. These grains are large and the surface to bulk ratio is very small.

As the diameter of the grain decreases, and becomes around twice the size of L_D, then the necks between grain particles become more resistant and dominate the gas response.

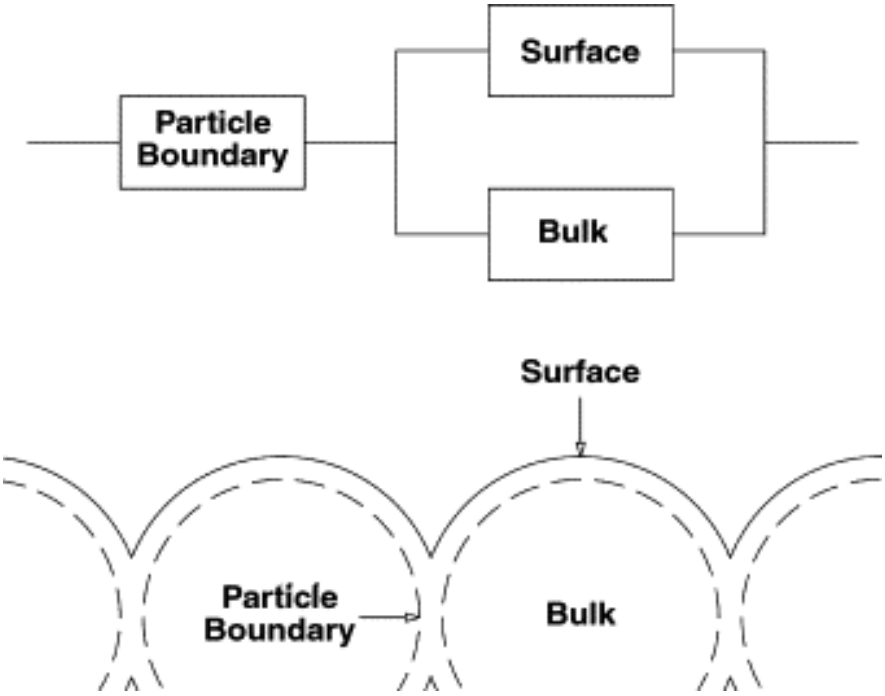

Figure 1.14. A simple equivalent circuit model, demonstrating the different resistances associated with sintered grains in a thick film gas sensor and their relative areas on gas sensing material the network of resistors representing the particle boundaries, the surface and the bulk and how these relate to the geometry of a solid composed of fused, approximately spherical particles. The dashed line in the lower diagram represents the depth to which the region defined as surface region reaches. This depth is equal to the Debye length. Figure adapted from images by Naisbitt *et.al.* (2006)[80].

When the grain size is even smaller, relative to the Debye length, the grain itself becomes most resistive, and gas response is determined by the entire grain, as the gas sensitive space charge region encompasses almost all the grain, removing the ineffective bulk region. This response is grain controlled and largely considered to be the most sensitive of the three models. The small size of grain particles and the high surface to bulk ratio contribute to the strong responsiveness of these materials. This model suggests that smaller sized particles lead to stronger responses.

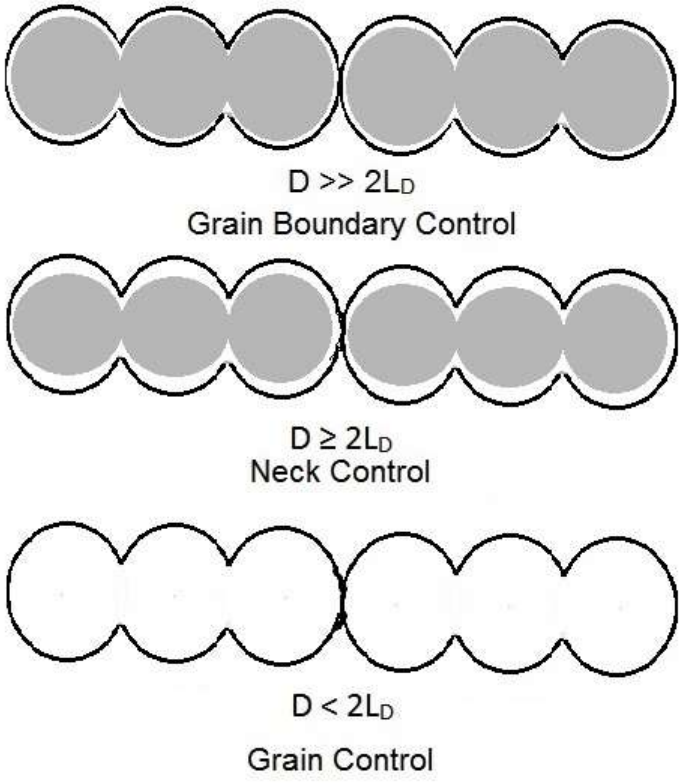

Figure 1.15. Schematic illustrating models demonstrating grain size effects in metal oxide gas sensors, the bulk region is shown in grey and the space charge region is shown in white. As grain size decreases, relative to the Debye length, the proportion of the grain occupied by the space charge layer increases, meaning that more of the material is tunable based on adsorbed species on the surface. Figure adapted from images by Afonja (2012)[77].

The grain-controlled model suggests that smaller grains lead to a larger response. This model should be considered in conjunction with the equivalent circuit model, which places a large resistance contribution from particle boundaries. As MOS particle size decrease, more particle boundaries occur between electrodes. For example, if the distance between two electrodes is 0.1 mm (100 µm) and the average particle size is 2 µm, 51 particle boundaries must be crossed between the electrodes. If on the same electrode substrate, a nanopowder with an average particle size diameter of 50 nm was used, 2001 particle barriers must be crossed between the electrodes, increasing the resistance in a sensor, impacting on the resistance and potentially the power requirements. An optimum size for the best D:L ratio whilst limiting the number of grain boundaries to cross must therefore be selected.

The gas sensing response of p-type sensors is largely considered to be weaker than in n-type materials. The reasons for this are based on the formation of the space charge layer

in the sensor material on adsorption of oxygen: n-type materials form a high resistance layer, while p-type materials form a low resistance layer, compared with the bulk material. As shown in Fig 1.16, in n-type materials, electrons must 'jump' over the space charge layer that is formed when oxygen atoms adsorb onto the sensor surface. In a p-type material, charge carriers generally flow through the lower resistance space charge layer. On interacting with a gas, changes of the adsorbed species at the sensor surface result in changes in the band bending. In a p-type material, large changes in the surface band bending of the material, does not result in a large change in resistance, relative to that of an n-type material, thus a smaller response is observed[81].

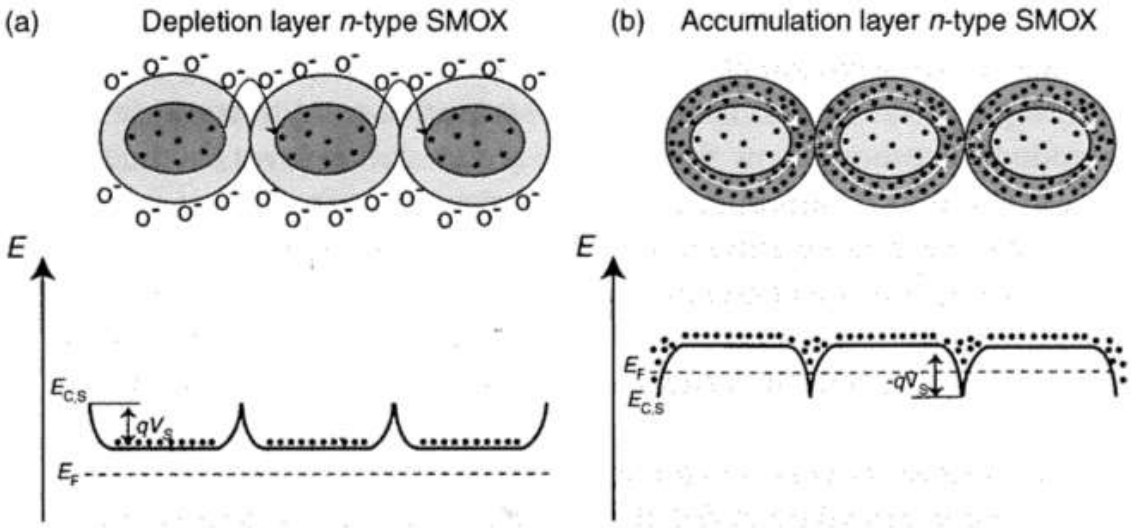

Figure 1.16. Demonstration of the band bending and charge carrier routes of n-type (a) and p-type (b) metal oxides. In n-type materials, charge carriers travel through the bulk material and require extra energy to overcome the space charge layer, while in p-type material, no extra energy is required to cross the space charge reason. As a result, in n-type material, changes in the band bending qV_s result in large changes in resistance, while in p-type material they do not. Adapted from images by Lee (2013)[76].

1.10. Selectivity in Gas Sensors

There is no single existing MOS gas sensor that is 100% selective to a single chemical gas[82]. This lack of selectivity is due to the reactive nature of the oxygen atoms adsorbed on the sensor surface, meaning many different chemical species can cause a similar response in the sensor. As a result of this, a great deal research has focussed on filtering

and decorating the sensor surface with elements that can be used to modify sensors and improve selectivity.

1.10.1. Electronic Noses

An electronic nose is an array of sensors and a programme of chemometric pattern recognition, used as an analytical instrument, in order to achieve specificity in detecting gases from a complex matrix.

MOS gas sensors have been incorporated into a number of electronic noses with a variety of applications, including the identification of tea[83], different types of alcoholic beverage[84], detection of spoilage in meat[85] and pesticides[86]. Sensors use different dopants, materials and operating temperatures to achieve a required fingerprint for a target gas. Gases are characterised by measuring three dynamic characteristics: transient slope (the rate of initial rapid increase when the gas is first detected), saturation slope (the slower rate of voltage increase as the senor reaches its greatest response), and maximum slope (measured when the sensor is closed off from the sample). Data from sensors is processed using mathematical procedures such as principle component analysis (PCA) or a support vector machine (SVM).

A number of different methods have been used to improve the selectivity of gas sensors, including the use of surface additives[87,88], nanoparticles[89,90,91], carbon nanotubes[92,93,94], and zeolites[95,96]. These dopants and additives use a range of mechanisms to achieve selectivity: many act as filters, excluding undesirable molecules from the sensor surface, or surface catalysts, to improve the sensor response of specific gases.

1.10.2. Metal Ion Doping

Doping is one of the most common methods of semiconductor modification. Doping involves the controlled introduction of well-defined impurities into semiconductor material and many scientists and engineers use this method to produce devices with interesting properties.

Doping of materials can affect the electronic properties of the material, by modifying the charge carrier concentration as well as the crystallite structure. Doping metal oxides with metals that are a higher oxidation state than the host metal, i.e. replacing Zn^{2+} in ZnO with In^{3+}, increases the electron density of the material, increasing the n-type characteristics in the metal oxide. Replacing the metal with an atom with fewer electrons, e.g. replacing Cr^{3+} with Ti^{4+} in chromium titanate ($Cr_{2-x}Ti_xO_3$), increases the p-type character of the metal oxide.

A number of n-type materials have undergone metal doping to investigate their sensing properties. Chakraborty *et.al*.[97] demonstrated that doping tin oxide (SnO_2) with 0.1 % and 0.5 % iron (Fe^{3+}) increased its responsiveness to methane and butane, this involved doping n-type materials to increase the electron density of the material, increasing its n-type behavior. Yoon *et.al.*[98] reported the doping of p-type NiO with iron in low doping levels (0.18-13.2%) and found that Fe doped sensors demonstrated enhanced responses to ethanol, xylene, benzene, toluene and carbon monoxide. This is due to an increase in the p-type behavior of the NiO by incorporation of Fe^{3+} into Ni^{2+} sites.

1.11. Zeolites

Zeolites are 3D aluminosilicate frameworks, composed of tetrahedral $[AlO_4]^{5-}$ and $[SiO_4]^{4-}$ anions, which share oxygen atoms to form uniformly sized cages and channels. Zeolites possess the overall empirical formula $M^{n+}{}_{x/n}\,[AlO_2]_x\,[SiO_2]_y.zH_2O$, an overall negative charge in the zeolite framework is balanced by the inclusion of a cation such as H^+, Na^+ or NH_4^+.

Due to their large band gap (several eV), electronic conductivity is not observed in zeolites. However, because mobile cations can hop between binding sites in the material, ionic conductivity is observed[99]. The activation energy and specific conductivity of zeolites vary depending on the framework type and nature of the cation present in the material. In a dehydrated state, the highest conductivity values have been observed in Na^+ compensated zeolites[100]. In a hydrated state, zeolites have been observed to conduct protons via a vehicle mechanism[101].

Zeolites can be classified according to their Si/Al ratio and the properties that arise from them. The lower the Si/Al ratio, the larger the negative charge within the zeolite (and the higher the counter ion concentration), this higher charge leads to increased hydrophilicity. Zeolites can be classified into three groups based on their Si/Al ratio, these are:

- Low silica zeolites, with Si/Al ratios of 1-1.5, such as zeolite A or X, these zeolites are hydrophilic.
- Medium silica zeolites, with Si/Al ratios of 2.5-10, such as zeolite Y or zeolite L, these zeolites are hydrophilic.
- High silica zeolites, with Si/Al ratios greater that 10 are very hydrophobic. Examples of these zeolites include zeolite beta and H-ZSM5.

If protons populate all the cation sites in the zeolite, each proton site is a strong Bronsted acid. Thus, increasing the Al/Si ratio in the zeolite framework increases the number of acid sites and the overall acidity of the zeolite. However, each acid site becomes a somewhat weaker Bronsted site as the population of protons increased. This is due to proton crowding in the zeolite pores[102].

The structure of the zeolite allows the material to function as a molecular sieve, filtering out molecules that are too big to fit into zeolite pores and channels, allowing molecules of the right size and shape to pass freely through. This property of zeolites is used in several industrial applications, including the petrochemical industry, as a catalyst in fluid catalytic cracking and in agrochemicals, as water moderators[103].

Zeolites have been integrated into gas sensors both as a sensing material and as an auxiliary phase. The use of zeolites as an auxiliary phase in gas sensing are divided into three major subgroups. The most common of these techniques is to apply a zeolite as an over layer, which is to print one or more layers of a zeolite material, over the top of a gas sensitive semiconductor. A number of studies demonstrate that overlaying a metal oxide semiconductor with zeolite material can lead to increases in selectivity, by

reducing the magnitude of response of some gases, but also enhance the magnitude of response to other gases. This is most notably reported by Binions *et. al.*[104] who demonstrated the use of H-LTA and H-ZSM5 over layers on top of thick films of tungsten trioxide (WO_3) and chromium titanate (CTO). These modifications caused a decrease in the responsiveness of the sensors to pulses of carbon monoxide and ethanol, however, an increase in the responsiveness to ethanol was observed with H-LTA modified chromium titanate. The pore structure of the zeolite material prevented specific analyte gases from reaching the surface of the metal oxide, and prevented a response from occurring.

Gas sensing material can also be incorporated directly into the zeolite material, whereby some sensitive material is incorporated into the cages. One example of this is detailed by Meier *et.al.*[105] who demonstrated a ruthenium complex was incorporated into the supercages of zeolite Y. The zeolite was mounted onto a silicon support and used as an oxygen sensor; the encapsulated zeolite demonstrated good responses dependent on the partial pressure of O_2.

The final method of zeolite modification is the formation of a zeolite - sensing material admixture. This involves incorporating zeolite material to the total sensing bulk, usually around 10-30% of the total material. This allows the sensing material to exist at the surface as well as deeper in the porous structure. The strong adsorption properties of the zeolite mean that gases can be 'held' within the metal oxide structure. Work by Peveler *et.al.*[106] included zeolites H-ZSM5 and TS-1 in tungsten trioxide and indium oxide sensors and recorded enhancements in sensitivity compared with their unmodified materials, to ethanol and nitrogen dioxide.

The use of impedimetric zeolite sensors has been extensively studied by Moos *et.al.* most notably the gas concentration dependent interaction of mobile protons in the zeolite pores being used as an impedance based selective ammonia sensor[107]. These sensors are based on the principle that when the zeolite material interacts with ammonia, the activation energy of conduction is decreased and ionic conductivity

occurs. Adsorption of ammonia molecules within the zeolite framework supports the proton transfer from one aluminium site to the next[108].

A hydrocarbon sensor, based on the Na-ZSM5 zeolite has also been developed[109]. Impedance spectroscopy (IS) measurements demonstrated a strongly increasing complex resistivity in the lower frequency range when hydrocarbons are introduced to a carrier gas flow. This sensor effect is highly selective towards hydrocarbons, showing no cross-sensitivities towards H_2, CO, NO, CO_2 or O_2.

These impedance-based effects are only observed if a thin layer of chromium oxide (Cr_2O_3) exists between the sensor electrodes and the zeolite[110]. Researchers have suggested that an interaction between chromium oxide and cations of the zeolite that takes place directly at the zeolite/chromium oxide interface is responsible for the sensor effect. However, it should be emphasised that up to now, there is no physical or electrochemical explanation of the sensor available[107].

1.12. Zeolites of Interest

This study incorporates four zeolites into metal oxide materials, with 30% of the total mass of printed material containing zeolite. This is based on previous research demonstrating 30% being the optimum composition of zeolite admixture[77].

The zeolites used in this study contain a range of pore diameters, structure types and Si/Al ratios (Table 1.3). All zeolites used are used in their protonated form.

Table 1.3. Properties of the four zeolite materials used in this study. All zeolites were supplied by zeolyst in the protonated form, with the exception of mordenite, which was supplied as NH_4^+ -mordenite and converted to H-mordenite as described by Bordiga *et.al,* (1995)[111].

Zeolite Name	Product no.	SiO_2/Al_2O_3 ratio	Surface area ($m^2\ g^{-1}$)	Pore diameter (Å)
Zeolite Y	CVB 600	5.2	660	7.35
Zeolite beta	CP 811E-75	75	664	5.95
Mordenite	CVB 21A	20	500	11.75
ZSM5	CVB 2802	140	400	5.55

1.12.1. Zeolite Y

Zeolite Y is a Fajuasite zeolite consisting of sodalite β-cages, connected through hexagonal D6R prisms (Fig 1.17). As a result, pores are perpendicular to each other and relatively large, with a 7.35 Å pore size, formed by 12 membered rings. Zeolite Y is commonly used in fluid catalytic cracking to convert high boiling fractions of crude oil into more valuable gasoline and diesel. Zeolite Y has been used in gas sensing to detect NO_X compounds[112,113] and carbon monoxide[114,115].

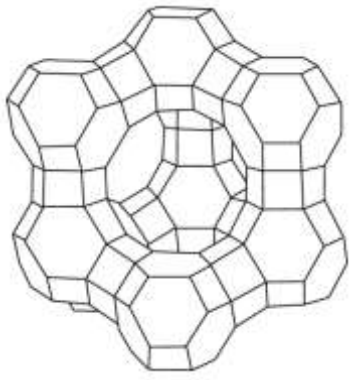

Figure 1.17. 3D schematic of zeolite Y, demonstrating the different structure types within the zeolite (each line corresponds to an Si-O-Si linkage). Figure adapted from Lutz (2014)[116].

1.12.2. Zeolite Beta

Zeolite beta is a high silica zeolite, giving the surface of this zeolite organophilic-hydrophobic selectivity[117]. The zeolite possesses a three-dimensional 12 membered ring pore system, with a pore diameter of 5.95 Å. Zeolite beta was developed by Mobil™ for use in petrochemical cracking, later to be replaced by ZSM5[118]. Zeolite beta has been used previously as a molecular sieve for separating toluene[119] as well as cracking of paraffin[120] and the disproportionation of isopropyl benzene[121].

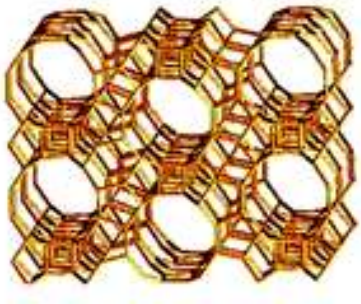

Figure 1.18. Schematic of zeolite beta in which micro pores are defined by the framework of the material (each line corresponds to an Si-O-Si linkage). Figure adapted from Hugon *et.al. (2000)*[122].

1.12.3. Mordenite

Mordenite is an orthorhombic zeolite with one-dimensional channels, meaning that the channels through the zeolite flow in only one direction. Mordenite is used frequently in the petrochemical industry for the acid catalysed isomerisation of alkanes and aromatics. It has been used in gas sensing to detect short chain hydrocarbons[123]and carbon monoxide[123].

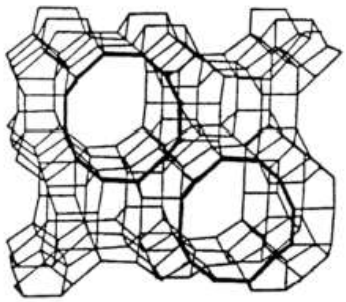

Figure 1.19. Schematic representation of the framework of mordenite (each line corresponds to an Si-O-Si linkage). Figure adapted from Hugon *et.al.* (2000)[123].

1.12.4. ZSM5

Zeolite Socony Mobil–5 (ZSM5) is a zeolite belonging to the pentasil family. Patented by the Mobil™ oil company in 1972[124], it is widely used in the petroleum industry as a catalyst for hydrocarbon isomerisation reactions. The zeolite is made up of several pentasil units linked together by oxygen bridges to form pentasil chains. Pentasil units consist of eight, five-membered rings. ZSM5 has estimated pore sizes of 5.4-5.6 Å[125]. The regular 3-D structure and acidity of ZSM5 mean that the material has been utilised in a number of acid catalysed reactions, including the isomerization and alkylation of hydrocarbons[126], such as the isomerisation of m-xylene to p-xylene. During this shape selective reaction, para-xylene has a much higher diffusion coefficient than meta-xylene, allowing para-xylene to traverse through the pores and diffuse out of the catalyst quickly and gain a high yield[127].

Figure 1.20. A pentasil unit, the building blocks of ZSM5 (each line corresponds to an Si-O-Si linkage). Figure adapted from Hugon *et.al.* (2000)[123].

1.13. Target Gases of Interest

This study will focus largely on five target vapours, commonly found in clandestine environments. All gases used were supplied by BOC as compressed gases.

1.13.1. Toluene

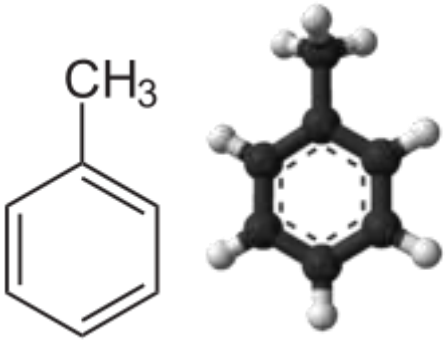

Figure 1.21. Skeletal and 3D structures of toluene. Carbon atoms are shown in grey and hydrogen atoms in white. The bond angle between carbon atoms is 120°. Structures produced using ChemDraw (2D) and Arguslab (3D).

Toluene is a colourless, combustible, water insoluble liquid at STP (25°C and 1 bar). Toluene was used at 2.5-40 ppm, as supplied by BOC. It is used in all three methods of methamphetamine synthesis as an organic solvent. Toluene is widely available to purchase as a common solvent. Toluene is found at non-clandestine environments in paint thinners, gasoline fuels, metal degreasers and in the production of insecticides. It is found in clandestine environments at concentrations of around 10-50 ppm in air. Toluene is also part of a group of common environmental pollutants known as BTEX (benzene, toluene ethyl benzene and xylene). BTEX compounds are commonly used in the manufacture of rubbers, dyes, detergents, pesticides and pharmaceuticals. Over time, toluene has replaced benzene in many industrial processes, due to benzene's high carcinogenicity.

1.13.2. Ethanol

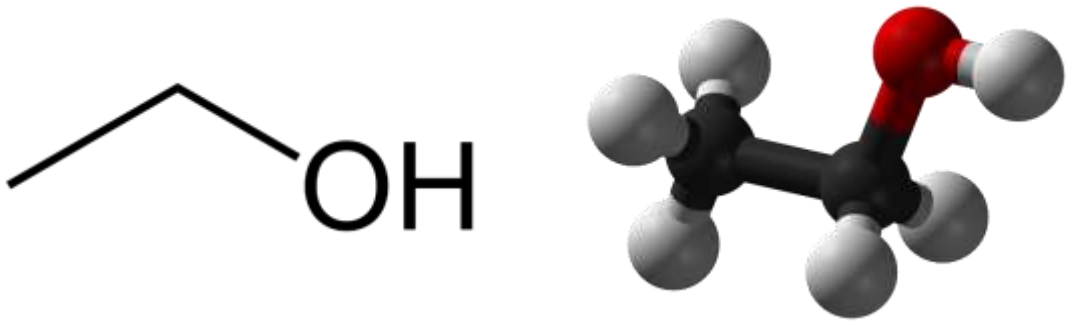

Figure 1.22. Skeletal and 3D structures of ethanol. Carbon atoms are shown in grey, oxygen atoms are red and hydrogen atoms are white. Structures produced using ChemDraw (2D) and Arguslab (3D).

Ethanol is a volatile, flammable, colourless liquid at standard temperature and pressure. Ethanol was used at concentrations between 5 and 80 ppm supplied by BOC. It is an important solvent, but is also used as a fuel, an intoxicant and in thermometers. It is found in low ppm and ppb concentrations[128] in methamphetamine labs, where it is used as a solvent in reductive ammination of P2P[129]. Ethanol vapour is found at levels between 50-100 ppm in the immediate environment around a clandestine methamphetamine laboratory[130]. Ethanol is mainly used in industrial processed such as fermentation and distillation, these processes can cause ethanol concentration in the air to exceed its threshold limit value of 1000 ppm, leading to irritation of the eyes, nose and skin as well as alcohol poisoning[131].

1.13.3. Acetone

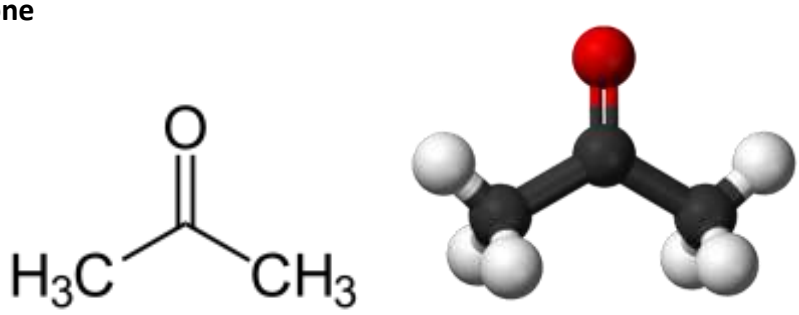

Figure 1.23. Skeletal and 3D structures of acetone. Carbon atoms are shown in grey, oxygen atoms as red and hydrogen atoms are white. Structures produced using ChemDraw (2D) and Arguslab (3D).

Acetone is a colourless, mobile and volatile liquid ketone, used at concentrations between 0.5 and 8 ppm by BOC. Acetone is miscible with water and as a result, serves as an important solvent. It is used in all methods of synthesis of methamphetamine as a solvent in the recrystallisation of the methamphetamine. For methamphetamine synthesis, acetone is obtained as a solvent, widely available from chemical suppliers. It is found in clandestine environments at concentrations below 10 ppm. Acetone is found in many household items including nail polish remover and paint thinner. Acetone is also known to be a key biomarker for patients with high levels of ketoacidosis, a side effect of diabetes.[132]

1.13.4. Nitrogen Dioxide

Figure 1.24. Skeletal and 3D structure of nitrogen dioxide. Nitrogen atoms are shown in blue and oxygen atoms are shown in red. The bond angle is 134.3°. Structures produced using ChemDraw (2D) and Arguslab (3D).

Nitrogen dioxide is a strong oxidant and toxic atmospheric pollutant and was used in concentrations between 0.05 and 0.8 ppm as supplied by BOC. It is frequently found in clandestine laboratories as a side product of the Birch reduction method[133]. In addition to this, the $–NO_2$ functional group is a sub structure of many chemicals used in the generation of Ammonia for clandestine uses[134].

Nitrogen dioxide is found as an intermediate in the manufacturing of nitric acid[135], and as a nitrating agent in the production of chemical improvised explosive devices (IEDs)[136] it is also found commonly as a product of internal combustion engines[137]. Exposure in the general population arises from cigarette smoke[138], butane & kerosene heaters and cooking stoves[139]. Cars, combustion engines and power plants are major causes of polluting nitrogen oxide gases (NO_x, x=1-2) in the air. Nitrogen dioxide is the most toxic

of these and has a threshold limit value of 3 ppm[140]. Overexposure to NO_2 can lead to respiratory problems such as asthma, bronchitis, emphysema and heart disease[141]. It is estimated that there are over 9000 deaths a year in London, related to NO_x exposure[142].

1.13.5. Ammonia

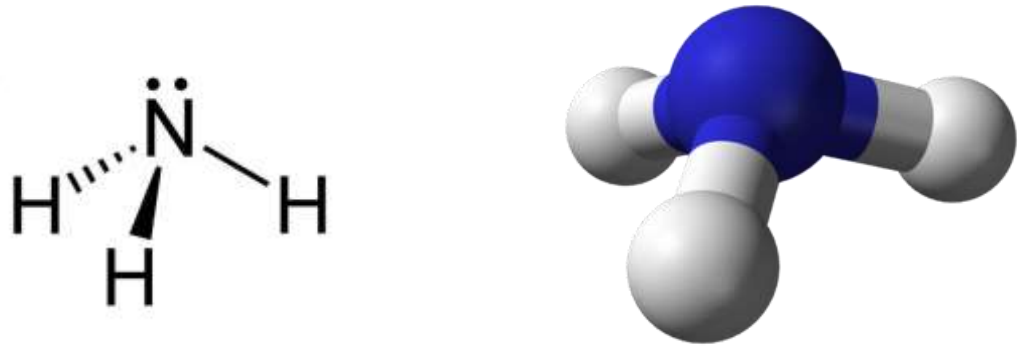

Figure 1.25. Skeletal and 3D structure of ammonia. Nitrogen atoms are shown in blue and hydrogen atoms are shown in white. Structures produced using ChemDraw (2D) and Arguslab (3D).

Ammonia is a strong, colourless, reducing gas. Ammonia was used at concentrations between 2.5 and 40 ppm, supplied by BOC. Widely used in many different methods of production of methamphetamine, primarily as a key ingredient of the Birch reduction method. The amine ($-NH_2$) group is a common functional group on several reagents found at clandestine locations, such as methylamine. Ammonia is found in a variety of cleaning products and fertilisers; however, it is usually obtained for clandestine use by theft, or even sale, from the agriculture industry.

Ammonia is usually obtained for clandestine synthesis methods from farmer's fields, where it is syphoned, or even sold, from large nurse tanks at farms. Anhydrous ammonia is used as an efficient and cost-effective fertilizer. Anhydrous ammonia vapour is corrosive and aggressively seeks out water, causing harm to the eyes, throat, sinuses and lungs[143].

Ammonia is also found as a major component of cleaning products[144], fuels[145], textiles[146] and refrigerants, where it is widely used in the industrial refrigeration of ice hockey rinks[147].

1.14. Objectives of This Study

The aim of this study is to investigate the use of semiconducting metal oxide gas sensors as a tool to detect chemicals used in the production of methamphetamine and to assess their potential to be incorporated into an electronic nose to detect clandestine methamphetamine production. For an array of sensors or electronic nose to be a successful analytical device, it must be:

- Highly sensitive to the target analytes.
- Possess good selectivity for the target in the presence of interfering gases.
- Have fast response and recovery times to the target gas.
- Show reproducible responses of the signal over multiple exposures to the test gas and power cycling.

In this study, zinc oxide, chromium titanate and vanadium pentoxide were modified using zeolite admixtures and metal ion doped material. To assess their gas sensing potential, sensors were exposed to gases commonly found in clandestine locations. Data was collected on the materials responses to all gases and classification techniques were performed for chemical fingerprint identification to assess the sensors ability to discriminate between gases to nominate the best candidates for inclusion in an electronic nose used to detect clandestine chemistry activity.

2 . Experimental

This chapter will detail the procedure of device fabrication as well as the design and operation of the gas sensing apparatus used to test sensors.

2.1 Material Fabrication

2.1.1. Zinc Oxide

Zinc oxide was used as supplied by Sigma Aldrich (Product code: 96479).

2.1.2. Chromium Titanate

Chromium titanate was produced from solid TiO_2 and Cr_2O_3 as described by Niemeyer *et.al.*[148]. Chromium (III) oxide, Cr_2O_3, was obtained from Sigma-Aldrich and sieved through a 38-micron sieve. This powder was dispersed in propan-2-ol (Sigma-Aldrich) and the titanium dioxide in propan-2-ol was added under ultrasonic agitation. After five minutes, 5 cm^3 of distilled water was added. After stirring and ultrasonic agitation for another 15 minutes the solvent was evaporated under reduced pressure in a rotary evaporator, with continuing ultrasonic agitation. The powder was dried at 120°C for two hours. Subsequently the powder was fired in recrystallised alumina crucibles for twelve hours at 1000°C in an elite thermal systems BRF15 furnace.

2.1.3. Vanadium Pentoxide

Vanadium pentoxide was used, as supplied by BDH Chemicals (Product code: 30565).

2.1.4. Indium Doped Zinc Oxide

Zinc oxide and indium doped ZnO were produced using a co-precipitation technique. To produce pure ZnO, zinc acetate ($Zn(OAc)_2.2H_2O$), supplied by Sigma-Aldrich, was fully dissolved in methanol. Subsequently, a 0.5 M solution of NaOH was added drop wise

over a period of 2 hours. The resulting precipitate was washed with ethanol and water and filtered. The precipitate was subsequently calcined at 700°C for 3 hours.

To produce indium doped ZnO, indium nitrate ($In(NO_3)_3.xH_2O$, (Alfa Asear)) was used as a doping agent and dissolved with suitable quantities of zinc acetate. This produced indium doped ZnO with 0.2, 0.5, 1 and 3-mol % indium.

2.2. Device Fabrication

Pure metal oxide sensors were fabricated as control samples in each chapter. These sensors featured 100% weight of the metal oxide.

Metal ion doped sensors were fabricated using 100 Wt % of each individual sample material. Zeolite modified metal oxide powders contained 30 Wt % zeolite mass. Inks were produced by grinding metal oxide and zeolite material. All powders were mixed with a texanol based organic vehicle (ESL-400, supplied by ESL Electro-Science) using a pestle and mortar, to produce a smooth homogenous suspension, which was subsequently used for screen-printing.

Materials were fabricated by printing inks onto 3 x 3 mm alumina substrate tiles; containing laser etched digitated electrodes and an integrated platinum heater track (electrode gap 0.15 mm, Fig. 2.1).

Screen-printing was performed on a DEK1202 printer. Ink was printed onto a strip of alumina substrates. A single sensor tile contains 196 (14 x 14) individual $9mm^2$ sensor tiles, containing interdigitated electrodes (Fig. 2.1). All tiles are scored for easy breaking of individual sensor tiles.

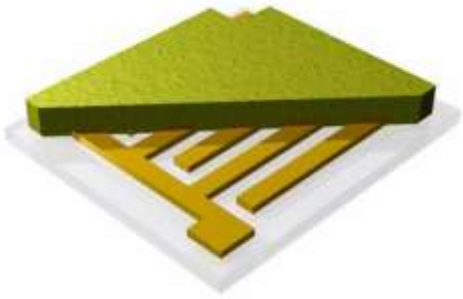

Figure 2.1. Individual sensor tile demonstrating interdigitated electrodes (0.15 mm gap) and thick film of screen-printed porous gas sensitive material. Image courtesy of City Technology Ltd.

A total of 5 layers of ink were printed on the substrate (~75 µm thickness). Between applications, the ink was dried under an infrared lamp for 20 minutes. Following application of all layers, individual sensors were fired for 1 hour at 600°C in an Elite Thermal Systems BRF15 furnace. The ramp rate of the furnace, to increase the temperature from room temperature to 600°C, was set at 5°C min^{-1} to prevent breakdown of the zeolite materials by rapid heating.

Figure 2.2. A printed strip of zinc oxide sensors.

Sensors were numbered 1-14, with 1 being the sensor tile closest to the head of the printer, and 14 being the sensor furthest from the printer head. In all cases, sensor number 6 was used, as a tile in the centre of the strip, it has been previously shown that this tile has the thickest film formed, due to its position in the printing process[70].

The sensors were bonded onto brass pins in a standard polyphenylene sulphide 4-pin sensor housing using platinum wire (0.0508 mm thickness, supplied by Alfa Aesar) and a MacGregor DC601 parallel gap resistance welder.

The heater track resistance of fully bonded sensors was measured by four-probe resistance measurement, using a Keithley 2464 multimeter, across the platinum base track of the sensor tile. These resistances were recorded to 4 decimal places.

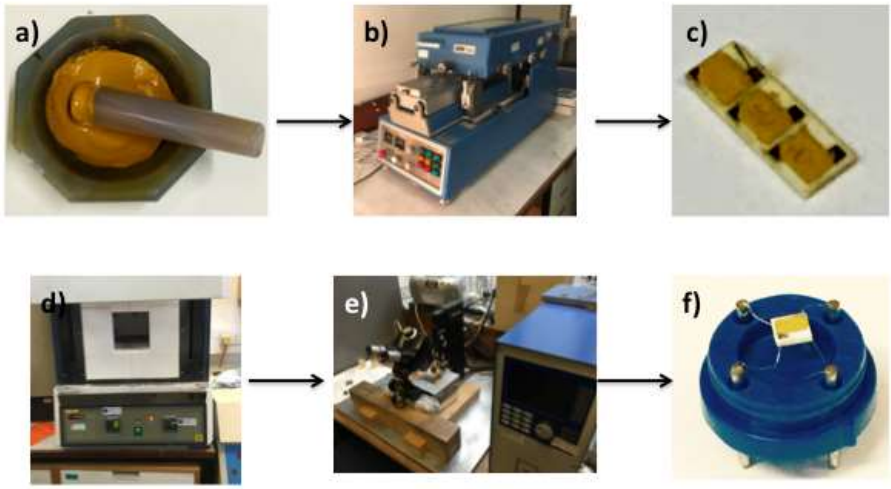

Figure 2.3. Steps in the fabrication of a sensor. a) demonstrates a MOS suspension (in this case V_2O_5), b) is a DEK 1202 screen printer, c) three V_2O_5 screen printed sensor chips, d) An Elite Thermal Systems furnace, e) MacGregor spot welder, f) a finalised sensor tile in its poly-phenylene sulphide housing, bonded with platinum wire.

2.3. Sensing Rig

All gas-sensing tests were performed on an in-house testing rig. This testing rig consists of a 12-port sensing chamber. The flow of gas into the chamber is controlled by four, Aera FC-7700CD mass flow controllers (MFCs) and six Burkert 0214 two-way solenoid

valves, connected through PTFE tubing. Air and target gases flow into the sensing chamber at a flow of 1000 cm^3/min.

The system is operated on an automated gas flow program (Table 2.2) written in Pascal, running on MS-DOS, by Keith Pratt.

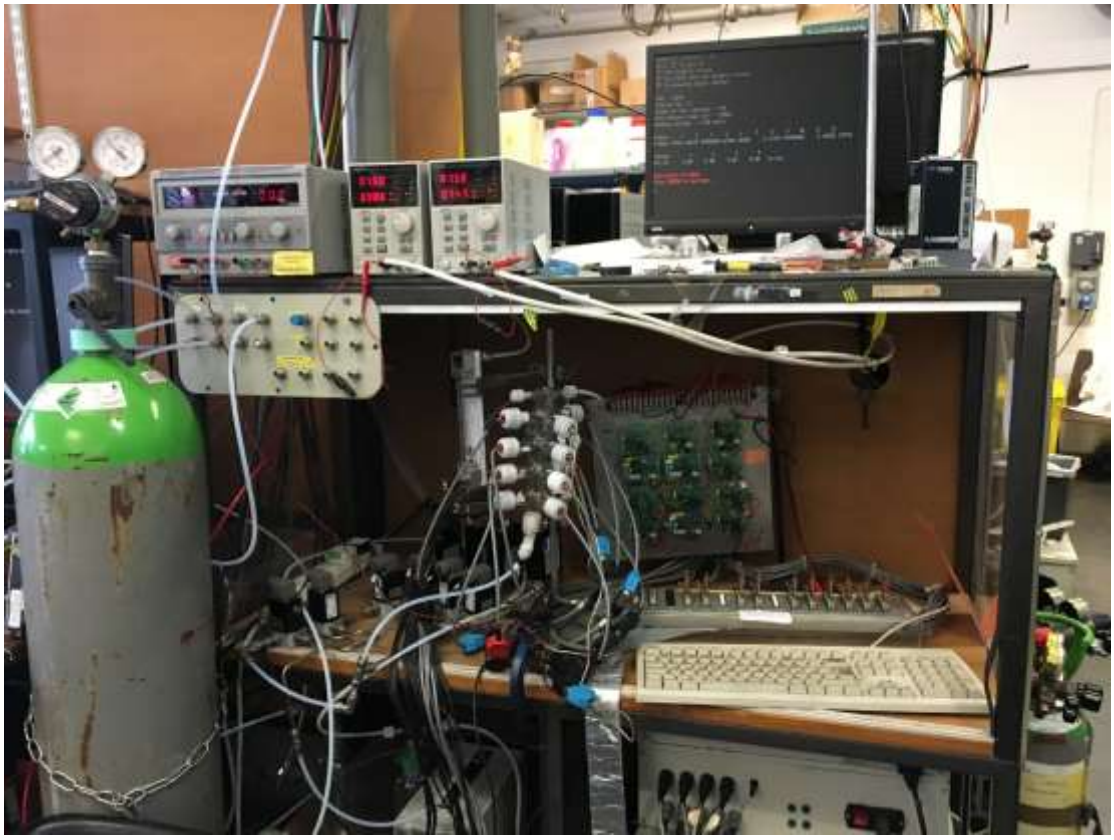

Figure 2.4. Gas sensing rig used in this investigation. The rig consists of a gas-sensing chamber, which can accommodate up to 12 ports. Gases are introduced in a controlled manner to the sensing chamber through four mass flow controllers and six solenoid valves.

Mass flow controllers (MFC) control the flow of gases from air and test gas cylinders to the sensor chamber, up to and including 1000 cm^3 min^{-1}. Solenoid valves (SV) control the entry of gases into the sensing chamber and operate under a binary setting. When solenoid valves are set to 0, the valve is closed, when set to 1, the valve is open and gas can travel through the tube. SV's 1-4 control gas entry to the sensing chamber from the corresponding mass flow controller, while SV 5-6 control the humidity loop, allowing humid air to enter the system.

The schematic of the in-house test rig (Fig. 2.5) demonstrates that there are 4 lines through which air and gas can travel. The red lines control the flow of air to the sensor chamber; dry air travels through MFC 1 and 2. When dry air is required, this continues directly to the sensor chamber, if humid air is required (RH = 50%), this travels through a humidifying loop where humid air enters the system between SV 5 and SV 6. Test gas travels through MFC 3, directly to the sensing chamber. The fourth gas line (green line) allows headspace analysis of a solid or liquid sample by extracting vapour in a Drechsel bottle. All the lines converge following the solenoid valves, and flow into the sensor chamber. Exhaust gas is removed without entering the atmosphere in which researchers are working.

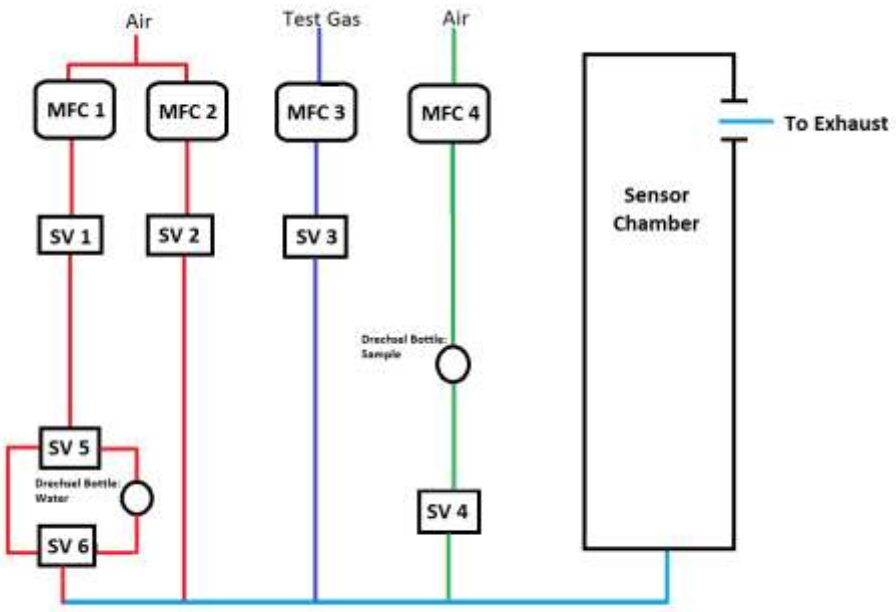

Figure 2.5. Schematic of the gas sensing rig flow diagram of in-house testing rig, with modification to channel 4 for sampling headspace of liquids and solids in the Drechsel bottle. Mass Flow Controllers (MFCs) and Solenoid Valves (SVs) 1-4 are located on their respective channels. SVs 5 and 6 control the proportion of humidity. Adapted from drawings by Dr William Peveler.

Sensors are heated to their respective operating temperatures using a Wheatstone bridge circuit board (Fig. 2.6), the driving voltage required to heat the sensor to a certain temperature was calculated using the resistance curve of platinum and the room temperature resistance of the sensor's platinum heater track, taken from four-point

resistance measurements. All sensors maintained stable temperatures over long time periods (up to 72 hours).

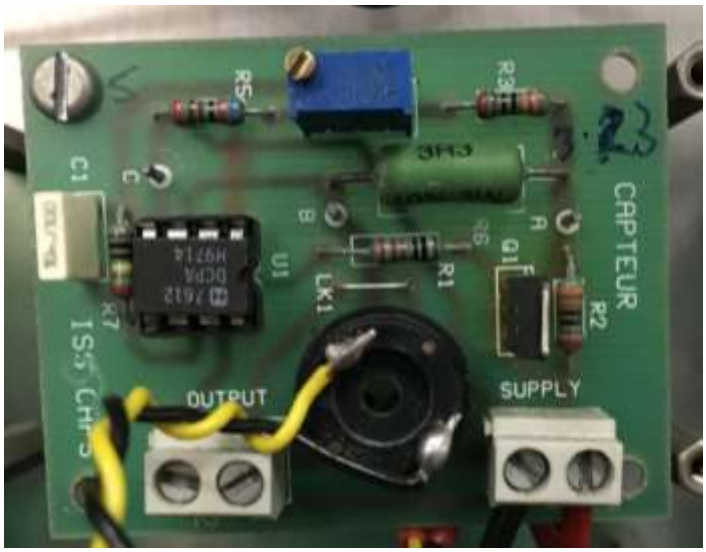

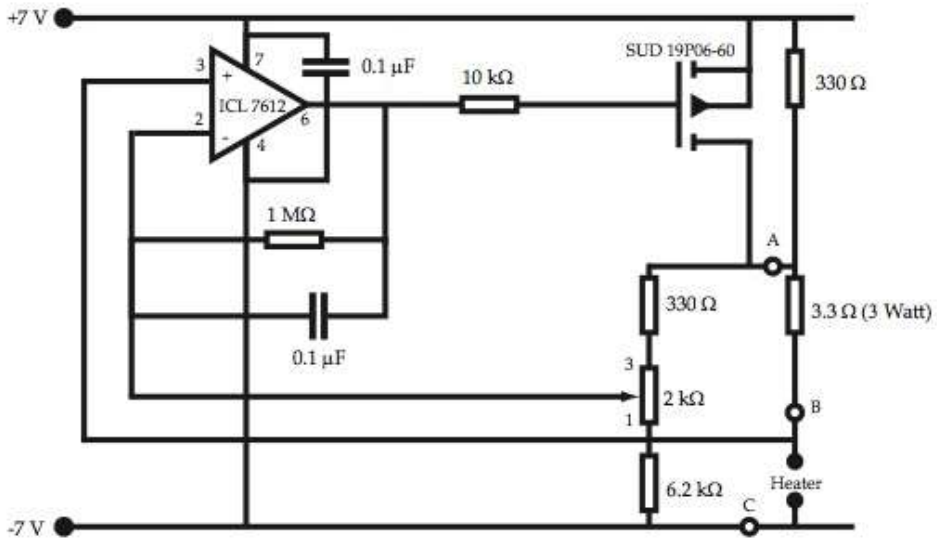

Figure 2.6. Photo and circuit diagram demonstrating Wheatstone bridge heater board used to control the voltage applied to the platinum heater track of each sensor. Points A, B and C are measurement pins for the attachment of two multimeters to adjust the resistance of the Pt wire and therefore the sensor temperature, via adjustment of the potentiostat. Adapted from drawings by Dr Ayo Afonja.

Circuit resistances for each sensor were measured using a potential divider circuit and amplifier. A serial resistor was selected for each sensor to modify the gain on the output measurement. This ensured that the data were kept within a measurable range for the analogue to digital converter card.

The sensor response was calculated from the resistance obtained in a two-step process. Firstly, the resistance obtained in its raw form from the rig refers to that of the potential divider circuit. This can be converted to sensor resistance by the following equation:

$$\mathrm{R_{Sensor}} = \left(\frac{(\mathrm{R2})}{(\mathrm{R1})}\right) \times \mathrm{R_{Output}}$$

In the equation R_{sensor} is the sensor resistance, R_{output} refers to the recorded resistance. R1 and R2 are the upper and lower socket resistance values as seen in figure 2.6. R1 is fixed at 2000 Ω; R2 varies depending on the sensor.

The response of the sensor is calculated as R/R_0 or R_0/R, dependent on the redox properties of the gas and the type of material (n-type or p-type). The baseline resistance value, R_0, of each individual sensor was calculated as the average resistance during the last 90 seconds of the initial air pulse, before the first gas pulse. This R_0 value is static and kept constant for subsequent pulses within the same experiment. This ensures that the response is recorded relative to the same R_0, and remains unaffected by a pre-conditioned gas sensing reactions, altering the resistance in the material.

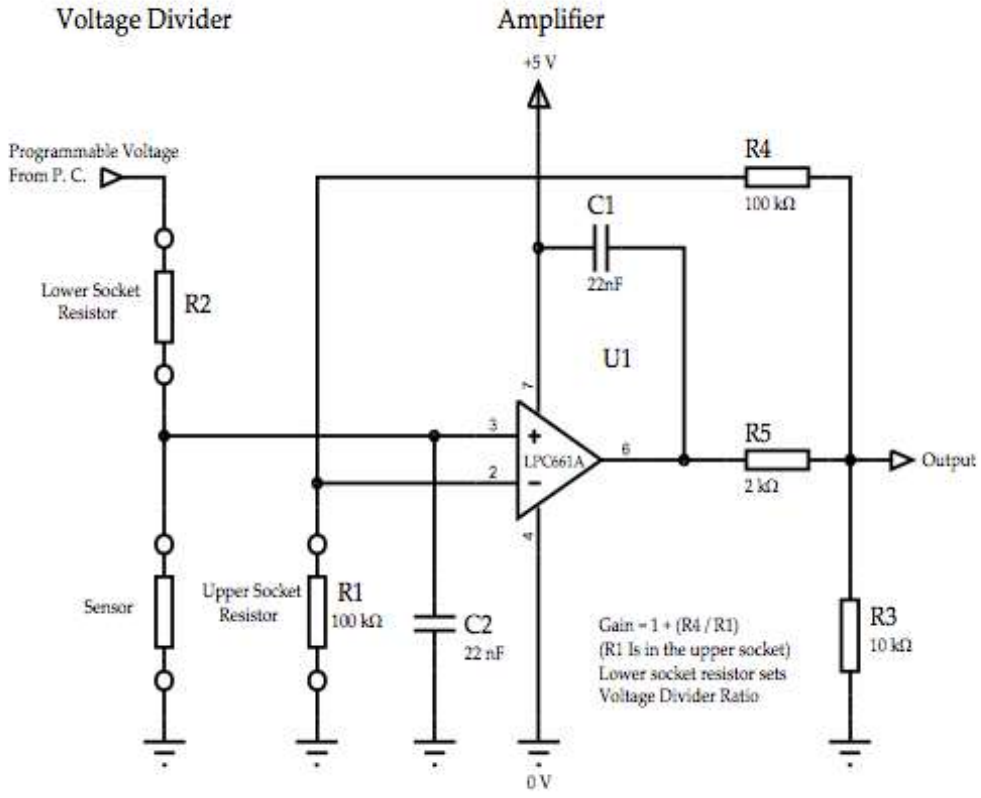

Figure 2.7. Circuit diagram for voltage divider and amplification board. The lower socket resistor value is not fixed and is changed depending on the sensor used in each experiment, all other capacitor and resistor values are fixed. Lower socket resistor (R2) value is changed to ensure the measurement of the sensor resistance is within the measurable range of the instrument (0-20 MΩ). Adapted from drawings by Dr Ayo Afonja.

For standard gas sensing experiments, sensors were exposed to pulses of air and gas supplied by BOC. Synthetic compressed air (CAS number: 132259-10-0) was used as a carrier gas. Table 2.1 lists the gases used in this study, their concentrations and their product numbers from BOC.

Table 2.1. Gases used in this thesis, with their source code and product number from BOC. The first part of the code refers to the gas and the concentration, the second part to the cylinder size and the final letter refers to the type of regulator required to connect the gas to the sensor rig, all regulators used were two stage regulators that differ by connection to the gas cylinder. All gas cylinders were balanced by compressed air.

Gas	Concentration (ppm)	Product number
Acetone	10	160475-AV-C
Acetone	100	164074-AV-C
Ammonia	50	151339-AK-C
Carbon Monoxide	1000	151518-AK-C
Ethanol	100	294645-AK-C
Methanol	100	172742-AV-C
n-butanol	100	164158-AV-C
Nitrogen dioxide	1	152639-AK-S
Toluene	50	156894-AV-B

Gases were used as percentages of their source concentration, with the remainder balanced by compressed air. For most experiments, sensors were initially exposed to a 40-minute (2400 second) pulse of air, to establish a baseline resistance. This initial air pulse was followed by five, 600-second pulses of gas, interspersed with 1200-second air pulses, to re-establish a baseline resistance. Resistance measurements were recorded every 10 seconds.

Table 2.2. Gas sensing program demonstrating pulses of 5, 10, 20, 40 and 80% of the source concentration of a gas in dry air. The gas flow through the rig is kept constant at 1000 cm^3/min. At the end of the test, there is a 30 second pulse where no gas flows and all solenoid valves are shut. This is to ensure no gas can escape into the system and any gas/air left in the sensing chamber is removed to exhaust before it is opened, ensuring researchers are not exposed to potentially harmful gases. SV refers to the solenoid valve number, with 1 being open and 0 being closed.

Time (S)	Air (cm^3/min)	Gas (cm^3/min)	SV1	SV2	SV3	SV4	SV5	SV6
2400	1000	0	0	1	0	0	0	0
600	950	50	0	1	1	0	0	0
1200	1000	0	0	1	0	0	0	0
600	900	100	0	1	1	0	0	0
1200	1000	0	0	1	0	0	0	0
600	800	200	0	1	1	0	0	0
1200	1000	0	0	1	0	0	0	0
600	600	400	0	1	1	0	0	0
1200	1000	0	0	1	0	0	0	0
600	200	800	0	1	1	0	0	0
1200	1000	0	0	1	0	0	0	0
30	0	0	0	0	0	0	0	0

2.3.1. Test Gas Conditions

All unmodified sensors and sensors modified with zeolite beta, zeolite Y, Mordenite and ZSM5 and indium oxide, were exposed to common volatile compounds, at concentrations between 5, 10, 20, 40 and 80 % of the source concentrations, supplied by BOC. All tests were carried out at a pressure of 1 atm. Tests were repeated in triplicate to ensure short-term repeatability.

Table 2.3. Concentrations of gas exposed to sensors, balanced by compressed air at a flow rate of 1000 cm^3 min^{-1}.

Gas	Source Concentration (ppm)	Test Concentrations (ppm)				
Acetone	10	0.5	1	2	4	8
Ammonia	50	2.5	5	10	20	40
Ethanol	100	5	10	20	40	80
Nitrogen Dioxide	1	0.05	0.1	0.2	0.4	0.8
Toluene	50	2.5	5	10	20	40
Methanol	100	5	10	20	40	80
n-butanol	100	5	10	20	40	80
Acetone	100	5	10	20	40	80
Methanol	100	5	10	20	40	80

The flow rates for all gas exposures were set to 1000 cm^3 min^{-1}, test gas pulses varied between 5% and 80% of the total flow, with pulse lengths set to 600 seconds. Before any exposure to test gases, sensors were exposed to clean air for 40 minutes to stabilise baseline resistance. Tests were performed at operating temperatures of 250°C, 300°C, 350°C, 400°C and 500°C.

2.3.2. Data Analysis

Once each experiment was completed, raw data was analysed using Microsoft Excel to obtain baseline resistance (R_0) which was calculated as the average resistance in the 2 minutes leading to the first test gas pulse, and R, the resistance at time, t. The magnitude of the response was calculated as the ratio of resistance to baseline resistance (R/R_0), and the reciprocal of that value (R_0/R), dependant on the sensor material and the redox properties of the target analyte (see Table 1.2).

2.4. Analysis of Exhaust Gas

To understand the mechanisms that occur when sensors are exposed to analyte gases, mass spectrometry techniques were used to analyse the exhaust gases following exposure to sensors. A novel experimental set up was built, that incorporated a small glass gas-sensing chamber, attached to a Hiden HPR60 Molecular Beam Mass Spectrometer System (Fig 2.8).

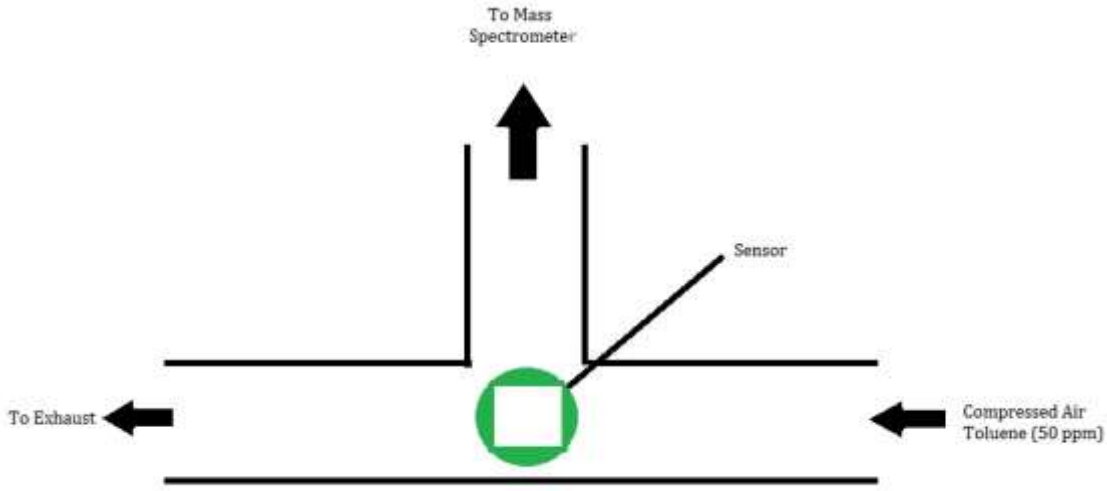

Figure 2.8. Schematic of the sensing chamber used in the analysis of exhaust gas. Air/toluene was supplied to the sensor at a constant flow rate of 1000 cm^3 min^{-1}, following reaction at the sensor, gas flowed out to exhaust where it was safely disposed of through a fume cupboard, while a portion was delivered to the mass spectrometer for analysis of the components of the air matrix.

Initially sensors were exposed to compressed air for a 10-minute exposure to establish equilibrium between adsorbed oxygen at the sensors surface and the atmosphere. Toluene was supplied to at a constant concentration of 50 ppm (balanced by dry compressed air) into the sensing chamber at a flow rate of 1000 cm^3 min^{-1}. Data was recorded following an initial 120-second period to ensure a constant supply of toluene to the sensing chamber.

Peaks were scanned between m/z =0-200 to detect breakdown of products as well as the formation of adduct species that may have larger masses than the proposed analyte. A total of 15 scans were recorded over a 10-minute period. Following each gas pulse,

the sensing chamber and all gas lines were cleaned with a 15-minute purge of compressed air. The sensors used in this study (ZSM5 and mordenite modified ZnO sensors) had an operating temperature of 500°C and 400°C.

The results of this, and of other tests conducted on the sensor materials will be discussed over the following chapters. The next chapter will discuss the modification of zinc oxide with zeolites; devices have been fabricated as discussed in section 2.2 and tested against five gases.

3. Zeolite Modification of Zinc Oxide

This chapter details the modification of zinc oxide with zeolite beta, Y, mordenite and ZSM5. The sensors have been fabricated and tested against five gases commonly found at clandestine locations.

3.1. Introduction

Zinc oxide is a compound semiconductor with a band gap of 3.4 eV at room temperature[149]. An n-type material, it is used in a wide variety of applications including gas sensors, UV resistive coatings, surface acoustic wave (SAW) devices, and filters[150]. Zinc oxide crystals are composed of alternating layers of zinc and oxygen atoms in a wurtzite hexagonal close packed structure. In this structure, oxygen ions are arranged in a hexagonal close packing arrangement, with zinc ions occupying half the tetrahedral interstitial portions, with the same hexagonally close packed arrangement (Fig. 3.1).

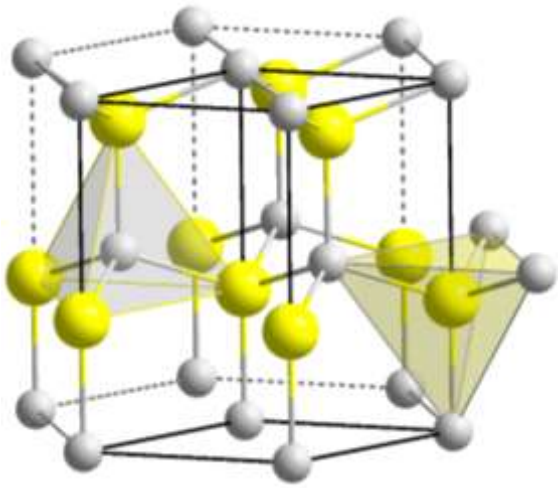

Figure 3.1. Wurtzite structure demonstrating the hexagonally close packed arrangement of ZnO, showing oxygen ions as white spheres, and zinc ions as yellow spheres[151].

Zinc oxide materials have been widely used as dielectric ceramic, pigment, catalyst and sensing material[152], due to the high chemical stability, low dielectric constant, large electromechanical coupling coefficient and high luminous transmittance of the substance.

The gas sensing properties of zinc oxide were first demonstrated in 1962 by Seiyama *et.al.*[153] and zinc oxide has since been found to be a versatile gas sensing material that has been used in sensor devices to detect carbon monoxide[154,155], hydrogen[156,157], nitrogen oxides[158,159], hydrocarbons[160,161], alcohols[162,163,164], ammonia[165,166,167] and disulphides[168]. The working temperature of ZnO gas sensors is generally quite high, around 400°C-500°C, and selectivity is generally poor. As a result of this, preparation methods and doping of ZnO gas sensors to reduce operating temperature and increase selectivity are major research topics[169,170].

3.2. Characterisation

3.2.1. Physical Appearance and Stability

Zinc oxide based sensors had an off-white colour both before and after calcination at 600°C. Sensors retained their composition in air after repeated heating over many months. Mild shock or impact pressure lead to crumbling, scarring and de-adhesion of the sensing element.

3.2.2. Surface Area Measurements

Surface area measurements of sensor materials were obtained using a Micromeritics TriStar II surface area analyser. The results obtained (Table 3.1) show large enhancements in all zeolite modified sensor materials. The largest surface area observed was found in zeolite beta modified ZnO. This large enhancement is a result of the inclusion of highly porous zeolite material, which, in addition to having a large surface area itself, is thought to open the microstructure, increasing pore size in the material.

Table 3.0.1. Surface area of ZnO and zeolite beta, Y, mordenite and ZSM5 modified ZnO.

Material	Surface Area ($m^2 g^{-1}$)
ZnO	3.3
ZnO/B	188.6
ZnO/Y	150.2
ZnO/MOR	103.3
ZnO/ZSM5	130.5

3.2.3. Scanning Electron Microscopy

Scanning electron micrographs were collected using a Jeol JSM-6301F microscope, in secondary electron imaging mode, using a 5 keV probe voltage. Images were recorded with SemAfore software.

The images (Fig. 3.2) show the porous nature of sensor materials and admixtures. The unmodified ZnO sensors microstructure demonstrates smooth circular platelets ranging in size from around 300 nm to 500 nm. The appearance of ZnO and zeolite beta admixture shows large “clumps” of ZnO, coated in angular grains of zeolite beta that vary in size between 0.1 and 0.4 μM at higher magnification, it is possible to see high surface area of small grains, around 100 nm in diameter. Zeolite Y and ZnO admixtures are again porous in nature, exhibiting a cavernous appearance, with grains of around 0.5 μM. At closer magnification, platelet like grains are visible, approximately 400 nm in diameter. The cavernous nature of gas sensors is most visible in a mordenite and ZnO admixture, the material made up of smooth non-uniform grains with an average size of around 600 nm.

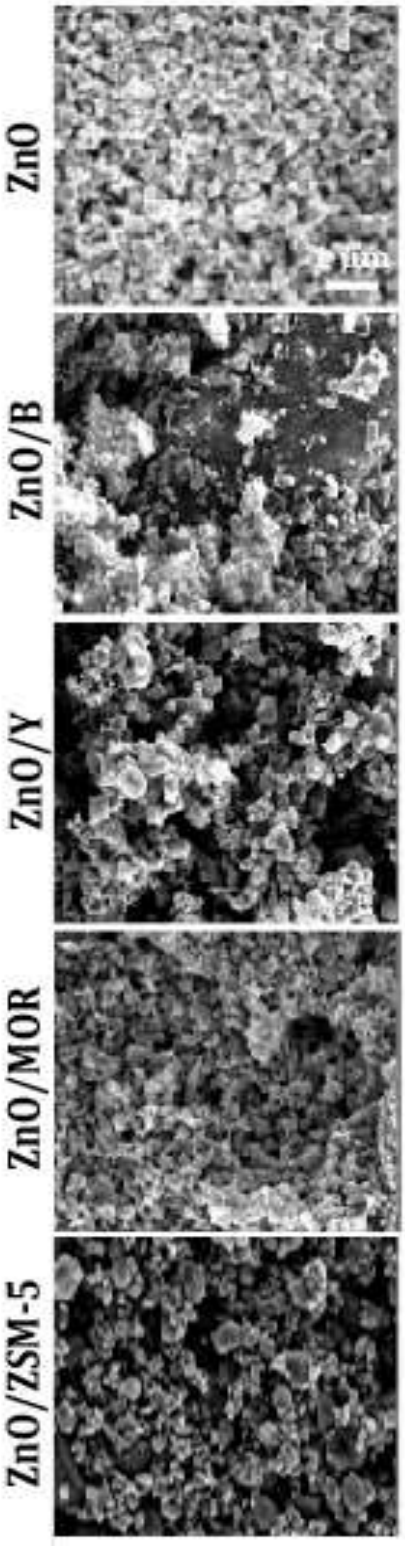

Figure 3.2. SEM images of ZnO and zeolite beta, Y, Mordenite and ZSM5 modified ZnO at a magnification of 10,000x.

3.2.4. X-Ray Diffraction

X-ray diffraction patterns were collected over the 2θ range 10° to 65°, step size 0.02°, on a Brucker GADDS D8 diffractometer using Cu Kα radiation (λ = 0.15418 nm). Diffraction patterns can be viewed in Fig. 3.3 and confirm the chemical make-up of the metal oxide and zeolite admixtures. All zinc oxide based materials show a wurzite single-phase structure with high crystallinity, which can be matched with the Joint committee on powder diffraction standard (JCPDS card no. 36-1451). With strong peaks at 2θ = 31.37°, 34.03°, 35.86°, 47.16°, 56.26° and 62.54°.

Diffraction patterns showing zeolite admixtures displayed characteristic peaks of each zeolite, however the intensity of these peaks is much smaller in magnitude than peaks relating to the ZnO structure. Additional phases in the modified sensor materials can lead to different gas responses in the sensor. The additional phases are likely due to agglomerated zeolite material, distributed throughout the sensor bulk.

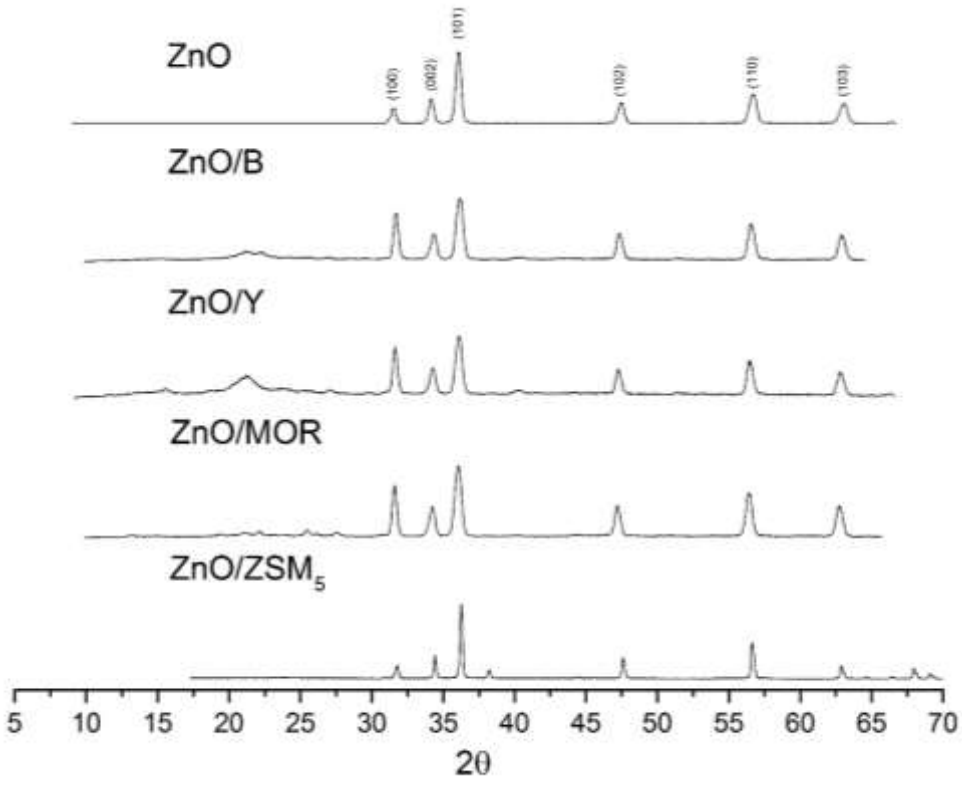

Figure 3.3. Diffraction patterns for all ZnO and zeolite admixed sensors, collected between 10° and 65°. The y-axis is normalised and offset for each spectrum.

3.2.5. Energy Dispersive X-Ray Spectroscopy

The atomic (Table. 3.2) and weight (Table. 3.3) percentages of ZnO and all zeolite modified sensors show similar zinc concentrations in all zeolite modified sensors; the introduction of zeolite raises the atomic percentages of aluminium, silicon and oxygen. The weight percentage of oxygen increases in zeolite-modified sensors, due to the large oxygen component of the zeolite.

Table 3.0.2. Atomic percentages of zeolite modified and unmodified zinc oxide sensors.

	Atomic Percentage (%)			
	Zn	**O**	**Al**	**Si**
ZnO	50	50	0	0
ZnO/B	36.4	54.1	0.5	9.0
ZnO/Y	37.2	51	2.9	8.9
ZnO/MOR	38.1	54.13	0.57	7.2
ZnO/ZSM5	37.2	48.7	0.4	13.7

Table 3.0.3. Weight percentages of zeolite modified and unmodified zinc oxide sensors.

	Weight Percentage (%)			
	Zn	**O**	**Al**	**Si**
ZnO	78.3	21.7	0	0
ZnO/B	33.3	42.6	1.2	21.9
ZnO/Y	32.4	44.2	6.0	17.4
ZnO/MOR	32.9	56.2	1.7	18.2
ZnO/ZSM5	32.6	45.1	0.3	22.0

3.2.6. Capacitance Measurements

Capacitance values of sensor materials (Table 3.4) were measured at operating temperatures of 500°C, 400°C and 300°C using a Keithly multimeter.

Table 3.0.4. Capacitance of ZnO and zeolite beta, Y, Mordenite and ZSM5 modified ZnO sensors at room temperature (~25°C), 350°C, 400°C and 500°C.

		Capacitance ($\mu F/m^2$)		
	RT	**350°C**	**400°C**	**500°C**
ZnO	65	10	15	1
ZnO/B	93	87.5	95	8
ZnO/Y	74	78.25	102.5	1
ZnO/MOR	91.2	175	460	10
ZnO/ZSM5	90.0	65	100	6

Capacitance is higher in all zeolite modified sensors than the unmodified ZnO sensor; this implies that more charge can be stored in the zeolite modified sensors than an unmodified ZnO sensor. The largest capacitance is observed in Mordenite modified ZnO.

3.3 Results

3.3.1. Baseline Resistance

Table 3.0.5. Baseline resistances of zeolite beta, Y, mordenite and ZSM5 modified and unmodified zinc oxide sensors.

	Resistance (Ω)		
	350°C	**400°C**	**500°C**
ZnO	8.6×10^5	4.2×10^5	7.2×10^4
ZnO/B	3.2×10^5	2.5×10^5	1.3×10^5
ZnO/Y	2.9×10^7	3.9×10^6	5.6×10^5
ZnO/MOR	1.3×10^6	1.0×10^6	3.7×10^5
ZnO/ZSM5	7.4×10^6	4.3×10^6	1.3×10^6

The baseline resistance of all sensors in dry air (Table. 3.5) show the resistance in zeolite-modified sensors is larger than the unmodified material. This is because the zeolite material acts as an insulator, inhibiting electron movement through the material. As temperature increases, the resistance in all sensors decreases, this is because as temperature increases, more electrons from the valence band acquire energy and jump to the conduction band and act as charge carriers.

3.3.2. Response to Ethanol

Zinc oxide and zeolite modified zinc oxide sensors were exposed to 5, 10, 20, 40 and 80 ppm ethanol. Tests were performed at operating temperatures of 350°C, 400°C and 500°C. Responses at 500°C (Fig. 3.4) show large enhancements in response for three of the four modified sensors (zeolite beta, Y and mordenite modified ZnO). The ZSM5 modified ZnO sensor reaches its maximum response considerably quicker than all other sensors. The ZSM5 modified sensor also reaches equilibrium on exposure to all concentrations of ethanol, unlike all the other sensors that do not reach a steady state in the 600-second gas pulse.

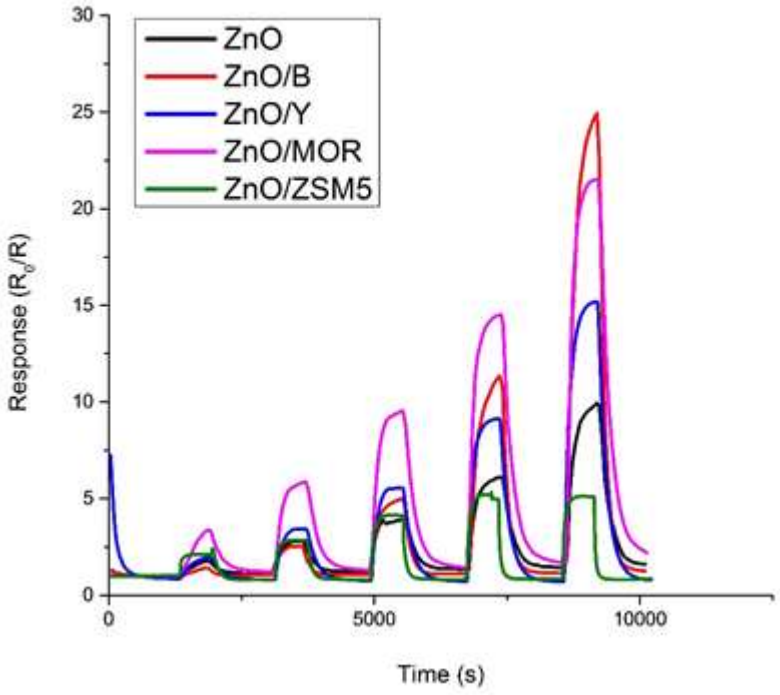

Figure 3.4. Response of ZnO and zeolite beta, Y, mordenite and ZSM5 modified ZnO sensors to 5, 10, 20, 40 and 80 ppm ethanol at an operating temperature of 500°C. Response is calculated as a function of baseline resistance R_0 that is, the sensor resistance in dry air.

The responses of all ZnO and zeolite modified ZnO sensors to ethanol at an operating temperature of 400°C (Fig. 3.5) shows a larger magnitude of response to unmodified ZnO than any of the zeolite modified ZnO sensors to concentrations of 80 ppm. Mordenite and zeolite Y show the smallest magnitude of response to ethanol at this operating temperature. Only ZSM5 modified ZnO reaches a steady state within the 600-second gas pulse. The recovery of zeolite beta modified ZnO is considerably slower than other zeolite modified ZnO sensors. Ethanol molecules may undergo acid catalysed dehydration to ethane molecules in the presence of zeolites, leading to a reduction in response in zeolite modified sensors.

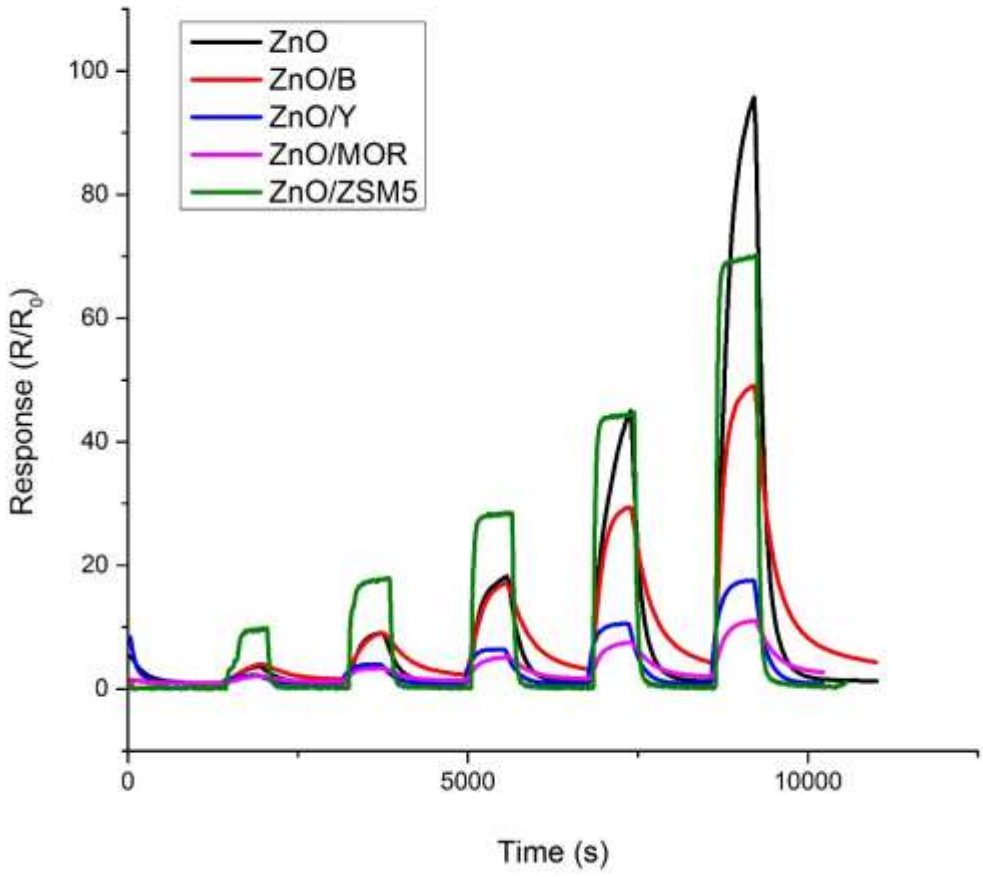

Figure 3.5. Response of ZnO and zeolite beta, Y, Mordenite and ZSM5 modified ZnO sensors to 5, 10, 20, 40 and 80 ppm ethanol at an operating temperature of 400°C. Response is calculated as a function of baseline resistance R_0 that is, the sensor resistance in dry air.

At an operating temperature of 350°C (Fig 3.6), ZSM5 modified ZnO demonstrates a magnitude of response considerably larger than other zeolite modified sensors, with a response of R_0/R= 57.6 to 80 ppm, during this time the ZSM5 modified sensor reaches equilibrium with the atmosphere. Following exposure to all gas pulses zeolite beta modified ZnO shows poor recovery back to the baseline resistance. This poor recovery in zeolite beta modified ZnO is observed at all operating temperatures. This slower recovery may be attributed to stronger adsorption at zeolite beta than other zeolites, increasing the concentration of ethanol close to the sensor surface and slowing the recovery during an air pulse.

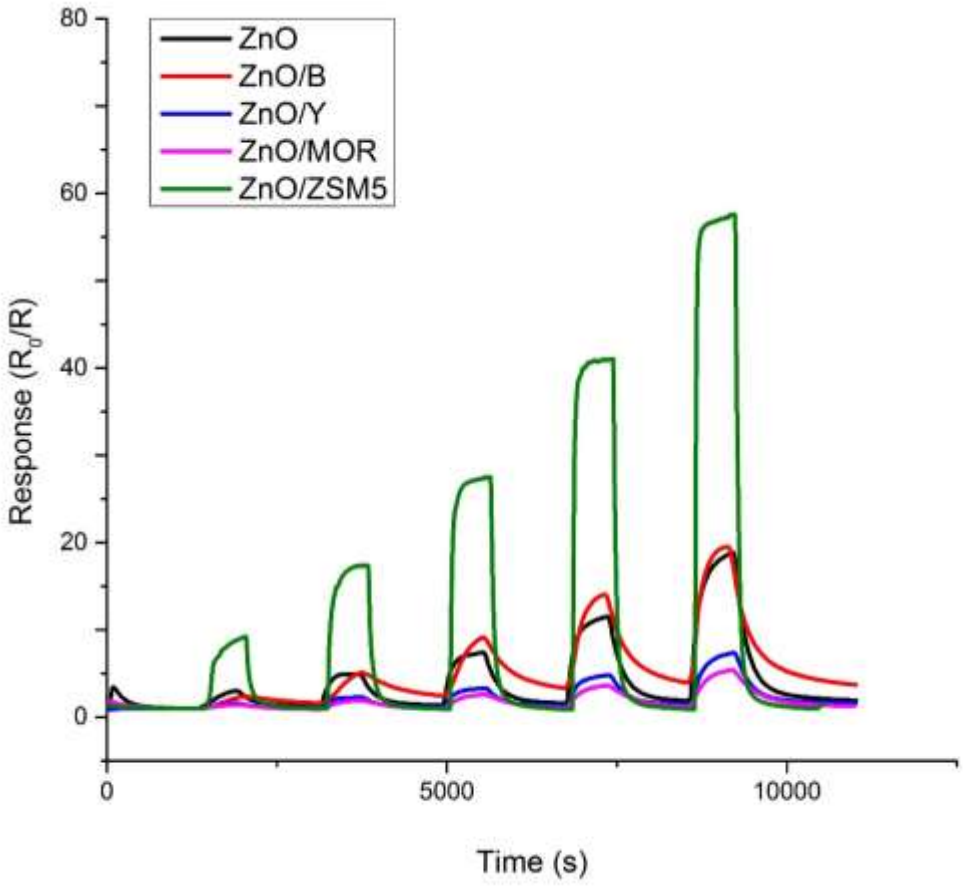

Figure 3.6. Response of ZnO and zeolite beta, Y, Mordenite and ZSM5 modified ZnO sensors to 5, 10, 20, 40 and 80 ppm ethanol at an operating temperature of 350°C. Response is calculated as a function of baseline resistance R_0 that is, the sensor resistance in dry air.

The maximum response to ethanol pulses at 350°C, 400°C and 500°C (Fig. 3.7) shows all sensors demonstrating their largest responses at 400°C. Unmodified ZnO displays the largest response at 400°C (R_0/R = 95.7 to 80 ppm ethanol). ZSM5 modified ZnO also display strong responses to ethanol, with responses to 80 ppm of R_0/R = 68.3 and R_0/R = 57.6 at 400°C and 350°C respectively. A number of authors report the dehydration of ethanol over H-ZSM5[171,172,173], this dehydration leads to a number of other species, most commonly ethane and water. However, the formation of oxonium and carbenium ions has also been reported[174], these positively charged ions have the potential to react with negatively charged oxygen ions at the sensor surface and lead to a larger magnitude of response in the sensor than ethanol or other molecules.

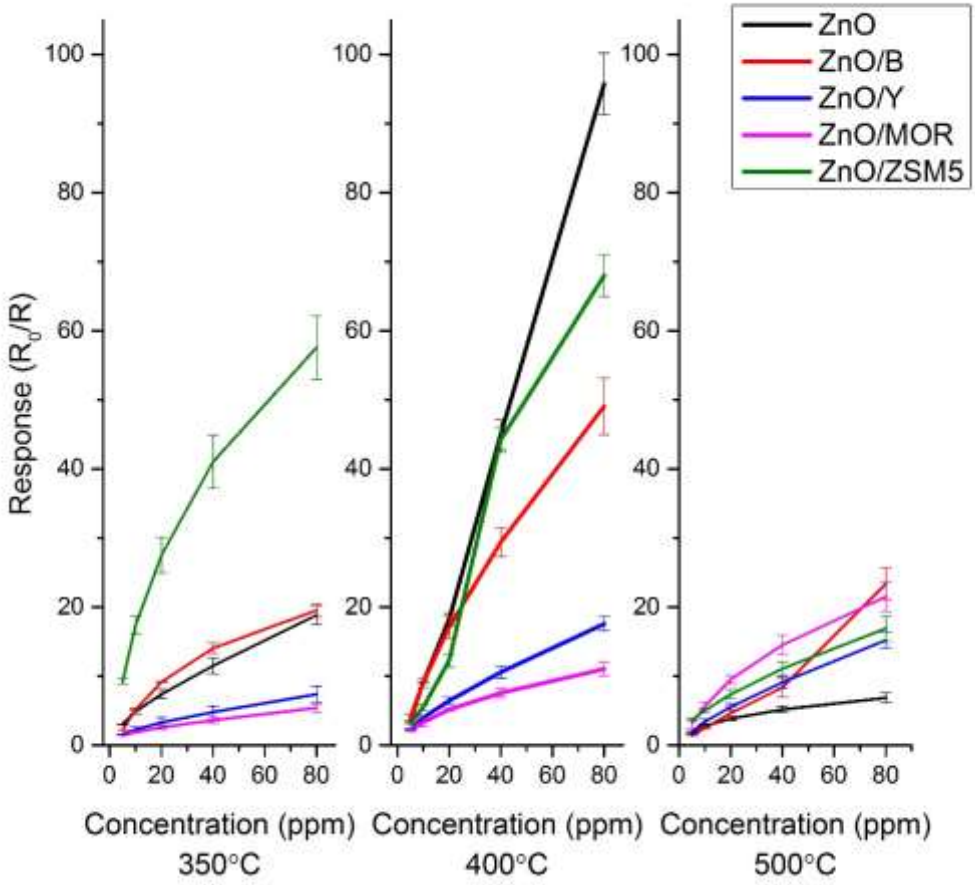

Figure 3.7. Response (± 1 S.D.) of ZnO based sensors (unmodified ZnO and zeolite beta, Y, mordenite and ZSM5 admixtures) to concentrations of 5-80 ppm ethanol at temperatures of 350°C, 400°C, 500°C. Response is calculated as a function of baseline resistance R_0 that is, the sensor resistance in dry air.

The response time (T_{res}), the time taken to reach 90% of the maximum response was calculated for an 80 ppm pulse of ethanol (Table 3.6) and show that the response time of ZSM5 modified ZnO is considerably shorter than that of other sensors. The H-ZSM5 zeolite has previously demonstrated strong uptake of ethanol[175], leading to a dehydration reaction to produce ethane and water which this is likely to be the reason for the much shorter response time observed here. As operating temperature increases, the response time for each sensor decreases. This decrease in response time with increasing temperature is likely to be a result of a faster rate of reaction at the sensor surface, resulting in electrons being liberated from the adsorbed oxygen bond to the sensor surface more quickly.

Table 3.0.6. Response times for ZnO and zeolite beta, Y, mordenite and ZSM5 modified ZnO on exposure to 80 ppm ethanol at an operating temperature of 350°C, 400°C and 500°C.

	Response time (s, ±5)		
Sensor	**350°C**	**400°C**	**500°C**
ZnO	300	510	350
ZnO/B	450	450	360
ZnO/Y	400	350	250
ZnO/MOR	530	430	420
ZnO/ZSM5	50	40	20

To test the repeatability of all ZnO sensors, materials were exposed to 3 pulses of 80 ppm ethanol at 400°C. These tests were repeated 1 week, 2 weeks, 4 weeks, 8 weeks and 12 weeks after the first test. The average response of these tests (Fig. 3.8) shows good repeatability over the 12-week period. The relative standard deviation of each sensor (Table 3.7) shows that all sensor responses vary by less than 7% over this period, indicating good precision on exposure to ethanol.

There are some minor fluctuations in the response and these can be attributed to two factors, the experiment spans three months and the changing season can have an impact on the sensor performance, varying humidity, temperature and UV intensity can all influence the surface properties[176]. The storage conditions of the sensor can also have an impact on its performance, particulate matter such as dust, pollen and soot can cause damage to the sensor surface and result in a change in sensor performance.

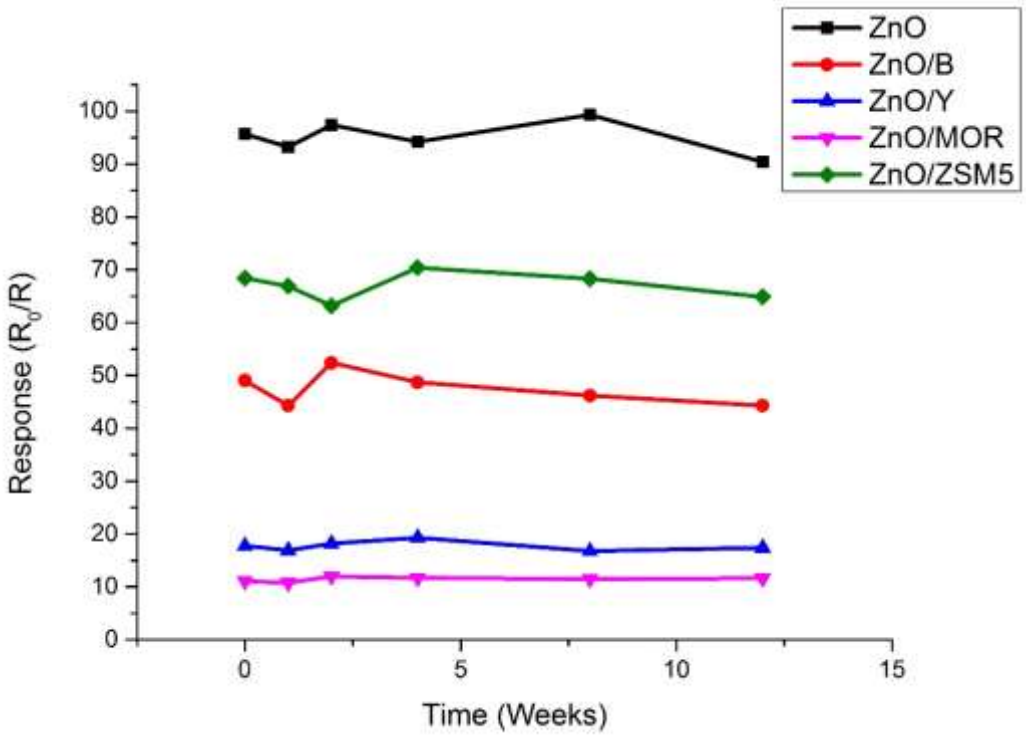

Figure 3.8. Response of ZnO based sensors (unmodified ZnO and zeolite beta, Y, mordenite and ZSM5 admixtures) to 80 ppm ethanol at an operating temperature of 400°C over a 12 week period.

Table 3.0.7. Relative standard deviation of response for ZnO and zeolite beta, Y, mordenite and ZSM5 modified ZnO on exposure to 80-ppm ethanol over a 12-week period (n=6).

Sensor	**%RSD**
ZnO	3.0
ZnO/B	6.1
ZnO/Y	4.8
ZnO/MOR	3.6
ZnO/ZSM5	3.6

3.3.3. Response to Nitrogen Dioxide

Unmodified ZnO and zeolite beta, Y, mordenite and ZSM5 modified ZnO sensors were exposed to 50, 100, 200, 400 and 800 ppb of nitrogen dioxide at operating temperatures

of 350°C, 400°C and 500°C. Responses at 500°C (Fig. 3.9) show large enhancements in zeolite modified sensors, when compared to the unmodified ZnO material. The largest enhancement at 500°C is observed with ZnO/Y, with a response R/R_0= 33.1, compared with the unmodified ZnO response of R/R_0= 2.75, to 800 ppb. Zeolite beta also has a significantly larger response to 800 ppb, with R/R_0=20.6.

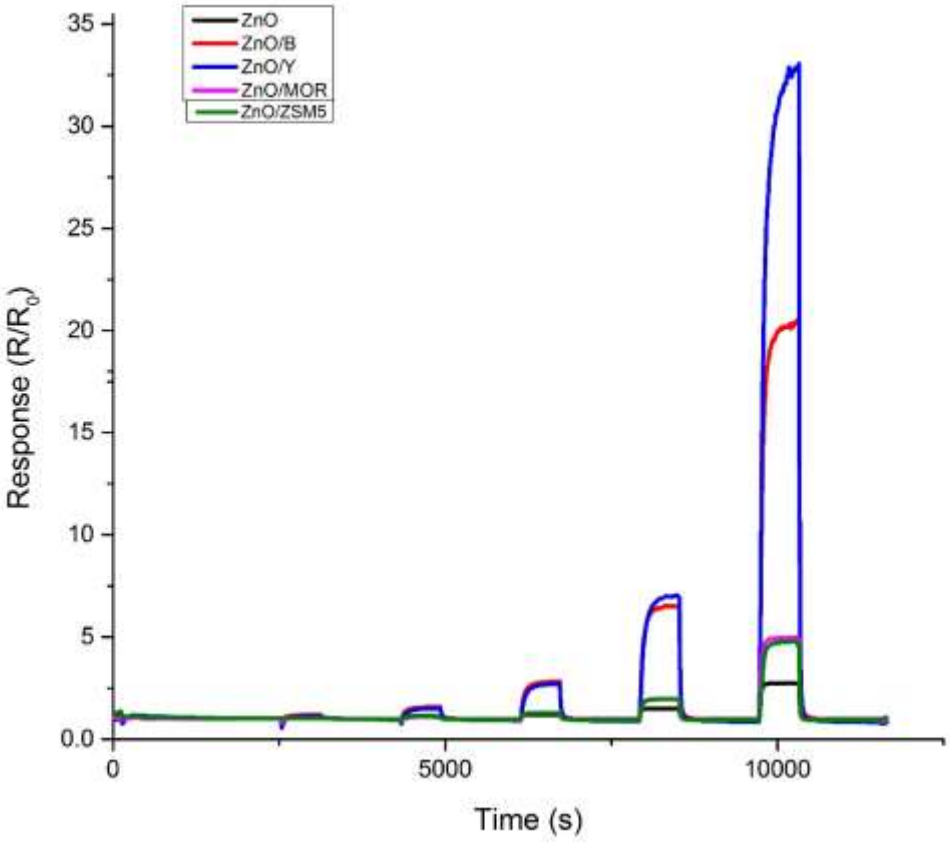

Figure 3.9. Response of ZnO and zeolite beta, Y, mordenite and ZSM5 modified ZnO sensors to 50, 100, 200, 400 and 800 ppb nitrogen dioxide at an operating temperature of 500°C. Response is calculated as a function of baseline resistance R_0 that is, the sensor resistance in dry air.

The responses of ZnO and zeolite modified ZnO sensors to nitrogen dioxide at an operating temperature of 400°C (Fig 3.10) demonstrate significantly larger magnitudes of response in zeolite Y modified ZnO than all other materials. The response of ZSM5 modified ZnO is found to be noisy on exposure to 800 ppb nitrogen dioxide, thought to be due to inconsistent adsorption/desorption at the sensor surface during the gas pulse.

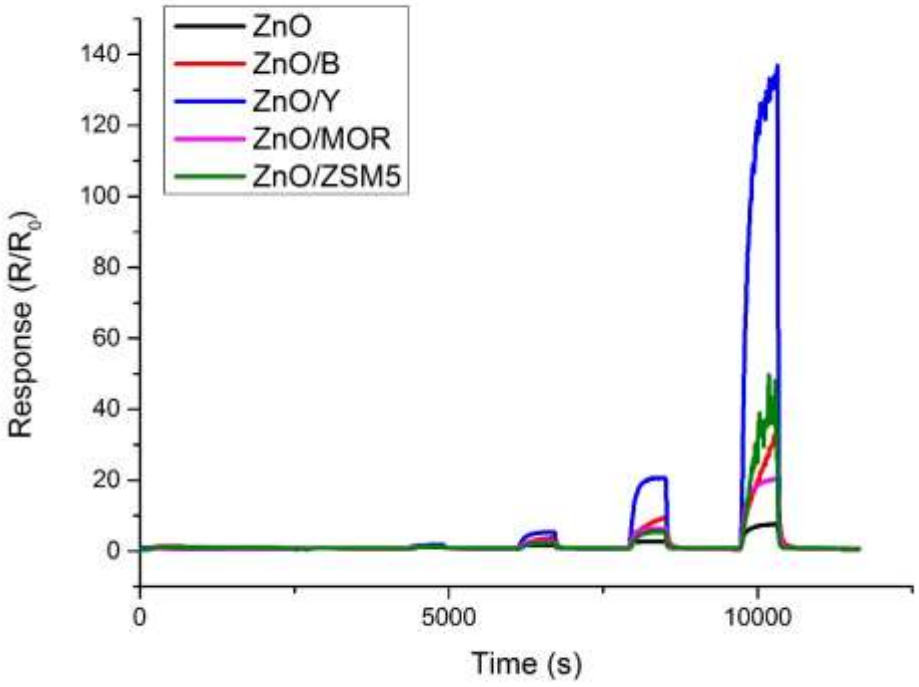

Figure 3.10. Response of ZnO and zeolite beta, Y, mordenite and ZSM5 modified ZnO sensors to 50, 100, 200, 400 and 800 ppb nitrogen dioxide at an operating temperature of 400°C. Response is calculated as a function of baseline resistance R_0 that is, the sensor resistance in dry air.

At an operating temperature of 350°C (Fig 3.11), mordenite modified ZnO demonstrates a maximum response of R/R_0 = 142.7 to 800 ppb nitrogen dioxide, this is the largest response observed on exposure to nitrogen dioxide. The smallest magnitude of response was observed with ZnO, which gave a noisy response that did not give a suitable or stable response during any gas pulse. None of the sensors, at an operating temperature of 350°C, achieved a steady state response during any 600-second nitrogen dioxide pulse.

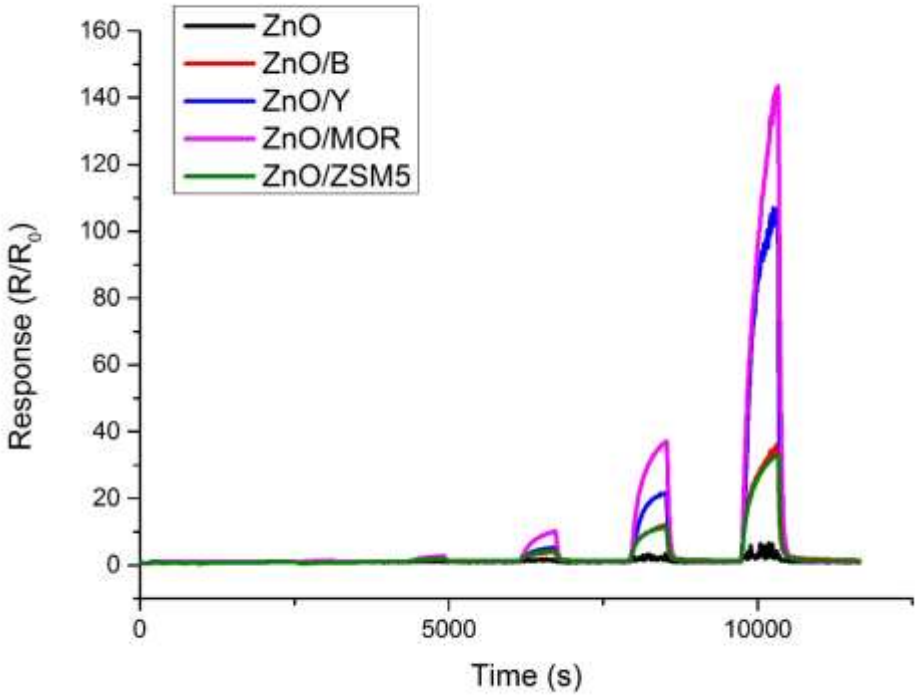

Figure 3.11. Response of ZnO and zeolite beta, Y, mordenite and ZSM5 modified ZnO sensors to 50, 100, 200, 400 and 800 ppb nitrogen dioxide at an operating temperature of 350°C. Response is calculated as a function of baseline resistance R_0 that is, the sensor resistance in dry air.

The responses to 50 ppb and 100 ppb nitrogen dioxide (Fig. 3.12) show an unexpected response at all temperatures. Initially, on the introduction of 50 ppb NO_2 the resistance in the materials decreases, in the case of zeolite Y modified ZnO, to half its baseline resistance, before it begins to increase, in the expected way, this occurs to a lesser extent on the introduction of 100 ppb. On the introduction of 200 ppb, the expected increase in resistance occurs, with no initial decrease. This is most likely due to some reducing gas caught in the gas-sensing rig, despite thorough cleaning of the system between experiments.

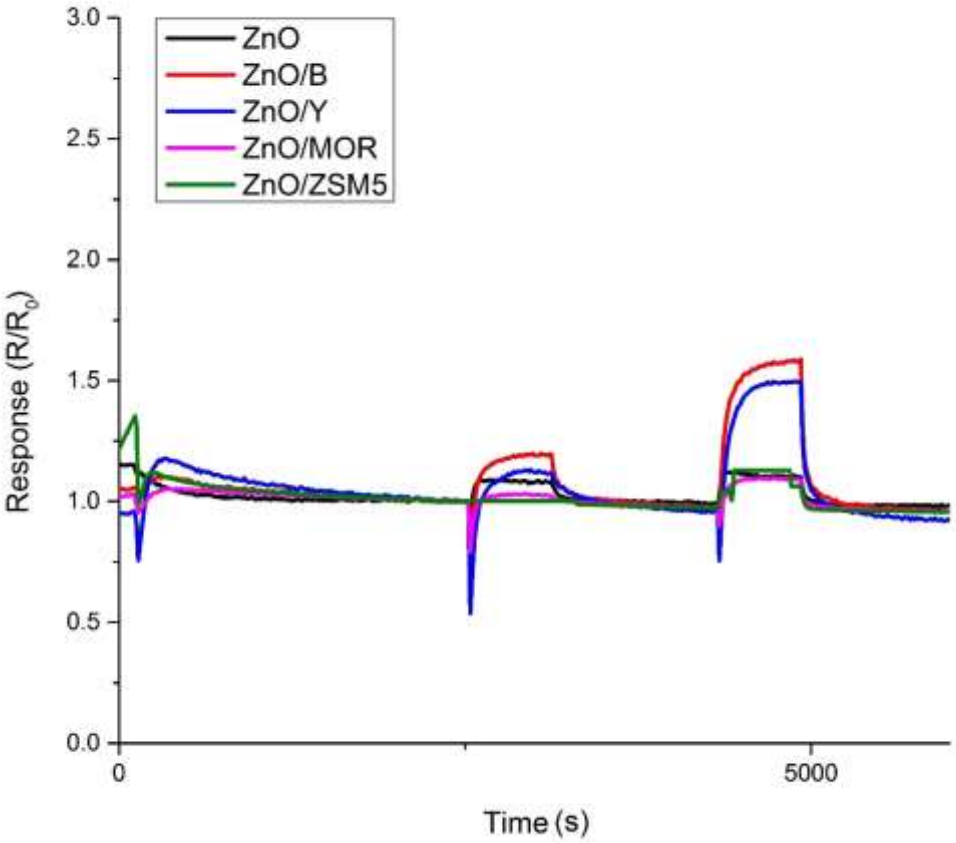

Figure 3.12. Response of unmodified ZnO and zeolite beta, Y, mordenite and ZSM5 to 50 and 100 ppb nitrogen dioxide at an operating temperature of 500°C. Response is calculated as a function of baseline resistance R_0 that is, the sensor resistance in dry air.

Response of ZnO and zeolite modified ZnO sensors to all concentrations of nitrogen dioxide at operating temperatures of 350°C, 400°C and 500°C (Fig. 3.13) show large enhancements in responsiveness of the zeolite modified sensors, compared with the unmodified ZnO. Zeolite Y shows the largest magnitude of response at 500°C and 400°C, with the largest response of R/R_0= 134.0. At an operating temperature of 350°C, Mordenite modified ZnO shows the largest magnitude of response, with R/R_0 = 142.7 to 800 ppb. The response of Mordenite modified ZnO increases dramatically at 350°C, when compared to the responses at 400°C and 500°C. Zeolite beta and ZSM5 modified ZnO show similar responses at 350°C and 400°C, which are larger in magnitude than those observed at 500°C.

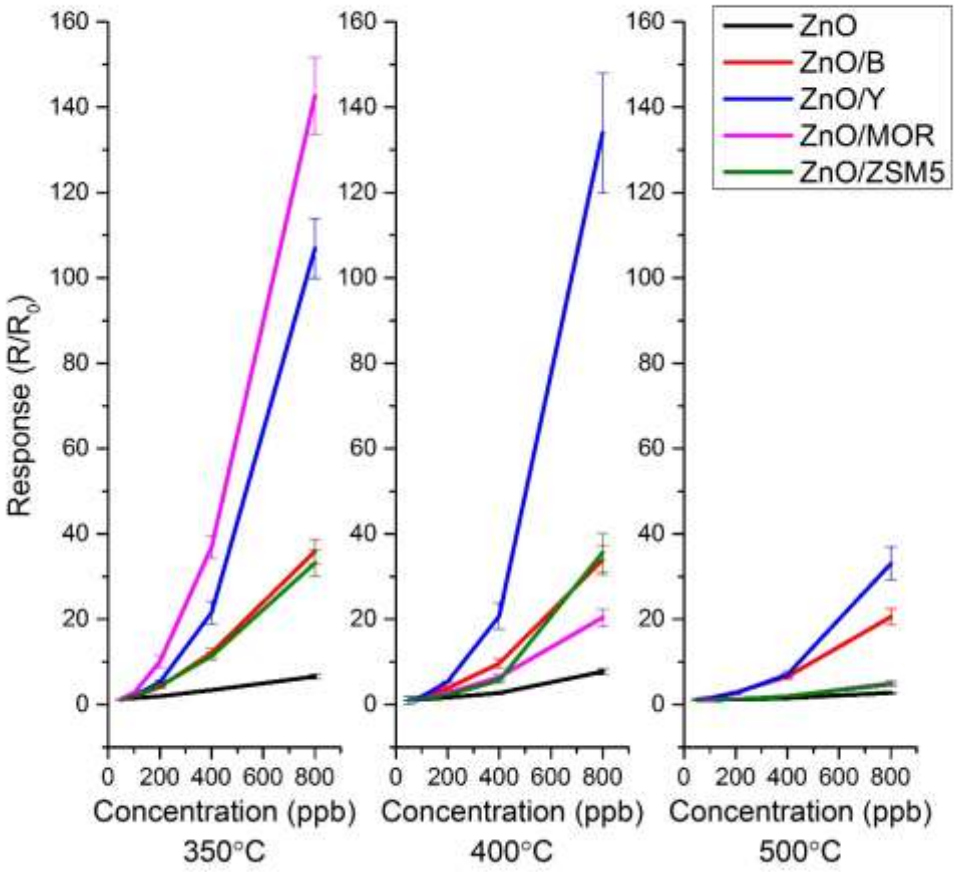

Figure 3.13. Response of ZnO and zeolite beta, Y, Mordenite and ZSM5 modified ZnO to concentrations of 50-800 ppb nitrogen dioxide, at operating temperatures of 350°C, 400°C and 500°C. Response is calculated as a function of baseline resistance R_0 that is, the sensor resistance in dry air.

The considerably large response observed in the mordenite modified zinc oxide senor can be attributed to the one-dimensional pore structure of mordenite. Other zeolites used in this study possess three-dimensional pore structures, leading to collisions between analyte species; the one-dimensional mordenite structure means the nitrogen dioxide molecules are only able to travel in one direction, increasing the likelihood of collisions with the gas sensitive surface.

The large responses observed with zeolite Y modified zinc oxide at an operating temperature of 350°C can be attributed to the larger pore size of the zeolite. Zeolites with smaller pore diameters result in a lower rate of nitrogen dioxide molecules diffusing through the zeolite material and reaching the gas sensitive surface.

The response times (T_{res}) on exposure to 800 ppb nitrogen dioxide (Table 3.8) show longer response times in all zeolite modified sensors. The longest response times recorded were found for mordenite and zeolite beta modified ZnO, these response times are dramatically reduced at higher temperatures, however at 350°C, the time taken to reach 90% of the maximum response is more than 7 minutes. All response times decrease with increasing temperature, a result of the greater rate of reaction at higher temperatures, resulting in electrons being removed at a faster rate.

Table 3.0.8. Response times for unmodified ZnO and zeolite beta, Y, mordenite and ZSM5 modified ZnO on exposure to 800 ppb nitrogen dioxide.

	Response time (s ±5)		
Sensor	**350°C**	**400°C**	**500°C**
ZnO	180	160	30
ZnO/B	430	370	90
ZnO/Y	390	280	140
ZnO/MOR	470	240	50
ZnO/ZSM5	190	170	120

3.3.4. Response to Acetone

All zinc oxide and zeolite modified zinc oxide sensors were exposed to 0.5, 1, 2, 4 and 8 ppm acetone at operating temperatures of 350°C, 400°C and 500°C. All sensors show the expected n-type behaviour (a decrease in resistance on contact with acetone molecules). Results of exposure at 500°C (Fig. 3.14) show that at 0.5 ppm, only the ZSM5 modified sensor shows a response (with R_0/R = 2.4). At 500°C, the unmodified ZnO sensor exhibits the largest magnitude of response (R_0/R = 18.0 to 8 ppm). All zeolite-modified sensors reach an equilibrium response within the 600-second pulse. The zeolite Y modified ZnO sensor exhibits a different response on exposure to acetone than to ethanol and nitrogen dioxide. After an initial decrease in resistance, there is a small increase, before the response settles at a value slightly lower than the initial maximum response. This response shape is observed with all sensors on exposure to 1 ppm, as well as with ZSM5 modified ZnO on exposure to 0.5 ppm. This response suggests that

acetone reacts at the zeolite surface, producing a less reactive species (such as ethane, methane or propane) resulting in a reduction in response.

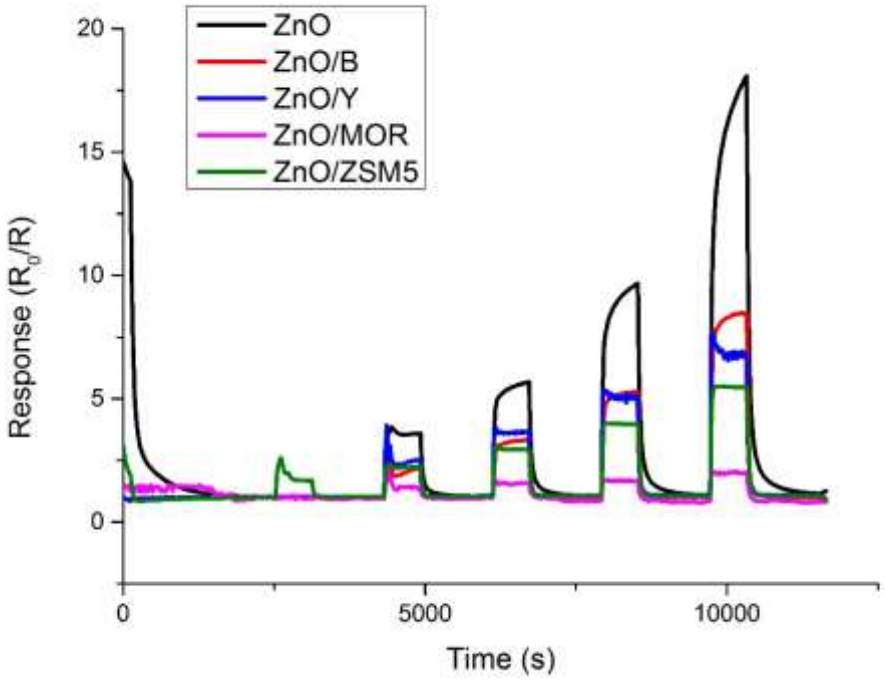

Figure 3.14. Response of ZnO and zeolite beta, Y, mordenite and ZSM5 modified ZnO to concentrations of 0.5, 1, 2, 4 and 8 ppm acetone, at operating temperatures of 500°C. Response is calculated as a function of baseline resistance R_0 that is, the sensor resistance in dry air.

The responses to acetone at an operating temperature of 400°C (Fig 3.15) show that, unlike at an operating temperature of 500°C, all sensors demonstrated a response to 0.5 ppm acetone. At lower acetone concentrations (0.5-2 ppm) the ZSM5 modified sensor is found to be the most responsive, while at higher acetone concentrations (4-8 ppm) zeolite beta modified ZnO is found to be more responsive, with a response of $R_0/R = 35.6$ to 8 ppm of acetone. During the acetone gas pulses all sensors, except for zeolite beta modified ZnO, reach an approximate steady state response. The zeolite beta modified ZnO responses do not plateau at concentrations above 2 ppm.

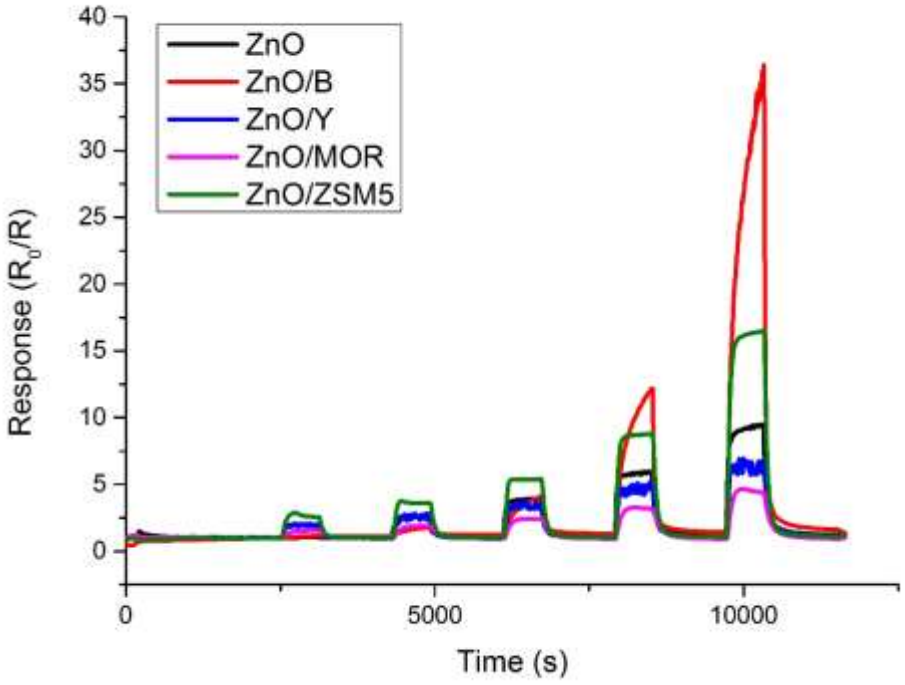

Figure 3.15. Response of ZnO and zeolite beta, Y, mordenite and ZSM5 modified ZnO sensors to 0.5, 1, 2, 4 and 8 ppm acetone at an operating temperature of 400°C. Response is calculated as a function of baseline resistance R_0 that is, the sensor resistance in dry air.

At an operating temperature of 350°C (Fig 3.16) the response of ZnO and zeolite modified ZnO sensors to concentrations of 0.5-8 ppm acetone show large responses of ZSM5 modified ZnO (R_0/R = 41.1 to 8 ppm). All other zeolite modified and unmodified sensors demonstrate considerably poorer responses (R_0/R = 6 - 12). Zeolite modified sensors show poorer recovery than the unmodified ZnO sensor.

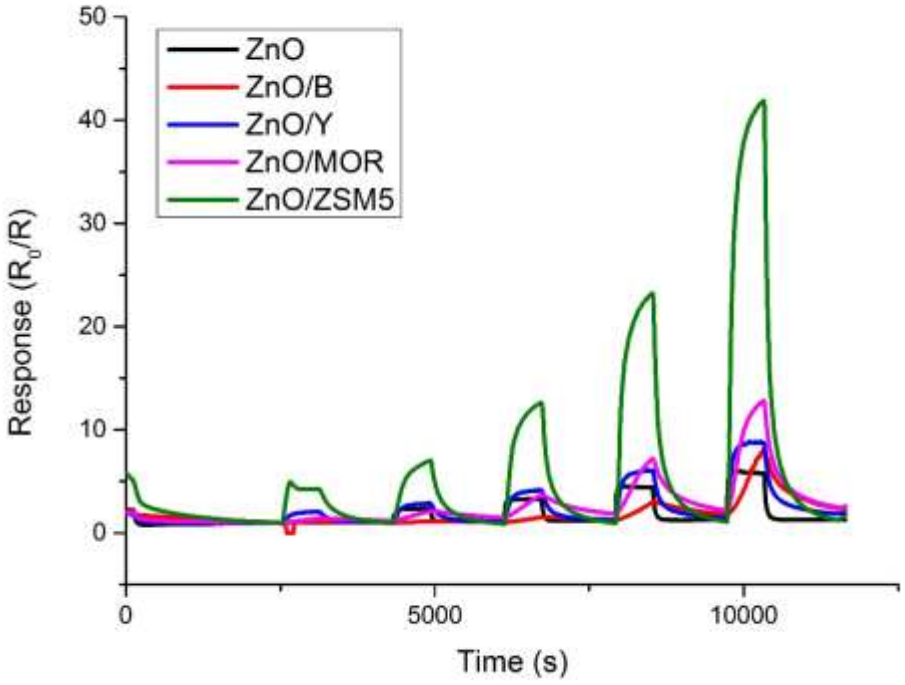

Figure 3.16. Response of ZnO and zeolite beta, Y, mordenite and ZSM5 modified ZnO sensors to 0.5, 1, 2, 4 and 8 ppm acetone at an operating temperature of 350°C. Response is calculated as a function of baseline resistance R_0 that is, the sensor resistance in dry air.

At lower temperatures, 400°C and 350°C (Fig. 3.17) zeolite modified sensors exhibit a larger magnitude of response than the unmodified ZnO sensor. At an operating temperature of 500°C, the unmodified sensor is found to be most responsive, potentially due to dehydration of the acetone at the zeolite surface to alkane or alkene molecules and water, which are less responsive than the acetone molecule. At an operating temperature of 400°C, ZSM5 and zeolite beta modified ZnO demonstrate a larger response than the unmodified ZnO, with responses of R_0/R = 47.8 and R_0/R = 24.1 to 8 ppm respectively. At an operating temperature of 350°C, all sensors display a larger magnitude of response to 8 ppm of acetone. Zeolite beta modified ZnO exhibits a relatively weak response at lower concentrations, and is less responsive than unmodified ZnO at concentrations of 4 ppm and below. At 350°C, ZSM5 modified ZnO exhibits the largest magnitude of response with R_0/R= 41.1 to 8 ppm.

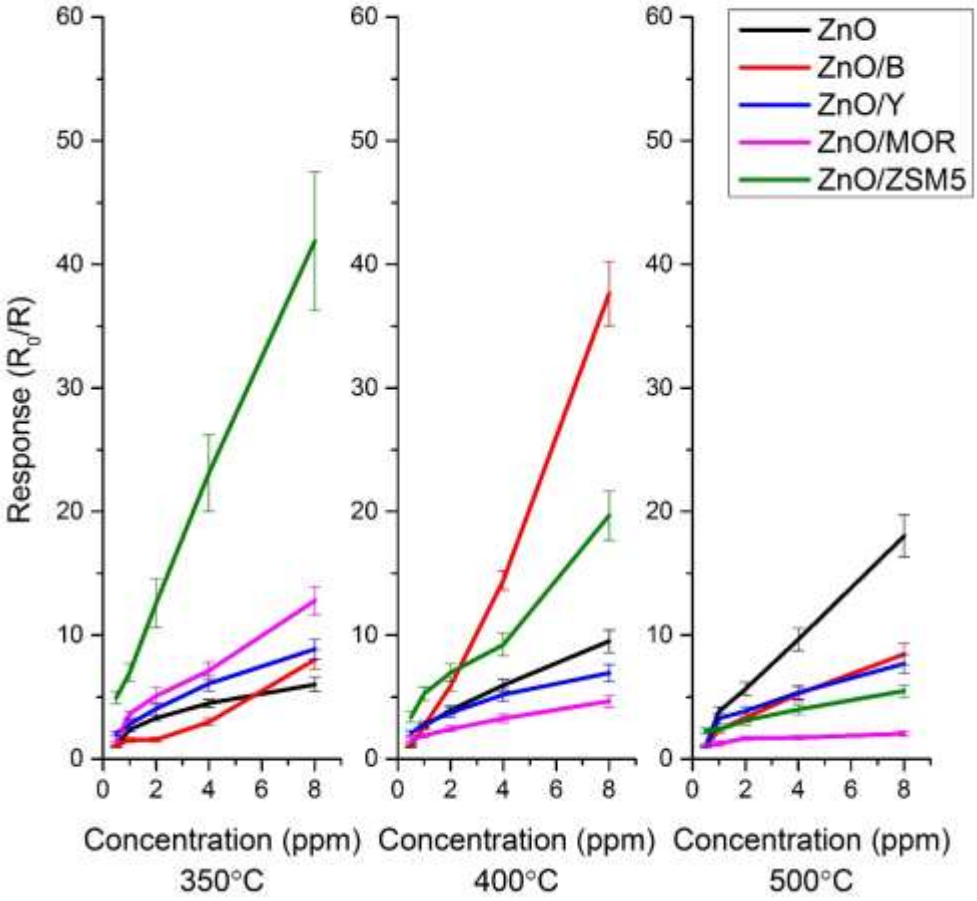

Figure 3.17. Response (± 1 S.D.) of ZnO based sensors (unmodified ZnO and zeolite beta, Y, mordenite and ZSM5 admixtures) to concentrations of 0.5-8 ppm acetone at temperatures of 350°C, 400°C, 500°C. Response is calculated as a function of baseline resistance R_0 that is, the sensor resistance in dry air.

The response times on exposure to 8-ppm acetone (Table 3.9) show large variations in the time taken to reach 90% of the maximum response. As temperature increases from 350°C to 400°C, the response time in all sensors is reduced, by at least 60%, with the largest reduction in mordenite modified ZnO (from 450 s to 80 s). This reduction in response time continues as operating temperature increases from 400°C to 500°C.

Table 3.0.9. Response times for unmodified ZnO and zeolite beta, Y, mordenite and ZSM5 modified ZnO on exposure to 40-ppm toluene.

	Response time (s, ±5)		
Sensor	**350°C**	**400°C**	**500°C**
ZnO	290	100	40
ZnO/B	480	120	60
ZnO/Y	100	90	30
ZnO/MOR	450	80	30
ZnO/ZSM5	110	100	40

3.3.5. Response to Toluene

All ZnO based sensors were exposed to 2.5, 5, 10, 20 and 40 ppm toluene at operating temperatures of 350°C, 400°C and 500°C. The responses to these concentrations at 500°C (Fig 3.18) show a fast response and recovery to every pulse of toluene in all sensors except for ZSM5 modified zinc oxide. While the ZSM5 modified ZnO sensor demonstrates the largest magnitude of response ($R_0/R = 64.2$) the sensor exhibits a noisy response and undergoes long response and recovery times. These long response and recovery times may be attributed to reactions occurring at the zeolite surface, producing multiple chemical species that go on to react at the zeolite surface.

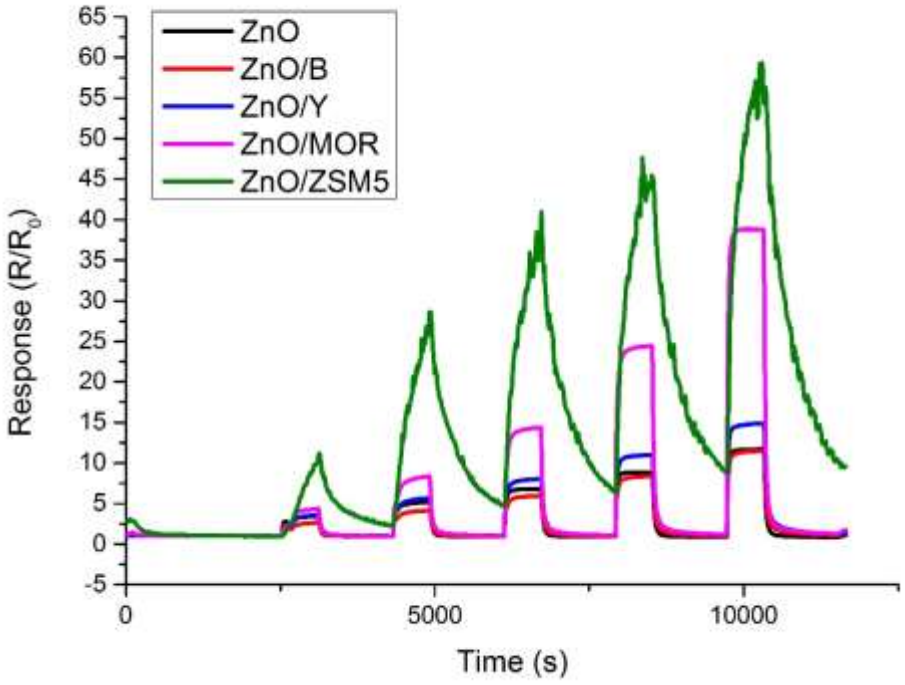

Figure 3.18. Response of ZnO and zeolite beta, Y, mordenite and ZSM5 modified ZnO sensors to 2.5, 5, 10, 20 and 40 ppm toluene at an operating temperature of 500°C. Response is calculated as a function of baseline resistance R_0 that is, the sensor resistance in dry air.

The responses to toluene exposure at an operating temperature of 400°C (Fig. 3.19) demonstrates that ZSM5, Mordenite and zeolite Y modified ZnO show enhancements in the responsiveness to toluene when compared to the unmodified ZnO. The Mordenite modified ZnO sensor shows a response indicative of zeolite activity when exposed to 10, 20 and 40 ppm toluene. The response to these concentrations reaches a maximum before declining, during the gas pulse and then returning to the baseline resistance on exposure to air. All other sensors undergo the expected response with toluene exposure. The ZSM5 modified ZnO sensor shows the largest magnitude of response, with R_0/R = 60.2 to 40 ppm of toluene.

The peak shape of mordenite modified ZnO suggests that the toluene molecules undergo a change at the zeolite surface. At higher concentrations (10, 20, 40 ppm) an initial increase at the beginning of the pulse is followed by a decrease in response. This

is potentially due to toluene being catalytically converted to alkane or alkene molecules or other materials that are less responsive at the zinc oxide surface.

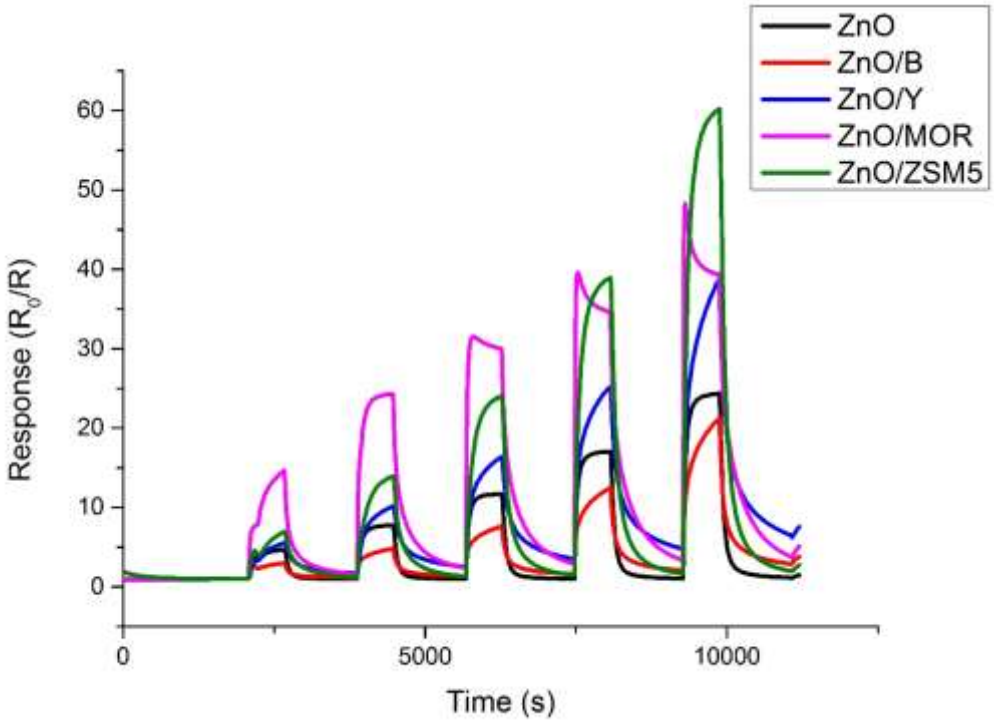

Figure 3.19. Response of ZnO and zeolite beta, Y, mordenite and ZSM5 modified ZnO sensors to 2.5, 5, 10, 20 and 40 ppm toluene at an operating temperature of 400°C. Response is calculated as a function of baseline resistance R_0 that is, the sensor resistance in dry air.

On exposure to toluene at an operating temperature of 350°C (Fig 3.20) ZnO and zeolite modified sensors demonstrate responses that are smaller in magnitude than at other operating temperatures. The ZSM5 modified sensor again shows the largest response (R_0/R =34.2 to 40 ppm of toluene). The mordenite modified sensor once again shows a similar response to that observed at an operating temperature of 400°C (Fig 3.19), likely due to zeolite catalysed reactions within the sensor material. Zeolite modified sensors show slower recovery that that observed in the unmodified ZnO sample, with no sensor recovering fully after the final gas pulse of 8 ppm.

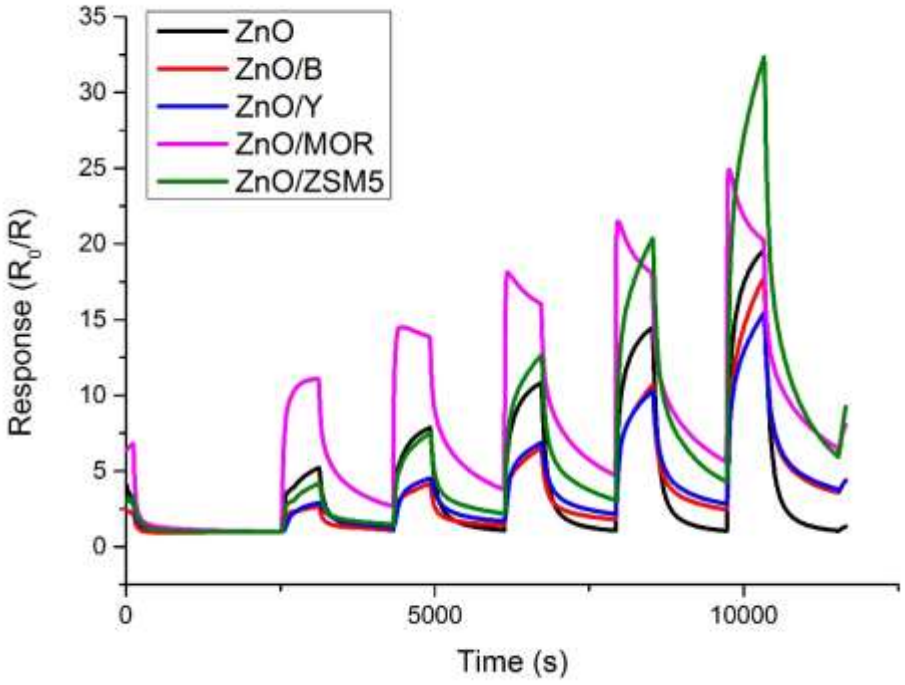

Figure 3.20. Response of ZnO and zeolite beta, Y, mordenite and ZSM5 modified ZnO sensors to 2.5, 5, 10, 20 and 40 ppm toluene at an operating temperature of 350°C. Response is calculated as a function of baseline resistance R_0 that is, the sensor resistance in dry air.

At operating temperatures between 350°C and 500°C (Fig. 3.21), mordenite and ZSM5 modified ZnO are shown to be consistently the most responsive ZnO based sensors on exposure to toluene. Zeolite beta modified sensors are shown to be less responsive than unmodified ZnO at all temperatures.

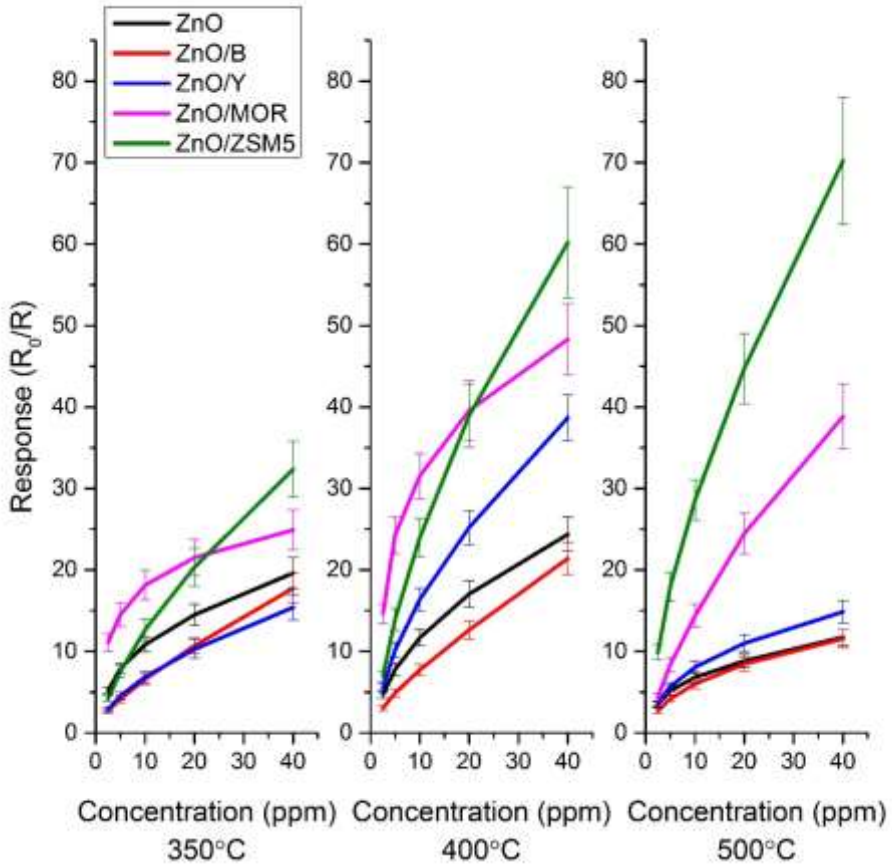

Figure 3.21. Response (± 1 S.D.) of ZnO based sensors (unmodified ZnO and zeolite beta, Y, mordenite and ZSM5 admixtures) to concentrations of 2.5-40 ppm toluene at temperatures of 350°C, 400°C, 500°C. Response is calculated as a function of baseline resistance R_0 that is, the sensor resistance in dry air.

Table 3.0.10. Response times for unmodified ZnO and zeolite beta, Y, Mordenite and ZSM5 modified ZnO on exposure to 40-ppm toluene.

	Response time (s, ±5)		
Sensor	**350°C**	**400°C**	**500°C**
ZnO	260	100	30
ZnO/B	310	290	50
ZnO/Y	340	270	30
ZnO/MOR	280	70	40
ZnO/ZSM5	380	190	50

The response times for all sensors on exposure to 80 ppm toluene (Table 3.10) show faster response times (<1 minute) than observed for other species, at an operating temperature of 500°C. This fast response is not observed at lower operating temperatures. The response times of all zeolite modified sensors were longer than the unmodified sensors, as observed with other species.

3.3.6. Response to Ammonia

All ZnO based sensors were exposed to 2.5, 5, 10, 20 and 40 ppm ammonia, at operating temperatures of 350°C, 400°C and 500°C. Responses at 500°C (Fig. 3.22) show generally smaller magnitude of response than to similar concentrations of other analyte gases seen in this chapter. The magnitude of response to ZSM5, mordenite and zeolite beta modified ZnO is found to be larger in magnitude than unmodified ZnO. Zeolite Y modified ZnO is found to be slightly smaller in magnitude than the unmodified sensor. The unmodified ZnO sensor and the ZSM5 modified sensor reach an equilibrium response at all concentrations. At higher concentrations, zeolite beta, Y and mordenite modified ZnO display an abnormal peak shape, where a maximum is reached quickly, then the magnitude of response decreases, before returning to the baseline response on the reintroduction of compressed air. This is similar to the peak shape observed with mordenite modified ZnO on exposure to toluene at operating temperatures of 400°C and 350°C (Fig 3.23 & 3.24). The reasons for this abnormal peak shape are likely due to conversion of ammonia to N_2 and H_2 at the zeolite surface, resulting in less reactive species and a lower response to the converted chemical species.

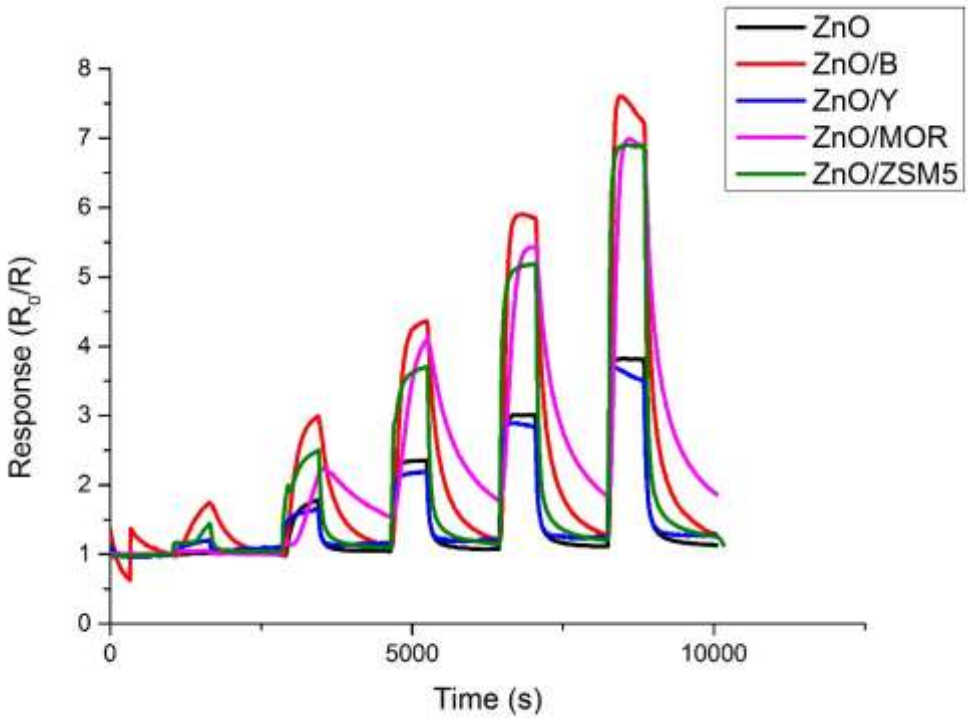

Figure 3.22. Response of ZnO and zeolite beta, Y, mordenite and ZSM5 modified ZnO sensors to 2.5, 5, 10, 20 and 40 ppb ammonia at an operating temperature of 500°C. Response is calculated as a function of baseline resistance R_0 that is, the sensor resistance in dry air.

At an operating temperature of 400°C (Fig 3.23) the response of ZSM5 and mordenite modified ZnO were found to be more responsive than unmodified ZnO, this may be due to the increased acidity of these zeolites compared to ZnO and the other zeolite modified sensors. Zeolite beta and Y modified sensors show response shapes similar to those observed at an operating temperature of 500°C, suggesting that ammonia undergoes acid catalysis and breaks down to less reactive species at the zeolite surface.

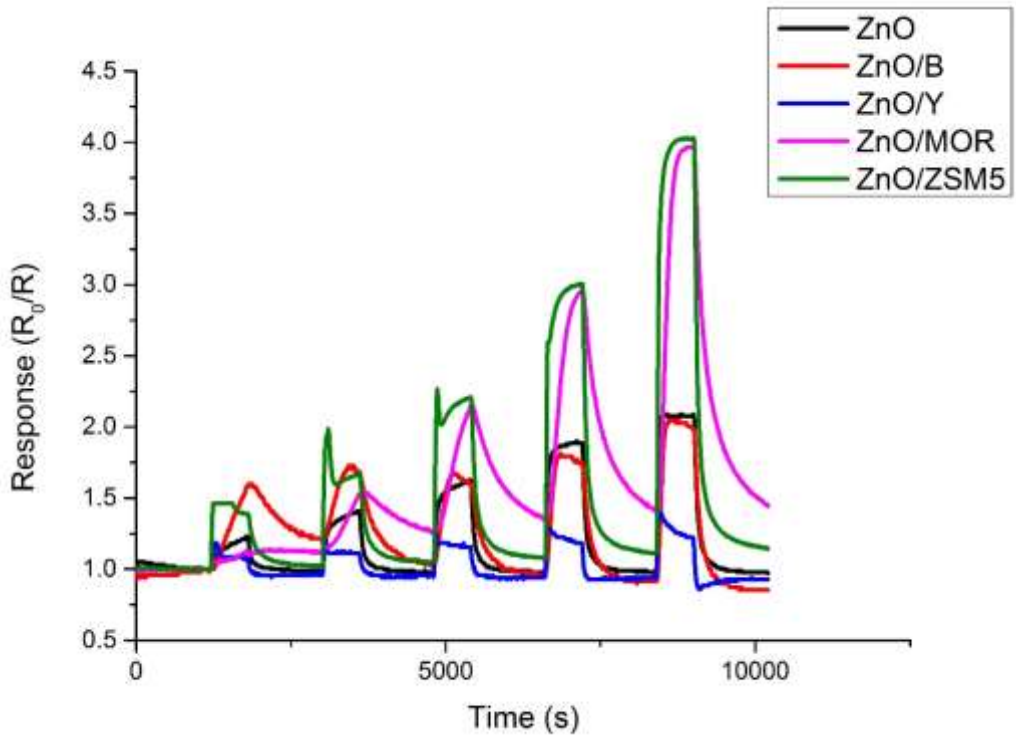

Figure 3.23. Response of ZnO and zeolite beta, Y, mordenite and ZSM5 modified ZnO sensors to 2.5, 5, 10, 20 and 40 ppb ammonia at an operating temperature of 400°C. Response is calculated as a function of baseline resistance R_0 that is, the sensor resistance in dry air.

At an operating temperature of 350°C (Fig 3.24), zeolite beta modified zinc oxide does not record any response to ammonia, at any concentration. ZSM5 modified ZnO is found to be the most responsive, with an abnormal peak shape that reaches a maximum response, then drops dramatically before plateauing, suggesting a zeolite catalysed conversion of ammonia molecules. Zeolite Y modified ZnO and unmodified zinc oxide show a similar response peak shapes to ZSM5 modified ZnO, suggesting a catalytic conversion of ammonia.

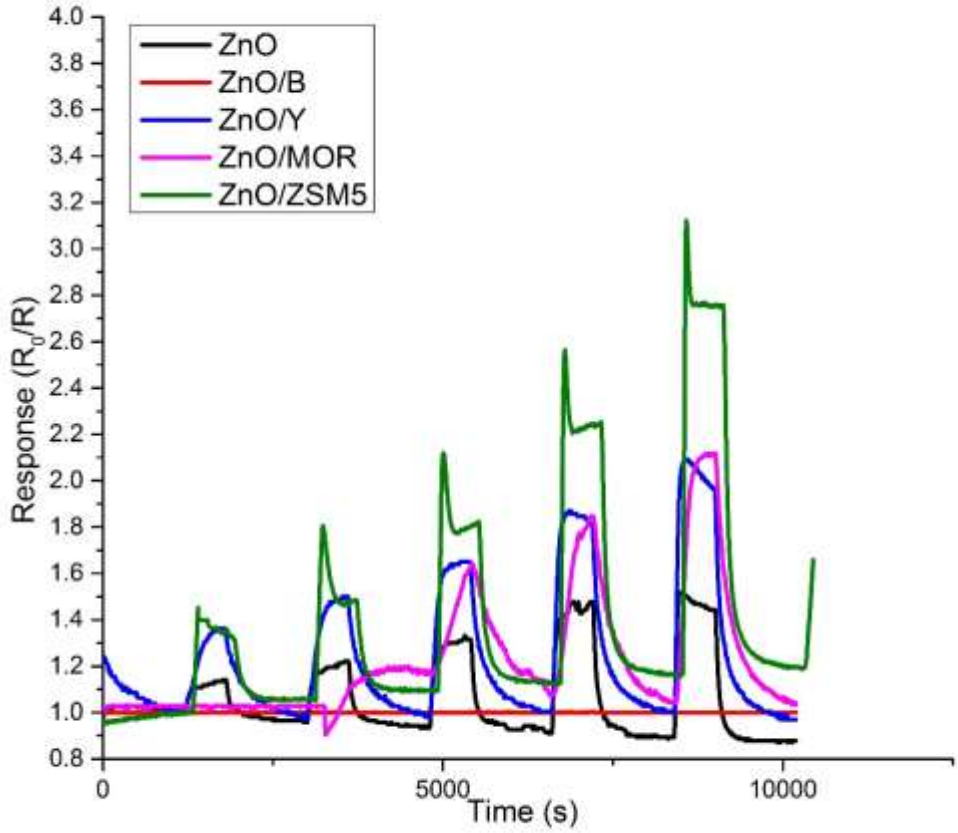

Figure 3.24. Response of ZnO and zeolite beta, Y, mordenite and ZSM5 modified ZnO sensors to 2.5, 5, 10, 20 and 40 ppb ammonia at an operating temperature of 400°C. Response is calculated as a function of baseline resistance R_0 that is, the sensor resistance in dry air.

The responsiveness of all sensors decreases as temperature decreases. Responses to ammonia at 350°C, 400°C and 500°C (Fig. 3.25) show zeolite beta modified ZnO, despite the relatively strong response to ethanol at 500°C (R_0/R = 7.8 to 40 ppm ammonia), demonstrates a poor response at 400°C and no response to ammonia at any concentration at 350°C. At operating temperatures of 350°C and 400°C, ZSM5 modified ZnO shows the largest magnitude of response to ammonia at all temperatures, with responses of R_0/R = 4.1 and R_0/R = 3.1 to 40 ppm at 350°C and 400°C respectively. Only ZSM5 and mordenite modified ZnO show enhancement over the unmodified ZnO sensor at all operating temperatures.

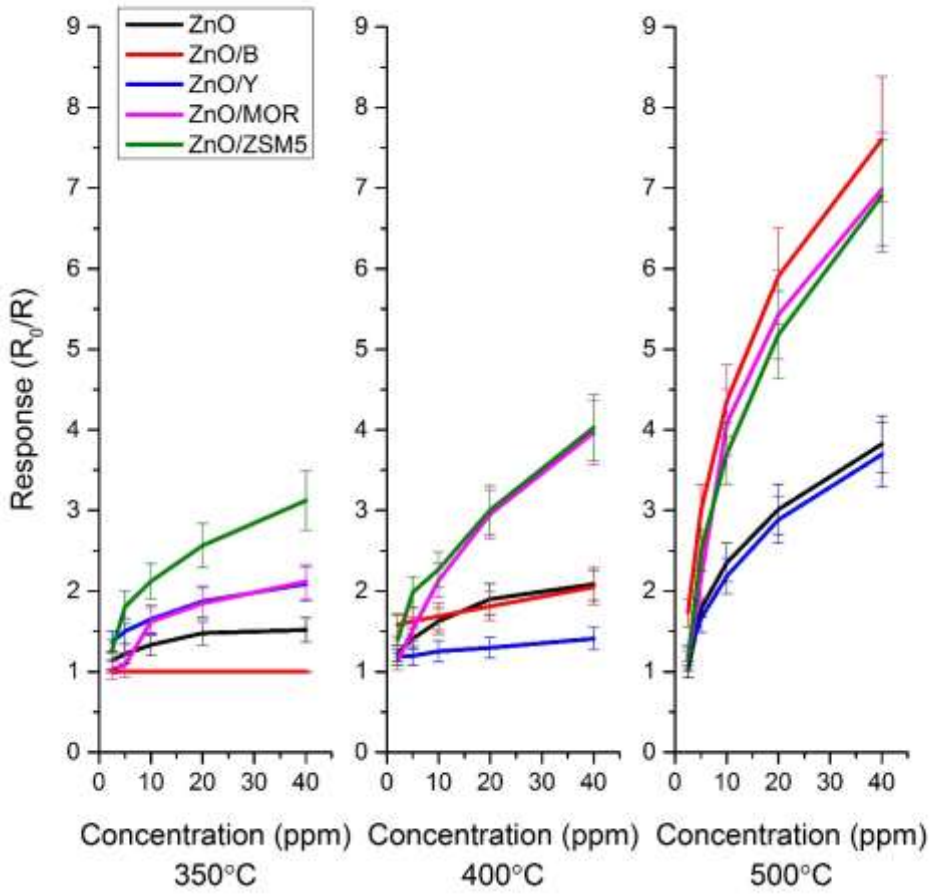

Figure 3.25. Response (± 1 S.D.) of ZnO based sensors (unmodified ZnO and zeolite beta, Y, mordenite and ZSM5 admixtures) to concentrations of 2.5-40 ppm ammonia at temperatures of 350°C, 400°C, 500°C. Response is calculated as a function of baseline resistance R_0 that is, the sensor resistance in dry air.

The response times on exposure to 40-ppm ammonia (Table 3.11) are faster than on exposure to any other analyte gas in this study, this is due to the abnormal peak shapes seen by zeolite beta, Y and mordenite modified ZnO, where the maximum response is reached quickly, then declines. There is not a significant difference between the response times of the unmodified ZnO sensor and zeolite modified sensors, except for mordenite modified ZnO, which has far longer response times than other ZnO sensors. The change in temperature also has little effect on the response time of the sensors.

Table 3.0.11. Response times for unmodified ZnO and zeolite beta, Y, mordenite and ZSM5 modified ZnO on exposure to 40 ppm ammonia.

	Response time (s, ±5)		
Sensor	**350°C**	**400°C**	**500°C**
ZnO	40	40	30
ZnO/B	-	40	40
ZnO/Y	60	30	20
ZnO/MOR	190	180	180
ZnO/ZSM5	80	40	30

3.4. Different Counter-Ion Use in Mordenite Modified ZnO

For exposure to ethanol, toluene, acetone ammonia and nitrogen dioxide, protonated zeolites were used to modify ZnO based sensors. Hydrogen is the smallest possible counter ion (consisting of one proton). Mordenite modified sensors were fabricated with 2 different counter ions, Na^+ and NH_4^+. These sensors were tested against 40-ppm toluene at 500°C and 400°C and subsequently retested every 2 hours. These zeolites were used as supplied by Zeolyst.

The results of these experiments at an operating temperature of 400°C (Fig. 3.26) show that during the first test, all three sensors have similar responses to 40 ppm toluene (R_0/R = 39.8 - 48.3), following this test, the response of NH_4- and Na- mordenite decreases in magnitude in subsequent tests, this continues to test 4. At test 4, the Na-mordenite modified ZnO response to 40 ppm has dropped from R_0/R = 45.0 to R_0/R = 29.6, while NH_4-mordenite modified ZnO response to 40 ppm had dropped from R_0/R= 29.8 to R_0/R= 15.5. This reduction in magnitude of response is rectified by heating NH_4- and Na- mordenite modified ZnO to an operating temperature of 550°C for 1 hour. The test immediately after this (test 5) shows that the responses to 40 ppm are similar to the responses in test 1.

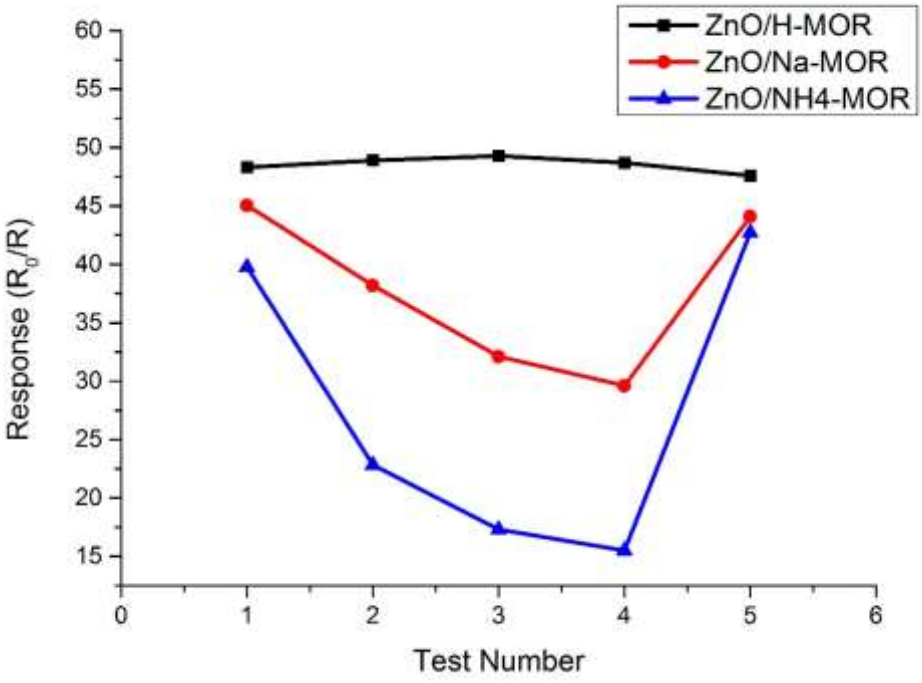

Figure 3.26. Consecutive responses of three mordenite modified ZnO (with NH_4, Na and H mordenite) to 40-ppm toluene. Tests were conducted 2 hours apart. After test 4, all sensors were heated to 550°C for one hour. Response is calculated as a function of baseline resistance R_0 that is, the sensor resistance in dry air.

3.5. Response to Humidity

Zinc oxide and zeolite beta, Y, mordenite and ZSM5 modified ZnO were exposed to a 600 second pulse of humid air (RH = 50%) at operating temperatures of 500°C, 400°C and 350°C. All sensors experience an increase in response on interaction with humid air. The largest increase in resistance is observed in zeolite Y modified ZnO; all other sensors show responses to humid air that are lower in magnitude.

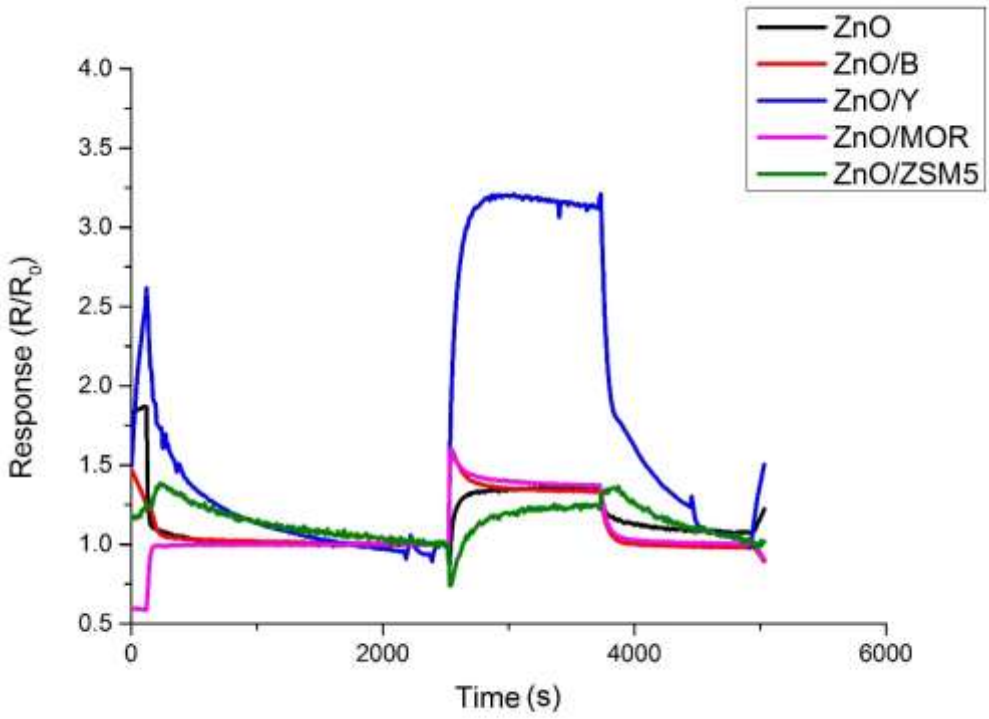

Figure 3.27. Response of ZnO based sensors (unmodified ZnO and zeolite beta, Y, mordenite and ZSM5 admixtures) to a 600 second pule of humid (RH = 50%) at a temperature of 500°C. Response is calculated as a function of baseline resistance R_0 that is, the sensor resistance in dry air.

The effect of humid air at operating temperatures between 350°C and 500°C (Fig. 3.28) shows that in most sensors (apart from zeolite Y modified ZnO) the response on interaction with humid gas increases with decreasing temperature. Zeolite Y modified ZnO has the opposite effect, with increasing operating temperature the change in resistance increases. Zeolite Y modified ZnO is far more responsive to humid air than any other sensor, with $R/R_0 = 3.3$ as opposed to $R/R_0 = 1.2$ for ZSM5 modified ZnO.

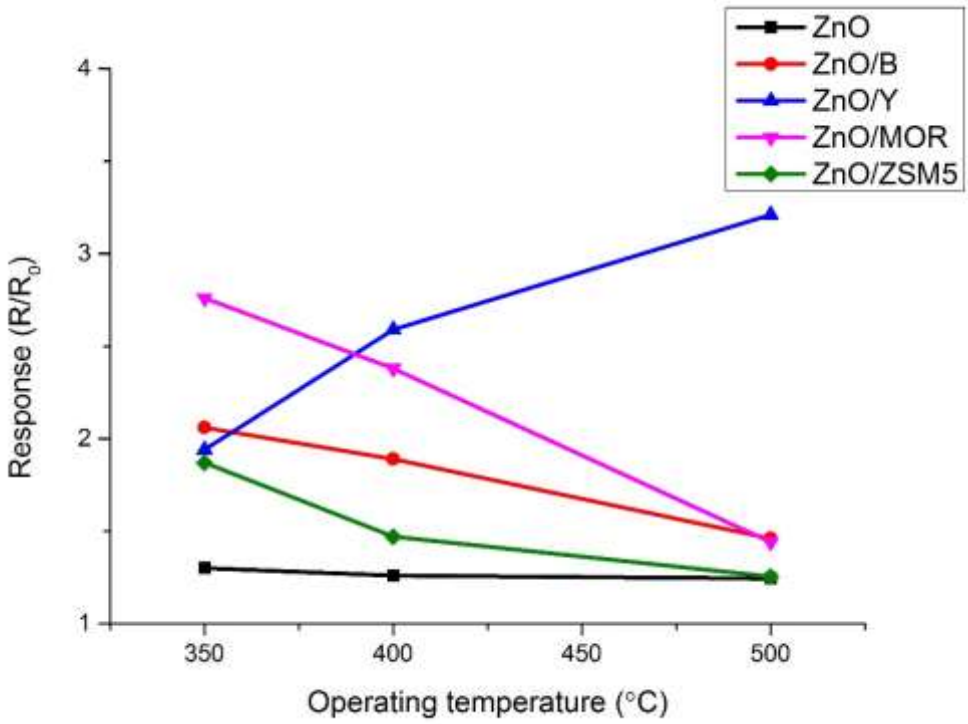

Figure 3.28. Response of ZnO based sensors (unmodified ZnO and zeolite beta, Y, mordenite and ZSM5 admixtures) to humid air (RH = 50%) at temperatures of 350°C, 400°C, 500°C. Response is calculated as a function of baseline resistance R_0 that is, the sensor resistance in dry air.

3.6 Exposure to Multiple Gases

To assess how ZnO based sensors interact with more complex air mixtures, unmodified ZnO and all zeolite modified ZnO sensors were exposed to three different mixes of gas, these were: ammonia/nitrogen dioxide and acetone/ethanol mixtures. Ammonia and nitrogen dioxide are expected to give opposing responses ad a result of their redox properties. Ethanol and acetone demonstrate responses of a similar order of magnitude to similar concentrations of these gases. The results of these are listed below.

3.6.1. Exposure to Ammonia and Nitrogen Dioxide

All ZnO based sensors were exposed to a mixture of nitrogen dioxide and ammonia. The concentrations used are displayed in Table 3.13

Table 3.13. Concentrations of ethanol and acetone in each gas pulse that unmodified ZnO and zeolite beta, Y, mordenite and ZSM5 modified ZnO were exposed to.

Ammonia (ppm)	Nitrogen dioxide (ppm)
40	0
30	0.2
20	0.4
10	0.8
0	1

The responses of each pulse (Fig. 3.29) show that there is a reduction in response when exposed to two gases, as opposed to each gas individually. These species have opposing reactions, and so to an extent, the responses cancel each other out. The response to nitrogen dioxide is the predominant, even at low concentrations (around 200 ppb), the reason for this is that nitrogen dioxide can react directly with the sensor surface, as opposed to ammonia, which reacts with oxygen atoms adsorbed to the surface. Nitrogen dioxide is able to react with the surface directly due to a lone electron on the nitrogen atom.

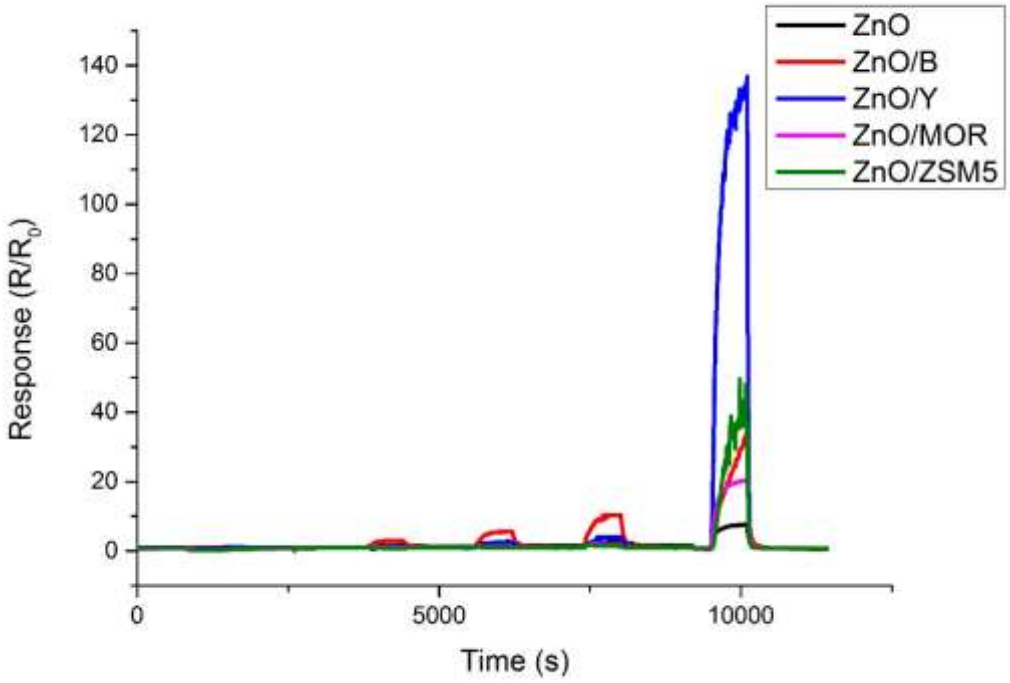

Figure 3.29. Response of ZnO based sensors (unmodified ZnO and zeolite beta, Y, mordenite and ZSM5 admixtures) to mixtures of 0-40 ppm ammonia and 0-1 ppm nitrogen dioxide at an operating temperature of 350°C. Response is calculated as a function of baseline resistance R_0 that is, the sensor resistance in dry air.

3.6.2. Exposure to Ethanol and Actone

Sensors were exposed to mixtures of ethanol and acetone at concentrations between 20 and 80 ppm (Table. 3.14).

Table 3.14. Concentrations of ethanol and acetone in each gas pulse that unmodified ZnO and zeolite beta, Y, mordenite and ZSM5 modified ZnO were exposed to.

Ethanol (ppm)	Acetone (ppm)
80	0
60	20
40	40
20	60
0	80

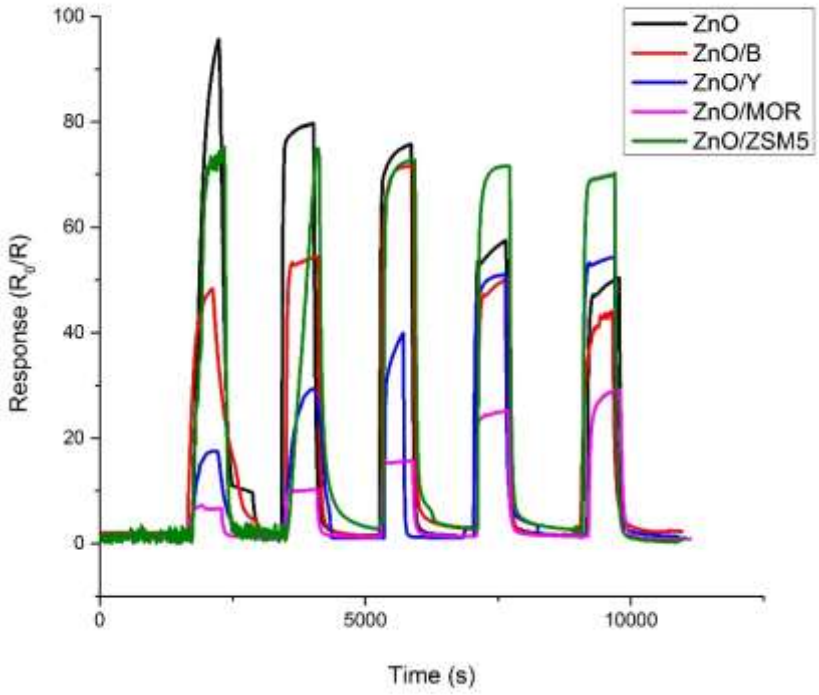

Figure 3.30. Response of ZnO based sensors (unmodified ZnO and zeolite beta, Y, mordenite and ZSM5 admixtures) to pulses of 80 ppm ethanol, 60 ppm ethanol and 20 ppm acetone, 40 ppm of both ethanol and acetone, 40 ppm ethanol and 60 ppm acetone and 80 ppm acetone at an operating temperature of 400°C. Response is calculated as a function of baseline resistance R_0 that is, the sensor resistance in dry air.

In the response to acetone and ethanol (Fig 3.30), it is interesting to note the varying peak shape that occurs with each subsequent gas pulse, the reason for the changing peak shape is likely to be due to competing reactions at the sensor surface between ethanol and acetone molecules, also acid catalysed reactions that may take place between acetone and ethanol molecules. Will result in different products at different gas compositions. Under acidic conditions it is possible for ketone and alcohol molecules to form an acetal molecule and water. Zeolite beta modified ZnO is the only sensor material that shows an enhancement in response when exposed to a mixture of gases as opposed to purely just acetone or ethanol, this is possibly due to the formation of acetal molecules under acidic conditions.

3.7. Analysis of Sensor Exhaust Gas

To understand the mechanisms undergone when sensors are exposed to analyte gases, mass spectrometry techniques were implemented to analyse the exhaust gases following exposure to sensors. A novel experimental set up was built, as discussed in section 2.4, which incorporated a small gas-sensing chamber, attached to a Hiden *HPR60* Molecular Beam Mass Spectrometer System. A flow of 50 ppm toluene at a flow rate of 1000 cm^3 min^{-1} was supplied to each sensor in a sensor chamber that was attached to the input of mass spectrometer (Figure 2.3).

The mass spectrum analysis of unmodified ZnO on exposure to 50 ppm toluene at 500°C (Fig 3.31) shows that two peaks dominate the spectrum, at m/z = 28, this peak is attributed to nitrogen gas (N_2). Nitrogen is the dominant chemical species in the atmosphere and so it is expected that it should be the most abundant gas in this sample. The second dominant peak is observed at m/s = 32, this is attributed to oxygen (O_2).

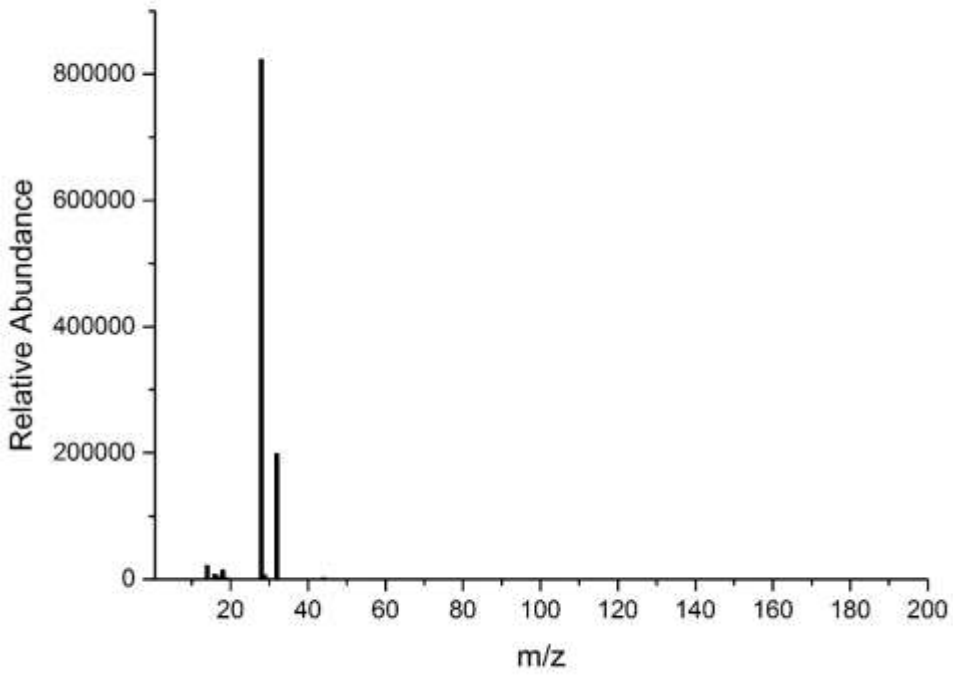

Figure 3.31. Mass spectrum analysing exhaust gas following exposure of a ZnO sensor to a pulse of 50 ppm toluene at an operating temperature of 500°C.

In order to analyse gases that are present at much lower concentrations than nitrogen and oxygen in the gaseous sample, an inset of the mass spectra, demonstrating the analysis of unmodified ZnO, mordenite and ZSM5 modified ZnO during exposure to toluene at 500°C and 400°C are shown in Figs 3.32 and 3.33. No peaks were observed above m/z = 100 and so this data has not been included in the figures.

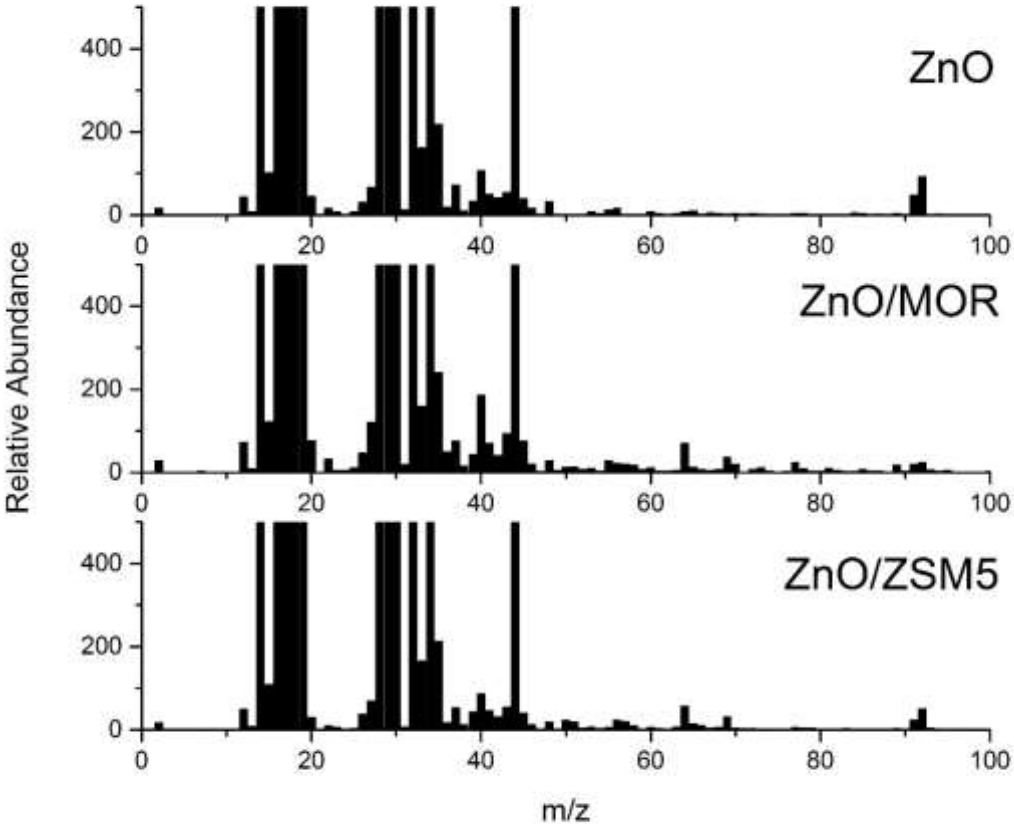

Figure 3.32. Mass spectra of exhaust gas following exposure of zinc oxide and mordenite and ZSM5 modified ZnO to toluene at an operating temperature of 500°C.

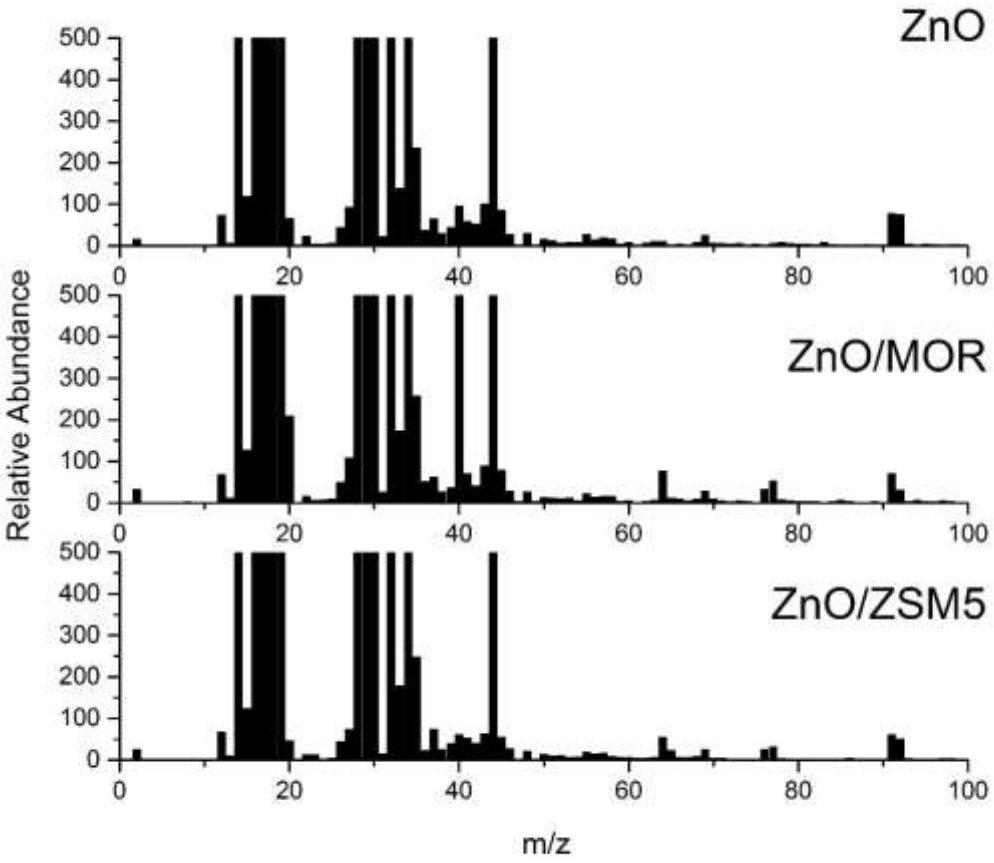

Figure 3.33. Mass spectra of exhaust gas following exposure of zinc oxide and mordenite and ZSM5 modified ZnO to toluene at an operating temperature of 400°C.

Analysis of the specific peaks in spectra of ZnO exhaust gas (Table 3.15) showed that there were significant increases in the CO_2 and H_2O above atmospheric concentrations: this is expected as toluene undergoes full oxidation to these products:

$$C_6H_5CH_3 + [O] \rightarrow CO_2 + H_2O$$

Both these species are observed in the mass spectra obtained and are present at higher concentrations in the zeolite modified samples, suggesting that more material is oxidised in the zeolite modified sensor samples, resulting in larger magnitudes of response to toluene using zeolite modified sensors than the unmodified sensor. The mass spectra also show that peaks corresponding to toluene (m/z = 92) are smaller

following exposure to zeolite modified sensors, indicating that a greater proportion of toluene is adsorbed at the sensor surface when zeolite material is present.

Table 3.15. Average peak height (n = 15) of peaks representing H_2O, CO_2 and toluene concentrations in the atmosphere following a 50-ppm exposure of toluene in dry air at an operating temperature of 500°C.

m/z ratio	No Sensor	ZnO	ZnO/MOR	ZnO/ZSM5
18	1620	1737	5389	2340
44	1430	1670	4172	2216
92	120	82	23	50
R_0/R (40 ppm)	n/a	11.7	38.9	72.4

Table 3.16. Average peak height (n = 15) of peaks representing H_2O, CO_2 and toluene concentrations in the atmosphere following a 50-ppm exposure of toluene in dry air at an operating temperature of 400°C.

m/z ratio	No Sensor	ZnO	ZnO/MOR	ZnO/ZSM5
18	1630	5204	24992	16096
44	1390	3324	5479	4764
92	120	74	30	50
R_0/R (40 ppm)	n/a	24.4	48.3	60.2

In addition to the increases in peak height showing increased production of water and carbon dioxide, several extra peaks are observed following exposure of toluene to zeolite-modified sensors. These additional peaks are found predominantly at masses above m/z = 50, suggesting a breakdown of the toluene molecule into benzene (suggested by a peak at m/z = 77), pentadiene (m/z = 65) and butadiene (m/z = 52). Examples of these species can be found in Figure 3.34. This suggests that toluene molecules are adsorbed and broken down to smaller molecules, such as benzene ions and C-C_5 chains. A single toluene molecule can be broken down into two or more alkene molecules, resulting in more species to react at the sensor surface. In addition to a larger number of species adsorbing at the surface, the full oxidation of molecules smaller than toluene (for example ethane, propene or benzene) would require lower activation

energies than the full oxidation of toluene, to produce water and carbon dioxide molecules.

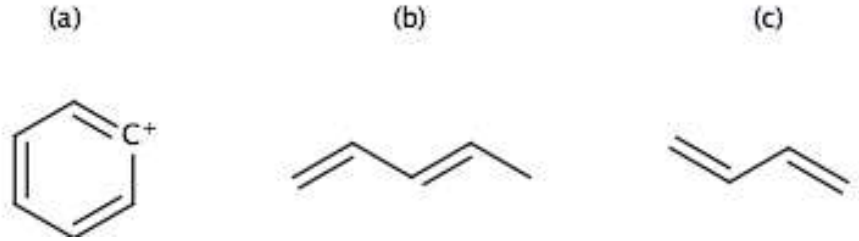

Figure 3.34. Examples of ions observed in mass spectrums of exhaust gases following exposure of ZnO and mordenite and ZSM5 modified ZnO sensors to toluene, (a) shows a benzene ion, (m/z= 77), (b) shows a 1,3-pentadiene (m/z = 65) and (c) shows 1,3-butadiene (m/z = 52). All three molecules are components of toluene and may be present if C-C and C=C bonds in the toluene molecule are broken.

A significant peak is observed in spectra referring to exhaust gas from mordenite modified ZnO, at m/z = 40, this is not observed in mass spectra from exhaust gases of unmodified ZnO or ZSM5 modified ZnO. The peak is significantly larger at an operating temperature of 500°C. This may refer to a C_3H_4 molecule, which may be the result of a breaking of the benzene ring and subsequent rearrangement resulting in the formation of 1,2-propadiene or propyne (Fig 3.35).

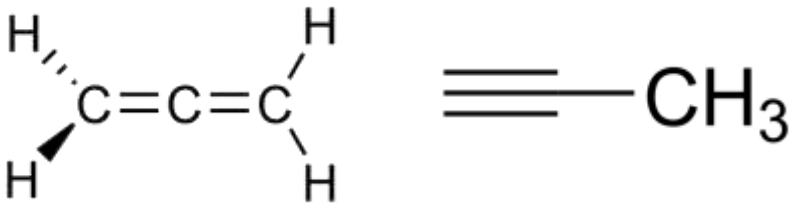

Figure 3.35. Structure of 1,2-propadiene (left) and propyne (right) molecules, likely candidates for the peak observed at m/z = 40 following the exposure of toluene to mordenite modified ZnO.

On comparison with exposure to pure toluene not exposed to a gas sensor, it is clear that these four peaks represent molecules that are not present, in large amounts, on the breakdown of toluene due to fragmentation within the mass spectrometer, indicating that these four products are a result of the breakdown of toluene at the gas sensor surface.

Table 3.17 Average peak height (n = 15) of of m/z = 40, 52, 65 and 77 in the atmosphere following a 50-ppm exposure of toluene in dry air and on exposure to ZnO and mordenite and ZSM 5 modified ZnO gas sensors at an operating temperature of 500°C.

m/z ratio	No Sensor	ZnO	ZnO/MOR	ZnO/ZSM5
40	20.1	106.0	185.3	86.0
52	6.3	10.6	9.3	17.2
65	2.8	12.0	23	46.6
77	0.66	14.1	69.3	31.3
R_0/R (40 ppm)	n/a	11.7	38.9	72.4

Table 3.18 Average peak height (n = 15) of of m/z = 40, 52, 65 and 77 in the atmosphere following a 50-ppm exposure of toluene in dry air and on exposure to ZnO and mordenite and ZSM 5 modified ZnO gas sensors at an operating temperature of 400°C.

m/z ratio	No Sensor	ZnO	ZnO/MOR	ZnO/ZSM5
40	10.0	108.4	14647.8	64.2
52	0.6	4.6	31.6	11.1
65	2.0	48	94.8	50.1
77	0.6	11.6	44.1	38.1
R_0/R (40 ppm)	n/a	24.4	48.3	60.2

3.8. Discussion

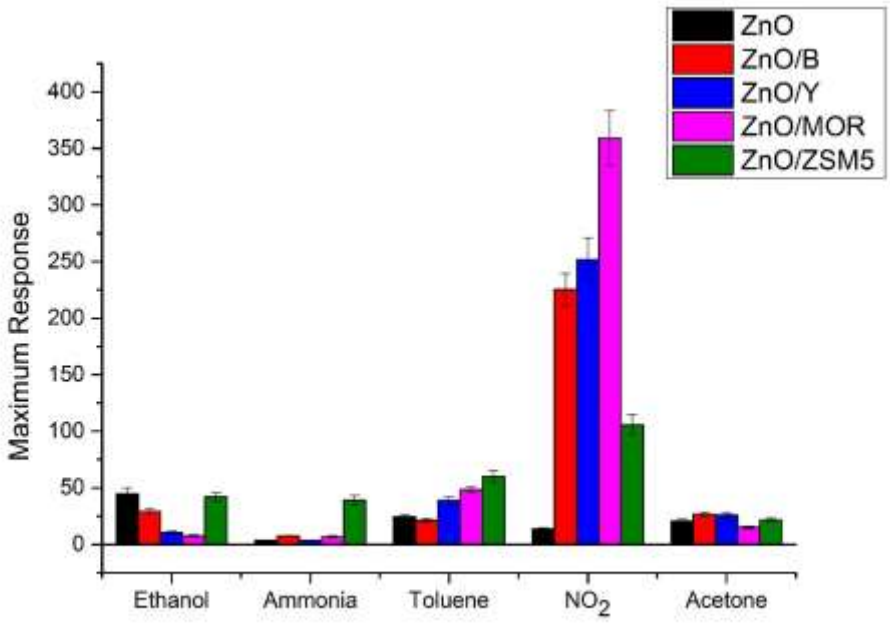

Figure 3.36. Response of ZnO based sensors (unmodified ZnO and zeolite beta, Y, mordenite and ZSM5 admixtures) to 40 ppm pulse of ethanol, ammonia, toluene, nitrogen dioxide and acetone at an operating temperature of 400°C.

Zinc oxide, and zeolite beta, Y, mordenite and ZSM5 modified ZnO sensors produced responses to all five gases used in this study. The strongest responses observed were on exposure to nitrogen dioxide. Enhancements in the magnitude of response were observed with most gases in the zeolite modified sensors, compared with the unmodified sensor.

The enhancement in sensor response is likely due to several factors. The surface areas of sensor materials (Table 3.1) demonstrates that zeolite modified sensors have a much larger surface area than unmodified ZnO. This allows for a more open microstructure, as seen in SEM analysis (Fig. 3.3). This more open microstructure provides more convenient channels for the penetration of gas molecules to the whole sensor and allows analyte molecule to probe deeper into the material, accessing ZnO and chemisorbed oxygen ions covering more ZnO material than available in the unmodified sensor.

Zeolite materials are known for their strong adsorbent properties. On exposure to an analyte gas, large amounts of target gas can be 'stored' at zeolite surface; this allows the zeolite to act as a preconcentrator, meaning that there is always a supply of target gas available to react. This is reflected in the slower response and recovery times observed in zeolite-modified sensors.

All the zeolites used in this study are well known acid catalysts and as such, target analytes are likely to undergo acid catalysed reactions, such as isomerisation, dehydration and catalytic cracking at the zeolite surface.

Capacitance measurements of all sensors (Table. 3.4) show that zeolite modified sensors all possess larger capacitance values than the unmodified ZnO sensor. This increase in capacitance is likely a result of the zeolite material possessing capacitive properties. The enhancements in responsiveness of the sensors could be related to this. The zeolite modified sensors possess the ability to store up charge when exposed to a target gas, the change in charge carrier concentration may release electrons that were stored at the zeolite and consequently reduce the resistance even further. This may explain some unusual peak shapes observed (Figs. 3.23 & 3.24).
Zeolites are well known for their catalytic properties. The results of this study, as well as the presence of the hydrogen counter ion suggest that all zeolites act as acid catalysts. Studies involving mass spectrometry analysis of the gas sensor rig (section 3.7) suggest that toluene may be converted, through a catalysed disproportionation reaction to benzene as well as multiple aliphatic hydrocarbons. Peak shapes observed on exposure to other gases, especially to ammonia and acetone, suggest a similar mechanism occurs at the zeolite surface, resulting in the breakdown of analyte molecules to other species that go on to react at the gas sensitive surface.

Unlike exposure to all other gases, when exposed to ethanol and in some cases, acetone, the magnitude response of unmodified ZnO is higher that all zeolite modified sensors. The full oxidation of ethanol occurs by the following reaction:

$$C_2H_5OH + 3O_2 \rightarrow 2CO_2 + 3H_2O$$

However, under acidic or basic conditions, the following reactions occur[177]:

$$C_2H_5OH \rightarrow C_2H_4 + H_2O \text{ (1)}$$

$$C_2H_5OH + O^- \rightarrow CH_3CHO + H_2O + e^- \text{ (2)}$$

The basic reaction (2) generates more electrons than the acidic reaction (1)[178]. Zinc oxide is amphoteric[179] meaning it can act as an acid or a base, therefore both reactions detailed above can occur at the sensor surface. All zeolites used were protonated, resulting in acid catalysis reactions at the sensor surface. These conditions were able to promote the acid based breakdown of ethanol seen in equation (1).

Additionally, under basic conditions, where acetaldehyde (CH_3CHO) is produced, the product can react further, resulting in further liberation of electrons in the sensor material. Acetaldehyde oxidises to ethanoic acid, which can fully break down to carbon dioxide and water.

$$CH_3CHO + O^- \rightarrow CH_3COOH + e^-$$

$$CH_3COOH + 4O^- \rightarrow 2CO_2 + 2H_2O + 4e^-$$

Therefore, the overall breakdown of ethanol under basic conditions releases six electrons into the bulk material, as opposed to the acidic reaction (observed in zeolite modified sensors), which produced ethene, which is very poorly oxidised.

The response of ZnO sensors upon exposure to nitrogen dioxide demonstrates a different type of response than with reducing gases, this is a because NO_2 can adsorb and interact directly with the sensor surface, as opposed to reacting solely with adsorbed oxygen species. NO_2 reacts with the sensor surface in the following way:

$$NO_{2\,(g)} + 3e^- \rightarrow NO^{2-}_{(ads)} + O^-_{(ads)}$$

$$NO^{2-}_{(ads)} + O^-_{(ads)} + e^- \rightarrow NO_{(g)+} + 2O^{2-}_{(ads)}$$

These reactions not only remove electrons from the material to facilitate the breakdown of nitrogen dioxide, but also produce more adsorbed oxygen species, thus lowering the charge carrier concentration in the material, and reducing the conductivity.

Sensors gave different magnitudes of response at different temperatures. There are several reasons for this; adsorption and desorption at the sensor surface are temperature activated, the physical properties of the material, such as charge carrier concentration, Debye length and work function are also temperature controlled. The rate of reaction for the oxidation/reduction of a specific test gas is dependent on the gas. Each sensors has a peak temperature for maximum sensitivity, below this maximum the rate of reaction is too slow to give the maximum possible response, whereas if the temperature is too high, the redox reaction proceeds so rapidly that the concentration of the test gas becomes diffusion limited and the concentration seen by the sensor approaches zero[180]. At such temperatures, redox reactions can take place at the sensor surface without producing a noticeable electric charge on the metal oxide material.

Mass spectrometric analysis of exhaust gas following exposure of toluene to ZnO and mordenite and ZSM5 modified ZnO shows that toluene undergoes the expected full oxidation to water and carbon dioxide. When zeolite modified sensors were analysed by mass spectrometry, additional peaks were found, indicating that the zeolite components of the sensor were breaking down toluene molecules into smaller chains as well as benzene. This breakdown enables more molecules to adsorb on the surface; these molecules contain fewer atoms and are smaller than the large toluene molecule (critical diameter of 6.7 Å), requiring less energy undergo oxidation and release electrons to the sensor.

Zeolite modified zinc oxide sensors show a larger magnitude of response to similar concentrations of NO_2 than WO_3 and In_2O_3 sensors[25], a larger response to ethanol than SnO_2 sensors[181] and a larger response to acetone than Fe_2O_3 gas sensors[182]. Zeolite modified ZnO sensors also show stronger responses to toluene than TiO_2[183] and WO_3 and demonstrated larger magnitudes of response to similar concentrations of ammonia than CuS[184] and SiO_2[185] based gas sensors.

3.9 Conclusion

A sensor array of five zinc oxide sensors, incorporating four different zeolites was manufactured. This is the first-time zeolites have been incorporated into zinc oxide, forming zeolite admixture sensors. Admixed sensors showed a large increase in responsiveness to NO_2 (from $R/R_0 = 6$ with unmodified ZnO to $R/R_0 = 142$, for ZnO doped with mordenite) and at higher temperatures, to ethanol (from $R_0/R = 7$ to $R_0/R = 23$).

Analysis of exhaust gas from sensors, following exposure to toluene, demonstrated catalytic breakdown of the analyte in the zeolite pores, allowing smaller hydrocarbon units to be oxidised at the gas sensitive surface.

Overall the ZnO series has demonstrated several key attributes to being a successful analytical device:

- The series has shown strong sensitivity to several target gases, in the low ppm and ppb range.
- Shown reproducible responses to changes in atmosphere over multiple exposures to test gases and power cycling.

The sensors have however lacked selectivity to many gases and shown generally long response times (> 100 seconds). These properties will be investigated using chromium titanate and vanadium pentoxide sensors.

The next chapter will cover the synthesis, fabrication and testing of chromium titanate sensors. The sensors have been modified under the same conditions as shown in this chapter, where the effects of zeolite modification on p-type materials are investigated.

4. Modification of Chromium Titanate

This chapter details the synthesis of chromium titanate (CTO) and the modification of chromium titanate sensors using zeolite beta, Y, mordenite and ZSM5. These sensors were characterised and tested against five gases commonly found at clandestine laboratories.

4.1. Introduction

Chromium Titanate ($Cr_{2-x}Ti_xO_3$, where x = 0.01-0.4) has been used as a commercial gas sensor in many devices, as well as in the production of solar cells[186] and paints[187]. Chromium titanate has several well-established gas sensing properties such as good baseline stability, selectivity towards reducing gases and negligible humidity influence. Chromium titanate is a p-type material; meaning its conductivity decreases in the presence of a reducing gas, exhibiting the opposite response that is shown by n-type zinc oxide (chapter 3) and vanadium pentoxide (chapter 5). The source of the p-type behaviour of chromium titanate comes from the substitution of Ti^{4+} for Cr^{3+} ions; this leads to the introduction of holes into the bulk material, and therefore p-type behaviour, where holes are the major charge carrier.

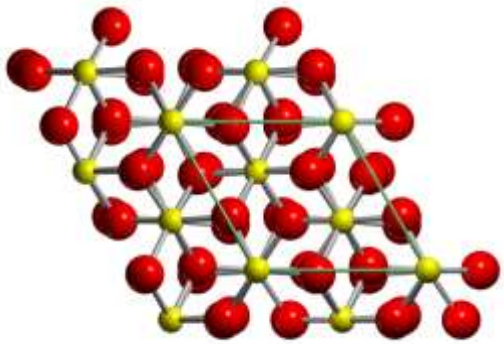

Figure 4.1. Eskolaite structure demonstrating hexagonally close packed oxygen atoms (red) and chromium (yellow) atoms in octahedral vacancies [188].

The structure of chromium titanate is based on the eskolaite crystal structure, similar to the chromium (III) oxide framework that is built up of hexagonal close packed oxygen (O^{2-}) ions with chromium (Cr^{3+}) ions occupying two-thirds of the octahedral interstices.

Titanium ions (Ti^{4+}) are substituted on to Cr^{3+} sites and the different charge is balanced by Cr vacancies. Titanium substituted ions usually group in three around a chromium vacancy[189].

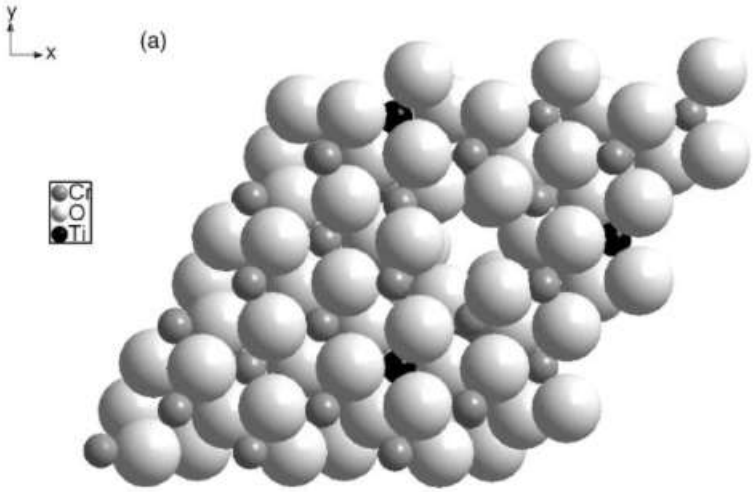

Figure 4.2. Computational model of (0001) face of CTO; three Ti^{4+} ions are charge balanced by a chromium vacancy[189].

Chromium titanate has been assessed for its gas sensing properties in several different studies and has been found to be responsive to carbon monoxide[190], hydrogen sulphide[191], ammonia[192] and liquid petroleum gas (a mixture of propane and butane)[193].

Zeolite materials have been used in conjunction with chromium titanate materials previously[194], this work has focused on using zeolites as overlayers to act as filters for particular molecular species. These materials were effective in filtering out medium sized alkane chains while allowing ethanol to pass through the zeolite pores to be detected by the sensor material.

In this chapter, chromium titanate was modified with four different zeolites, these were: zeolite beta, zeolite Y, mordenite and ZSM5. All five sensors were tested against five gases, ethanol, nitrogen dioxide, acetone, toluene and ammonia.

4.2. Characterisation

4.2.1. Physical Appearance of Sensors

All chromium titanate sensors have a green colour at room temperature, upon heating to 250°C-350°C, the sensor material changes to a black colour, heating above 450°C caused the sensor to glow red. The sensors retained their physical composition in air after repeated heating over many months, however significant shock or pressure on the sensor caused the material to crumble and lead to de-adhesion.

4.2.2. Surface Area Measurements

Surface area measurements of chromium titanate and zeolite modified materials were performed using a Micromeritics TriStar II surface area analyser. The surface area for each powder (Table 4.1) show large enhancements in all zeolite modified materials. The largest enhancement is shown in zeolite beta modified chromium titanate. Zeolite beta has the largest surface area of all the zeolites used in this study. These large enhancements in surface area are as a result of the large surface areas of the zeolite material.

Table 4.1. Surface areas of unmodified CTO and beta, Y, mordenite and ZSM5 modified CTO.

Material	Surface Area ($m^2 g^{-1}$)
CTO	3.1
CTO/B	146.2
CTO/Y	119.3
CTO/MOR	104.7
CTO/ZSM5	68.9

4.2.3. X-Ray Diffraction

X-ray diffraction patterns (Fig. 4.3) confirm the chemical make-up of the metal oxide and zeolite admixtures. All chromium titanate XRD patterns display a major corundum crystal phase, with secondary peaks at 34° and 42°, identified as $CrTiO_3$ by match of observable peaks in JCPDS pattern 33-408. Chromium titanate is identified with peaks at 2θ= 37°, 36°, 66°, 63°, 55°, 51° and 43°. Zeolite peaks are observed, as expected. Additional phases are present in zeolite modified sensors, the diffraction pattern of zeolite beta modified chromium titanate contains additional peaks at 29.29°, 22.09° and 21.88°, characteristic of the zeolite. The diffraction pattern of zeolite Y modified chromium titanate contains additional peaks at 12.43° and a cluster of peaks at around 22°. The diffraction pattern of mordenite modified chromium titanate contains additional peaks at 13.45°, 22.20° and 25.63°. All are characteristic of their respective zeolites. ZSM5 modified chromium titanate contains additional peaks around 28.09° and 29.65° and 22.26° and 23.78°. Additional phases in the modified sensor materials can lead to different gas responses in the sensor. The additional phases are likely due to agglomerated zeolite material, distributed throughout the sensor bulk.

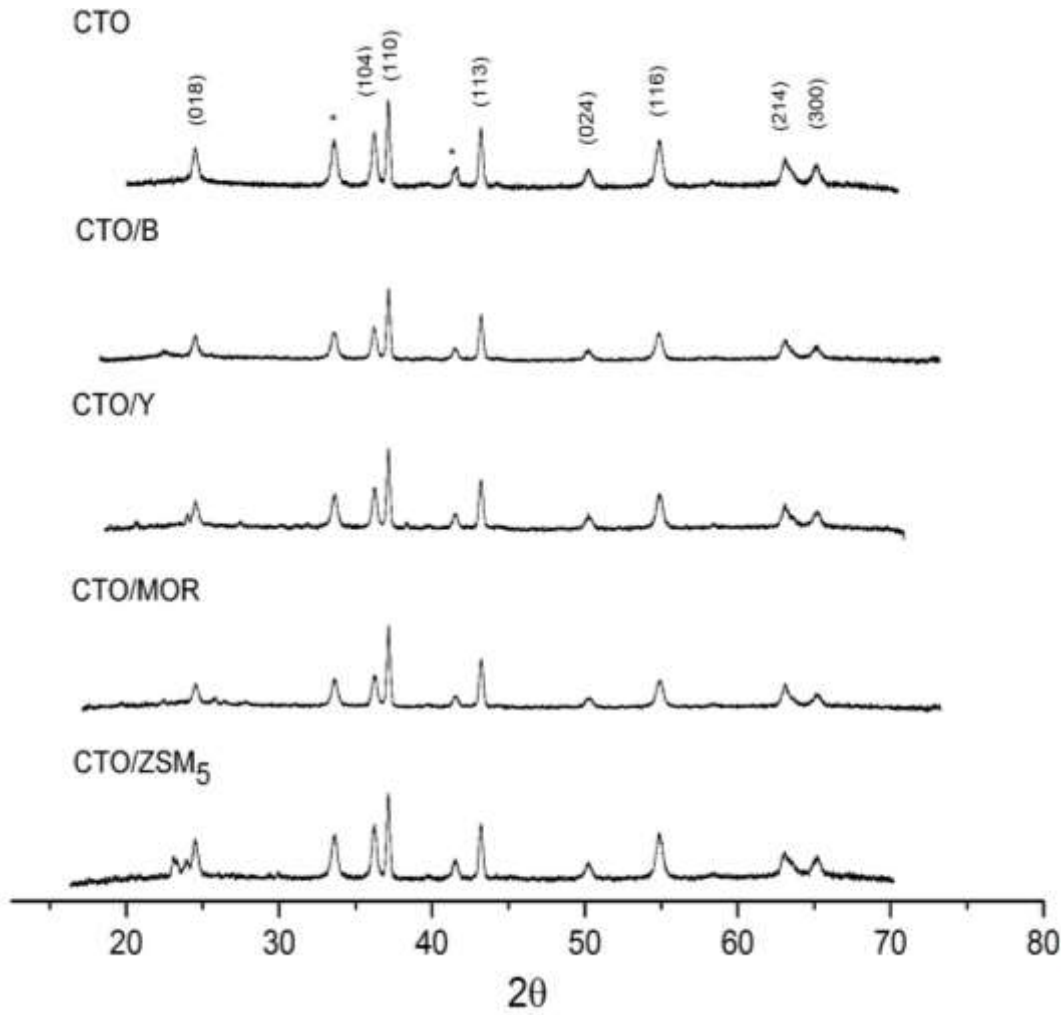

Figure 4.3. Diffraction patterns for all CTO and zeolite admixed sensors, collected between 10° and 65°. The y-axis is normalised and offset for each spectrum. * peaks represent a second phase, identified at $CrTiO_3$ by match of observable peaks in JCPDS pattern 33-408.

4.2.4. Scanning Electron Microscopy

SEM images for all five sensors at 10,000x and 20,000x magnification are shown in Fig 4.4, these demonstrate the porous nature of the sensor surface. Unmodified chromium titanate shows an average grain size diameter of around 100 nm, both zeolite beta and Y modified chromium titanate sensors show well-sintered grains with diameters of around 100 nanometers. Mordenite modified chromium titanate shows platelets of varying size in the order of several hundred nanometers. ZSM5 modified chromium titanate consists of large particles, with average diameter greater than 100 nm. All zeolite-modified materials, show increased porosity, as compared to the pure chromium titanate material.

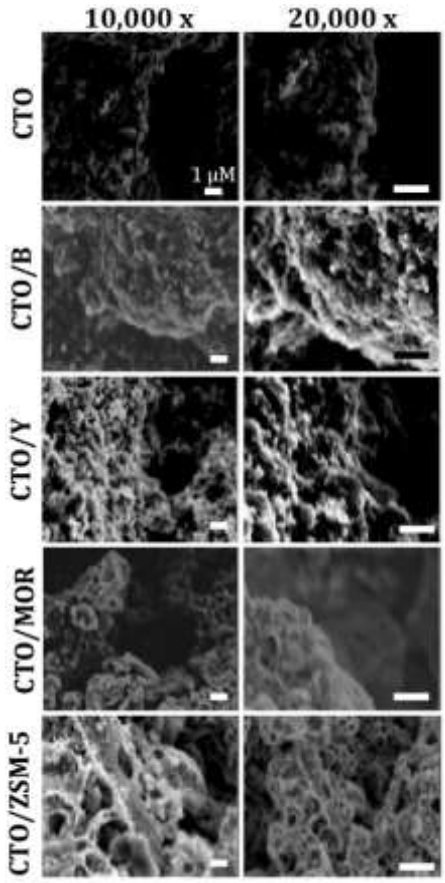

Figure 4.4. SEM images of CTO and zeolite modified CTO at 10,000x and 20,000x.

4.2.5. Energy Dispersive X-Ray Spectroscopy

Results of elemental analysis with energy dispersive X-ray spectroscopy are shown both as atomic percentage (Table 4.2) and weight percentage (Table 4.3). These show similar chromium and titanium concentrations in all zeolite modified sensors; the introduction of zeolite raises the atomic percentages of aluminium, silicon and oxygen. The weight percentage of oxygen does not increase in zeolite-modified sensors, due to the larger relative mass of silicon and aluminium, compared with oxygen.

Table 4.2. Atomic percentages of zeolite modified and unmodified chromium titanate sensors.

	Atomic Percentage (%)				
	Cr	**Ti**	**O**	**Al**	**Si**
CTO	35.6	3.1	61.3	0	0
CTO/B	24.4	2.7	63.4	0.5	9.0
CTO/Y	26.8	2.7	59.7	2.9	8.9
CTO/MOR	27.0	2.4	62.2	0.57	7.2
CTO/ZSM5	25.7	2.7	59.0	0.4	13.7

Table 4.3. Weight percentages of zeolite modified and unmodified chromium titanate sensors.

	Weight Percentage (%)				
	Cr	**Ti**	**O**	**Al**	**Si**
CTO	62.1	5.02	32.9	0	0
CTO/B	47.4	4.7	37.8	0.5	9.0
CTO/Y	49.9	4.5	33.7	2.9	8.9
CTO/MOR	52.53	3.9	35.6	0.57	7.2
CTO/ZSM5	48.64	4.1	34.4	0.4	13.7

4.3. Results

4.3.1. Background Resistance

Table 4.4. Baseline resistances of zeolite modified and unmodified chromium titanate sensors.

	Resistance (Ω)		
	250°C	**300°C**	**350°C**
CTO	3.0×10^5	9.2×10^5	3×10^4
CTO/B	9.0×10^6	9.3×10^6	1.5×10^6
CTO/Y	1.6×10^7	1.2×10^7	3.5×10^6
CTO/MOR	2.7×10^7	3×10^6	7.0×10^5
CTO/ZSM5	5.8×10^7	4.3×10^6	9.7×10^5

The background resistance in air, of unmodified chromium titanate and zeolite modified chromium titanate is shown in Table 4.4. The first observation to be noted is that all zeolite-modified materials have a larger resistance than unmodified chromium titanate, at the same operating temperature. In most cases, this is at least one order of magnitude larger; in some cases, it is two orders of magnitude higher. The reason for this is that chromium titanate is a one-phase system, while the zeolite modified material to a two-phase system. In the zeolite modified chromium titanate sensors, the two-phase systems, the mostly insulating zeolite material restricts the mobility of charge carriers and so increases the resistance within the sensor.

As the operating temperature of the sensor increases, the resistance of the sensor in air decreases, this is due to the conductivity of the semiconductor material increasing as a result of electrons having energy to “jump” from the valence band to the conduction band, increasing the concentration of holes in the material. Thermal promotion will also increase the number of electron carriers.

4.3.2. Response to Ethanol

Chromium titanate sensors were exposed to 600-second pulses of ethanol at 5, 10, 20, 40 and 80 ppm, separated by 1200-second pulses of dry air. Results at an operating temperature of 350°C are shown in Fig. 4.5. Unmodified chromium titanate shows a weak response at all temperatures (e.g. R/R_0 = 1.08 to 80 ppm ethanol); all zeolite-modified sensors display responses with larger magnitudes than the unmodified material. The zeolite beta modified sensor shows the largest response to ethanol (R/R_0 ≈ 6.8 to 80 ppm ethanol). This response is however, noisy on exposure to ethanol at all temperatures, as is the response of zeolite Y modified chromium titanate. This noise is not seen in other sensors and may be a result of non-uniform adsorption at the sensor surface.

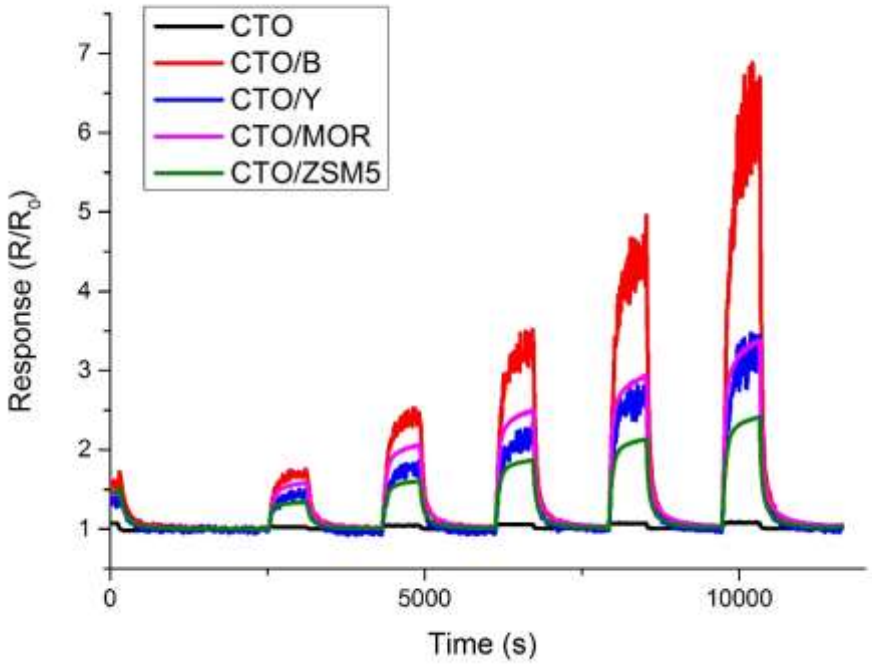

Figure 4.5. CTO based sensors (unmodified CTO and zeolite beta, Y, mordenite and ZSM5 admixtures) response to 5, 10, 20, 40 & 80 ppm ethanol, at an operating temperature of 350°C. Response is calculated as a function of baseline resistance R_0 that is, the sensor resistance in dry air.

The response of chromium titanate and zeolite modified CTO sensors to ethanol at an operating temperature of 300°C demonstrates a small magnitude of response to all concentrations in the unmodified chromium titanate sensor (R/R_0 = 1.3 to 80 ppm). The mordenite and ZSM5 modified chromium titanate sensors were found to be most responsive to ethanol at an operating temperature of 300°C. The response of mordenite modified chromium titanate snows a noisy response to an 80-ppm pulse of ethanol. None of the sensors used in this experiment reached a steady state in the 600-second gas pulse, except for unmodified chromium titanate.

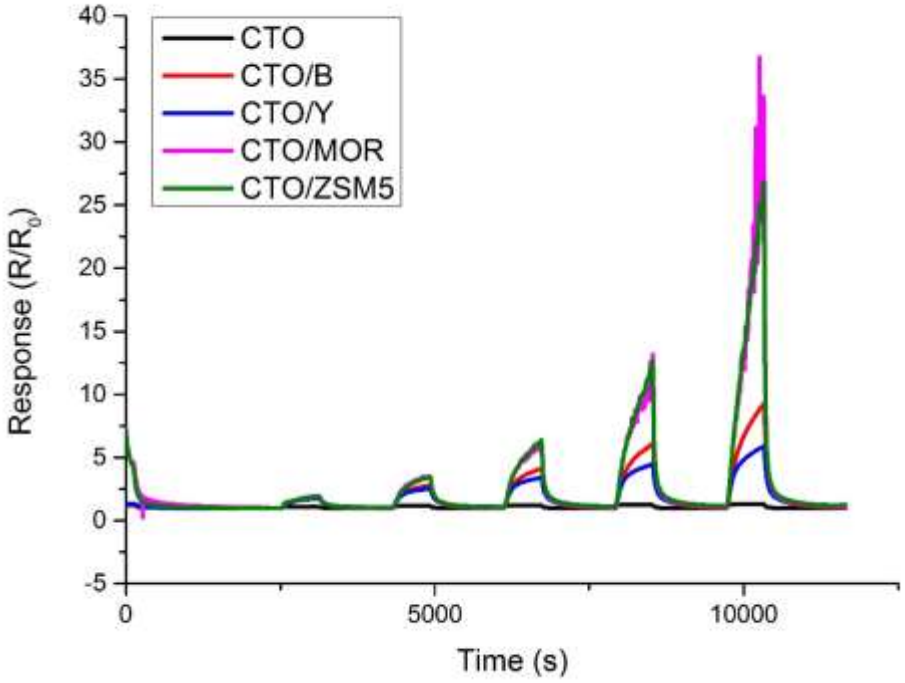

Figure 4.6. CTO based sensors (unmodified CTO and zeolite beta, Y, mordenite and ZSM5 admixtures) response to 5, 10, 20, 40 & 80 ppm ethanol, at an operating temperature of 300°C. Response is calculated as a function of baseline resistance R_0 that is, the sensor resistance in dry air.

The response transient of exposure to ethanol at operating temperatures of 250°C (Fig 4.7) demonstrates considerably larger magnitudes of response in mordenite and ZSM5 modified chromium titanate than in all other sensors. Both mordenite and ZSM5 modified sensors record responses of R/R_0 = 439 and R/R_0 = 462 respectively to pulses of 80 ppm. Only the unmodified chromium titanate sensor reaches a steady state in the

600-second gas pulse, all other sensors display a 'shark-fin' type response. The large response is likely due to reaction at the zeolite surface. Ethanol is well known to dehydrate at the ZSM5 surface to form ethene[195,196]. In addition to this it is likely that side products are formed, especially at lower operating temperatures due to incomplete dehydration of the alcohol at the zeolite surface, potentially resulting in the formation of carbocations, these positively charged ions would react strongly with the negatively charged oxygen ions at the sensor surface, resulting in a large response.

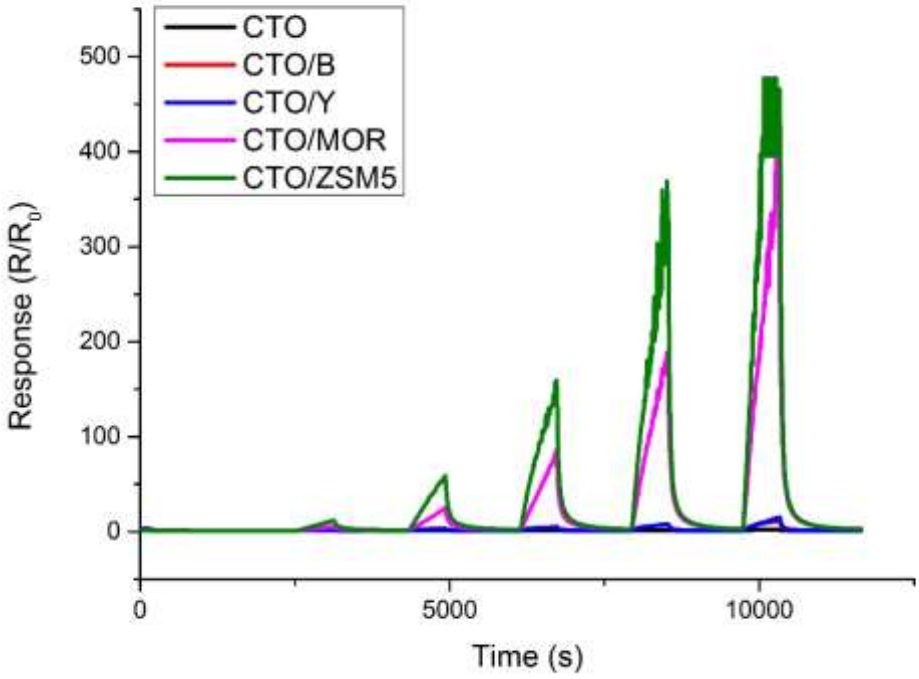

Figure 4.7. CTO based sensors (unmodified CTO and zeolite beta, Y, mordenite and ZSM5 admixtures) response to 5, 10, 20, 40 & 80 ppm ethanol, at an operating temperature of 250°C. Response is calculated as a function of baseline resistance R_0 that is, the sensor resistance in dry air.

Responses of chromium titanate sensors at 250°C, 300°C and 350°C (Fig 4.8) show that as the operating temperature of the sensor decreases, the magnitude of response of the sensor increases dramatically, especially in mordenite and ZSM5 modified chromium titanate sensors. Mordenite modified chromium titanate (R/R_0= 439 at 80 ppm ethanol) and ZSM5 modified chromium titanate (R/R_0= 462 at 80 ppm ethanol) show the largest responses to any gas in this chapter and significantly larger than observed with other materials. This large response combined with the relatively low operating temperatures

(and therefore lower power requirements), make these sensors in particular excellent candidates for electronic noses to detect ethanol. Despite the strong response of zeolite modified chromium titanate, unmodified chromium titanate sensors do not record a response of more than R/R_0=2 (R/R_0=1.3 to 80 ppm at 300°C, R/R_0=1.9 to 80 ppm at 250°C).

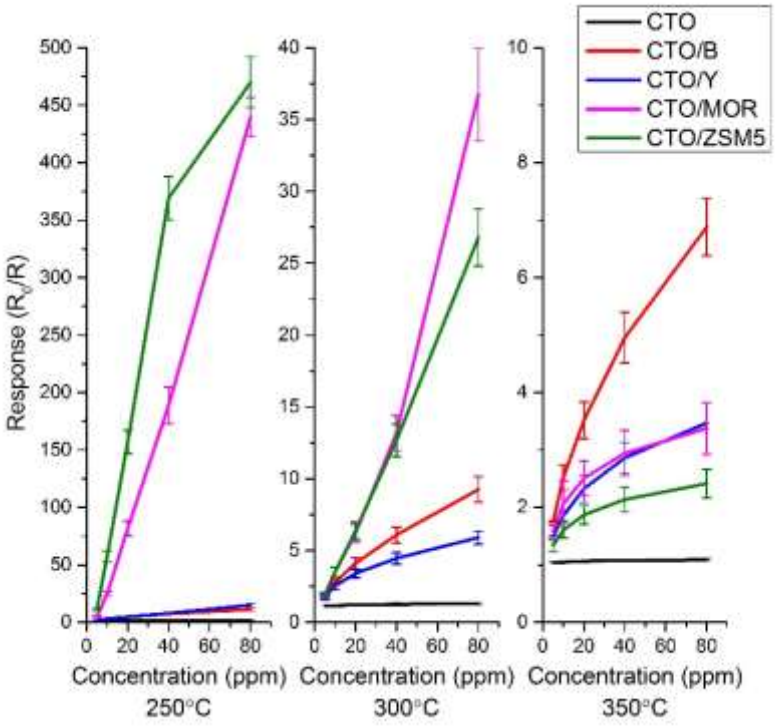

Figure 4.8. Response (± 1 S.D.) of CTO based sensors (unmodified CTO and zeolite beta, Y, mordenite and ZSM5 admixtures) to concentrations of 5-80 ppm ethanol at temperatures of 250°C, 300°C, 350°C. Response is calculated as a function of baseline resistance R_0 that is, the sensor resistance in dry air.

Sensors were exposed to three, 600-second pulses of 20 ppm of ethanol at an operating temperature of 300°C, interspersed with 1200-second dry air intermissions. These repeated concentrations generally show similar orders of magnitudes of response and similar peak shapes. The noisy peaks observed at 350°C of zeolite beta and Y modified chromium titanate are not observed with tests at 300°C and 250°C, indicating that the noise observed is temperature dependant.

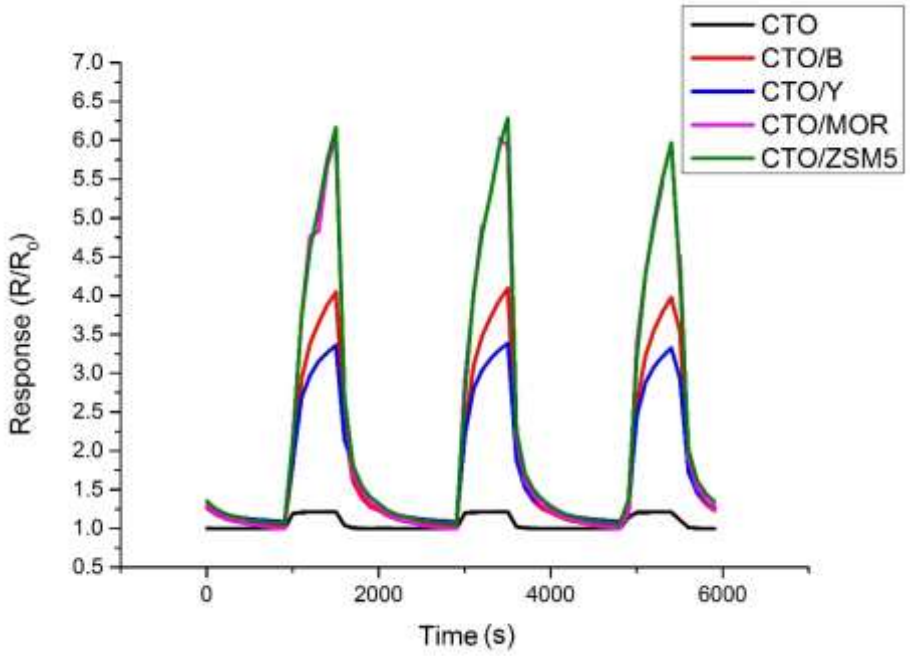

Figure 4.9. Responses of CTO based sensors (unmodified CTO and zeolite beta, Y, mordenite and ZSM5 admixtures) at an operating temperature of 300°C to three consecutive pulses of 20 ppm ethanol. Response is calculated as a function of baseline resistance R_0 that is, the sensor resistance in dry air.

Response times for chromium titanate and zeolite modified chromium titanate sensors on exposure to 80-ppm ethanol (Table 4.5) show a large increase in response times of zeolite modified sensors, compared to the unmodified sensor. This large increase is because a smaller proportion of the surface is gas sensitive; the majority of the surface is made up of chromium titanate grains coated in zeolite material. The target species (ethanol in this case) also adsorbs at the zeolite surface, preventing it from causing a response in the semiconductor material. Of the zeolite materials, zeolites Y and ZSM5 show the longest response times, this agrees with the responses of other sensor material to ethanol (section 3.3.3 and 5.3.3). The longer response time is attributed to strong adsorption of ethanol on these zeolites, as adsorption of the material on the zeolite prevents it from reacting at the chromium titanate grain surface. As temperature increase, the response time decreases, at higher temperatures, materials can react quicker, introducing electrons into the material at a faster rate and so producing a quicker response.

Table 4.5. Response times (± 5 s) for CTO based sensors (Pure CTO plus zeolite beta, Y mordenite and ZSM5 modified sensors) to 80-ppm ethanol.

	Response Time (s, ±5)		
	250°C	**300°C**	**350°C**
CTO	170	60	40
CTO/B	310	290	190
CTO/Y	490	330	110
CTO/MOR	330	320	90
CTO/ZSM5	410	360	170

4.3.3. Response to Nitrogen Dioxide

All zeolite modified and unmodified chromium titanate sensors were exposed to 50, 100, 200, 400 and 800 ppb of nitrogen dioxide. Sensor responses at 350°C (Fig. 4.8) show an interesting response shape, while during the 600 second pulse there is a net decrease in resistance, initially, there is an increase in resistance, that begins to recover and eventually give the expected response. This presents a larger drop in response, with lower concentrations of NO_2. The largest drop is response occurs with 50 ppb NO_2 (an increase of ~15% in resistance). This is likely due to reducing gases caught in the gas-sensing rig, either through adsorption to the walls of the gas lines or trapped in mass flow controllers. Overall, the sensors show relatively weak responses to NO_2 at 350 °C, with the maximum response to 800 ppm being with zeolite Y modified chromium titanate (R_0/R=1.22).

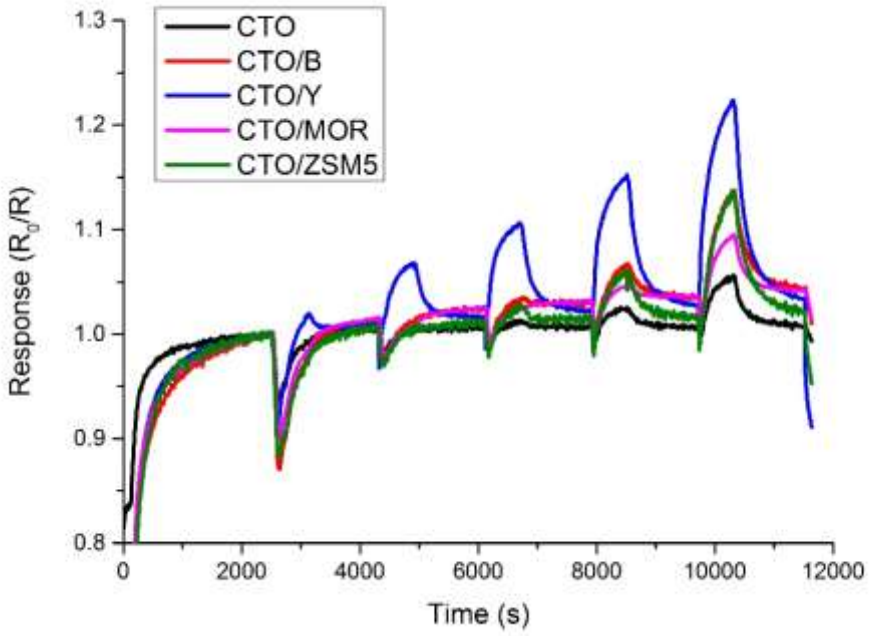

Figure 4.10. Responses of CTO and zeolite beta, zeolite Y, mordenite and ZSM5 modified CTO to pulses of 50, 100, 200, 400 and 800 ppb NO_2 at an operating temperature of 350°C. Response is calculated as a function of baseline resistance R_0 that is, the sensor resistance in dry air.

The responses of chromium titanate and zeolite modified chromium titanate at operating temperatures of 300°C and 250°C (Fig 4.11 and 4.12) to concentrations of nitrogen dioxide are generally poor, with all sensors displaying a response only at 800 ppb. At an operating temperature of 300°C, there is significant drift from baseline throughout the experiment, only the unmodified chromium titanate sensor maintains a stable baseline. This may be a result of influence from the zeolite, either electrically or chemically influencing the sensor response.

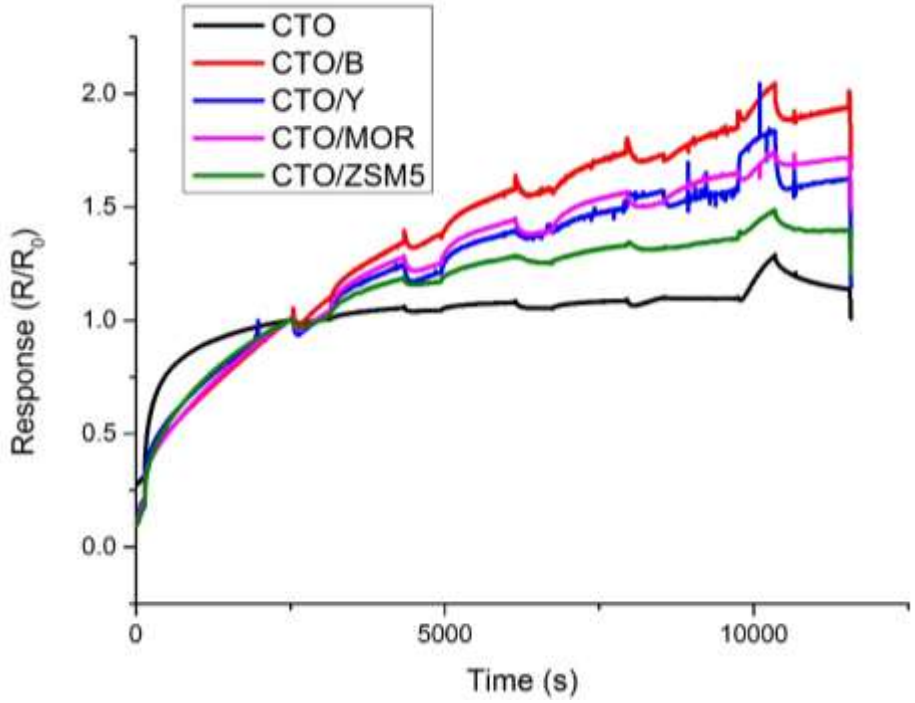

Figure 4.11. CTO based sensors (unmodified CTO and zeolite beta, Y, mordenite and ZSM5 admixtures) response to 5, 10, 20, 40 & 80 ppm ethanol, at an operating temperature of 300°C. Response is calculated as a function of baseline resistance R_0 that is, the sensor resistance in dry air.

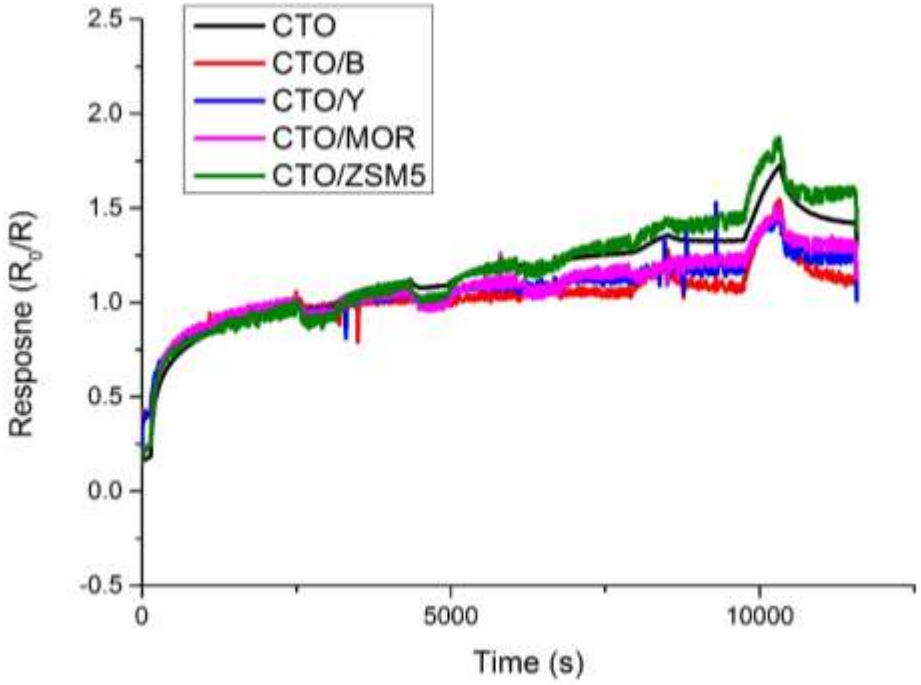

Figure 4.12. CTO based sensors (unmodified CTO and zeolite beta, Y, mordenite and ZSM5 admixtures) response to 5, 10, 20, 40 & 80 ppm ethanol, at an operating temperature of 250°C. Response is calculated as a function of baseline resistance R_0 that is, the sensor resistance in dry air.

The maximum response to NO_2 (Fig. 4.13) shows poor responses ($R_0/R < 2.1$) for all sensors in the presence of the gas. The largest responses were found to be zeolite beta and Y modified chromium titanate ($R_0/R= 2.04$ in both cases). The largest responses for zeolite beta, Y and mordenite modified chromium titanate were found at 300°C, while for unmodified chromium titanate and ZSM5 modified chromium titanate were observed at 250°C. The oxidising nature and therefore opposite response of NO_2 sensors compared to other gases used in this chapter mean that most sensors can achieve some level of selectivity to nitrogen dioxide. The unique peak shape and resistance change means that these responses are easily identifiable as evidence of nitrogen dioxide in the atmosphere. All zeolite modified chromium titanate sensors show an enhancement over unmodified chromium titanate at operating temperatures of 350°C and 300°C. When sensors are operating at 250°C, zeolite beta and ZSM5 modified chromium titanate show an enhancement over unmodified chromium titanate, however, zeolite Y and mordenite show a decrease in responsiveness relative to pure chromium titanate.

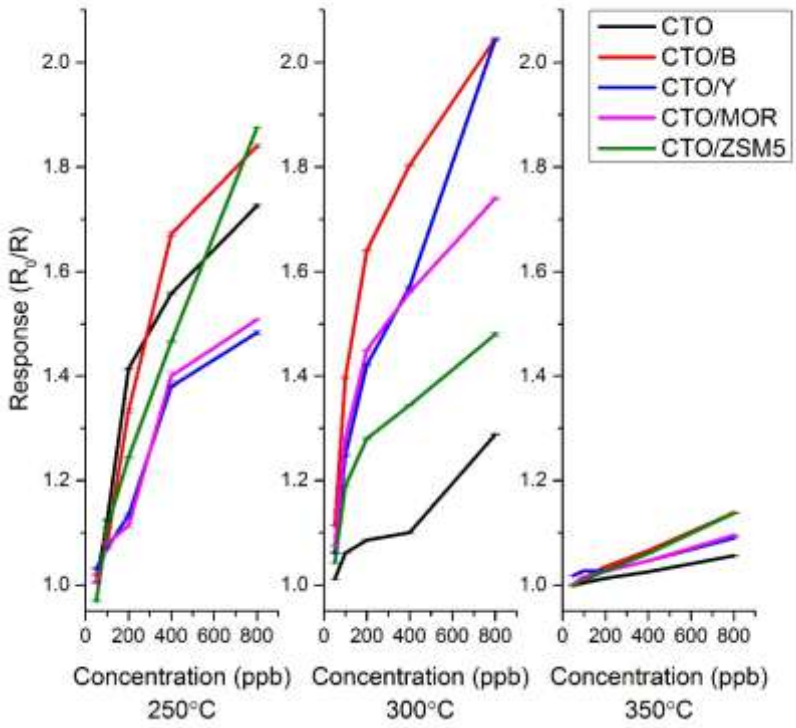

Figure 4.13. Response (± 1 S.D.) of CTO based sensors (unmodified CTO and zeolite beta, Y, mordenite and ZSM5 admixtures) to concentrations of 50-800 ppb nitrogen dioxide at temperatures of 250°C, 300°C, 350°C. Response is calculated as a function of baseline resistance R_0 that is, the sensor resistance in dry air.

4.3.4. Response to Toluene

Chromium titanate and zeolite modified chromium titanate sensors were exposed to 2.5, 5, 10, 20 and 40 ppm of toluene. The responses at 350°C (Fig. 4.14) show strong responses to toluene and considerable enhancements in the responsiveness of zeolite modified sensors when compared to the unmodified chromium titanate. None of the zeolite-modified sensors achieve an equilibrium response in the 600-second gas pulse. With the exception of ZSM5 modified chromium titanate, all sensors have a good recovery following each gas pulse. The ZSM5 modified chromium titanate sensor experiences a considerably longer recovery time following each gas pulse, compared to all other samples, this is related to the strong toluene adsorption properties of H-ZSM5[197] which prevents toluene molecules from leaving the material pores and oxygen from reabsorbing fully at the surface. Analysis of exhaust gas on exposure of toluene to zeolite modified zinc oxide (section 3.7) demonstrated that on exposure to zeolite modified sensors, toluene broke down into its constituent hydrocarbons, leading to an enhancement in response, this is also observed with zeolite modified chromium titanate at an operating temperature of 350°C.

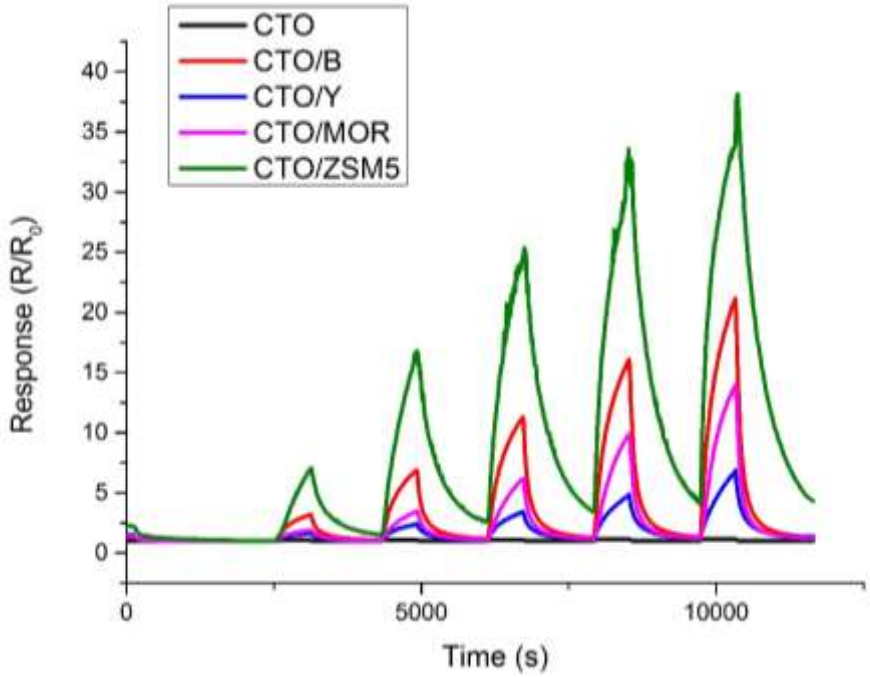

Figure 4.14 Response of CTO based sensors (unmodified CTO and zeolite beta, Y, mordenite and ZSM5 admixtures) to concentrations of 2.5, 5, 10, 20 and 40 ppm toluene at an operating temperature of 350°C. Response is calculated as a function of baseline resistance R_0 that is, the sensor resistance in dry air.

At an operating temperature of 300°C, chromium titanate and zeolite modified chromium titanate sensors are found to be more responsive to toluene than at other operating temperatures (Fig 4.15). The largest response is observed with zeolite beta (R/R_0 = 81.3 to 40 ppm). The response of zeolite Y modified chromium titanate is similar to responses observed with ZnO based sensors on exposure to toluene (Section 3.3.5), where an initial increase in response is followed quickly by a decrease. This response indicates the influence of zeolite-catalysed reactions occurring within the sensor material and potentially producing hydrocarbons, which are less reactive at the sensor surface than toluene. In this experiment, it is the zeolite Y modified CTO sensor that shows this response, whereas at 400°C and 500°C the mordenite modified ZnO sensor shows this peak shape on exposure to toluene (Figs 3.19 and 3.20).

The zeolite beta, Y and ZSM5 modified CTO sensors demonstrated poor recovery to baseline following exposure to toluene. Mordenite modified and unmodified chromium titanate sensors recover fully after exposure to toluene, however the mordenite modified sensor undergoes a slower recovery.

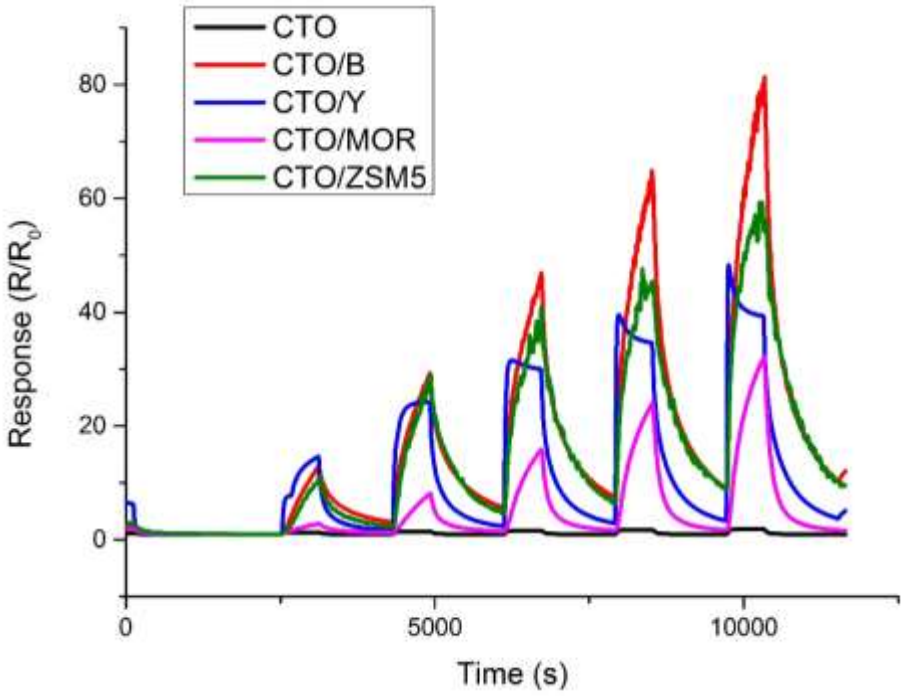

Figure 4.15. Response of CTO based sensors (unmodified CTO and zeolite beta, Y, mordenite and ZSM5 admixtures) to concentrations of 2.5, 5, 10, 20 and 40 ppm toluene at an operating temperature of 300°C. Response is calculated as a function of baseline resistance R_0 that is, the sensor resistance in dry air.

Mordenite modified chromium titanate sensors, when exposed to toluene at an operating temperature of 250°C (Fig 4.16), demonstrated enhanced responsiveness compared with all other sensors in the experiment. This large enhancement may be due to the monodirectional pore structure of the zeolite, which allows the relatively large toluene molecule to travel in and out of the zeolite on a single plane, whereas in other zeolites with three-dimensional pore structures, there is a greater chance of analyte gases being 'trapped' in the zeolite network. It has already been demonstrated that toluene undergoes acid catalysed breakdown at the zeolite surface resulting in a larger magnitude of response (Section 3.7). All zeolite-modified chromium titanate sensors undergo a poor recovery back to baseline following a gas pulse. This is potentially due toluene molecules trapped in the zeolite material reacting at the sensor surface.

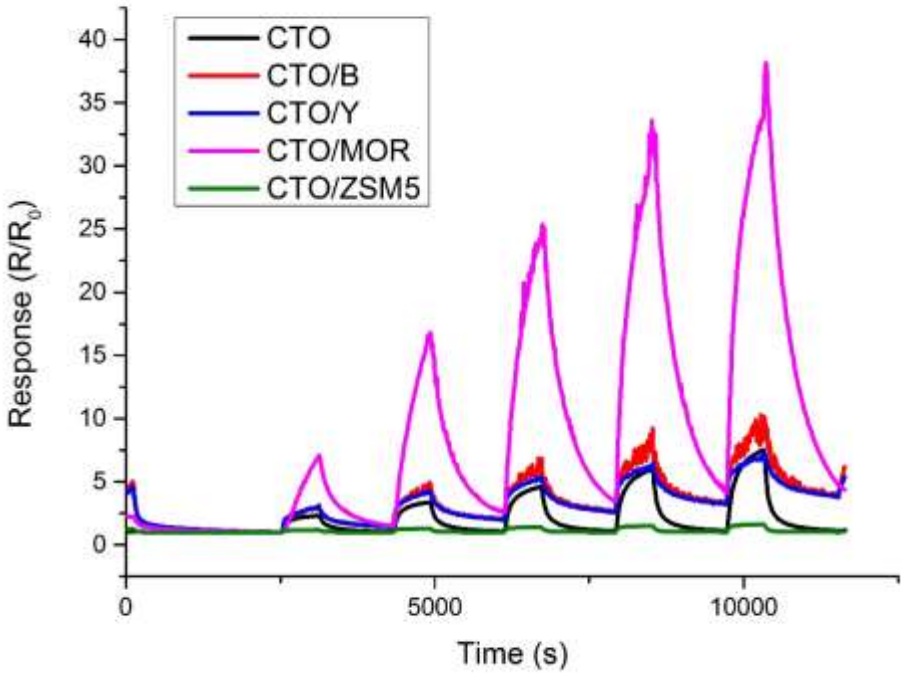

Figure 4.16. Response of CTO based sensors (unmodified CTO and zeolite beta, Y, mordenite and ZSM5 admixtures) to concentrations of 2.5, 5, 10, 20 and 40 ppm toluene at an operating temperature of 250°C. Response is calculated as a function of baseline resistance R_0 that is, the sensor resistance in dry air.

Response to toluene at all operating temperatures (Fig. 4.17) is poor for unmodified chromium titanate. The zeolite modified chromium titanate sensors all show strong responses at 250°C, 300°C and 350°C. The strongest responses for all sensors (with the

exception of mordenite modified chromium titanate) are observed at an operating temperature of 300°C. Mordenite modified chromium titanate has its largest magnitude of response to toluene at 250°C. At higher operating temperatures, mordenite is found to successfully break down toluene molecules into its constituent hydrocarbon chains (section 3.7), which is likely to occur at an operating temperature of 250°C as well.

The largest magnitude of response at any temperature is found with zeolite beta modified chromium titanate, with R/R_0 = 81.3 to 40 ppm toluene. ZSM5 and zeolite Y modified chromium titanate also show strong responsiveness to toluene at 300°C with R/R_0 > 45 to 40 ppm toluene.

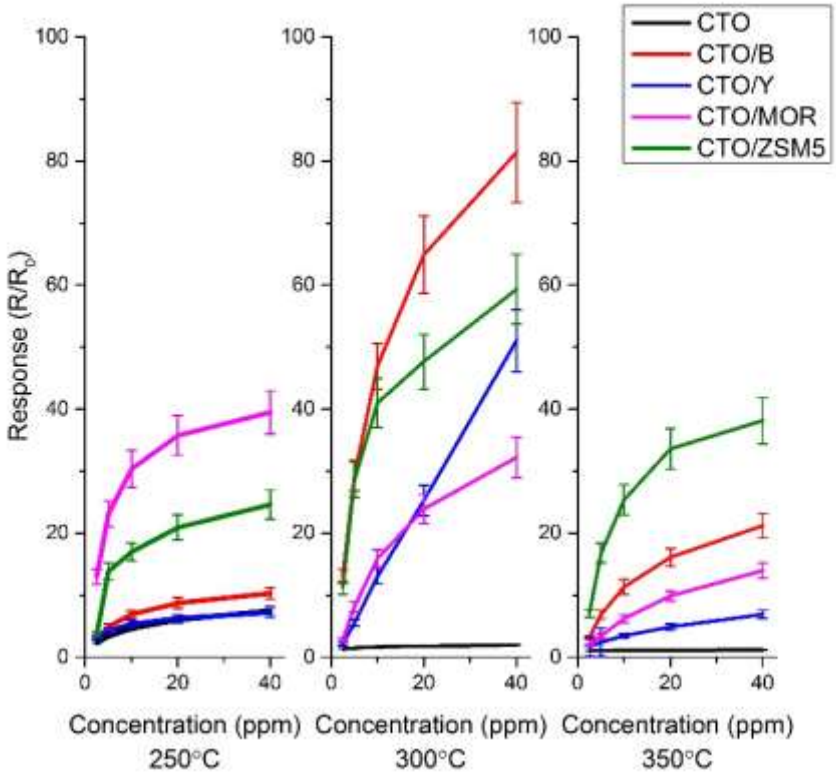

Figure 4.17. Response (± 1 S.D.) of CTO based sensors (unmodified CTO and zeolite beta, Y, mordenite and ZSM5 admixtures) to concentrations of 2.5-40 ppm toluene at temperatures of 250°C, 300°C, 350°C. Response is calculated as a function of baseline resistance R_0 that is, the sensor resistance in dry air.

The response times on exposure to toluene (table 4.6) are longer than that observed upon exposure to other gases, especially at 250°C, where the response time of all sensors is at least 4 minutes. The unmodified chromium titanate sensor shows faster

response times at 300°C and 350°C, while ZSM5 demonstrates the longest response time at all operating temperatures. ZSM5 has been shown to catalyse many different reactions with toluene, due to its strong and shape selective adsorption[198,199]. This strong adsorption prevents toluene gas molecules from adsorbing at the chromium titanate surface. However, it is likely that this adsorption is partly responsible for the considerably larger magnitude of response compared to the unmodified chromium titanate material.

Table 4.6. Response times (± 5 s) for CTO based sensors (unmodified CTO and zeolite beta, Y, mordenite and ZSM5 admixtures) to 40-ppm toluene.

	Response Time (s, ±5)		
	250°C	**300°C**	**350°C**
CTO	370	110	70
CTO/B	410	350	340
CTO/Y	240	240	210
CTO/MOR	290	240	210
CTO/ZSM5	420	380	370

4.3.5. Response to Acetone

All chromium titanate and zeolite modified chromium titanate sensors were exposed to 0.5, 1, 2, 4 and 8 ppm of acetone at operating temperatures of 250°C, 300°C and 350°C. Responses of all sensors at 350°C (Fig 4.18) are generally poor, with all responses below R/R_0 = 1.3. All zeolite-modified materials show an enhancement in response when compared with the unmodified material, the most responsive sensors were found to be ZSM5 and zeolite Y modified chromium titanate, with almost identical responses of R/R_0 ≈ 1.3. The zeolite Y modified sensor shows a nosier response than the ZSM5 counterpart.

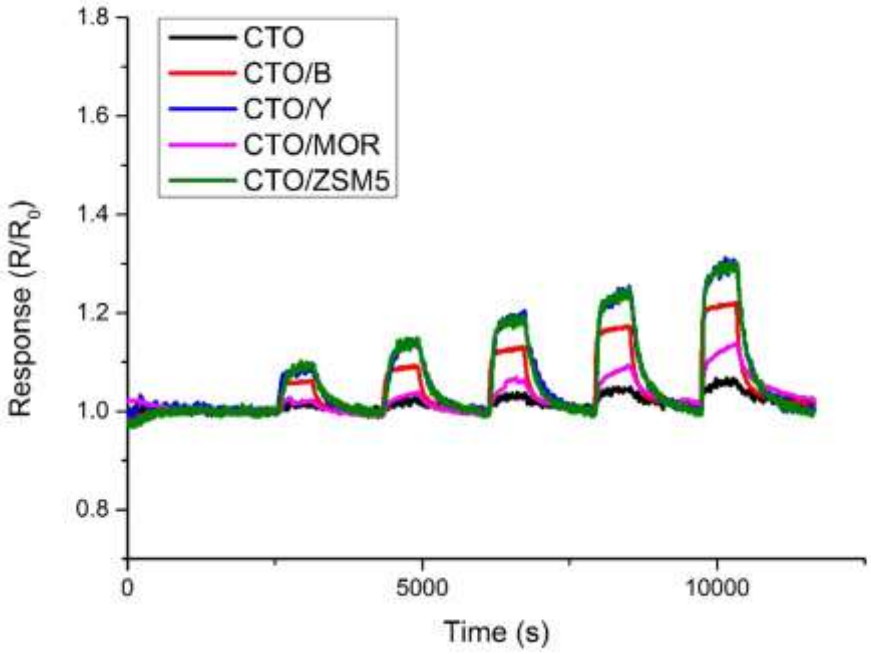

Figure 4.18. Response of CTO based sensors (unmodified CTO and zeolite beta, Y, mordenite and ZSM5 admixtures) to concentrations of 0.5, 1, 2, 4 and 8 ppm acetone at an operating temperature of 350°C. Response is calculated as a function of baseline resistance R_0 that is, the sensor resistance in dry air.

At an operating temperature of 300°C (Fig 4.19) chromium titanate and chromium titanate modified sensors are found to be more responsive to higher concentrations (≥ 2 ppm) of acetone, however are unresponsive to 0.5 ppm. The response of zeolite beta modified chromium titanate shows the largest response to acetone (R/R_0 =3.8 to 8 ppm acetone). All sensors undergo a poor recovery following a gas pulse.

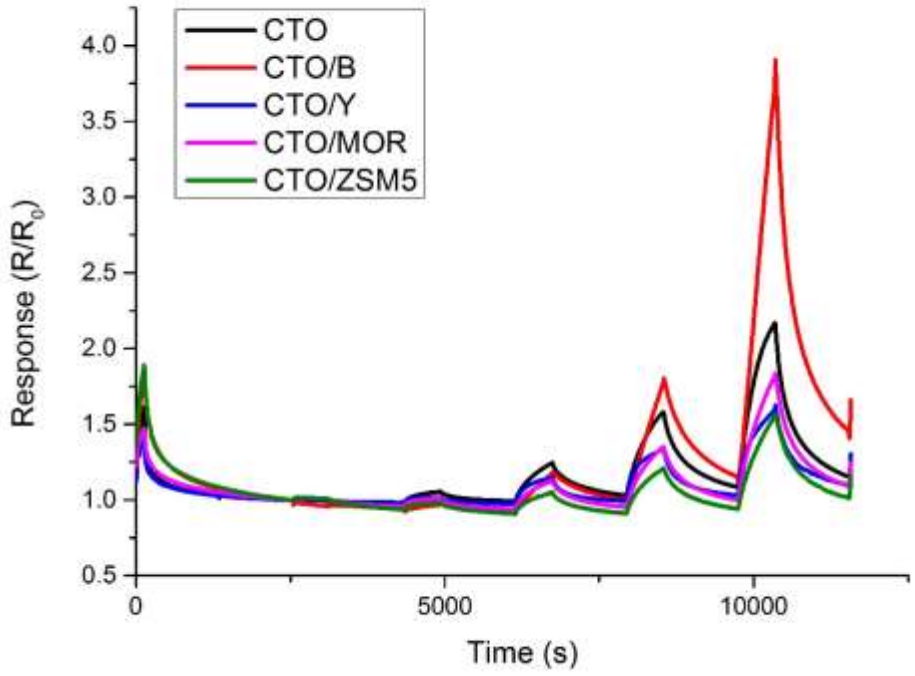

Figure 4.19. Response of CTO based sensors (unmodified CTO and zeolite beta, Y, mordenite and ZSM5 admixtures) to concentrations of 0.5, 1, 2, 4 and 8 ppm acetone at an operating temperature of 300°C. Response is calculated as a function of baseline resistance R_0 that is, the sensor resistance in dry air.

At an operating temperature of 250°C (Fig 4.20) the zeolite beta modified CTO sensor shows a large magnitude of response to acetone (R/R_0 = 43.1 to 8 ppm). This response is however, very noisy and would not be stable over a long period of time. All other chromium titanate based sensors show responses lower in magnitude, with the mordenite modified CTO sensors response to acetone of R/R_0 = 8.1 to 8 ppm. The responses of chromium titanate and zeolite Y, mordenite and ZSM5 are smoother and less noisy than the zeolite beta modified chromium titanate.

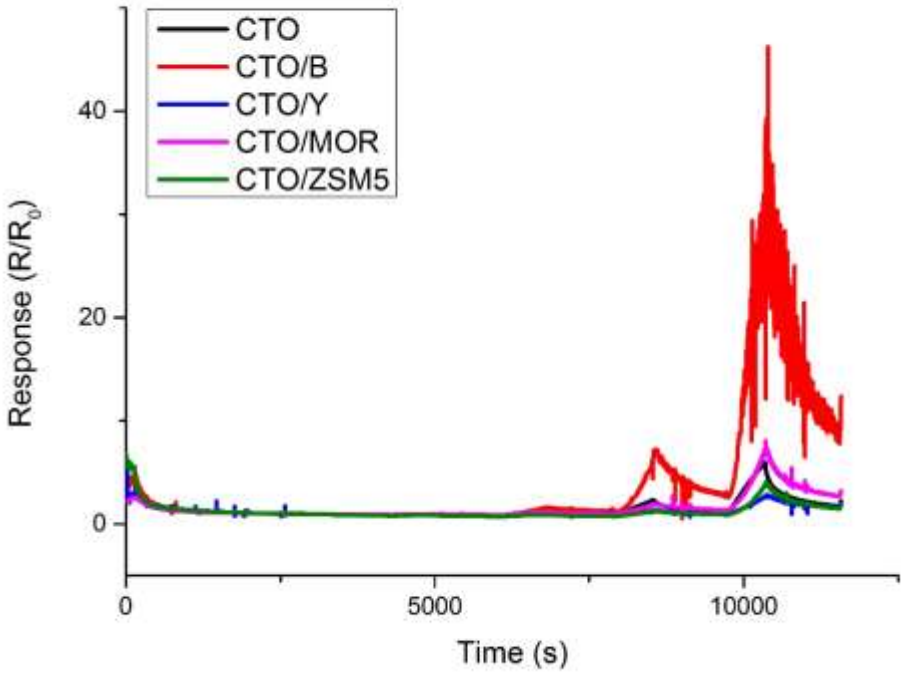

Figure 4.20. Response of CTO based sensors (unmodified CTO and zeolite beta, Y, mordenite and ZSM5 admixtures) to concentrations of 0.5, 1, 2, 4 and 8 ppm acetone at an operating temperature of 250°C. Response is calculated as a function of baseline resistance R_0 that is, the sensor resistance in dry air.

The response of chromium titanate and zeolite beta, Y, mordenite and ZSM5 modified sensors increases dramatically as the operating temperature decreases. The responses to acetone at all operating temperatures (Fig 4.21) are largest in magnitude at 250°C, the magnitude of response for zeolite beta modified chromium titanate is significantly larger than that of other sensors.

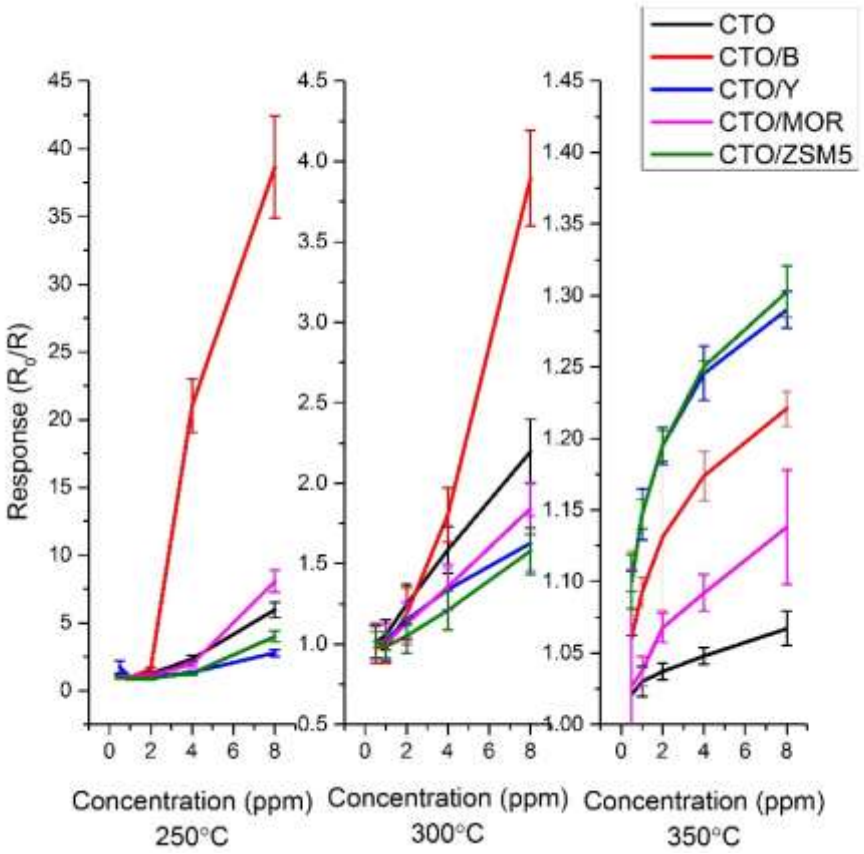

Figure 4.21. Response (± 1 S.D.) of CTO based sensors (unmodified CTO and zeolite beta, Y, mordenite and ZSM5 admixtures) to concentrations of 0.5-8 ppm acetone at temperatures of 250°C, 300°C, 350°C. Response is calculated as a function of baseline resistance R_0 that is, the sensor resistance in dry air.

Table 4.9. Response times (± 5 s) for CTO based sensors (unmodified CTO and zeolite beta, Y, mordenite and ZSM5 admixtures) to 8-ppm acetone.

	Response Time (s, ±5)		
	250°C	**300°C**	**350°C**
CTO	360	150	90
CTO/B	510	500	470
CTO/Y	380	230	180
CTO/MOR	460	390	340
CTO/ZSM5	380	320	270

4.3.6. Response to Ammonia

Chromium titanate and zeolite modified chromium titanate sensors displayed resistive responses on exposure to ammonia gas. Sensors were exposed to 2.5, 5, 10, 20 and 40 ppm ammonia at 250°C, 300°C and 350°C. Responses at 350°C (Fig. 4.22) show enhancements when compared to unmodified sensor, in zeolite beta, Y and ZSM5 modified sensors. The mordenite modified chromium titanate sensor shows a smaller magnitude of response than the unmodified sensor. The largest magnitude of response is observed in ZSM5 modified chromium titanate (R/R_0 = 2.63 to 40 ppm), with zeolite beta also showing a strong response (R/R_0 = 2.50 to 40 ppm). The peak shapes of all responses are free from noise and approach equilibrium in the 600 second gas pulse. All sensors recover to within 10% of their original baseline, with ZSM5 and zeolite beta showing slightly poorer recoveries than the three other modified sensors. Zeolite beta and ZSM5 have similar pore sizes (~6 Å); the similar enhancement in response may be due to adsorption or reaction at the surface, leading to the liberation of more electrons at the surface.

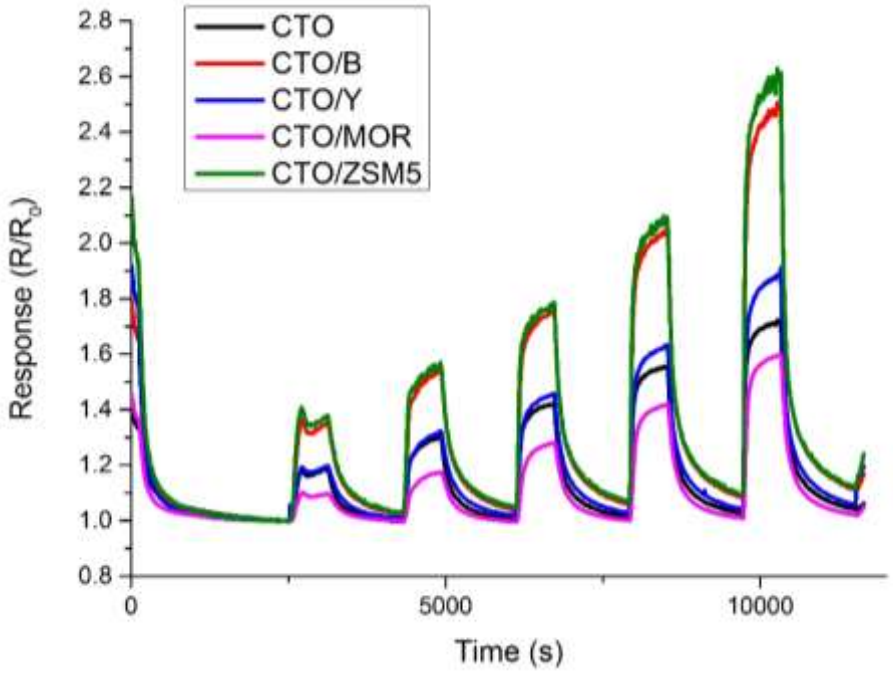

Figure 4.22. Response of CTO based sensors (unmodified CTO and zeolite beta, Y, mordenite and ZSM5 admixtures) to 2.5, 5, 10, 20 & 40 ppm ammonia, at an operating temperature of 350°C. Response is calculated as a function of baseline resistance R_0 that is, the sensor resistance in dry air.

The response transient of chromium titanate based sensors upon exposure to ammonia at 300°C (Fig 4.23) once again show significantly larger magnitudes of response in zeolite beta and ZSM5 modified chromium titanate sensors than all other sensors. All zeolite-modified sensors show enhancements in responsivity compared to the unmodified chromium titanate sensor.

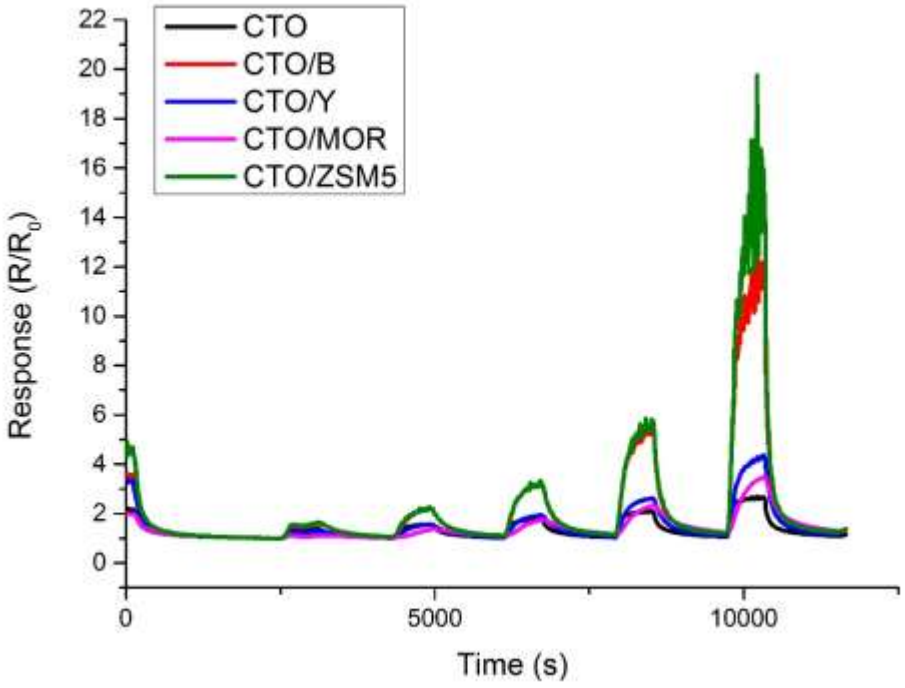

Figure 4.23. Response of CTO based sensors (unmodified CTO and zeolite beta, Y, mordenite and ZSM5 admixtures) to 2.5, 5, 10, 20 & 40 ppm ammonia, at an operating temperature of 300°C. Response is calculated as a function of baseline resistance R_0 that is, the sensor resistance in dry air.

At an operating temperature of 250°C (Fig 4.24), ZSM5 modified chromium titanate is shown to be the most responsive sensor to concentrations of ammonia above 5 ppm (R/R_0 = 8.4 to 40 ppm ammonia). Mordenite modified CTO is shown to be less responsive than the unmodified sensor on exposure to all concentrations of ammonia. All zeolite modified CTO sensors experience a slow response and a poor recovery back to baseline following each gas pulse.

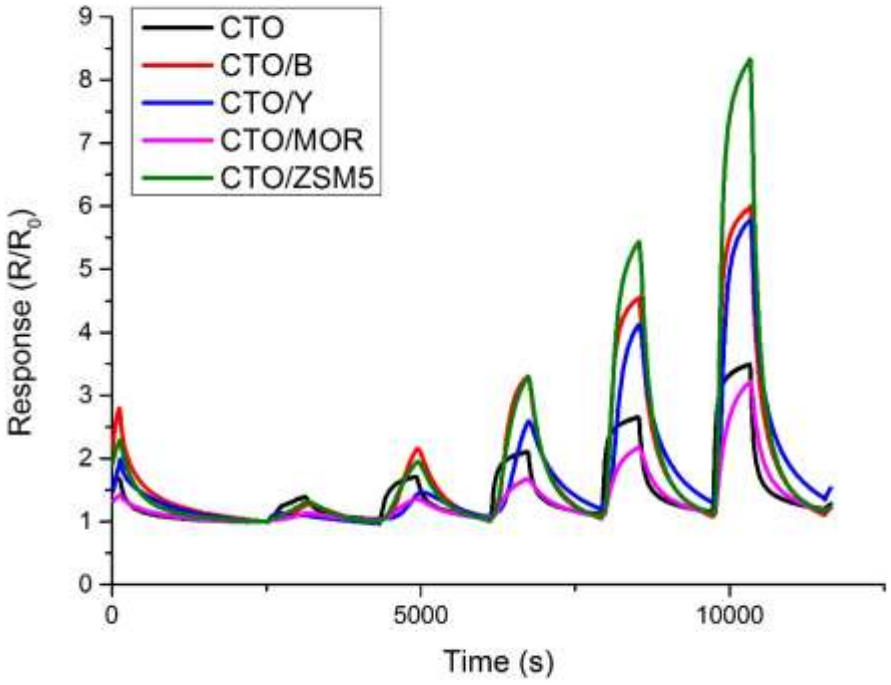

Figure 4.24. Response of CTO based sensors (unmodified CTO and zeolite beta, Y, mordenite and ZSM5 admixtures) to 2.5, 5, 10, 20 & 40 ppm ammonia, at an operating temperature of 250°C. Response is calculated as a function of baseline resistance R_0 that is, the sensor resistance in dry air.

Responses to all sensors to ammonia at 250°C, 300°C and 350°C (Fig. 4.25) show the largest responses in ZSM5 and zeolite beta modified chromium titanate, while all other sensors demonstrate a larger response at 250°C. At all temperatures, ZSM5 demonstrated the largest magnitude of response, with the largest response of R/R_0 = 19.75 to 40 ppm ammonia at an operating temperature of 300°C. At 350°C and 250°C unmodified chromium titanate shows slightly larger magnitudes of response than mordenite modified chromium titanate. All other zeolite-modified sensors demonstrate larger magnitudes of response than the unmodified sensor. At the zeolite surface, ammonia may potentially be broken down to nitrogen gas (N_2) an unreactive gas and hydrogen gas H_2, this reaction occurs at a greater rate under the acidic condition of the zeolites via the following reaction.

$$2NH_3 \rightarrow N_2 + 3H_2$$

At the gas sensitive surface, hydrogen gas, H_2, would react to form water H_2O, this reaction would likely take place at a greater rate than the oxidation of ammonia and therefore result in a larger magnitude of response, as observed with several of the zeolite modified sensors.

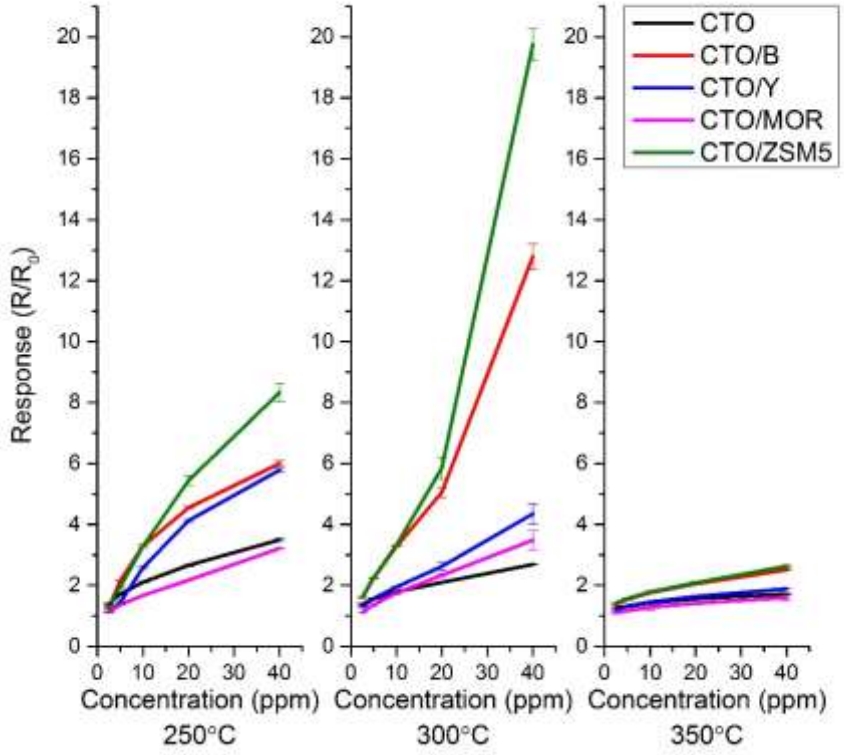

Figure 4.25. Response (± 1 S.D.) of CTO based sensors (unmodified CTO and zeolite beta, Y, mordenite and ZSM5 admixtures) to concentrations of 2.5-40 ppm ammonia at temperatures of 250°C, 300°C, 350°C. Response is calculated as a function of baseline resistance R_0 that is, the sensor resistance in dry air.

The response times for all chromium titanate sensors on exposure to 40-ppm ammonia is shown in Table 4.7. In all cases, zeolite modified sensors have longer response times that the unmodified chromium titanate. The longest response time observed was with mordenite modified chromium titanate, despite its small magnitude of response. Response time decreases with increasing temperature in all cases.

Table 4.7 Response times (± 5 s) for CTO based sensors (unmodified CTO and zeolite beta, Y, mordenite and ZSM5 admixtures) to 40-ppm ammonia

	Response Time (s, ±5)		
	250°C	**300°C**	**350°C**
CTO	180	140	90
CTO/B	260	230	220
CTO/Y	330	330	120
CTO/MOR	400	380	130
CTO/ZSM5	300	210	100

4.3.7. Responses to Humidity

Sensors were exposed to a 1200-second pulse of RH = 50% (Fig. 4.26). This pulse shows the resistance in all sensors increasing and establishing a new baseline at a higher resistance on exposure to humid air. The reason for this is that the oxygen atom in water molecules is less electronegative than that of an adsorbed oxygen ion at the sensor surface. Therefore, the ability of an adsorbed water molecule to attract electrons from the sensor, to form a hole accumulation later, is slightly less than that of a single adsorbed oxygen ion.

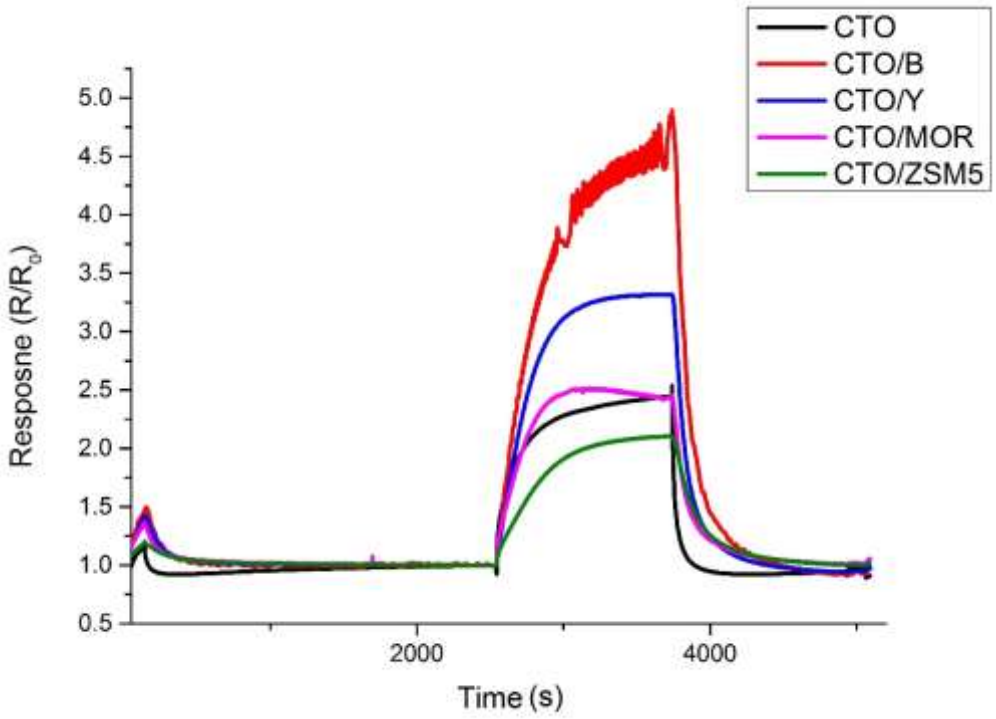

Figure 4.26. Response of CTO based sensors (unmodified CTO and zeolite beta, Y, mordenite and ZSM5 modified CTO) to a 600-second pulse of humid air (RH=50%). Response is calculated as a function of baseline resistance R_0 that is, the sensor resistance in dry air.

Change in humidity at 250°C, 300°C and 350°C (Fig 4.27) show that in unmodified chromium titanate and zeolite beta, Y and mordenite modified chromium titanate, there is a decrease in the influence of humidity with decreasing temperature. The ZSM5 modified chromium titanate sensor shows the opposite behaviour to the other sensors, by showing a larger response to a change in humidity at a lower operating temperature.

At 250°C unmodified chromium titanate, zeolite Y and mordenite modified chromium titanate show little response to the change in humidity. As the temperature increases, mordenite and unmodified chromium titanate continue to behave in similar manner with the introduction of humid air.

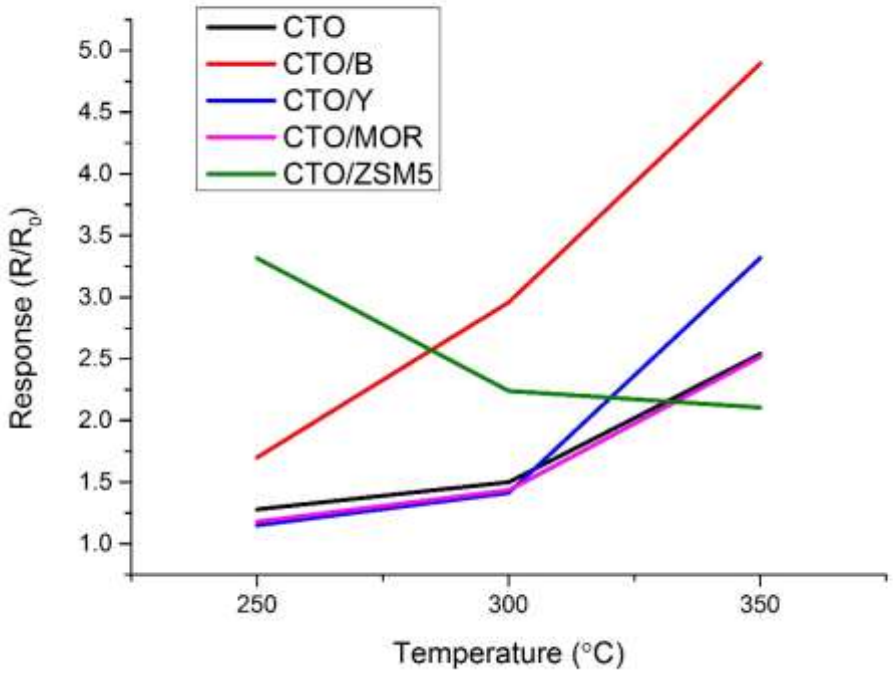

Figure 4.27. Change on response of CTO and zeolite modified CTO (zeolite beta, Y, mordenite and ZSM5) when exposed to humid air (RH= 50%) at 250°C, 300°C and 250°C. Response is calculated as a function of baseline resistance R_0 that is, the sensor resistance in dry air.

To assess the change in response when in a humid environment, sensors were exposed to two 600-second pulses of 50-ppm ethanol in dry air, after which relative humidity was increased to 50% and sensors were again subjected to two pulses of 50-ppm ethanol. The pulses in dry air are as expected in accordance with Fig. 4.4. When sensors are exposed to humidity, resistance increases and establishes a steady response. On exposure to ethanol, responses with similar peak shapes are observed, though in Fig. 4.18, these responses may appear larger in magnitude than in dry air, when R_0 is calculated in humid air, the responses are comparable between the two atmospheric conditions (Table 4.8).

Table 4.8. Responses of CTO and zeolite beta, Y, mordenite and ZSM5 modified CTO to 50 ppm ethanol at operating temperatures of 300°C and 250°C, in dry and humid air.

	Response (300°C)		Response (350°C)	
	RH=0%	RH=50%	RH=0%	RH=50%
CTO	1.09	1.04	1.06	1.02
CTO/B	5.28	4.35	5.13	4.70
CTO/Y	2.06	1.64	2.86	3.20
CTO/MOR	27.7	19.5	2.24	2.82
CTO/ZSM5	17.05	13.21	2.15	2.34

In many cases, the response observed in humid conditions is smaller in magnitude than in dry air. The reason for this is likely because water molecules occupy sites at the sensor surface, preventing reactions between the target gas and charged oxygen particles at the surface.

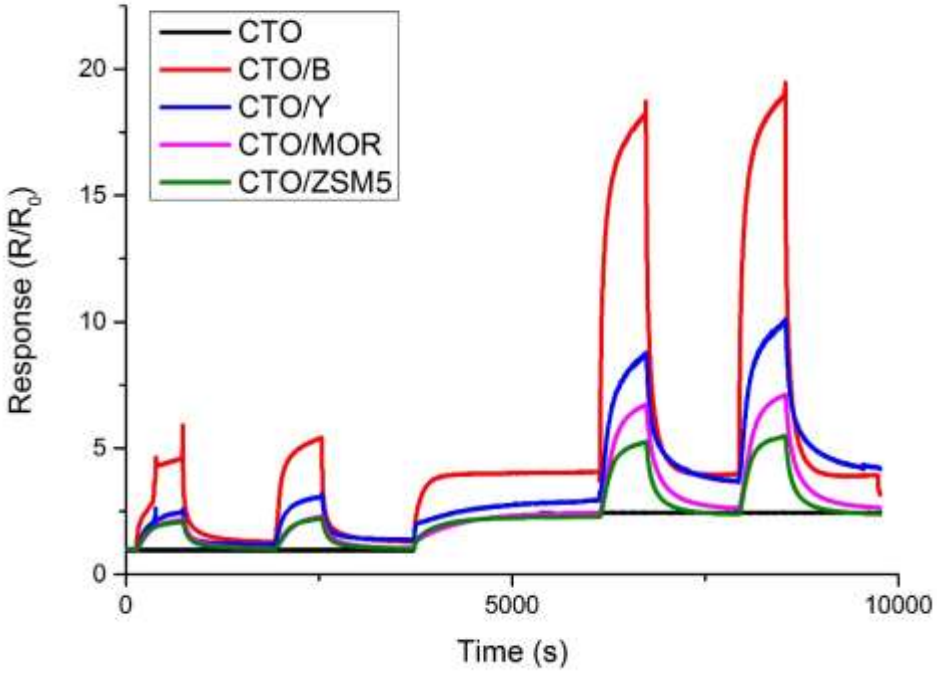

Figure 4.28. Response of pure CTO and zeolite beta, zeolite Y, mordenite and ZSM5 modified CTO to 50 ppm ethanol at 350°C in dry air and wet air (RH = 50%). Response is calculated as a function of baseline resistance R_0 that is, the sensor resistance in dry air.

4.3.8. Reactions to Multiple Gases

All chromium titanate and zeolite modified chromium titanate were exposed to mixtures of ethanol and ammonia. Sensors were exposed to 600 second alternating pulses of air and gas. Mixtures can be seen in table 4.9.

Table 4.9. Mixtures of ethanol and acetone exposed to CTO and zeolite modified CTO sensors.

Ethanol (ppm)	Ammonia (ppm)
80	0
60	20
40	40
20	60
0	80

The response to gas mixtures at 350°C (Fig. 4.29) shows the magnitude of response is in most cases between the responses for 80 ppm of pure ethanol and ammonia. This suggests that ammonia and ethanol compete for reaction 'space' at the sensor surface and reach equilibrium between the two species. It is interesting to note changes in the peak shape as well as the signal to noise ratio throughout the experiment, this may be due to the competing adsorption of the two gases, or reactions resulting in new compounds, such as amines or amides, having different adsorption properties than either ethanol or ammonia.

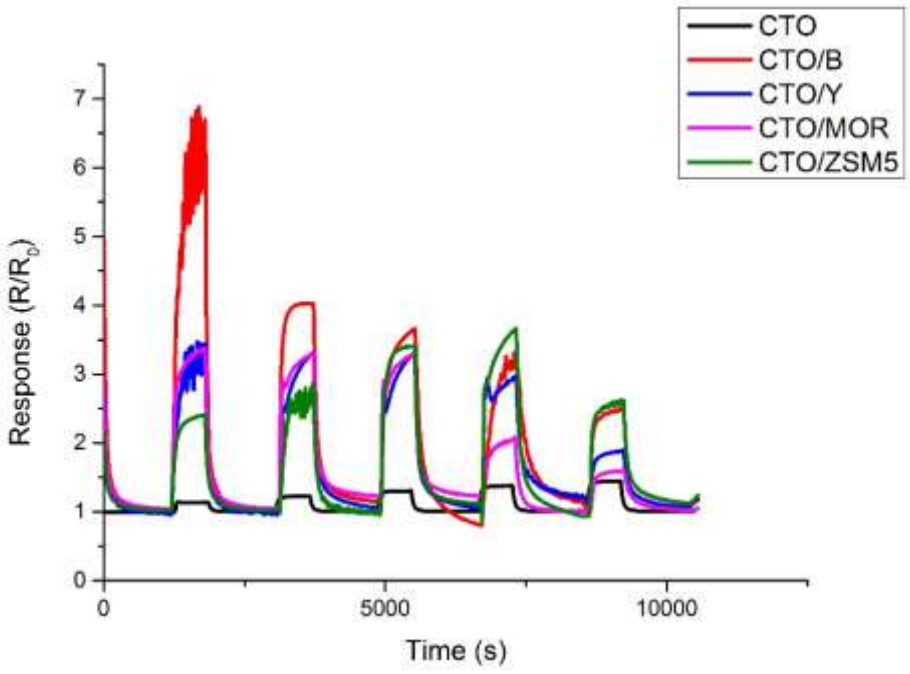

Figure 4.29. Maximum response of CTO and zeolite beta, Y, mordenite and ZSM5 modified CTO to pulses of 80 ppm ethanol, 60 ppm ethanol and 20 ppm ammonia, 40 ppm of both ethanol and ammonia, 40 ppm ethanol and 60 ppm ammonia and 80 ppm ammonia at an operating temperature of 350°C. Response is calculated as a function of baseline resistance R_0 that is, the sensor resistance in dry air.

The responses for mixed gas testing at 300°C (Fig. 4.31) show that the ZSM5 modified sensor demonstrates an enhancement in the multiple gas pulses, this implies that ethanol and ammonia react at the zeolite surface, producing a material (or materials) that produce a larger response in the chromium titanate sensor than either ethanol of ammonia on their own.

Such reactions have been identified by van der Gaag *et.al.*[200] who identified at temperatures between 600-650 K, that a range of gases including; ethane, diethyl ether, acetic aldehyde, ethylamine, pyridine and carbon dioxide can be produced through reactions between ethanol and ammonia. The production of such species this can contribute to an enhanced response.

Breakdown reactions (as proposed by van der Gaag[200]) that may occur at the zeolite surface are detailed in figure 4.30, and show that while ammonia and ethanol molecules

may react to form pyridines at the zeolite surface, an entire range of molecules can potentially form which may be more reactive, such as acetonitrile, ethanoic acid and ethyl ethanoate.

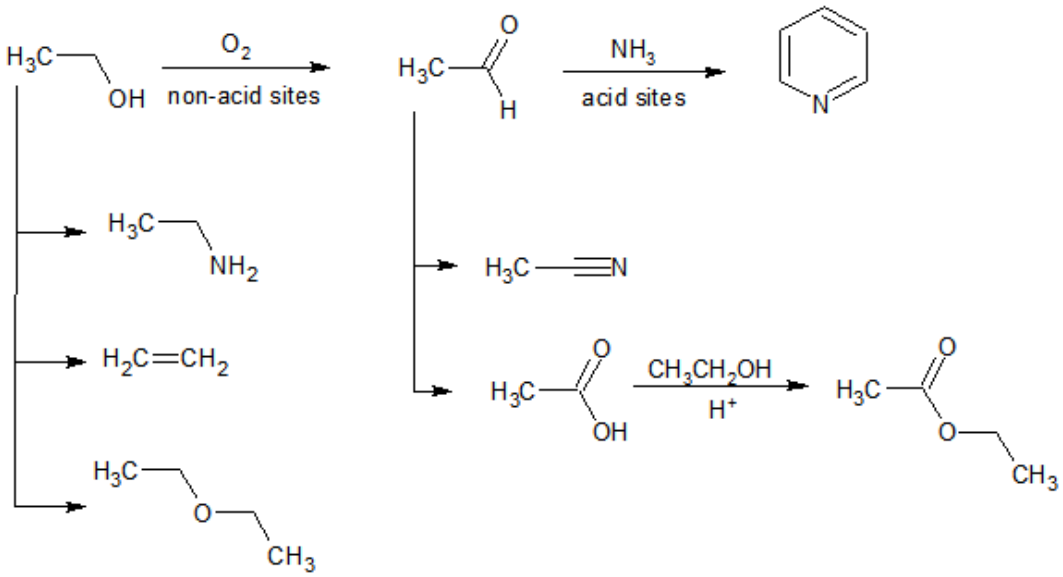

Figure 4.30. Potential reaction pathways of reactions between ethanol and ammonia at elevated temperatures at a zeolite surface, as proposed by van der Gaag[200]. Figure produced using ChemDraw.

A similar response is shown in zeolite beta modified chromium titanate, with the largest magnitude of response to a mix of 40-ppm ethanol and 40-ppm ammonia, which is potentially due to a similar mechanism.

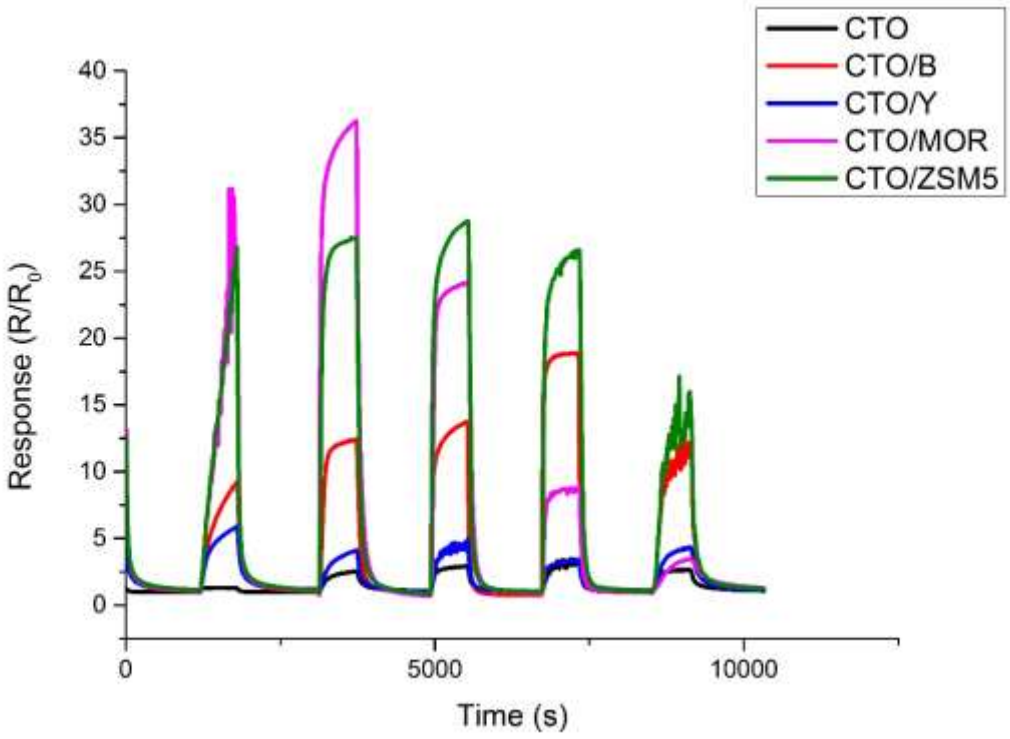

Figure 4.31. Maximum response of CTO and zeolite beta, Y, mordenite and ZSM5 modified CTO to pulses of 80 ppm ethanol, 60 ppm ethanol and 20 ppm ammonia, 40 ppm of both ethanol and ammonia, 40 ppm ethanol and 60 ppm ammonia and 80 ppm ammonia at an operating temperature of 350°C. Response is calculated as a function of baseline resistance R_0 that is, the sensor resistance in dry air.

Reactions to ammonia and ethanol mixtures at 250°C (Fig. 4.32) show similar response shapes to those observed at 300°C. The ZSM5 modified chromium titanate sensor has a non-linear decrease in responsiveness, with increasing ammonia concentration. Zeolite beta modified chromium titanate shows a larger response with mixtures of ammonia and ethanol than for pure exposure to either gas. Mordenite and zeolite Y modified chromium titanate as well as the unmodified sample continue respond as at 300°C and 350°C.

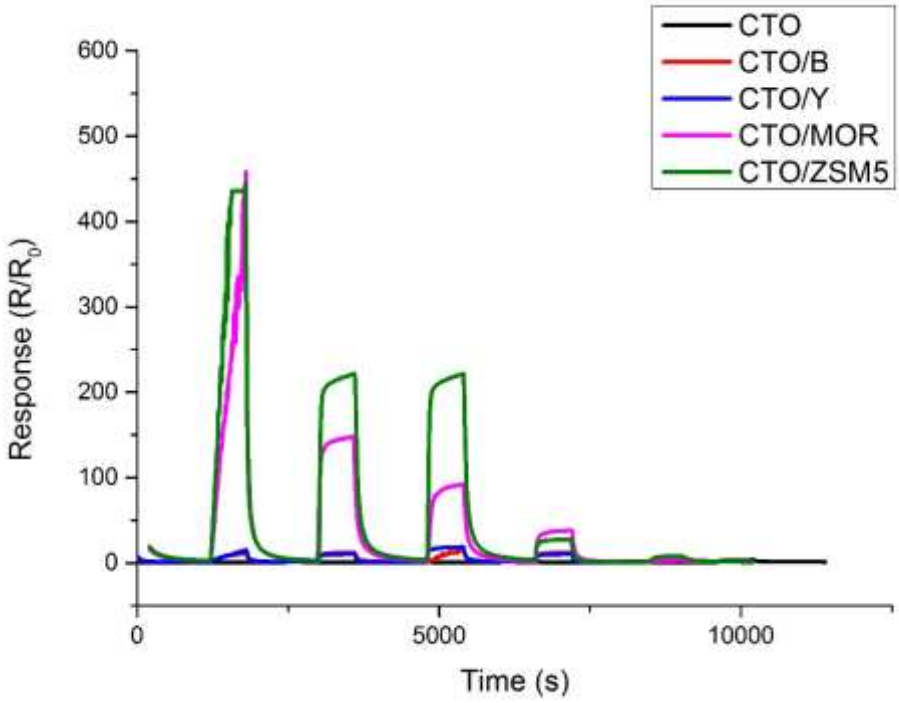

Figure 4.32. Maximum response of CTO and zeolite beta, Y, mordenite and ZSM5 modified CTO to pulses of 80 ppm ethanol, 60 ppm ethanol and 20 ppm ammonia, 40 ppm of both ethanol and ammonia, 40 ppm ethanol and 60 ppm ammonia and 80 ppm ammonia at an operating temperature of 350°C. Response is calculated as a function of baseline resistance R_0 that is, the sensor resistance in dry air.

4.3.9. Use of Different Counter Ions in Mordenite

In the chapter (and throughout this thesis) zeolites that are incorporated into the MOS sensor material have used protonated zeolites (where H^+ is used as a counter ion). Zeolites exist with different cations (Na^+, Cu^+, Co^+, NH_4^+, Gd^+ etc). Hydrogen ions were chosen for their small relative size. For comparison, mordenite modified chromium titanate sensors were produced using H-mordenite, Na-mordenite and NH_4-mordenite (used as supplied by zeolyst) and exposed to 80 ppm toluene, every 2 hours, at an operating temperature of 350°C.

Initial tests showed similar magnitudes of response to toluene for all three sensors. On subsequent tests, however, while H-mordenite showed consistent results over four tests, the magnitude of response in the NH_4 and Na-mordenite modified sensors showed a decrease in the magnitude of response (Fig. 4.33). Two methods were found to

"restore" the sensors and obtain similar responses to their initial tests. The first was to heat the sensor, using the Wheatstone bridge circuit, to a temperature of 550°C for 1 hour (Fig. 4.33).

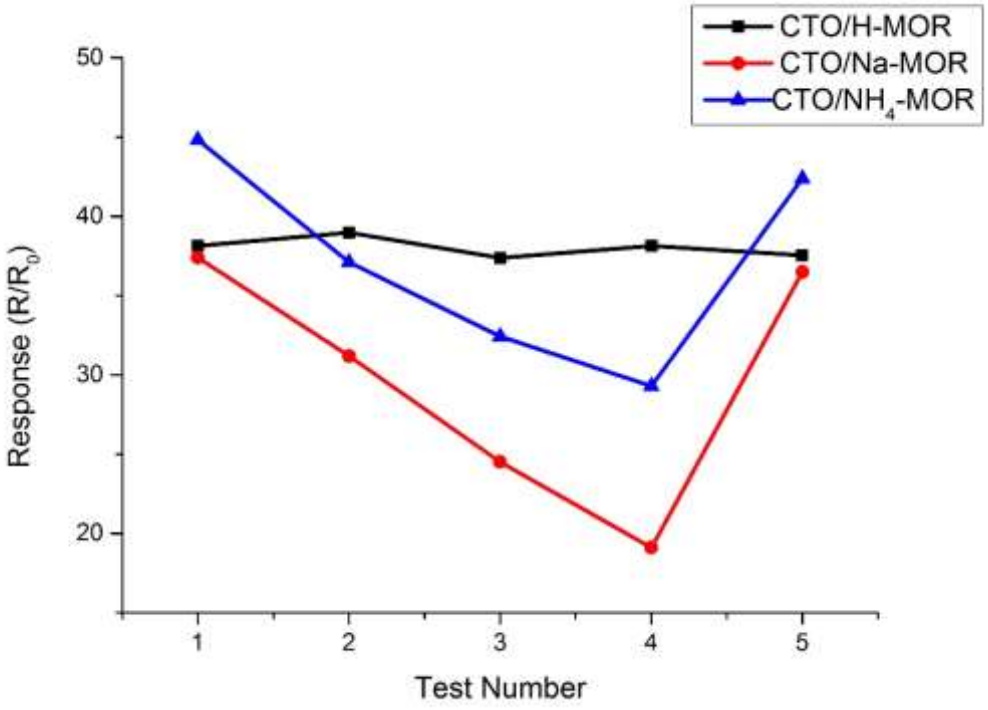

Figure 4.33. Consecutive responses of three mordenite modified CTO (with NH_4, Na and H mordenite) to 80-ppm toluene. Tests were conducted 2 hours apart. After test 4, all sensors were heated to 550°C for one hour. Response is calculated as a function of baseline resistance R_0 that is, the sensor resistance in dry air.

The second method for increasing the responsiveness of the zeolite modified sensors was for the sensors to undergo no gas testing for 72 hours, but remained at their 350°C operating temperature (Fig 4.34).

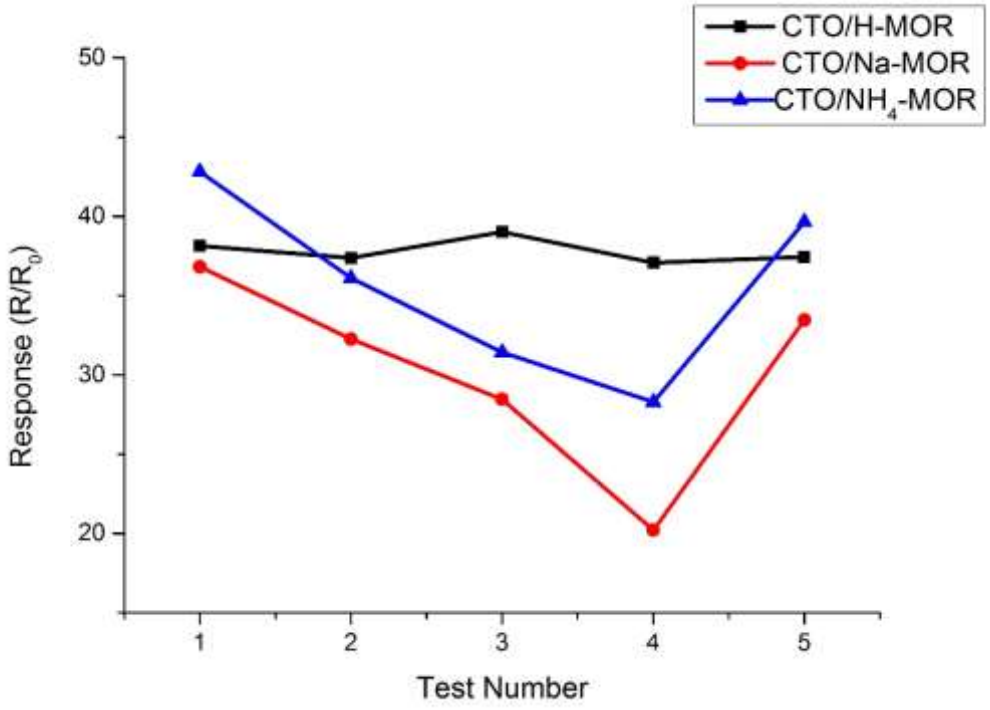

Figure 4.34. Consecutive responses of three mordenite modified CTO (with NH_4, Na and H mordenite) to 80-ppm toluene. Initially, tests were conducted 2 hours apart. After test 4, sensors underwent a downtime of 72 hours, during which all sensors remained heated at 350°C. Response is calculated as a function of baseline resistance R_0 that is, the sensor resistance in dry air.

This phenomenon suggests that with much larger cations than H^+ occupying the zeolite pores materials are adsorbed and "trapped" in the framework, unable to leave the network of pores to react at the sensor surface or leave the atmosphere completely. Eventually the zeolite structure becomes saturated and no more toluene can be adsorbed at the zeolite surface, reducing the magnitude of response. Heating the material to 550°C can give the adsorbed materials the energy to desorb at the sensor surface, while 'resting' the sensor at 350°C for 72 hours allows materials to desorb over a longer period. This desorption is not complete, as the sensors do not fully recover to the responses demonstrated on their first exposure to toluene.

4.4. Discussion

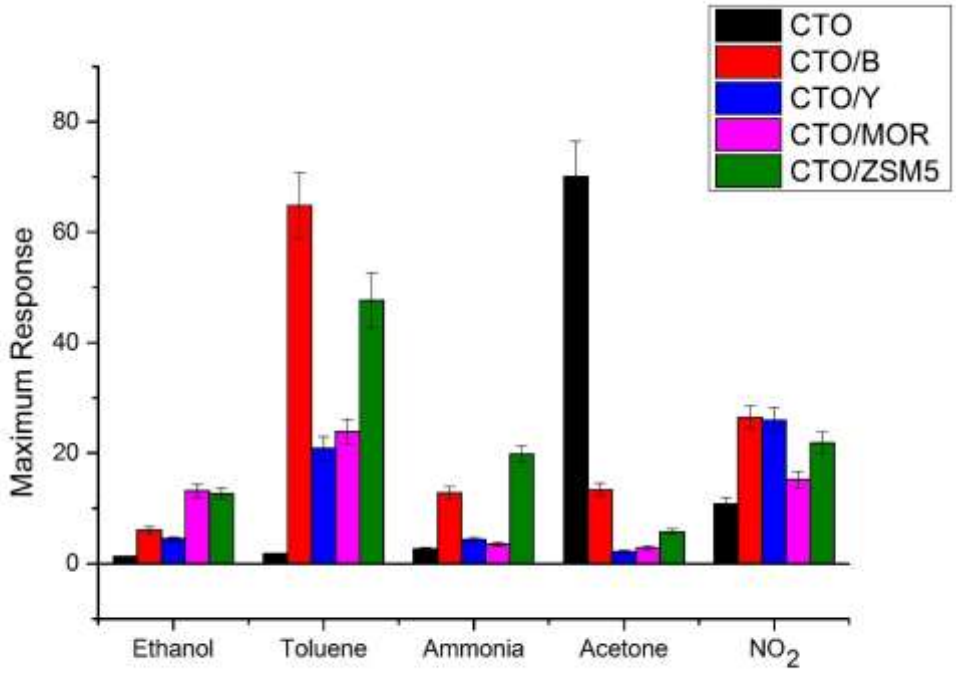

Figure 4.35. Response (R_0/R for all gases, except NO_2, which is R/R_0) of CTO sensors (unmodified CTO and zeolite beta, Y, mordenite and ZSM5 admixtures) at an operating temperature of 300°C to 40 ppm of a range of gases.

All sensors demonstrated strong responsiveness to the target gases they were exposed to in this investigation. Exposure to ethanol, toluene, ammonia and acetone led to an increase in the sensor resistance, while exposure to nitrogen dioxide led to a decrease. This is the opposite effect observed n-type sensors (Sections 3.3 and 5.3). The reason for this is that chromium titanate, as a p-type material, undergoes a different mechanism of action on contact with a target gas than the n-type sensors.

The difference in mechanism is due to the facts that, in n-type materials, electrons are the major charge carrier, while in p-type materials, holes are the charge carrier. With p-type material, a similar reaction occurs at the sensor surface as an n-type sensor, with oxygen initially adsorbing onto the surface, removing electrons and increasing the hole concentration, therefore increasing the conductivity in the sensor material.

When a reducing gas reacts with the sensor surface, electrons are reintroduced into the bulk, and occupy a hole site in the bulk material, reducing charge carrier concentration and therefore increasing the resistance of the sensor.

The largest response to ethanol was observed with mordenite and ZSM5 modified chromium titanate at an operating temperature of 250°C (R/R_0 = 439 and 462 respectively to a pulse of 80 ppm). This is compared to an unmodified sensor response of R/R_0 = 1.9. Both mordenite and ZSM5 have well documented adsorption properties for ethanol. Protonated mordenite has been shown to be successful in the dehydration of ethanol at temperatures between 180°C-300°C[201]. This dehydration leads to the production of ethylene, via diethyl ether. The active dehydration of the ethanol molecules in this study is attributed to the large number of Brønsted acid sites within the zeolite structure. Dehydration of ethanol on H-mordenite has also been observed via an ethoxy intermediate[202].

Responses to toluene are significantly larger in zeolite beta and Y modified chromium titanate sensors. The addition of these zeolites leads to several different reactions involving toluene. As demonstrated in section 3.7, toluene undergoes several acid catalysed reactions at the zeolite surface to its constituent hydrocarbon chains, these molecules undergo redox reactions at the gas sensitive surface and generate a larger response than the complete toluene molecule. As observed in section 3.7, mordenite and ZSM5 modified ZnO sensors experience the largest enhancement over the unmodified ZnO sensor, while zeolite beta and Y modified CTO show the largest enhancement. These sensors operate at different temperatures, with the CTO sensors operating at a lower temperature than zinc oxide sensors, meaning that zeolite beta and Y operate more effectively at lower operating temperature on exposure to toluene.

On response to low concentrations of acetone (<10 ppm) zeolite beta shows large enhancements in response when compared to other zeolite modified chromium titanate and unmodified chromium titanate sensors. Zeolite beta has been shown to convert acetone successfully to acetic acid (CH_3COOH), because of its Bronsted acid strength, which is midway between H-ZSM5 and H-Y[203]. It has also been reported that the

conversion of acetone on zeolite beta is highly selective for isobutylene ($CH_3C(CH_3)CH_3$) when compared to the reaction on H-ZSM5[204]. These reactions are temperature dependant. With a more electronegative carboxylic acid group, compared to the ketone functional group, more electrons are released during the breakdown of the molecule at the surface. The carboxylic acid can be deprotonated, forming hydroxyl ions at the surface, as well as reactions at the carbonyl group in the molecule.

Exposure to humidity (RH = 50%) led to an increase in resistance in all zeolite modified and unmodified sensors. When water molecules interact with the sensors, they form hydroxyl (OH^-) ions on the surface, directly introducing electrons into the bulk material. This decreases the charge carrier (hole) concentration and therefore increases the resistivity of the material. Responses to ethanol in the presence of humid air are observed to be slightly lower than exposures in dry air. This decrease in response is a result of hydroxyl ions competing with ethanol at the sensor surface, so fewer ethanol molecules oxidise at the sensor surface.

Zeolite modified sensors show improved responses to ethanol than sol-gel produced chromium titanate[205], thin film chromium titanate[206] and zeolite overlaid chromium titanate sensors[104]. These sensors also show stronger responses to acetone than iron(III) oxide[207] and nickel oxide[208], a stronger response to toluene than titanium dioxide[209] and tungsten trioxide[210] and stronger responses to ammonia than indium oxide[211].

4.5. Conclusion

Five chromium titanate based sensors were produced by combining the material with four zeolite materials. These sensors were exposed to five gases, both on their own and in combination to determine the effect of zeolite material in the gas sensing ability of chromium titanate and to assess the potential for incorporation into an electronic nose.

The addition of zeolites to the sensing material produces large increases in the sensitivity of the sensor, allowing detection of a range of gases to low ppm and ppb concentrations. The use of this zeolite array, in combination with machine learning

techniques (as discussed in chapter 7), can potentially enable a high level of selectivity in detecting the type of gas present, in a short space of time. This has been previously unseen in p-type material.

Overall the chromium titanate series has demonstrated a number of key attributes required for incorporation in a successful analytical device:

- The series has shown strong sensitivity to several target gases, in the low ppm and ppb range.
- Shown reproducible responses to changes in atmosphere over multiple exposures to test gases and power cycling.
- Possess good selectivity to target gases.

The sensors have however, like zeolite modified ZnO sensors, shown generally poor response times, this will be investigated further in the coming chapters with doped zinc oxide and vanadium pentoxide sensors.

The next chapter covers the modification of vanadium pentoxide. Where sensors were fabricated under the same conditions and in chapter 3 and 4. These sensors were tested with a number of gases, both individually and in mixtures.

5. Modification of Vanadium Pentoxide

Vanadium pentoxide (V_2O_5) sensors can be modified by the inclusion of zeolite beta, Y, mordenite and ZSM5. Sensors modified in this way were exposed to several gases commonly found at clandestine locations and the results of these experiments are discussed below.

5.1. Introduction

Vanadium pentoxide is a common metal oxide used in the catalysis industry and a principle precursor to alloys of vanadium[212]. As a result of its high oxidation state, vanadium pentoxide is both an amphoteric oxide and an oxidizing agent; it is an n-type semiconductor with a band gap of 2.2 eV[213].

Vanadium pentoxide is utilised in several devices based on the principle of charge transfer, such as electrochromic devices, optical switches and solar cells. Vanadium pentoxide has a high specific energy density[214] and high electrochemical and charge transfer activity[215]. This charge transport proceeds via electron hopping between V^{4+} (impurities) and V^{5+} centers, in accordance with the Mott model[216]. This property makes vanadium pentoxide fibres well suited for the construction of functional materials or novel devices, which can be operated under low temperature conditions.

Vanadium pentoxide has an orthorhombic unit cell structure and belongs to the Pmnm space group. Orthorhombic vanadium pentoxide is usually described as being made up of chains of edge sharing vanadium pentoxide square pyramids (Fig 5.1).

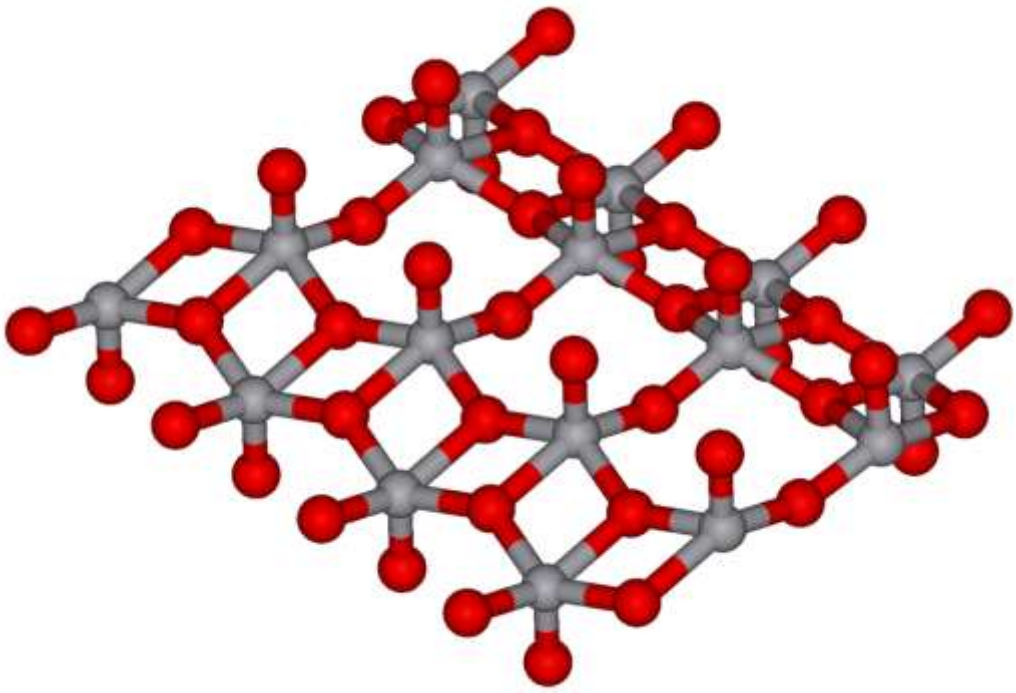

Figure 5.1. Schematic showing a monolayer of the orthorhombic structure of vanadium pentoxide, showing vanadium atoms in grey and oxygen atoms in red.

Previous research on the use of vanadium pentoxide as a gas sensing material has focused on the use of the material in nanofibres[217], nanorods[218] and nanobelts[219]. These are thin film sensors, which show responses to ethanol and other species with hydroxyl functional groups. The response of these sensors is quite low ($R_0/R \approx 1.5$ to 100 ppm of ethanol) when compared to other more conventional gas sensitive semiconductors, such as WO_3 ($R_0/R \approx 25$ to 100 ppm ethanol[220]) and SnO_2 ($R_0/R \approx 40$ to 100 ppm ethanol[221]). However, despite the relatively low responses to target gases, vanadium pentoxide sensors have been shown have good long-term stability, even after hundreds of tests[217].

In the context of the work presented in this thesis, five vanadium pentoxide based gas sensors were produced, incorporating four zeolite materials as admixtures into the material. The zeolites incorporated were: zeolite beta, zeolite Y, mordenite and ZSM5. Details of sensor fabrication can be found in section 2.2. These sensors were then tested

against five common analyte gases, both as lone gases, and as mixtures. In line with other work presented here, tests were conducted at 250°C, 300°C and 350°C.

5.2. Characterisation

5.2.1. Physical Appearance of Sensors

All vanadium pentoxide sensors have an orange colour at room temperature, upon heating to 250°C-350°C, the sensor material changes to a deep red colour. The sensors retained their composition in air after repeated heating over many months, however significant shock or pressure on the sensor caused the material to crumble and lead to de-adhesion.

5.2.2. Surface Area Measurements

Surface area measurements of vanadium pentoxide and zeolite-modified powders are shown in Table 5.2. All zeolite-modified materials show significant enhancements in their surface area.

Table 5.1. Surface area measurements of zeolite modified and unmodified vanadium pentoxide powders.

Material	Surface Area (m^2/g)
V_2O_5	2.4
V_2O_5/B	131.8
V_2O_5/Y	103.7
V_2O_5/MOR	110.1
V_2O_5/ZSM5	72.3

Beta modified vanadium pentoxide shows the largest increase in the series, while ZSM5 shows the smallest enhancement, however, the surface area of ZSM5 modified vanadium pentoxide is still more than 30 times the surface area of pure vanadium

pentoxide. This large enhancement is due to the large porous surface area of the zeolite materials.

5.2.3. Scanning Electron Microscopy

Scanning electron microscopy images of all sensors at 5,000x and 20,000x magnifications are illustrated in Fig. 5.2. Unmodified vanadium pentoxide shows smooth, platelet like grains, with diameters of approximately 1 µm and a thickness of around 350 nm. The platelets are all different shapes, but are of a similar size. Zeolite modified sensors show highly porous zeolite structures covering the vanadium pentoxide grains. The ZSM5 modified sensor shows the largest particle size of the zeolite-modified sensors, while the beta modified material shows the smallest particle size. This agrees with the BET measurements, which determined that ZSM5 modified vanadium pentoxide had the smallest surface area of all modified sensors, and beta had the largest surface area. All sensors have a cavernous appearance.

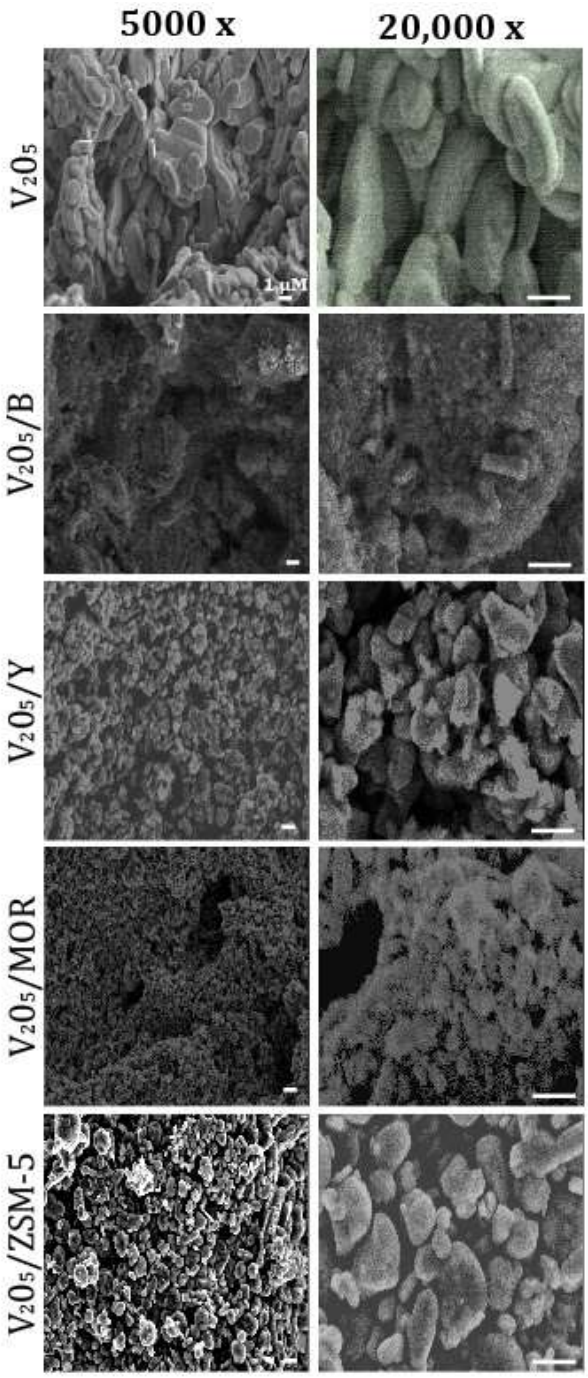

Figure 5.2. SEM images of all V_2O_5 sensors at 5000x and 20000x (Scale bars represent 1 μm).

5.2.4. Energy-Dispersive X-ray Spectroscopy

Results of elemental analysis with energy dispersive X-ray spectroscopy are shown both as atomic percentage (Table 5.3) and weight percentage (Table 5.4). These show similar vanadium concentrations in all zeolite modified sensors; however the introduction of zeolite raises the atomic percentages of aluminium, silicon and oxygen. The weight

percentage of oxygen does not increase in zeolite-modified sensors, due to the larger relative mass of silicon and aluminium, compared to oxygen.

Table 5.2. Atomic percentages of zeolite modified and unmodified vanadium pentoxide sensors.

	Atomic Percentage (%)			
	V	**O**	**Al**	**Si**
V_2O_5	41.8	58.2	0	0
V_2O_5/B	15.2	65.9	0.5	18.4
V_2O_5/Y	16.9	63.5	5.4	14.2
V_2O_5/MOR	14.0	69.8	1.5	14.8
V_2O_5/ZSM5	12.0	68.5	0.8	18.7

Table 5.3. Weight percentages of zeolite modified and unmodified vanadium pentoxide sensors.

	Weight Percentage (%)			
	V	**O**	**Al**	**Si**
V_2O_5	30.4	69.6	0	0
V_2O_5/B	32.85	44.72	0.49	21.9
V_2O_5/Y	35.7	41.9	6.0	17.4
V_2O_5/MOR	31.2	48.9	1.7	18.2
V_2O_5/ZSM5	25.0	52.7	0.3	22.0

5.2.5. X-Ray Diffraction

Diffraction patterns of vanadium pentoxide and zeolite modified Vanadium pentoxide (Fig 5.3) show the expected orthorhombic vanadium pentoxide (JCPDS card no. 41-1426) structure. Zeolite modified vanadium pentoxide samples show some additional peaks corresponding to zeolite XRD patterns. This indicated that the orthorhombic structure of vanadium pentoxide is the dominant structure in the zeolite. Zeolite beta modified

V_2O_5 shows a significantly larger peak at 2θ = 36°, corresponding to the (401) plane; this is not easily explained and may in fact be due to instrumental errors in collecting data from the highly charged plane.

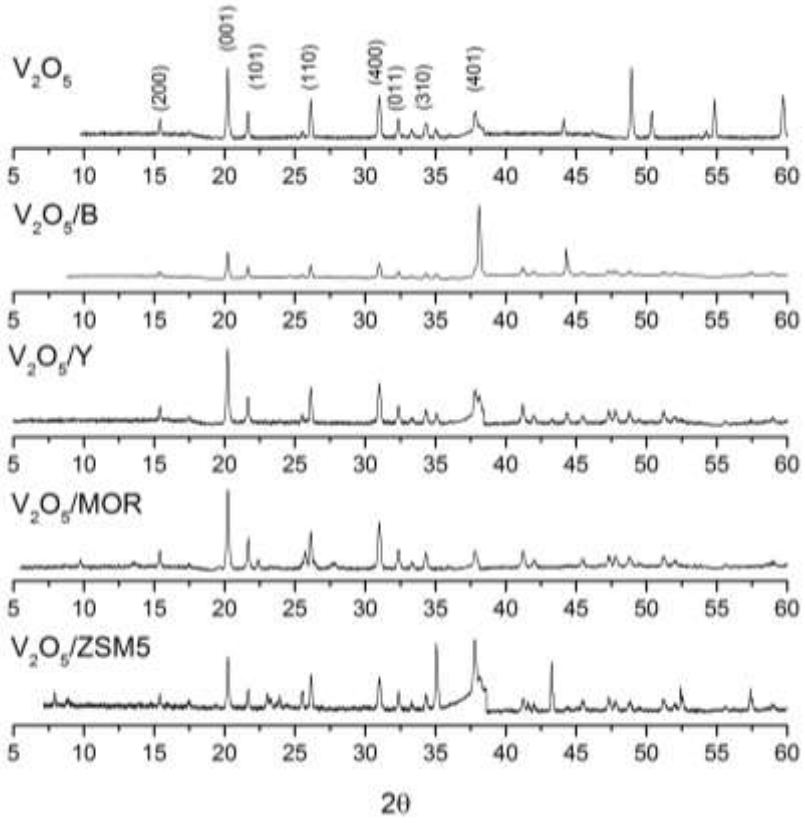

Figure 5.3. X-ray diffraction patterns of V_2O_5 and zeolite beta, Y, mordenite and ZSM5 modified V_2O_5, demonstrating the orthorhombic structure of V_2O_5 (indexed against JCPDS #001- 0359).

5.3. Results

5.3.1. Baseline Resistance

The average baseline resistance for each sensor is shown in Table 5.4. In all cases, the modified sensors show significantly increased resistance, compared to the unmodified vanadium pentoxide. This increased resistance is to be expected as zeolite materials are generally insulating and will consequently increase the resistance in the material. As temperature increases, baseline resistance decreases, this is because at higher temperatures electrons in the valence band will have energy to occupy higher energy levels in the conduction band and become charge carriers.

Table 5.4. Baseline resistances of zeolite modified and unmodified vanadium pentoxide sensors.

Sensor	Resistance (Ω)		
	250°C	**300°C**	**350°C**
V_2O_5	2760	2280	2053
V_2O_5/B	2.3×10^8	7.8×10^7	1.1×10^7
V_2O_5/Y	4.8×10^8	1.8×10^7	4.4×10^6
V_2O_5/MOR	2.3×10^6	6.1×10^5	4.3×10^4
V_2O_5/ZSM5	1.7×10^6	1.96×10^5	1.2×10^5

5.3.2. Exposure to Ethanol

Sensors were exposed to 5, 10, 20, 40 & 80 ppm of ethanol at temperatures of 350°C, 300°C & 250°C. Exposure to ethanol caused a decrease in resistance in all sensors. Zeolite modified sensors were found to have a significantly larger response than the unmodified vanadium pentoxide. Results for exposure at 350°C are shown in Fig 5.4. The peak shape of the mordenite and zeolite Y is a typical “shark-fin” shape, showing that, in the allotted time, the sensors did not reach a steady state. The responses of pure vanadium pentoxide and the beta and mordenite modified sensors show a small degree of noise, especially in air, which is thought to be because of inconsistent oxygen adsorption/desorption. Despite these issues, significant enhancements are observed during the 600-second gas pulses.

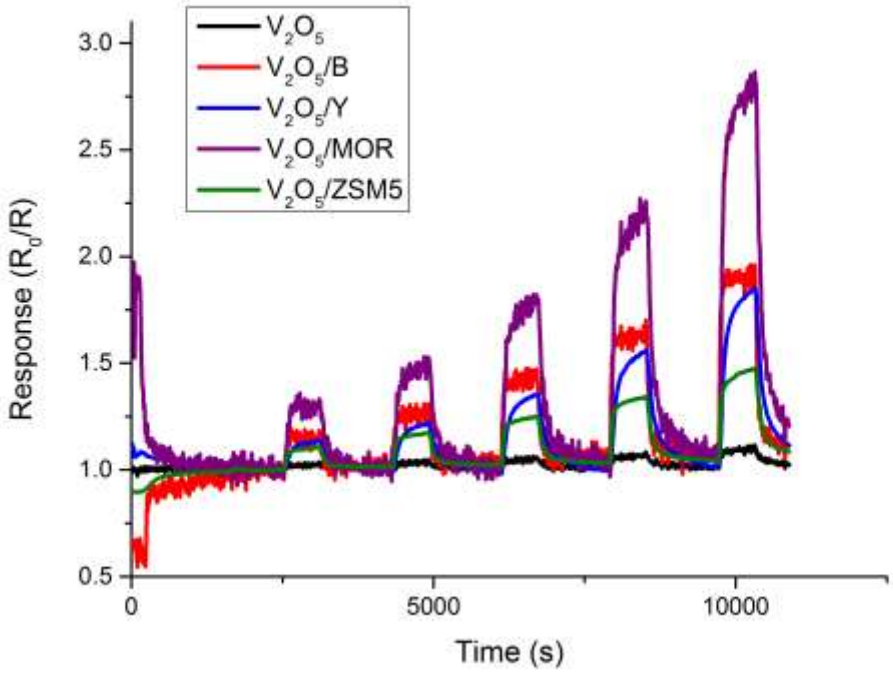

Figure 5.4. V_2O_5 based sensors (unmodified V_2O_5 and zeolite beta, Y, mordenite and ZSM5 admixtures) response to 5, 10, 20, 40 & 80 ppm ethanol, at an operating temperature of 350°C. Response is calculated as a function of baseline resistance R_0 that is, the sensor resistance in dry air.

To test the short-term repeatability of the sensors they were then exposed to three consecutive 600-second pulses of 80-ppm ethanol (Fig. 5.5). For each individual sensor, the magnitude of response was similar to those observed in Fig 5.4, and each sensor had a similar peak shape during all three-gas pulses, indicating a similar response and recovery sequence. Apart from mordenite-modified vanadium pentoxide, all sensors could reach an approximate steady state during the 600-second pulse.

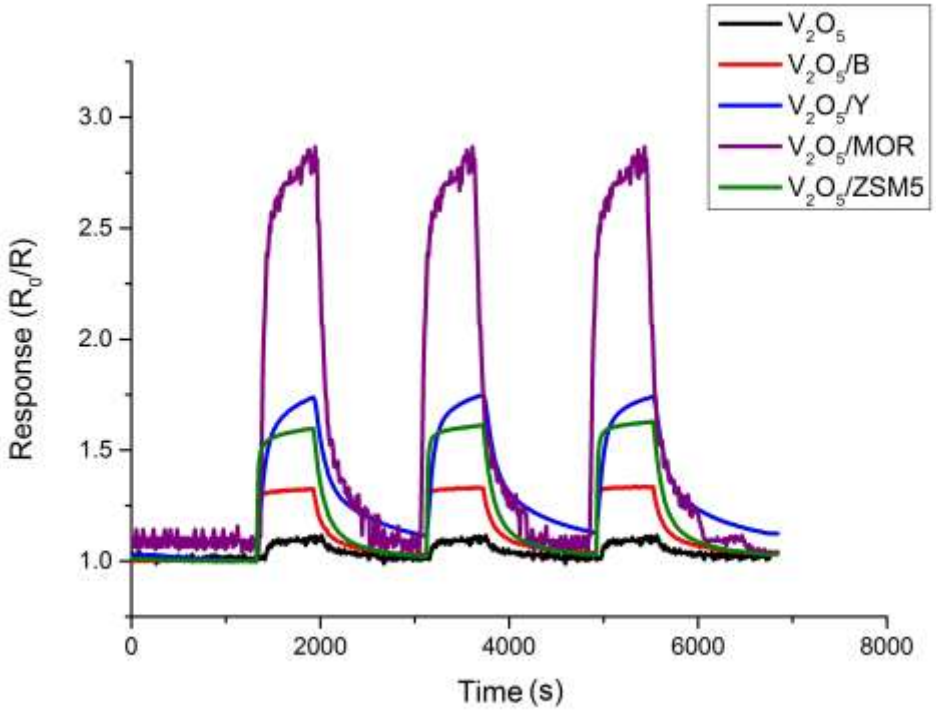

Figure 5.5. Responses of V_2O_5 based sensors (unmodified V_2O_5 and zeolite beta, Y, mordenite and ZSM5 admixtures) at an operating temperature of 350°C to three consecutive pulses of 80-ppm ethanol. Response is calculated as a function of baseline resistance R_0 that is, the sensor resistance in dry air.

The response of vanadium pentoxide and zeolite modified sensors to ethanol at 300°C (Fig 5.6) is significantly noisier; especially in mordenite modified vanadium pentoxide. The magnitudes of response are slightly higher than those observed at 350°C. At this temperature, all zeolite-modified sensors show an enhancement in response compared to the unmodified vanadium pentoxide sensor.

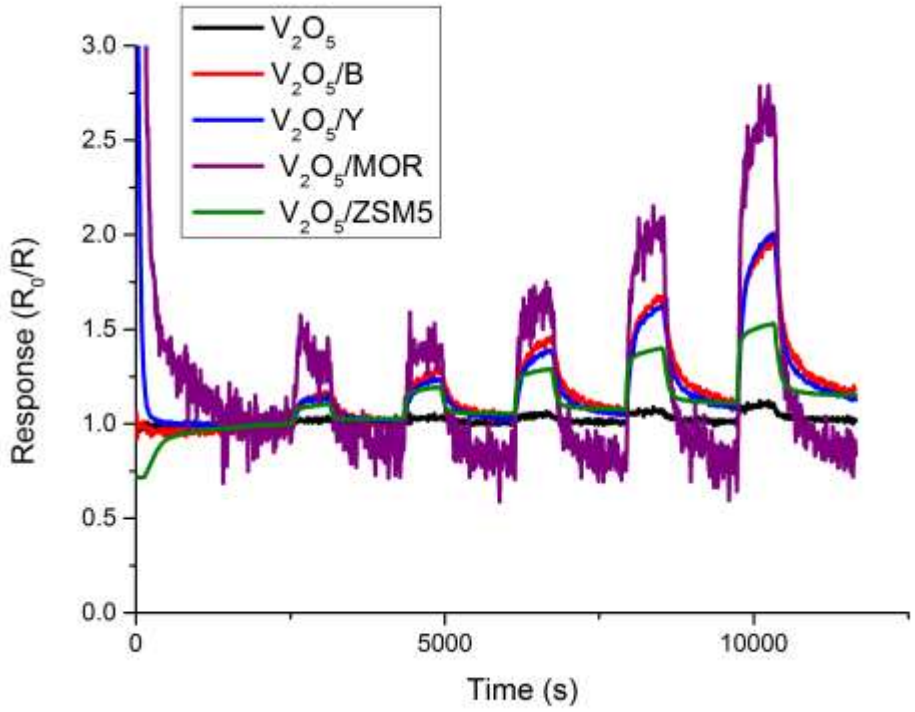

Figure 5.6. V_2O_5 based sensors (unmodified V_2O_5 and zeolite beta, Y, mordenite and ZSM5 admixtures) response to 5, 10, 20, 40 & 80 ppm ethanol, at an operating temperature of 300°C. Response is calculated as a function of baseline resistance R_0 that is, the sensor resistance in dry air.

The response of vanadium pentoxide and zeolite modified sensors to ethanol at 250°C show significant enhancement in zeolite Y modified vanadium pentoxide compared with all other sensors (Fig 5.7). This is not seen at other operating temperatures with ethanol. This large enhancement may be due to the larger pore diameter observed with zeolite Y, compared to other zeolite structures, meaning that ethanol molecules are able to diffuse freely through the zeolite directly to the gas sensitive surface, whereas in zeolites with smaller pore diameters, ethanol molecules will collide with the pore walls. All zeolite modified sensors show enhancement in response compared with the unmodified vanadium pentoxide sensor.

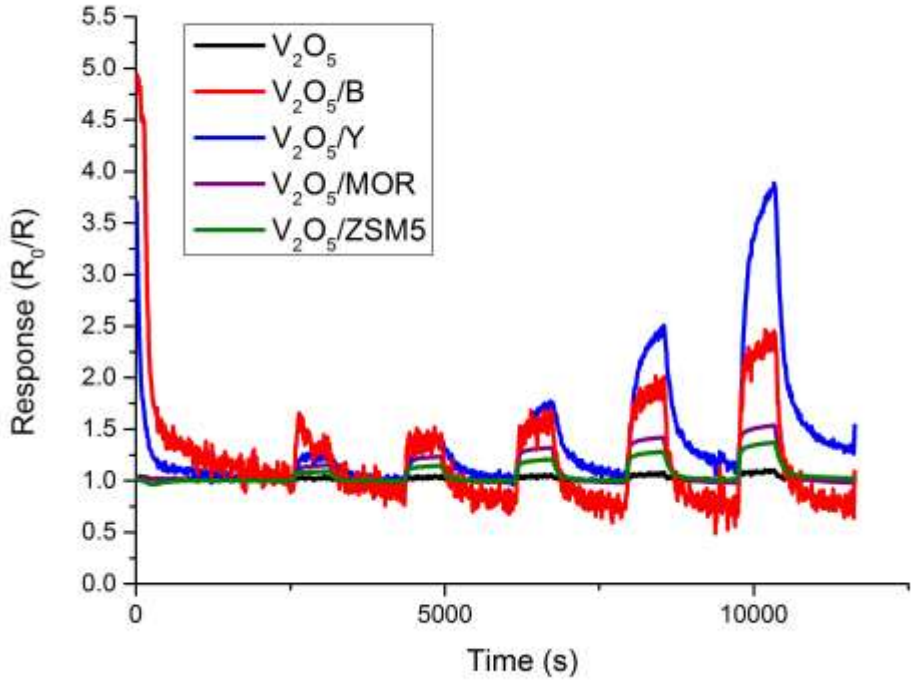

Figure 5.7. V_2O_5 based sensors (unmodified V_2O_5 and zeolite beta, Y, mordenite and ZSM5 admixtures) response to 5, 10, 20, 40 & 80 ppm ethanol, at an operating temperature of 250°C. Response is calculated as a function of baseline resistance R_0 that is, the sensor resistance in dry air.

The maximum responses of all sensors are displayed in Fig. 5.8. Across the temperature range, there is an increase in the responsiveness of the zeolite beta and Y modified sensors as temperature decreases, with the response of zeolite Y modified ZnO to 80 ppm ethanol rising from R_0/R= 1.85 at 350°C to R_0/R= 3.88 at 250°C. Conversely the other modified sensors decrease in responsiveness from 350°C to 250°C.

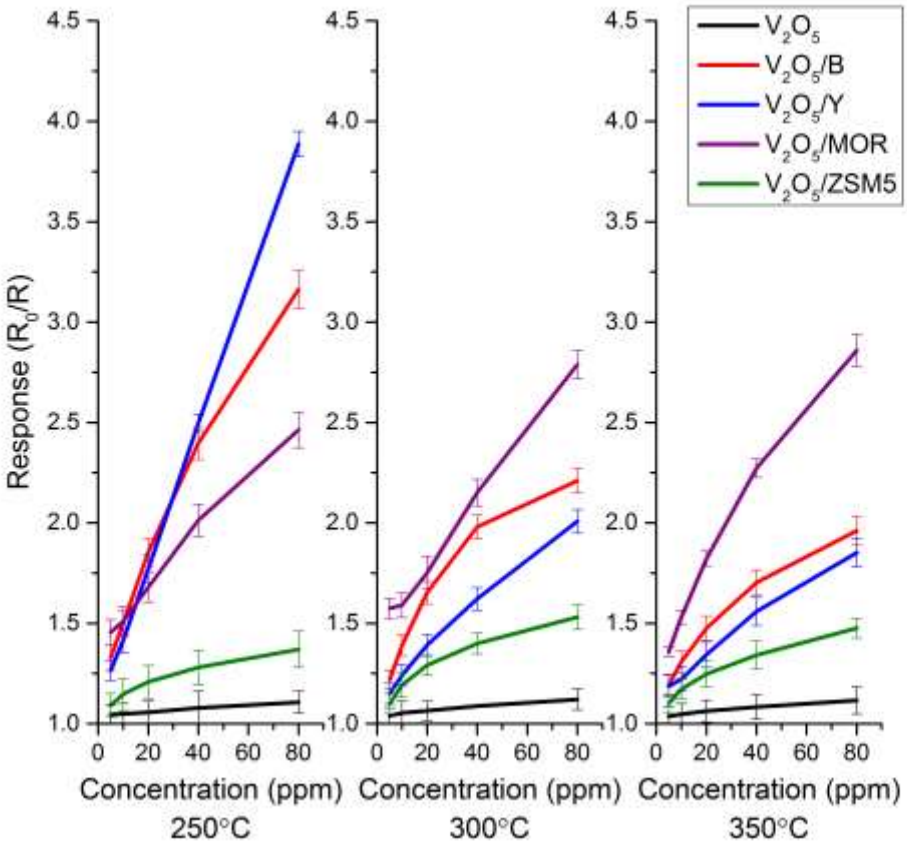

Figure 5.9. Response (± 1 S.D.) of V_2O_5 based sensors (unmodified V_2O_5 and zeolite beta, Y, mordenite and ZSM5 admixtures) to concentrations of 5-80 ppm ethanol at temperatures of 250°C, 300°C, 350°C. Response is calculated as a function of baseline resistance R_0 that is, the sensor resistance in dry air.

The response time, τ_{res}, is defined as the time taken for the sensor response to reach 90% of its maximum value. The response times for 80-ppm ethanol pulses are shown in Table 5.5.

Table 5.5. Response times (± 5 s) for V_2O_5 based sensors to 80-ppm ethanol.

Sensor	Response time (s, ±5)		
	250°C	**300°C**	**350°C**
V_2O_5	90	70	80
V_2O_5/B	80	60	60
V_2O_5/Y	310	220	250
V_2O_5/MOR	170	170	160
V_2O_5/ZSM5	170	160	190

These results show that response times are independent of the actual response; the largest response does not give the largest response time and does not vary dramatically with temperature. The response times for zeolite beta modified sensors are significantly shorter than for other zeolite-modified sensors at all temperatures. Zeolite Y modified sensors show the longest response time; the adsorption characteristics of ethanol with zeolite Y are well documented[222,223,] and support this result. The adsorption of ethanol at the zeolite surface may slow the reactivity at the vanadium pentoxide grain surface and consequently slow the response time.

5.3.3. Exposure to Nitrogen Dioxide

Sensors were exposed to 50, 100, 200, 400 & 800 ppb of nitrogen dioxide at temperatures of 350°C, 300°C & 250°C. Exposure to nitrogen dioxide caused a resistive response (an increase in sensor resistance) in all sensors, however, exposure to this gas produces an interesting peak shape, where by an initial decrease in resistance is observed, followed by an increase in resistance. Most likely due to some reducing gas trapped in the rig, despite thorough cleaning of the instrumentation.

The magnitude of response of zeolite-modified sensors was larger than that of unmodified Vanadium pentoxide. The largest observed response was that of mordenite modified vanadium pentoxide, which gave a response of R/R_0 = 7.57. The responses observed upon exposure to nitrogen dioxide are far smoother than those of ethanol exposure, indicating the more consistent adsorption/desorption properties of this analyte.

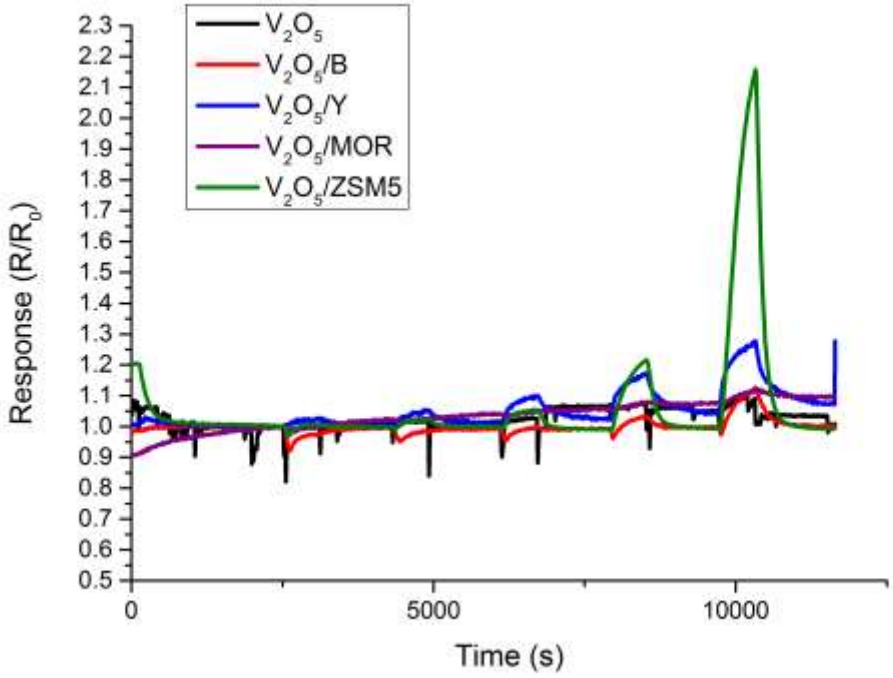

Figure 5.10. Response of V_2O_5 sensors (unmodified V_2O_5 and zeolite beta, Y, mordenite and ZSM5 admixtures) to 50, 100, 200, 400 & 800 ppb of NO_2 at an operating temperature of 350°C. Response is calculated as a function of baseline resistance R_0 that is, the sensor resistance in dry air.

At an operating temperature of 300°C (Fig 5.11) enhancements in all zeolite modified sensors are observed compared to the unmodified vanadium pentoxide sensor. Zeolite beta, Y and ZSM5 show similar magnitudes of response to all concentrations of nitrogen dioxide however, mordenite shows significant enhancement as well as poor recovery and a noisy response.

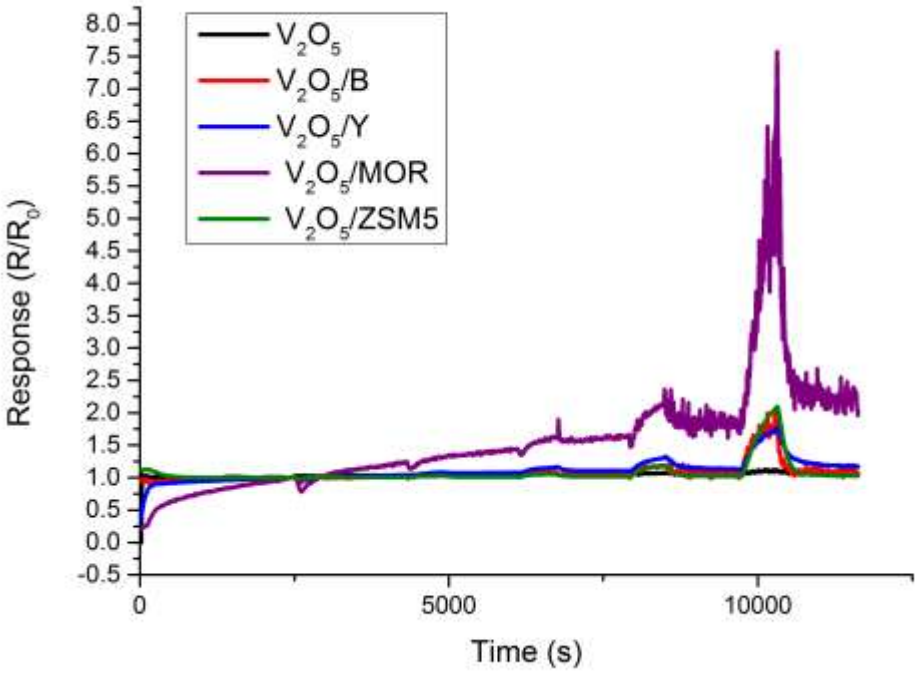

Figure 5.11. Response of V_2O_5 sensors (unmodified V_2O_5 and zeolite beta, Y, mordenite and ZSM5 admixtures) to 50, 100, 200, 400 & 800 ppb of NO_2 at an operating temperature of 300°C. Response is calculated as a function of baseline resistance R_0 that is, the sensor resistance in dry air.

At an operating temperature of 250°C all vanadium pentoxide and zeolite modified vanadium pentoxide sensors show poor responses compared to other operating temperatures, as well as poor baseline drift and recovery (Fig 5.12). This poor performance at lower operating temperature may be due to inconsistent reactions between the sensor surface and nitrogen dioxide as well as inconsistent adsorption of oxygen at the sensor surface, resulting in an unstable baseline resistance. Mordenite modified vanadium pentoxide was found to be responsive above 400 ppb, however there is significant baseline drift at this operating temperature, potentially due to gradual increase in oxygen atoms adsorbing onto the vanadium pentoxide surface, resulting in an increase in the sensor resistance and a failure to reach equilibrium with the environment. Mordenite modified sensors have been found to show significant enhancements with other n-type materials (section 3.3.3), this enhancement is thought to be due to the monodimensional pore structure, which allows direct access to the gas sensitive surface in a direct manner, as opposed to a 3D structure.

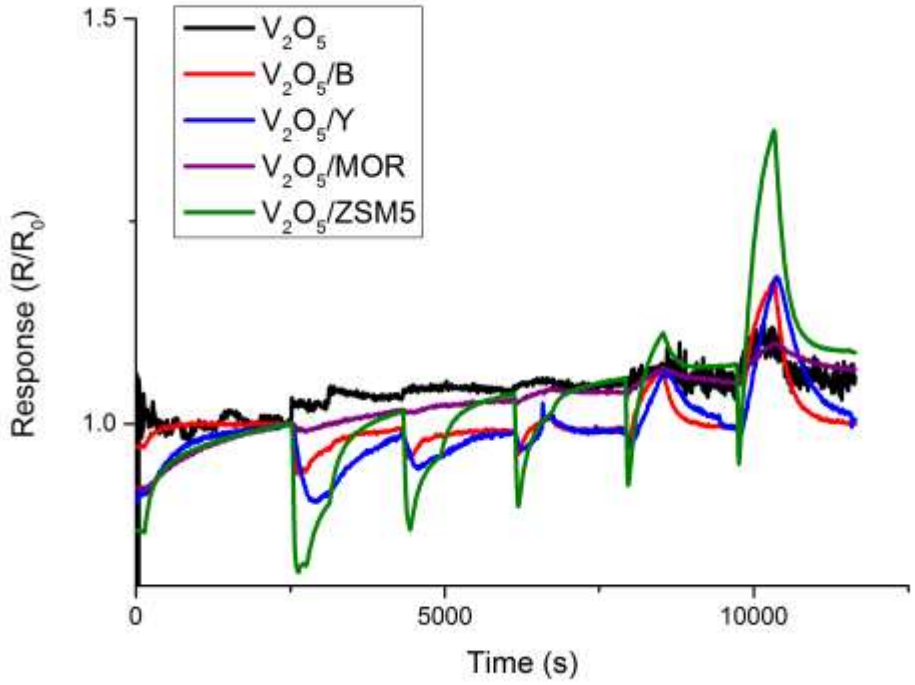

Figure 5.12. Response of V_2O_5 sensors (unmodified V_2O_5 and zeolite beta, Y, mordenite and ZSM5 admixtures) to 50, 100, 200, 400 & 800 ppb of NO_2 at an operating temperature of 250°C. Response is calculated as a function of baseline resistance R_0 that is, the sensor resistance in dry air.

The maximum responses of all sensors at several temperatures are shown in Fig. 5.13. Zeolite modified vanadium pentoxide sensors show larger magnitudes of response at all temperatures, compared to the unmodified sensor, especially in mordenite modified vanadium pentoxide at 300°C. This sensor is significantly more responsive at 300°C than at other temperatures, where the mordenite modified sensor has responses similar to those of unmodified vanadium pentoxide. All other sensors have their largest responses at 350°C, and this magnitude of response decreases as the operating temperature of the sensor decreases.

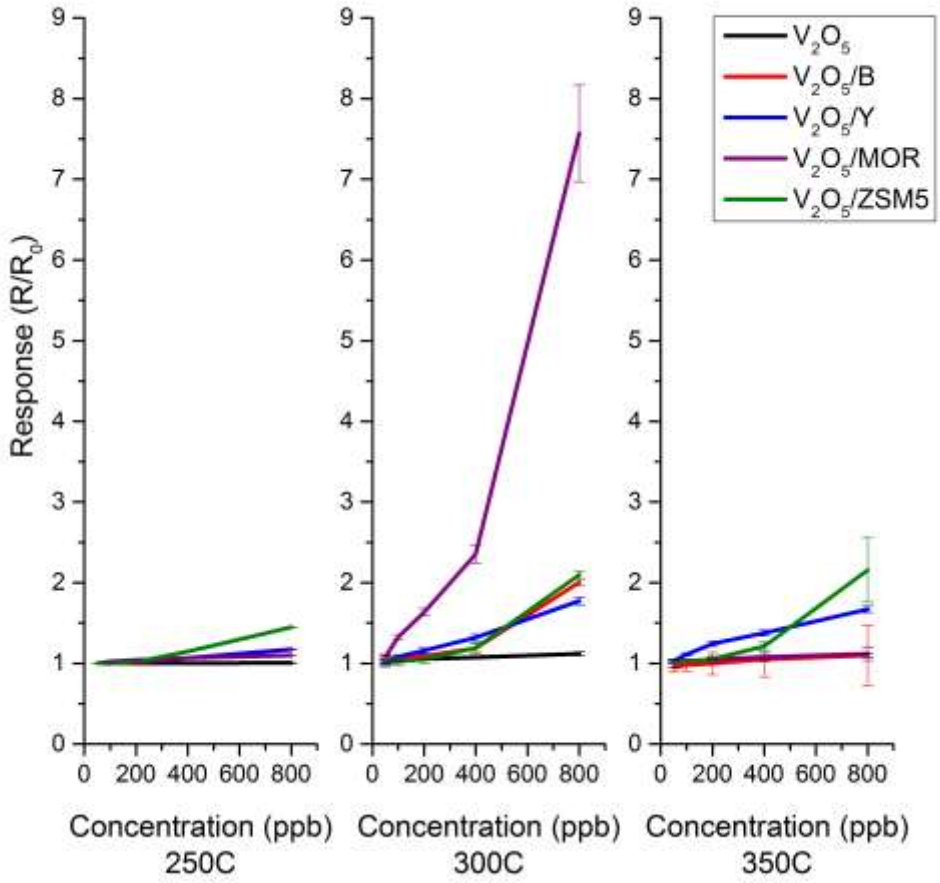

Figure 5.13. Response (± 1 S.D.) of V_2O_5 based sensors (unmodified V_2O_5 and zeolite beta, Y, mordenite and ZSM5 admixtures) to concentrations of 50-800 ppb nitrogen dioxide at temperatures of 250°C, 300°C, 350°C. Response is calculated as a function of baseline resistance R_0 that is, the sensor resistance in dry air.

5.3.4. Exposure to Toluene

Sensors were exposed to 2.5, 5, 10, 20 and 40 ppm of toluene at 250°C, 300°C & 350°C. All modified sensors produced responses at all concentrations, zeolite Y modified vanadium pentoxide gave a significantly larger response at all temperatures. Unmodified vanadium pentoxide did not produce a distinguishable response to any concentration of toluene within the testing range.

At an operating temperature of 350°C (Fig 5.14), zeolite modified vanadium pentoxide sensors show enhancements over the unmodified sensor. The largest enhancement in response is observed with zeolite Y modified vanadium pentoxide, with a maximum

response of R_0/R = 1.82 to 40 ppm toluene. The peak shape of zeolite beta modified vanadium pentoxide shows a steady state is reached at most concentrations. The zeolite Y modified sensor shows a shark fin response that does not reach saturation at any concentration. All sensors appear to recover back to their initial resistance, the recovery is however, slow and only just achieved in the 1200-second interval.

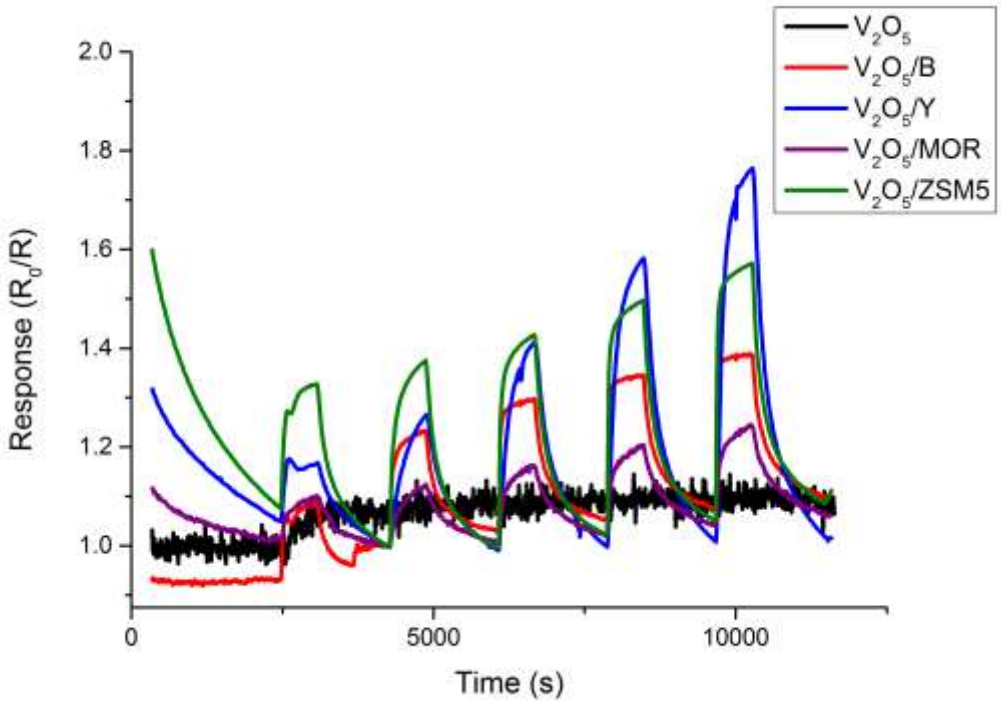

Figure 5.14. Response (± 1 S.D.) of V_2O_5 based sensors (unmodified V_2O_5 and zeolite beta, Y, mordenite and ZSM5 admixtures) to concentrations of 2.5, 5, 10, 20 and 40 ppm toluene at an operating temperature of 350°C. Response is calculated as a function of baseline resistance R_0 that is, the sensor resistance in dry air.

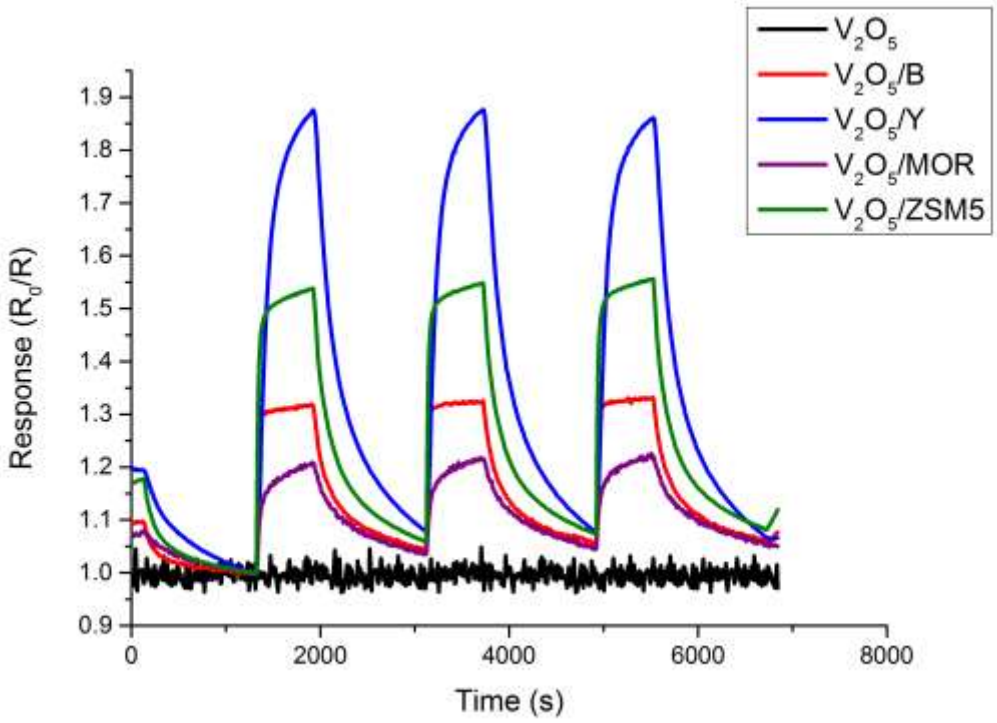

Figure 5.15. Responses of V_2O_5 based sensors (unmodified V_2O_5 and zeolite beta, Y, mordenite and ZSM5 admixtures) at an operating temperature of 350°C to three consecutive pulses of 40-ppm toluene. Response is calculated as a function of baseline resistance R_0 that is, the sensor resistance in dry air.

The repeatability of the sensors was tested with an experiment that exposed the sensors to three consecutive 600-second pulses of 40-ppm toluene at 350°C (Figure 5.15). Once again, the unmodified vanadium pentoxide sensor gave no response to the target gas, while with all other materials, a strong consistent response was observed. At 40-ppm, the ZSM5 and beta modified sensors achieved a steady state response, while mordenite and zeolite Y modified sensors did not quite achieve this, though the mordenite appears to plateau towards the end of the 600 second pulse. The magnitude of all responses observed are consistent and all sensors display similar peak shape. The magnitude of subsequent responses is similar, despite an incomplete recovery. At the beginning of the first response, all sensors have an $R_0/R = 1.0$, at the beginning of the second pulse, zeolite modified sensors have responses of $R_0/R = 1.05$-1.08, this is most likely a result of toluene molecules that are still chemisorbed at the sensor surface. The increased response at the beginning of the pulse does not affect the magnitude of response,

suggesting that equilibrium between the sensor surface and the atmosphere is reached regardless of the presence of any species at the sensor surface initially.

At an operating temperature of 300°C (Fig 5.16), zeolite Y modified vanadium pentoxide shows a significantly larger magnitude of response than any other sensors. The response of zeolite Y modified vanadium pentoxide does however, show very poor recovery and the response does not return to baseline following exposure to toluene. Other zeolite-modified sensors reach a steady state during the 600-second gas pulse. Recovery of all sensors is poor with no responses returning fully to baseline following exposure to 40-ppm toluene.

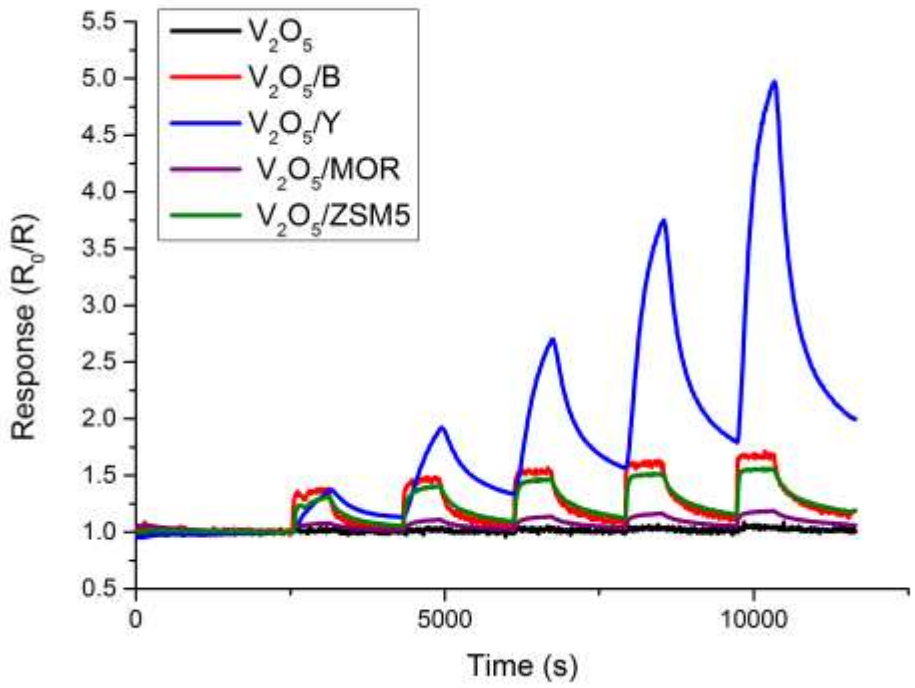

Figure 5.16. Response (± 1 S.D.) of V_2O_5 based sensors (unmodified V_2O_5 and zeolite beta, Y, mordenite and ZSM5 admixtures) to concentrations of 2.5, 5, 10, 20 and 40 ppm toluene at an operating temperature of 300°C. Response is calculated as a function of baseline resistance R_0 that is, the sensor resistance in dry air.

At an operating temperature of 250°C, sensor response to toluene was generally poor, with no response greater than R_0/R = 3.2 to 40 ppm toluene (Fig 5.17). Zeolite beta and Y modified vanadium pentoxide show the largest enhancements in response, this is likely due to breakdown of toluene molecules into constituent parts that can react at

the sensor surface. Zeolite beta and Y may, at lower operating temperatures, be more efficient at the acid catalysed breakdown of toluene than mordenite and ZSM5 modified sensors. At operating temperatures of 400°C and 500°C, ZSM5 and mordenite modified ZnO sensors are found to be more responsive to toluene than unmodified ZnO (as detailed in section 3.7), this is thought to be due to the breakdown of toluene into pentadiene, butadiene and other short chain hydrocarbon molecules at the zeolite surface. Zeolite Y modified vanadium pentoxide shows a poor recovery to baseline following each gas pulse, potentially due to increased adsorption and poor desorption from the sensor this may be due to the super cage structure of zeolite Y which is able to adsorb toluene molecules more efficiently.

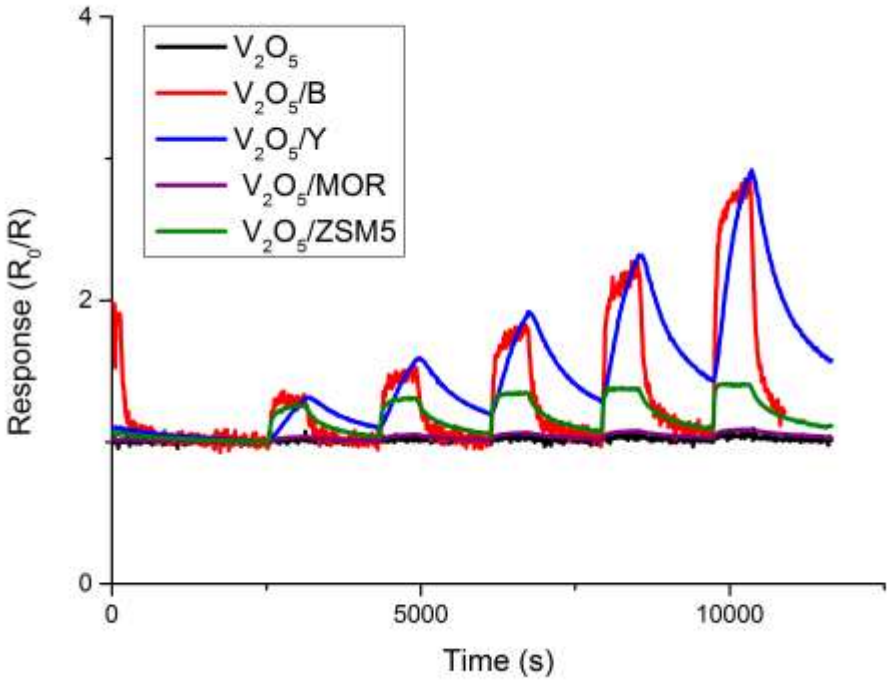

Figure 5.17. Response (± 1 S.D.) of V_2O_5 based sensors (unmodified V_2O_5 and zeolite beta, Y, mordenite and ZSM5 admixtures) to concentrations of 2.5, 5, 10, 20 and 40 ppm toluene at an operating temperature of 250°C. Response is calculated as a function of baseline resistance R_0 that is, the sensor resistance in dry air.

Figure 5.18 illustrates the response of all sensors across all operating temperatures to pulses of toluene. Large enhancements in the response of zeolite Y modified vanadium pentoxide are observed compared to unmodified vanadium pentoxide, this response reaches a maximum at 300°C. Beta, mordenite and ZSM5 modified sensors also reach

maximum responsiveness at 300°C, however the enhancement in zeolite Y modified vanadium pentoxide is far larger than the enhancement in other sensors.

The pore diameter of zeolite Y is larger than zeolite beta, mordenite or ZSM5, therefore relatively large toluene molecules (compared to other analyte gases used in this study) are able to successfully diffuse through the zeolite which results in fewer collisions with channel walls and allows a greater proportion of toluene molecules to reach and react at the gas sensitive surface.

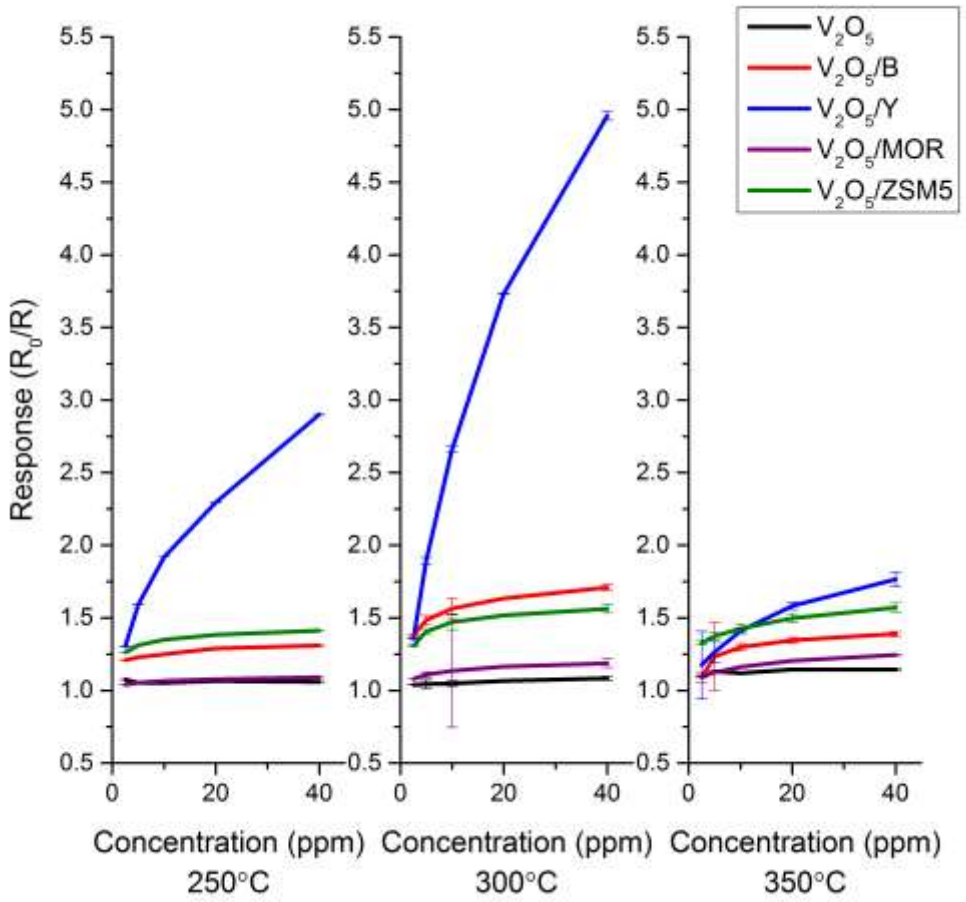

Figure 5.18. Response (± 1 S.D.) of V_2O_5 based sensors (unmodified V_2O_5 and zeolite beta, Y, mordenite and ZSM5 admixtures) to concentrations of 2.5-40 ppm toluene at temperatures of 250°C, 300°C, 350°C. Response is calculated as a function of baseline resistance R_0 that is, the sensor resistance in dry air.

The response times for vanadium pentoxide based sensors on exposure to 40-ppm toluene are detailed in Table 5.6. The response times for exposure to toluene are generally longer than those for other gases, especially at lower temperatures. Generally,

there is a decrease in response time as the operating temperature increases, potentially due to an increased rate of reaction at the sensor surface.

Table 5.6. Response times (± 5 s) for V_2O_5 based sensors (unmodified V_2O_5 and zeolite beta, Y, mordenite and ZSM5 admixtures) to 40-ppm toluene.

Sensor	Response time (s, ±5)		
	250°C	**300°C**	**350°C**
V_2O_5	100	120	60
V_2O_5/B	190	130	90
V_2O_5/Y	260	210	180
V_2O_5/MOR	240	120	110
V_2O_5/ZSM5	160	90	60

5.3.5. Exposure to Acetone

All sensors were exposed to 0.5, 1, 2, 4 and 8 ppm acetone at 250°C, 300°C and 350°C. All sensors produced responses that resulted in a decrease in resistance.

At an operating temperature of 350°C (Fig 5.19), the magnitude of response of the zeolite Y modified vanadium pentoxide sensor is considerably higher than the other sensors; this response exhibits a shark-fin shape and does not reach a steady state in the 600-second gas pulse. All other sensors reach an approximate steady state. The recovery of all sensors is good, with resistances returning to their initial baseline.

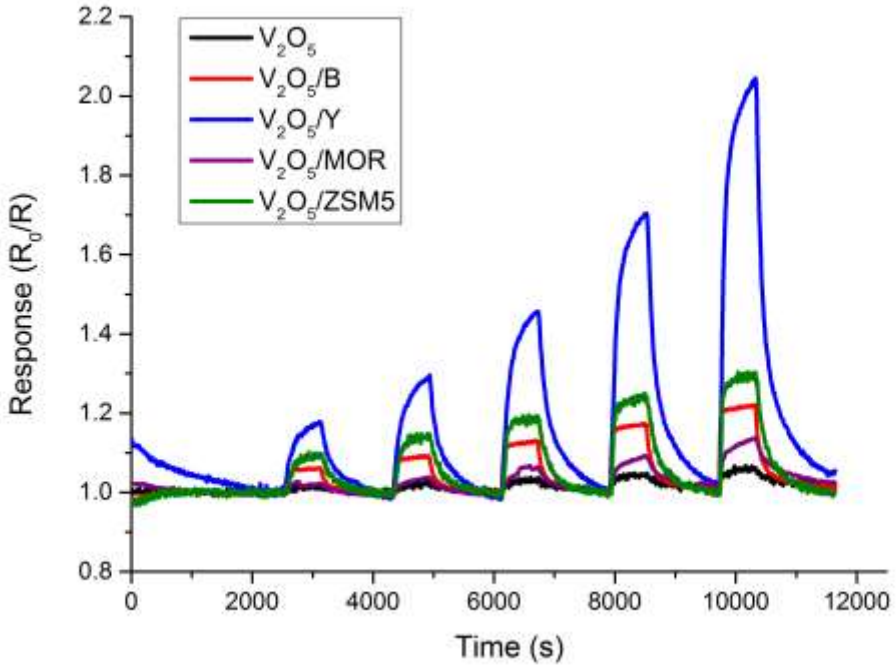

Figure 5.19. V_2O_5 based sensors (unmodified V_2O_5 and zeolite beta, Y, mordenite and ZSM5 admixtures) response to 0.5, 1, 2, 4 & 8 ppm acetone, at an operating temperature of 350°C. Response is calculated as a function of baseline resistance R_0 that is, the sensor resistance in dry air.

At an operating temperature of 300°C (Fig 5.20) the response of all vanadium pentoxide and zeolite modified vanadium pentoxide sensors (except for mordenite modified vanadium pentoxide) are found to show non-ideal recovery. Zeolite beta and ZSM5 modified vanadium pentoxide sensors do not return to their baseline response following a gas pulse, while the recovery of zeolite Y shows significant baseline drift and the sensor is unable to re-establish a stable baseline following a gas pulse. Despite the poor baseline stability, zeolite Y modified vanadium pentoxide shows the largest magnitude of response with R_0/R = 1.79 to 8 ppm acetone. The unmodified vanadium pentoxide sensor shows a poor response to all concentrations of acetone.

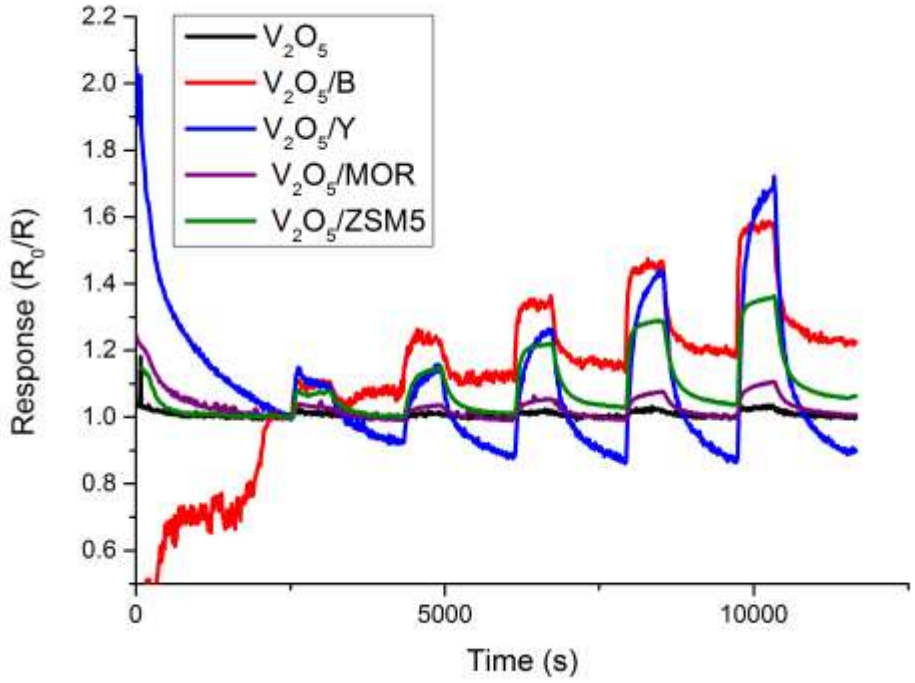

Figure 5.20. V_2O_5 based sensors (unmodified V_2O_5 and zeolite beta, Y, mordenite and ZSM5 admixtures) response to 0.5, 1, 2, 4 & 8 ppm acetone, at an operating temperature of 300°C. Response is calculated as a function of baseline resistance R_0 that is, the sensor resistance in dry air.

At an operating temperature of 250°C (Fig 5.21) the response of zeolite beta modified vanadium pentoxide is especially noisy, the sensor is unable to establish a baseline and while relatively strong responses are recorded, these are not accurate, due to significant baseline drift and noise in the signal. Zeolite Y, mordenite and ZSM5 modified vanadium pentoxide sensors show more stable responses, with the response of mordenite modified vanadium pentoxide demonstrating a response of R_0/R = 2.05 to 8 ppm acetone. The recovery of mordenite and ZSM5 modified vanadium pentoxide following a gas pulse is found to be quick, while zeolite Y recovery is poor and zeolite beta does not recover at all. The unmodified vanadium pentoxide sensor again shows poor responsivity to acetone at all concentrations.

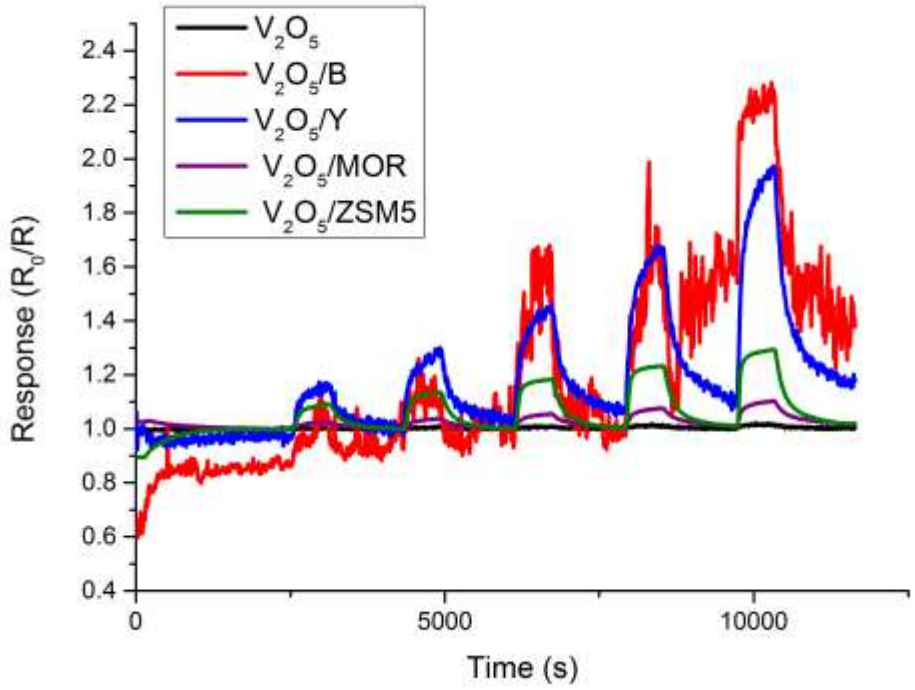

Figure 5.21. V_2O_5 based sensors (unmodified V_2O_5 and zeolite beta, Y, mordenite and ZSM5 admixtures) response to 0.5, 1, 2, 4 & 8 ppm acetone, at an operating temperature of 250°C. Response is calculated as a function of baseline resistance R_0 that is, the sensor resistance in dry air.

Responses of all vanadium pentoxide based sensors to acetone (Fig. 5.22) increase slightly as operating temperature decreases. The exception to this is the zeolite Y modified sensor, which shows a maximum response at 350°C. Zeolite beta modified vanadium pentoxide shows the largest response of any sensor to acetone, with a maximum response of R_0/R= 2.3 to a concentration of 8 ppm. The repeatability of all sensors is generally good, especially at 350°C.

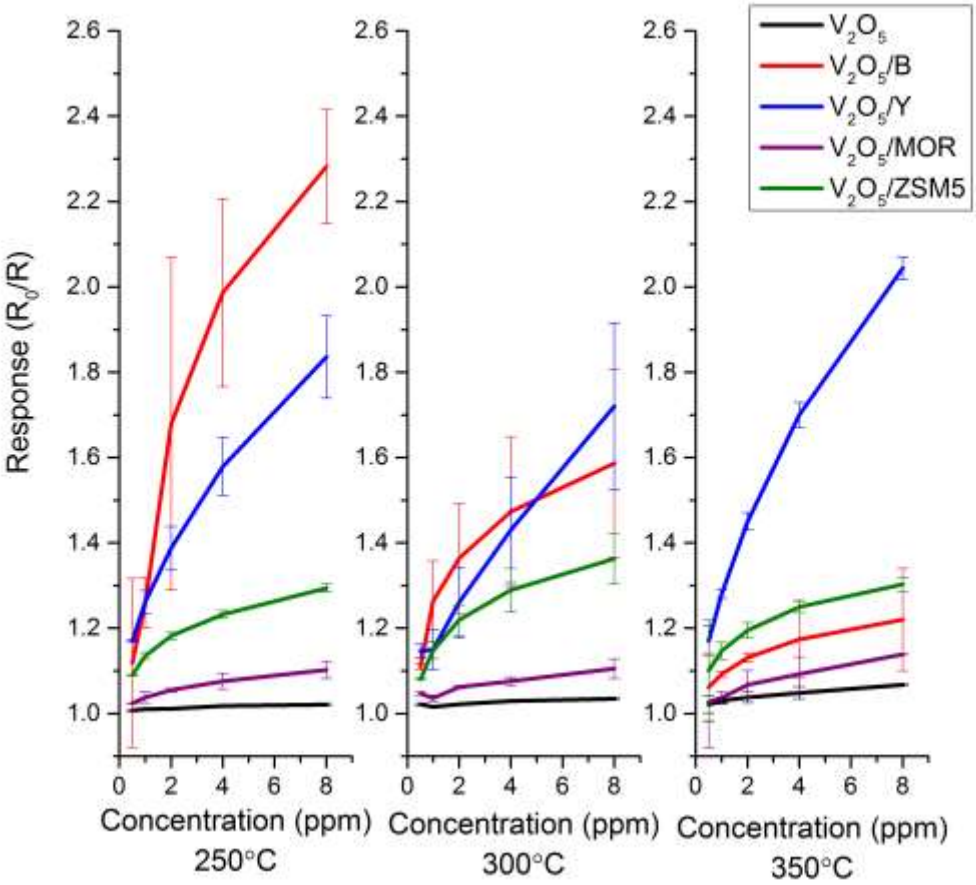

Figure 5.22 Response (± 1 S.D.) of V_2O_5 based sensors (unmodified V_2O_5 and zeolite beta, Y, mordenite and ZSM5 admixtures) to concentrations of 0.5-8 ppm acetone at temperatures of 250°C, 300°C, 350°C.

Response times on exposure to 8-ppm acetone (Table 5.7) generally decrease with increasing temperature. This is likely because of a faster rate of reaction at the sensor surface at higher temperature. An exception to this is observed with mordenite modified vanadium pentoxide, this is likely due to the poor response of mordenite modified vanadium pentoxide and the poor signal to noise ratio observed at 400°C which means that the response time is perceived to be short. Zeolite modified sensors all have longer response times that the unmodified sensor, this is a result of the gas sensitive semiconductor material being more accessible to the target gas, whereas the zeolite material has the potential to provide hindrance to target gas, attempting to reach the sensor surface.

Table 5.7. Response times (± 5 s) for V_2O_5 based sensors (unmodified V_2O_5 and zeolite beta, Y, mordenite and ZSM5 admixtures) to 8-ppm acetone.

Sensor	Response time (s, ±5)		
	250°C	**300°C**	**350°C**
V_2O_5	110	70	60
V_2O_5/B	170	80	40
V_2O_5/Y	290	280	210
V_2O_5/MOR	140	200	120
V_2O_5/ZSM5	190	120	90

5.3.6. Exposure to Ammonia

Exposure to 2.5, 5, 10, 20, 40 ppm of ammonia resulted in generally poor responses from vanadium pentoxide modified sensors at 350°C (Fig. 5.23). The largest response came from zeolite Y modified vanadium pentoxide with a response of $R_0/R = 1.27$. Despite this slightly stronger response, the recovery of this sensor in particular is poor; the resistance is unable to reach its initial R_0 value after any gas pulse. The resistance of all sensors is noisy, a result of potentially poor ammonia adsorption at the sensor surface. None of the sensors reach a steady state during their 600-second gas pulse on exposure to ammonia.

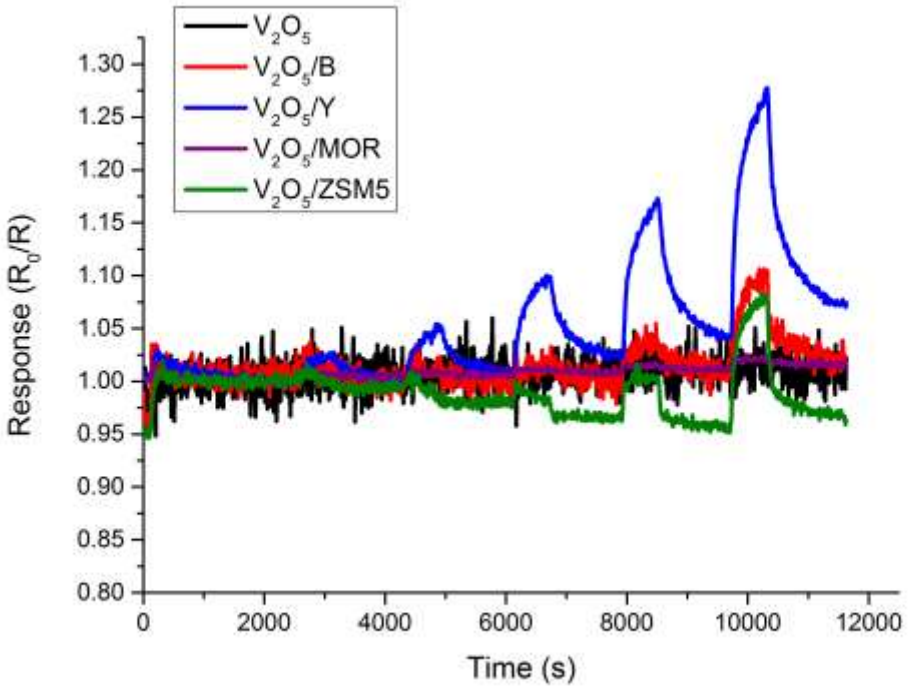

Figure 5.23. V_2O_5 based sensors (unmodified V_2O_5 and zeolite beta, Y, mordenite and ZSM5 admixtures) response to 2.5, 5, 10, 20 & 40 ppm ammonia, at an operating temperature of 350°C. Response is calculated as a function of baseline resistance R_0 that is, the sensor resistance in dry air.

At an operating temperature of 300°C (Fig 5.24) the responses of vanadium pentoxide and zeolite modified vanadium pentoxide sensors to ammonia show poor responses, that are attributed more to background noise, rather than the presence of any analyte gas. On exposure to ammonia, no single sensor presents a significant response to any concentration of gas.

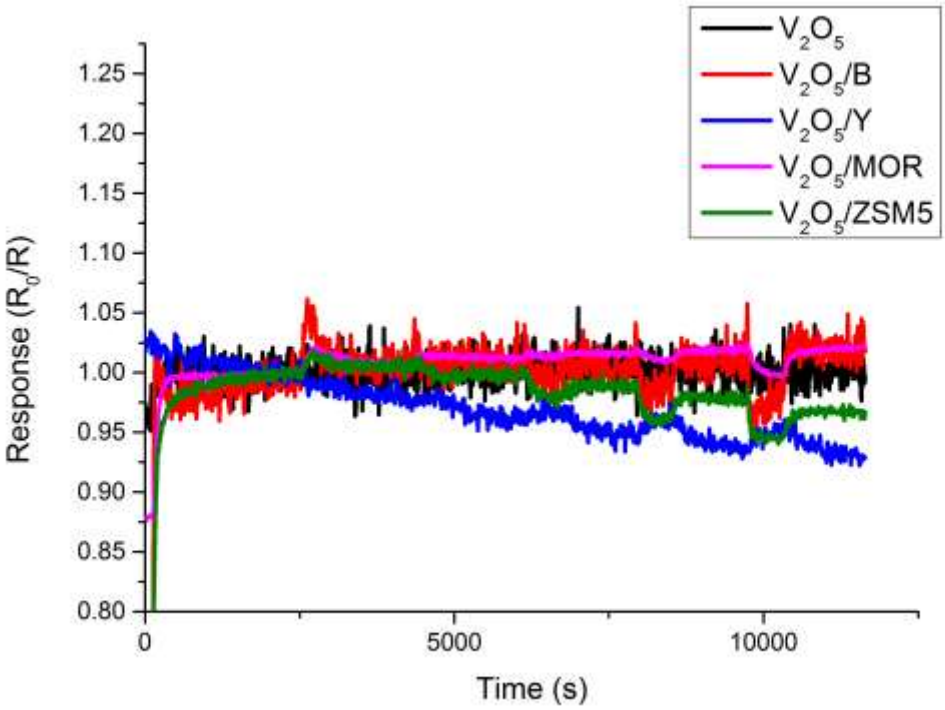

Figure 5.24. V_2O_5 based sensors (unmodified V_2O_5 and zeolite beta, Y, mordenite and ZSM5 admixtures) response to 2.5, 5, 10, 20 & 40 ppm ammonia, at an operating temperature of 300°C. Response is calculated as a function of baseline resistance R_0 that is, the sensor resistance in dry air.

At an operating temperature of 250°C (Fig 5.25) responses of vanadium pentoxide based sensors again show poor response to ammonia responses are unidentifiable at concentrations below 40 ppm, with only the zeolite beta modified vanadium pentoxide sensor demonstrating a response above $R_0/R = 1.2$. This response was to 40 ppm of ammonia.

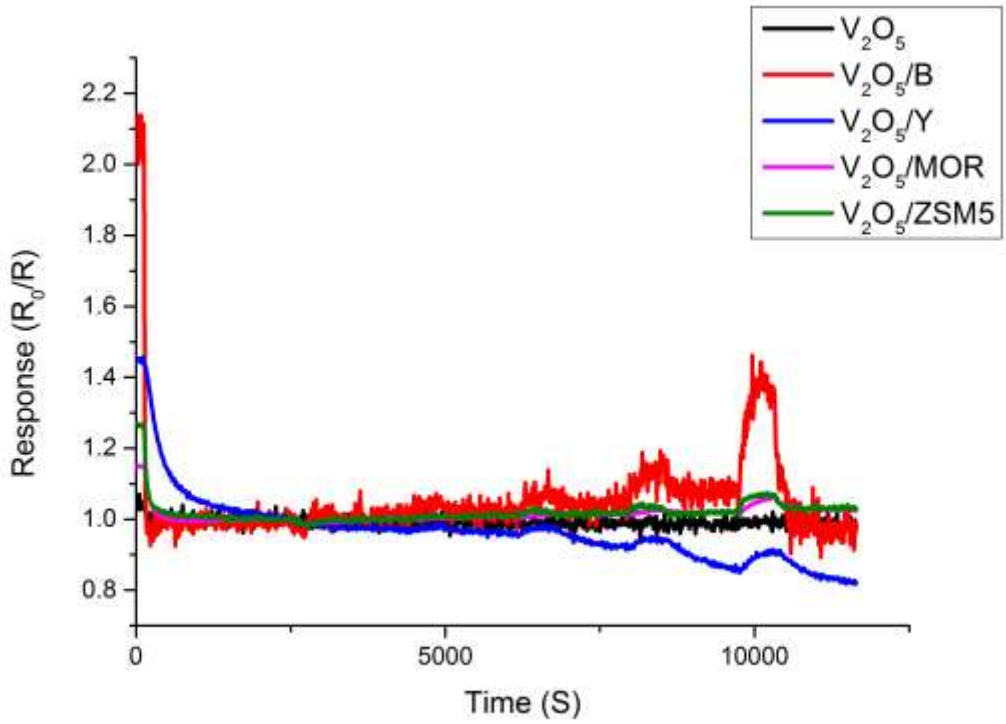

Figure 5.25. V_2O_5 based sensors (unmodified V_2O_5 and zeolite beta, Y, mordenite and ZSM5 admixtures) response to 2.5, 5, 10, 20 & 40 ppm ammonia, at an operating temperature of 250°C. Response is calculated as a function of baseline resistance R_0 that is, the sensor resistance in dry air.

The majority of vanadium pentoxide modified and unmodified sensors show poor responses upon exposure to ammonia at different temperatures (Fig. 5.26). The exception to this being zeolite Y modified vanadium pentoxide at 350°C and 300°C, and zeolite beta modified vanadium pentoxide at 250°C, even in these cases the responses are poor when compared with most other responses in this thesis. Interestingly, the strong responses of zeolite Y modified vanadium pentoxide at 350°C and 300°C becomes reversed at 250°C, that is, above 300°C, resistance decreases on contact with ammonia, however, at 250°C, resistance increases on contact with ammonia. A similar phenomenon is observed with H-ZSM5 at 350°C. Following the first pulse of ammonia (2.5 ppm) the recovery of the sensor appears to lower the resistance of the sensor, below its initial baseline, this occurs again after the second pulse of ammonia (5 ppm). The magnitude of response of these early pulses of ammonia, while decreasing in resistance as expected, is unable to return to the initial baseline. This means that the response appears with an R_0/R value less than 1.

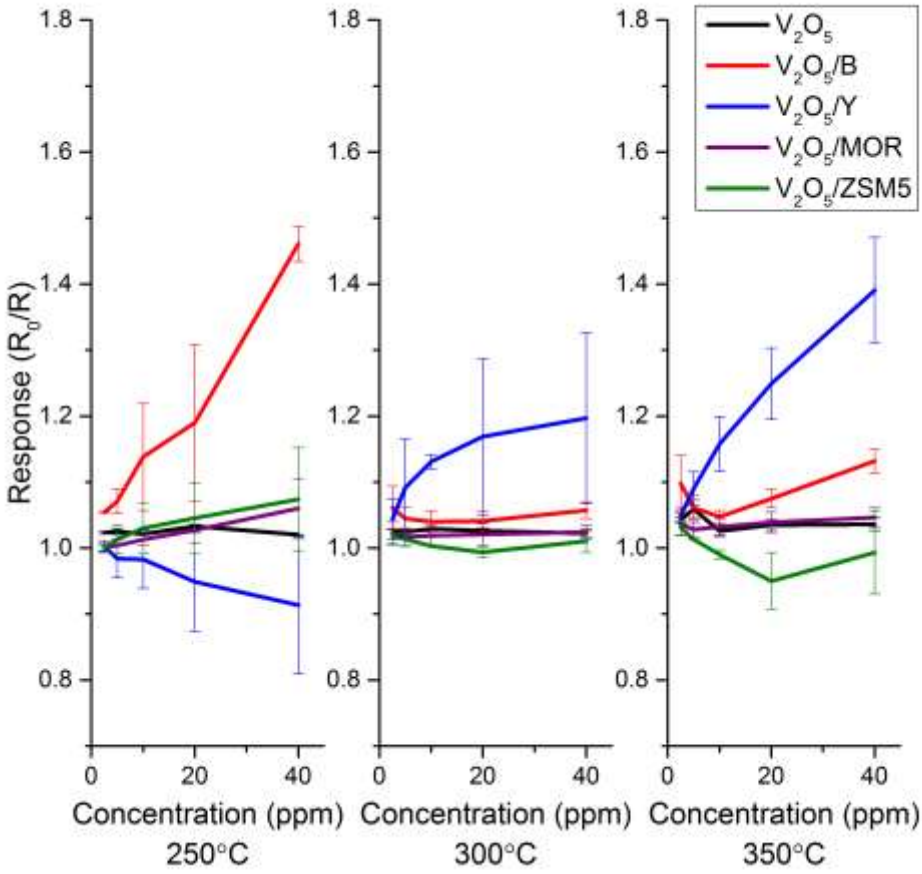

Figure 5.26. Response (± 1 S.D.) of V_2O_5 based sensors (unmodified V_2O_5 and zeolite beta, Y, mordenite and ZSM5 admixtures) to concentrations of 2.5-40 ppm ammonia at temperatures of 250°C, 300°C, 350°C. Response is calculated as a function of baseline resistance R_0 that is, the sensor resistance in dry air.

Response times for all sensors (Table 5.8) are generally quite high, with zeolite beta and Y showing the largest response times (greater than 200 seconds). Mordenite and ZSM5 modified vanadium pentoxide based sensors show response times comparable to vanadium pentoxide. The low responses of these sensors ($R_0/R < 1.1$) indicate that this low response time is more indicative of a poor response than a fast reaction at the sensor surface. Response times tend to increase with increasing operating temperature, the exception being mordenite modified vanadium pentoxide. The increase in response time with increasing operating temperature is not observed with other sensors, this increase is likely due to the poor response. The response transients at operating

temperatures of 300°C and 250°C show that the signal to noise ratio is very low, meaning that the response is not significantly larger than background noise experienced by the sensor.

Table 5.8. Response times (± 5 s) for V_2O_5 based sensors (unmodified V_2O_5 and zeolite beta, Y, mordenite and ZSM5 admixtures) to 40-ppm ammonia.

	Response time (s, ±5)		
Sensor	**250°C**	**300°C**	**350°C**
V_2O_5	70	80	90
V_2O_5/B	210	230	280
V_2O_5/Y	120	160	200
V_2O_5/MOR	90	70	80
V_2O_5/ZSM5	100	90	70

5.3.7. Exposure to Multiple Gases

In addition to observation of the sensors and their response to a single test gas, all vanadium pentoxide based sensors were exposed to a mixture of test gases. Sensors were exposed to 2400 seconds of air, followed by the introduction of 50 ppm ethanol, after an 1800 second period, 25 ppm of acetone was also introduced to the system for 600 seconds. Following this pulse, the ethanol-air baseline re-equilibrated, followed by a 50-ppm pulse, before returning to ethanol, then to baseline air.

Table 5.9. Experimental parameters for ethanol/acetone exposure experiment

Time (s)	Percentage of flow		
	Air	**Ethanol**	**Acetone**
2400	100	0	0
1800	50	50 (50 ppm)	0
600	25	50 (50 ppm)	25 (25 ppm)
1200	50	50 (50 ppm)	0
600	0	50 (50 ppm)	50 (50 ppm)
1200	50	50 (50 ppm)	0
1200	100	0	0

The response of all vanadium pentoxide sensors is shown in Fig 5.27. Initially, on exposure to ethanol, sensors undergo a conductive response (decrease in resistance); after a short period of time all sensors reach a steady state. On exposure to acetone, the response increases further. Following the first acetone pule, where the atmosphere contains 50-ppm ethanol, zeolite Y, mordenite and ZSM5 modified sensors do not recover fully to their initial, pre-acetone resistance. On exposure to 50-ppm acetone (atmospheric composition: 50 ppm ethanol, 50 ppm acetone), responses increase further, with zeolite Y showing the largest response ($R_0/R = 3.15$). Zeolite Y, mordenite and ZSM5 sensors again do not fully recover following the second acetone pulse. The recovery following the return to just compressed air (no acetone or ammonia) is significantly better, due to the increased oxygen concentration. Zeolite beta modified vanadium pentoxide performs particularly well in this experiment. While it does not have as large a magnitude of response as other zeolite modified sensors, the response and recovery during every phase of the experiment is quick and efficient, the establishment of a new baseline is quick and the recovery back to the initial response is good.

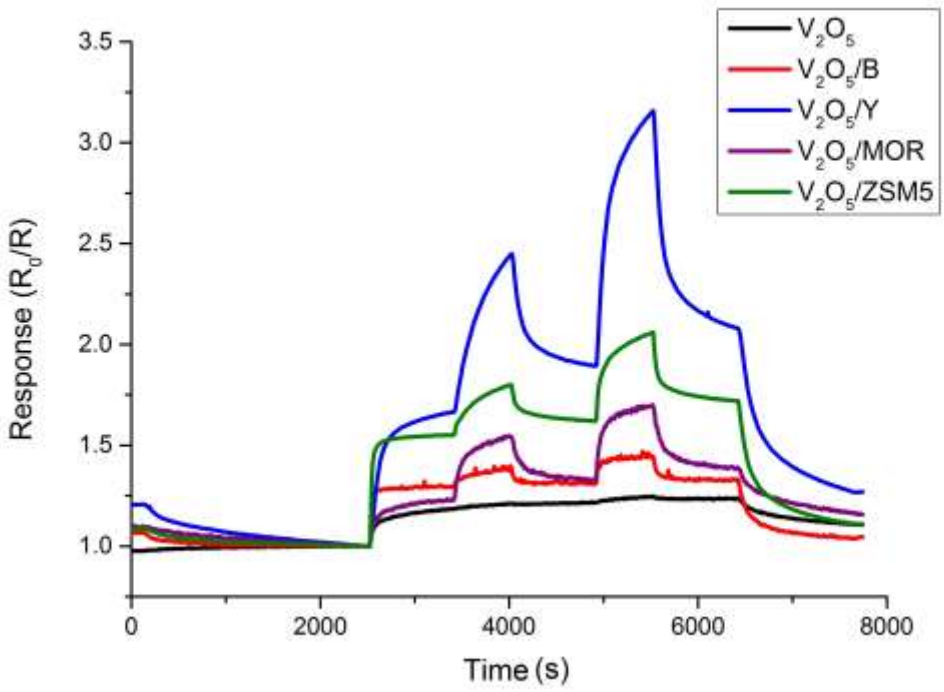

Figure 5.27. Exposure of V_2O_5 sensors, at an operating temperature of 350°C, to 50 ppm ethanol with pulses of 25 ppm and 50 ppm acetone. Response is calculated as a function of baseline resistance R_0 that is, the sensor resistance in dry air.

A similar experiment was performed using ethanol and nitrogen dioxide. Nitrogen dioxide, as an oxidising gas, results in a different response (an increase in sensor resistance, as opposed to a decrease observed with reducing gases). The experiment details are illustrated in Table 5.10. Ethanol was introduced to the system at a concentration of 50 ppm, followed by 250 and 500 ppb pulses of nitrogen dioxide on top of the ethanol.

The response to this experiment (Fig 5.28) shows a decrease in resistance when sensors are exposed to ethanol. When nitrogen dioxide is introduced into the system, the resistance of all sensors decreases further, this is the opposite response observed elsewhere in the thesis. On exposure to other n-type materials (sections 3.3.3 and 5.3.3) the resistance of sensors increases on exposure to nitrogen dioxide. This may be due to gas phase reactions between ethanol and nitrogen dioxide to produce a nitro group-containing compound. Gas phase reactions between primary alcohols and nitrogen dioxide have been observed previously[224] and may account for this unexpected

response. One would expect to see a decrease in resistance on the introduction of ethanol, followed by a decrease increase in resistance on the introduction of NO_2.

Table 5.10. Experimental parameters for ethanol/NO_2 exposure experiment.

Time (s)	Percentage of flow		
	Air	Ethanol	NO_2
2400	100	0	0
1800	50	50 (50 ppm)	0
600	25	50 (50 ppm)	25 (0.25 ppm)
1200	50	50 (50 ppm)	0
600	0	50 (50 ppm)	50 (0.5 ppm)
1200	50	50 (50 ppm)	0
1200	100	0	0

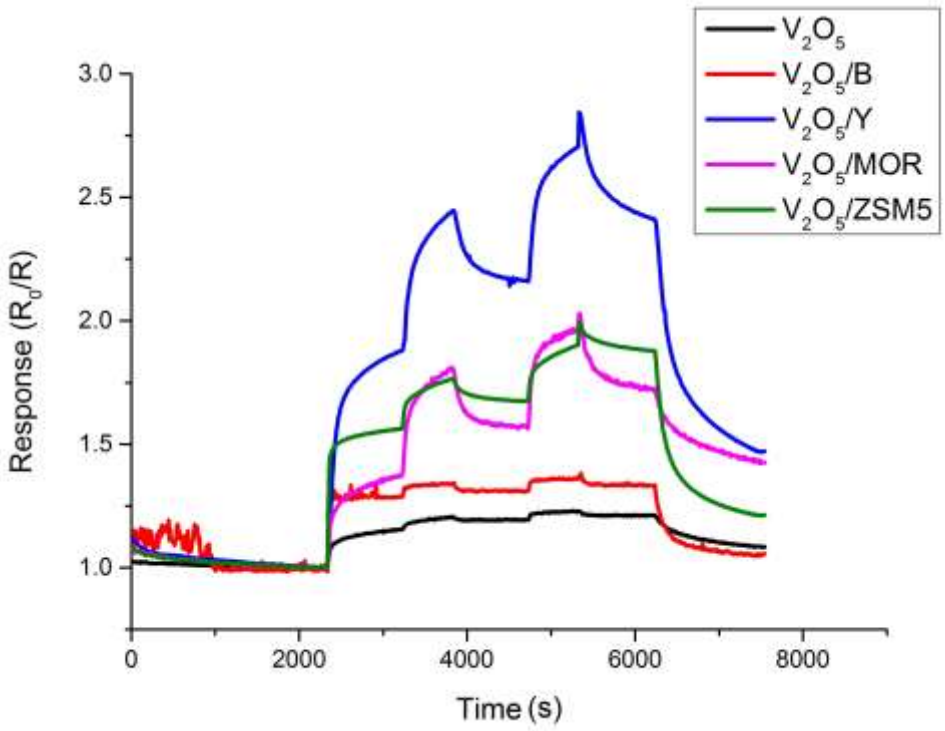

Figure 5.28. Exposure of V_2O_5 sensors to 50-ppm ethanol, with 250 and 500 ppb pulses of NO_2. Response is calculated as a function of baseline resistance R_0 that is, the sensor resistance in dry air.

5.4. Discussion

The maximum response of all screen-printed unmodified and zeolite admixture modified vanadium pentoxide sensors to 40 ppm of the five gases used in this study are shown in Fig. 5.29. These results show that vanadium pentoxide sensors show little to no sensitivity towards ammonia at the concentrations utilised. Pure vanadium pentoxide shows very poor responsiveness towards all gases used at 40 ppm. Of the four gases that the vanadium pentoxide and zeolite modified vanadium pentoxide sensors showed some response to, each has a different profile, i.e., different modified sensors show different ordered responses for example, with ethanol, the responsiveness of sensors are, in descending order; V_2O_5/MOR, V_2O_5/Y, V_2O_5/ZSM5, V_2O_5/B and V_2O_5, whereas acetone exposure at the same concentration has a different order of sensor responses; V_2O_5/Y, V_2O_5/B, V_2O_5/ZSM5, V_2O_5/MOR and V_2O_5. These differences in the order of responsiveness, as well as the different ratios of response give the sensor array some degree of selectivity, with each gas having a unique 'chemical fingerprint'.

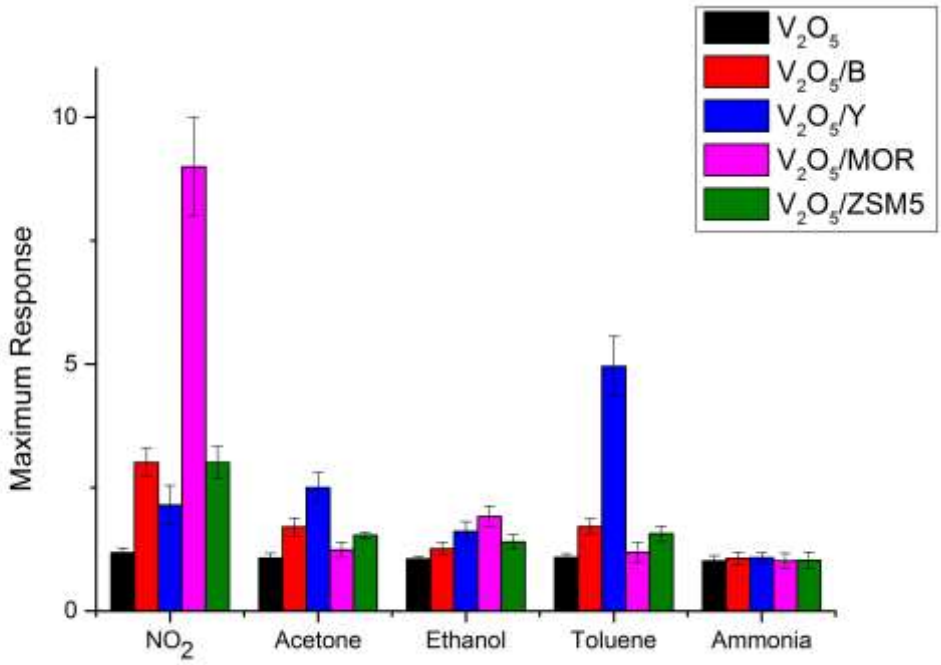

Figure 5.29. Response (R_0/R for all gases, except NO_2, which is R/R_0) of V_2O_5 sensors (unmodified V_2O_5 and zeolite beta, Y, mordenite and ZSM5 admixtures) at an operating temperature of 300°C to 40 ppm of a range of gases.

When reducing agents, such as ethanol, acetone, toluene and ammonia, interact with adsorbed oxygen at the sensor surface, electrons are reintroduced into the bulk. In all materials an increased concentration of gas, results in a larger magnitude of response. This increased magnitude of response is a direct result of an increased partial pressure in the immediate environment around the sensor surface and more available species to react with the vanadium pentoxide surface.

Nitrogen dioxide exhibits the opposite effect to all other gases; this is a result of its oxidising properties, as nitrogen dioxide can act as a free radical[225]. This free radical behaviour enables the nitrogen dioxide to react directly with the surface, as opposed to the adsorbed oxygen at the surface, making the vanadium pentoxide far more sensitive to nitrogen dioxide than to other gases and enabling a response in the ppb range as opposed to the ppm range observed for other analytes. Nitrogen dioxide reacts at the surface based on the following scheme:

$$NO_{2(g)} + 3e^- \rightarrow NO^{2-}_{(ads)} + O^-_{(ads)}$$

$$NO^{2-}_{(ads)} + O^-_{(ads)} + e^- \rightarrow NO_{(g)} + O^{2-}_{(ads)}$$

This complete reaction results in the introduction of more oxygen atoms at the sensor surface. The increased oxygen concentration leads to an increase in the thickness of the depletion layer, aided by the removal of electrons from the bulk material and therefore an increase in the resistance of the semiconductor material. The adsorption of O^- is very interesting step in reaction, because the O^- ions assist the adsorbed oxidising ions in taking electrons from the metal oxide surface, increasing the resistance further.

Zeolite modified sensors show increased responsiveness to all gases. There are a number of reasons for this increased activity at the sensor surface. Table 5.1 shows that zeolite modified materials have significantly larger surface areas (30-50 times larger) than the pure vanadium pentoxide material, this increased surface area, a result of the

inclusion of very absorbent material, means that target gases can be absorbed to the surface and catalysed into smaller molecules, resulting in more molecules available for reaction for example, toluene is known to breakdown to a number of hydrocarbon species, including propane, butane and ethane, in the presence of H-ZSM5 at temperatures of 250°C-450°C (as detailed in section 3.6).

$$C_7H_9 + 7H^+ \rightarrow 3C_2H_4 + CH_4$$

This reaction uses hydrogen ions, available as counter ions from the zeolite, to break down a single toluene molecule into four hydrocarbon molecules, which can then react independently with the sensor material.

In the data shown, ammonia has significantly smaller magnitudes of response than that observed with other reducing gases. In some cases, such as exposure of gases to pure vanadium pentoxide and mordenite modified vanadium pentoxide sensors, the response is not significantly larger than the background resistance. The proposed reactions at the vanadium pentoxide sensor surface are:

$$2NH_{3(g)} + 3O^-_{(ads)} \rightarrow N_{2(g)} + 3H_2O_{(g)} + 3e^-$$

$$2NH_{3(g)} + 5O^-_{(ads)} \rightarrow NO_{(g)} + 5e^-$$

$$2NH_{3(g)} + 4O^-_{(ads)} \rightarrow N_2O_{(g)} + 3H_2O_{(g)} + 4e^-$$

The reaction pathway is dependent on the availability of oxygen at the sensor surface; ammonia produces fewer electrons per adsorbed oxygen at the sensor surface than other gases. Ammonia is also known to strongly chemisorb to zeolite materials[226], which may result in ammonia gas molecules not reaching the more active vanadium pentoxide surface. These poor results could also be a result of water vapour accumulation at the sensor surface, although this is unlikely at high temperatures[227].

Response times for MOS sensors are generally longer than other types of sensor such as infrared gas sensors (with reaction times < 3 s); this is because of the slower reaction time at the sensors surface. Reaction times are independent of the response of the sensor to that gas, the largest magnitude of response does not necessary mean the longest response time. Unmodified vanadium pentoxide usually has a shorter response time than the zeolite-modified counterparts. This is a result of the availability of semiconductor surface where target molecules can react.

An example of this is with ethanol adsorption on zeolite Y. With unmodified vanadium pentoxide, 100% of the surface area is gas sensitive area, whereas although the zeolite modified sensor is 43 times larger, this area is made mostly of porous zeolite, only approximately 2% of the surface area is metal oxide, able to react with the target gas and produce an electronic response. Zeolite Y is, in addition, a hydrophilic zeolite[228], meaning that water adsorbs well onto the surface of the zeolite, preventing it from reacting with the sensor and slowing the response time further, while hydrophobic zeolite beta has response times similar to unmodified vanadium pentoxide.

Zeolite Y modified vanadium pentoxide demonstrates a larger magnitude of response than other zeolite modified sensors in many cases. This larger response may be due to the larger pore diameter than other zeolites uses in this study. A larger channel in the zeolite allows molecules to diffuse with less likelihood of collision with the walls of the channel and allow molecules to reach the gas sensitive surface at a greater rate than in zeolites with smaller pore diameters.

Response times for all sensors decrease with increasing temperature, this is a result of increased rate of reaction at higher temperatures. The response of the sensor is dependent on a reaction at the surface, which liberates an adsorbed oxygen species on the surface to affect the conductivity of the material. When this reaction occurs at a higher temperature, more oxygen atoms are liberated at a faster rate until equilibrium is reached, therefore at higher temperatures, sensors have a faster response time.

The vanadium pentoxide sensors were able to identify the presence of a second gas, from a complex atmosphere containing ethanol and acetone. This is illustrated as a difference in response between exposure to acetone in air and acetone in an ethanol and air combination. The order of responsiveness of sensors is different for the acetone/ethanol combination compared to exposure of only ethanol or acetone. This order of responsiveness is unique to ethanol/acetone combination and could act as a way of detecting more complex gas mixtures.

When exposed to ethanol, sensors reached a steady state and could establish a new baseline, upon exposure to acetone, the magnitude of order of response changes, in the expected fashion.

When a nitrogen dioxide and ethanol mix is introduced, an unexpected response occurs. On the addition of ethanol, the expected decrease in resistance occurs, and reaches a relatively steady state. Nitrogen dioxide is then introduced, and the resistance increases further. Initially, as ethanol has reached a steady state, it is easy to presume that the surface is at equilibrium with the immediate atmosphere, and that any new gas is competing for available space at the sensor surface. When vanadium pentoxide sensors were exposed to nitrogen dioxide with no conflicting gases, the peak shape was unique, in that resistance decreased, then immediately increased. This is not observed, upon the addition of nitrogen dioxide and ethanol together, suggesting that a potential third species is introduced, either from the two gases reacting in the gas phase, at the sensor surface or in the zeolite mix.

Bartolomeu *et.al.*[229] suggest the following reaction of nitrogen dioxide and ethanol over H-ZSM5 at temperate of above 120°C:

$$NO_2 + C_2H_5OH \rightarrow NO + CH_3CHO + H_2O$$

This leads to the production of acetaldehyde, a species chemically similar to acetone, possessing one less methyl group. The peak shape and enhancement in magnitude of response is similar to those observed with ethanol and acetone.

When compared to other sensors (sections 3.3, 4.3 And 6.3), the response of these vanadium pentoxide based sensors is, with few exceptions, very poor. There are no sensors with a response to any gas above R/R_0 or $R_0/R = 6$. This low response is likely related to the small depletion region of the vanadium pentoxide grains. The size of the depletion region is broadly defined as:

$$\text{Thickness of depletion layer} \propto \frac{1}{\sqrt{N}}$$

Where N is the charge carrier density. It is observed from the baseline resistance of the sensors that unmodified vanadium pentoxide has a low resistance (several orders of magnitudes lower than those of zinc oxide or chromium titanate (See Table 3.6 & 4.7). This low resistance implies that the charge carrier density is high therefore, the depletion layer thickness is quite small. When gases react at the sensor surface and remove adsorbed oxygen from the surface, the depletion region changes in size, in the case of reducing gases, the depletion region shrinks and so resistance decreases. As the depletion region is already small and resistance is low then the removal of adsorbed species on the surface will have a relatively smaller effect than if removed from a metal oxide grain with a large depletion region. All modified zeolite sensor materials exist as a two-phase system, and the inclusion of zeolites does not affect the size of the depletion region. The large enhancement in resistance is a result of the insulating zeolite materials blocking the path of charge carriers in the materials.

Zeolite modified sensors do however show enhancements in the responsiveness of vanadium pentoxide sensors when compared with other methods of modification, namely vanadium pentoxide nanobelts[230] and mixed metal oxides[231].

Despite the poor responses of the sensors studied in this chapter, there are a number of reasons to indicate these sensors could be incorporated into an electronic nose. Most importantly, the unstable response to ammonia and nitrogen dioxide is interesting, while there are many metal oxide sensors that are highly sensitive to both

ammonia[232,233] and nitrogen dioxide[234,235], few are insensitive to these gases, and the absence of a response, as part of a 3 or 4 sensor array can provide evidence to the presence of these gases. The response time of a sensors to a gas varies depending on the species detected, therefore analysis of the magnitude of response and the response time for these sensors can give an indication of the class of gas present.

5.5. Conclusion

A series of five gas sensors, based on vanadium pentoxide and modified with four zeolites have been fabricated, characterised and tested for their gas sensing properties against five gases commonly found at clandestine locations. The sensors were found to show strong, repeatable responses to ethanol, toluene, and acetone, while responses to ammonia and nitrogen dioxide were poor. Zeolite modification was found to increase the responsiveness of sensors to all gases. Exposure to multiple gases showed that the sensors can detect a change in the ambient environment. The increase in response of zeolite-modified sensors is attributed to a combination of increased surface area, resulting in an increase in the adsorption of target gases and catalytic activity of the zeolite.

The next chapter examines indium doping of ZnO sensors. ZnO has been doped with 0.2-3% indium using a co-precipitation method, and investigates as a potential ethanol sensor.

6 Indium Doped Zinc Oxide

This chapter focuses on the doping of zinc oxide with indium via a co-precipitation method. Five different materials (unmodified zinc oxide and 0.2%, 0.5% 1% and 3% indium doped zinc oxide, IZO) were produced using this method and tested for their gas sensing properties. The electronic properties of the material were also assessed.

6.1 Introduction

The electronic properties of zinc oxide solids can be tuned via the incorporation of various dopants, usually group 13 elements such as Aluminum[236], Gallium[237] and Indium[238]. Doping zinc oxide materials with these elements replaces Zn^{2+} ions with higher valence M^{3+} ions, increasing impurities in the material through the introduction of new materials with differing electronic properties.

Many different doping techniques have been developed to produce both thick and thin film gas sensors, including; co-sputtering[239], thermal evaporation[240], pulsed laser deposition[241] and ball milling[242].

Different dopants and doping levels can be used to vary the electrical, structural, magnetic properties of semi-conducting oxides[243]. A variation in the type of dopant and doping level can therefore crucially affect the gas sensing properties of these materials, particularly their sensitivity for the detection of vapours such as ethanol.

The influence of Al, In, Cu, Fe, Sn, doping on ZnO thin films has been evaluated by Miki Yoshida *et.al*, who observed increased sensitivity in Al and Sn doped films[244]. Nickel doping of ZnO thin films has been shown to lower their operating temperature[245], and Cheng *et.al* investigated the use of ZnO nano particulate films to detect a variety of alcohols[246]. Aluminium doped ZnO has shown conductivity enhancements as well as improved transparency[247,248].

In this study, indium doped zinc oxide (IZO) powders were synthesised, characterised and tested for their ability to monitor low concentrations of various test gases in air. Doped and pure zinc oxide powders were prepared using a low cost, scalable co-

precipitation technique. This is a robust and reliable technique, which is easy to implement, as it does not require any expensive or complex equipment. Co-precipitation techniques (as discussed in section 2.1.4) have been used to produce a wide range of gas sensing materials in previous investigations[249,250].

6.2 Characterisation

6.2.1. Surface Area

Surface area measurements were performed using a Micromeritics TriStar II surface area analyser. The Surface area of all ZnO and IZO materials (Table 6.1) shows little variation with changing indium concentration. There is a small increase with increasing indium concentration, but this increase is far smaller than those observed on zeolite inclusion (section 3.1). There is a 66% increase in surface area of 3% In doped ZnO compared to the unmodified ZnO material, this is compared to an increase of around 6000% increase in surface are following zeolite modification (section 3.2.2).

Table 6.1. Surface areas of ZnO and 0.2%, 0.5%, 1% and 3% indium doped ZnO.

Material	Surface area (m^2/g)
ZnO	2.79
IZO (0.2%)	3.21
IZO (0.5%)	4.01
IZO (1%)	4.12
IZO (3%)	4.19

6.2.2. Scanning Electron Microscopy

Scanning Electron Microscopy (SEM) images of the sensor surface were recorded at 50,000x magnification (Fig. 6.1) these images show the porous nature of the materials.

Figure 6.1.a shows ZnO with an average grain size of 120 nm, whereas Fig 6.1.b shows hexagonal grains approximately 140 nm in diameter. Fig 6.1.c displays hexagonal grains, with an average grain diameter of 145 nm and Fig 6.1.d shows IZO (1%) with grain displaying less hexagonal characteristic, which were larger in diameter, approximately 200-250 nm. In Fig 6.1.e, IZO (3%), larger fused grains around 180 nm in diameter can be observed and Fig 6.1.f shows a sensors substrate with printed metal oxide material, for reference. The images show that as indium content increases, the hexagonal characteristics of the material become more defined. However, above 0.5% doping, the material loses its hexagonal characteristic, and larger, less uniform, grains are formed.

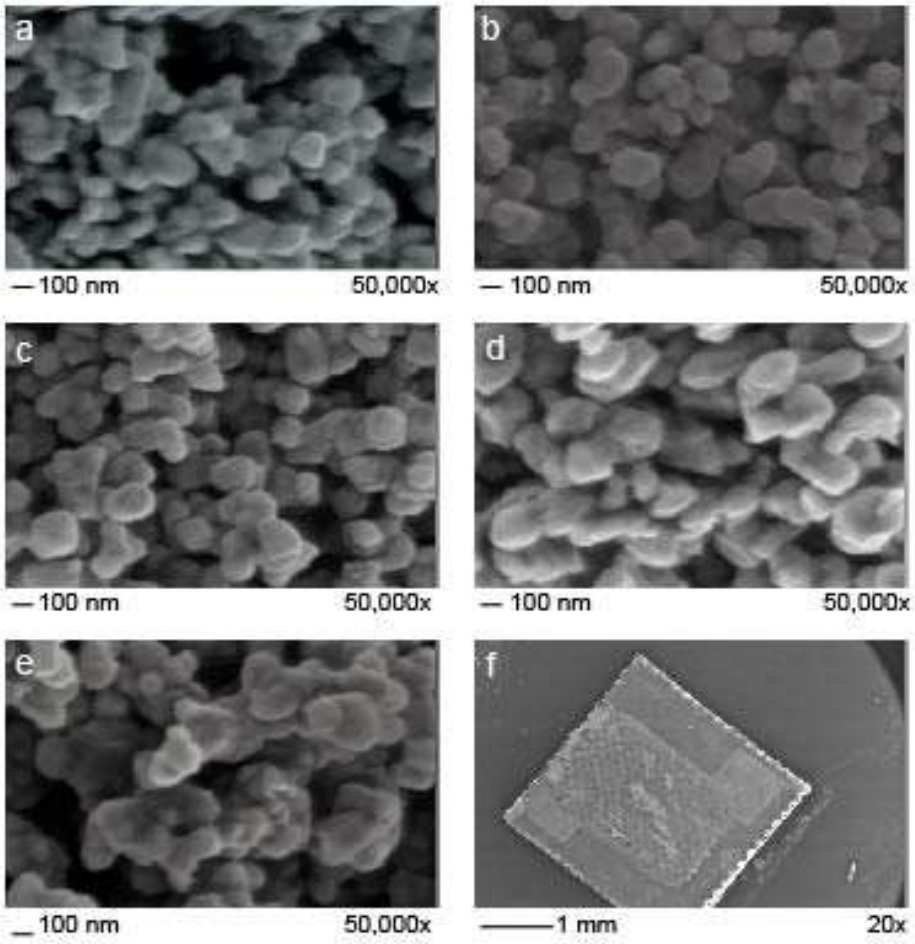

Figure 6.1. SEM micrographs of indium doped sensor chips. All images are at 50,000x magnification. a) ZnO, b) IZO (0.2%), c) IZO (0.5%), d) IZO (1%), e) IZO (3%) f) screen printed ZnO sensor.

6.2.3. Energy Dispersive X-ray Spectroscopy

The atomic (Table 6.2) and weight (Table 6.3) percentages of ZnO and IZO sensors show similar oxygen concentrations in all doped sensors, however with increasing indium concentrations, a decreasing zinc percentage is observed.

Table 6.2. Atomic percentages of unmodified zinc oxide and indium doped zinc oxide sensors.

	Atomic Percentage (%)		
	Zn	**O**	**In**
ZnO	53.0	47.0	0
IZO (0.2%)	52.7	46.9	0.2
IZO (0.5%)	52.4	46.5	0.5
IZO (1%)	52.0	46.9	0.9
IZO (3%)	50.0	47.1	2.9

Table 6.3. Weight percentages of unmodified zinc oxide and indium doped zinc oxide sensors.

	Weight Percentage (%)		
	Zn	**O**	**In**
ZnO	76.5	23.5	0
IZO (0.2%)	74.0	24.4	1.6
IZO (0.5%)	76.0	22.1	1.9
IZO (1%)	74.9	21.4	3.7
IZO (3%)	71.8	19.1	9.1

6.2.4. X-Ray Diffraction

X-ray diffraction patterns were collected for all samples (Fig. 6.2). All zinc oxide based materials show a predominant wurzite phase structure with high crystallinity, which can be matched with the Joint Committee on Powder Diffraction Standards (JCPDS card no. 36-1451) and literature studies on ZnO[251]. All samples display strong peaks at 2θ =

31.37°, 34.03°, 35.86°, 47.16°, 56.26° and 62.54°. No additional peaks were found in undoped ZnO. In indium doped ZnO, while the ZnO wurzite phase remains predominant, two low intensity peaks are observed (marked with *) showing the formation of an In_2O_3 corundum phase (JCPDS, No. 65,3170). The intensity of these peaks increases with increasing indium doping. These peaks are clearly visible in 1% and 3% IZO materials, in lower doped IZO and ZnO, the materials are single phased. This suggests that all indium added above 0.5% doping level is added as In_2O_3 and not as doped indium to the sample.

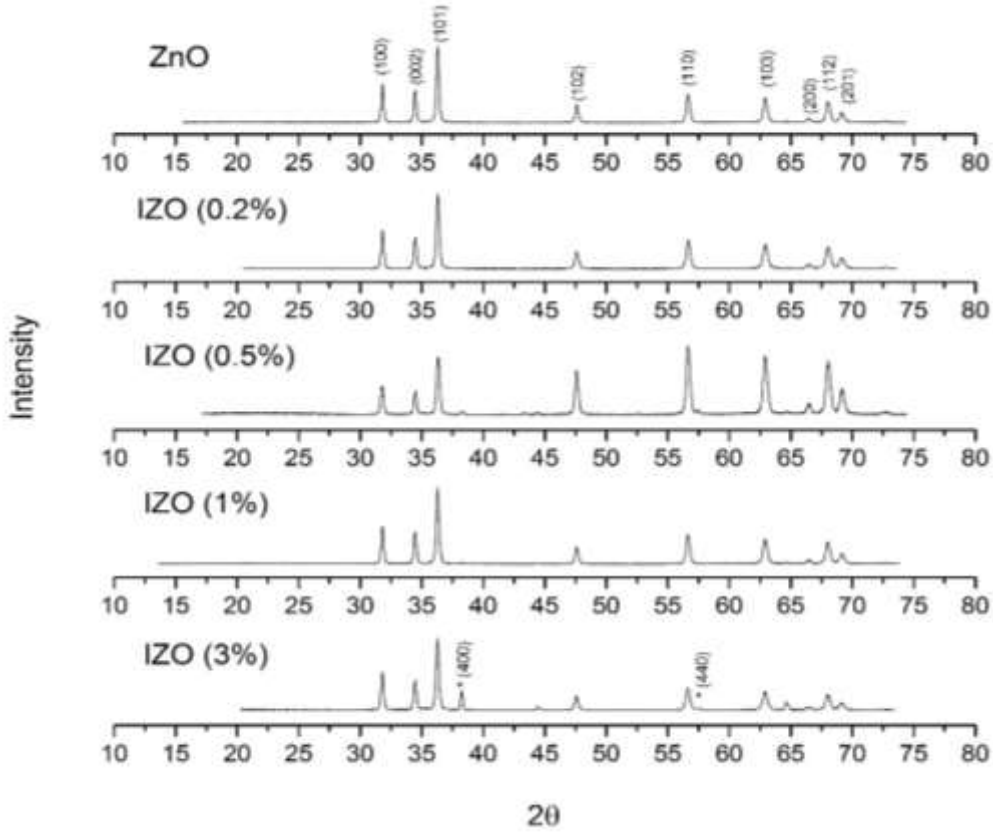

Figure 6.2. Diffraction patterns for ZnO and IZO sensors, collected between circa 10° and 75°. Peaks denoted with a * refer to the formation of an In_2O_3 corundum phase. The y-axis is normalised and offset for each spectrum. Principle peaks are indexed according to their standards from the literature[252].

6.2.5. Electrical Conductivity

The dc conductivity of the undoped and doped ZnO pellets were measured at room temperature using a Keithley 2400 Source Meter.

The conductivity of all samples was calculated from the linear region of I-V curves (Fig. 6.3). The dc conductivity was calculated using the following equation:

$$\sigma = \frac{t}{RA}$$

Where σ is the dc conductivity, t is the thickness, A is the area and R is the resistance of the samples, σ has the units: Ω^{-1} cm^{-1}.

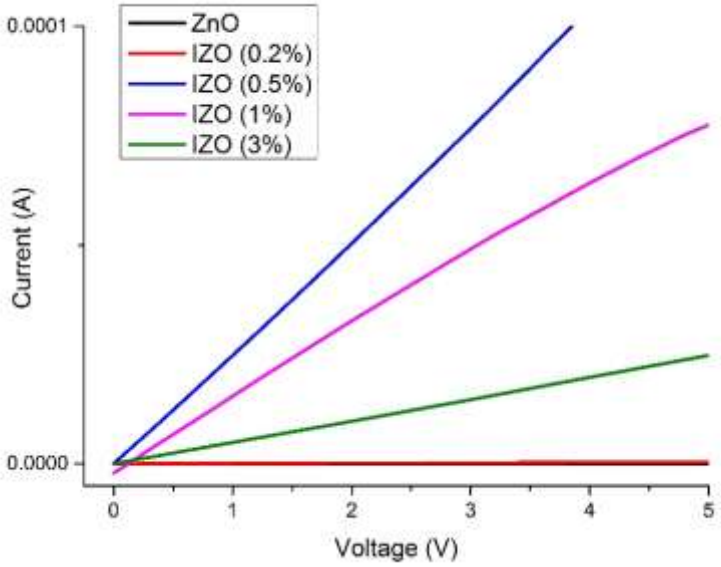

Figure 6.3. Variation in current with voltage at room temperature in ZnO and 0.2%, 0.5%, 1% and 3% indium doped ZnO.

The magnitude of conductivity in indium-doped materials is higher than the unmodified ZnO (Fig 6.4). This increase can be explained by two reasons: firstly, the increase in electrons leads to an increase in carrier concentration as a result of indium incorporation[253]. Secondly a large increase in the dopant concentration may cause the formation of a degenerate semi-conductor (a semiconductor with such a high level of doping that the material starts to act more like a metal than as a semiconductor) with high conductivity. The increased carrier concentration in the degenerate semiconductor can also lead to metallic behaviour of the In-doped ZnO[254].

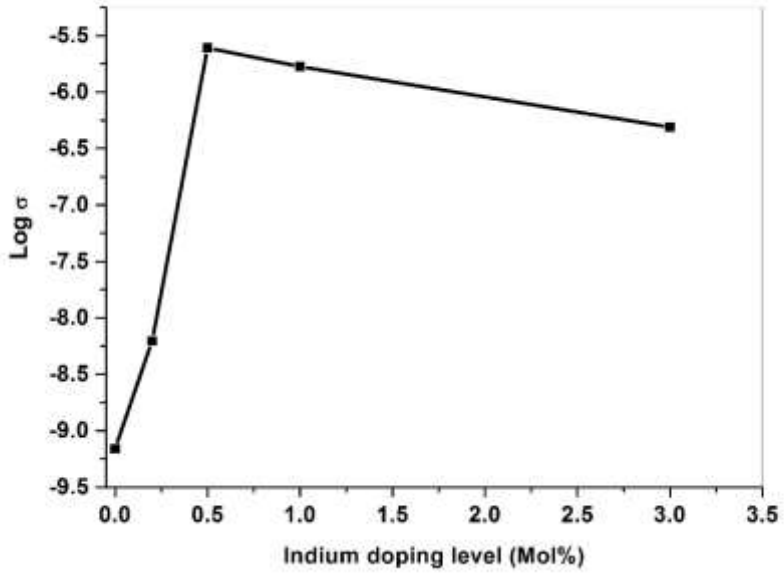

Figure 6.4. Variation in logσ with indium doping level.

In IZO materials with 1% and 3% indium, a decrease in conductivity is observed (Fig. 6.4). This decrease can be explained by the high dopant concentration increasing the probability of the ionized impurity centre scattering charge carriers, which can influence the electronic mobility, reducing the conductivity. This may also have contributed to the fusing of grains observed in Fig. 6.1[255].

The effects of metal impurities on the electrical conductivity of ZnO have been studied in detail, many researchers propose that dopants may enhance the excess oxygen concentration in the grain boundary region of the material and preferentially form a potential barrier[256,257]. Therefore, the electrical conductivity of the indium doped zinc oxide samples is apparently higher than that of the undoped ZnO, and the grain boundary is more resistive than the grain. Conductivity increases with increasing indium concentration, to 0.5%, and then reduces; this reduction in the conductivity may be due to the inactivity of added dopant atoms and the formation of a minor In_2O_3 phase as well as other morphological phase changes. The most likely explanation for this is that above 0.5% doping, all the extra indium that is added to the system is added as In2O3 and not as doped indium into the sample.

6.3. Results

6.3.1. Baseline Resistance

The baseline resistance of ZnO and all IZO sensors (Table 6.4) shows that the resistance of indium-doped sensors is lower that the undoped ZnO, indicating a larger charge carrier concentration. This is to be excepted based on the results observed in section 6.2.5 that showed an increase in conductivity in all IZO materials, especially in materials with low doping levels (< 1%).

Table 6.4. Baseline resistance of ZnO and 0.2%, 0.5%, 1% and 3% indium doped ZnO at operating temperatures of 350°C, 400°C, 500°C.

	Resistance (Ω)		
	350°C	**400°C**	**500°C**
ZnO	$1.5x10^8$	$1.7x10^6$	$6.3x10^5$
IZO (0.2%)	$2.3x10^6$	$1.5x10^4$	$1.3x10^4$
IZO (0.5%)	$5.5x10^5$	$1.7x10^4$	$1.2x10^4$
IZO (1%)	$2.9x10^6$	$2.1x10^6$	$3.7x10^5$
IZO (3%)	$3.0x10^6$	$2.0x10^6$	$2.8x10^5$

6.3.2. Exposure to Ethanol

All ZnO and IZO sensors were exposed to 5, 10, 20, 40 and 80 ppm ethanol at operating temperatures of 350°C, 400°C and 500°C. At an operating temperature of 500°C (Fig. 6.5) enhancements in responses can be observed in the lower percentage doped IZO sensors (0.2-0.5%) compared to the undoped ZnO sensor. The sensors doped with the highest percentage of indium (1-3%) are found to be less responsive, with 3% indium doped ZnO found to be not responsive at all. This is potentially due to over doping of the ZnO material.

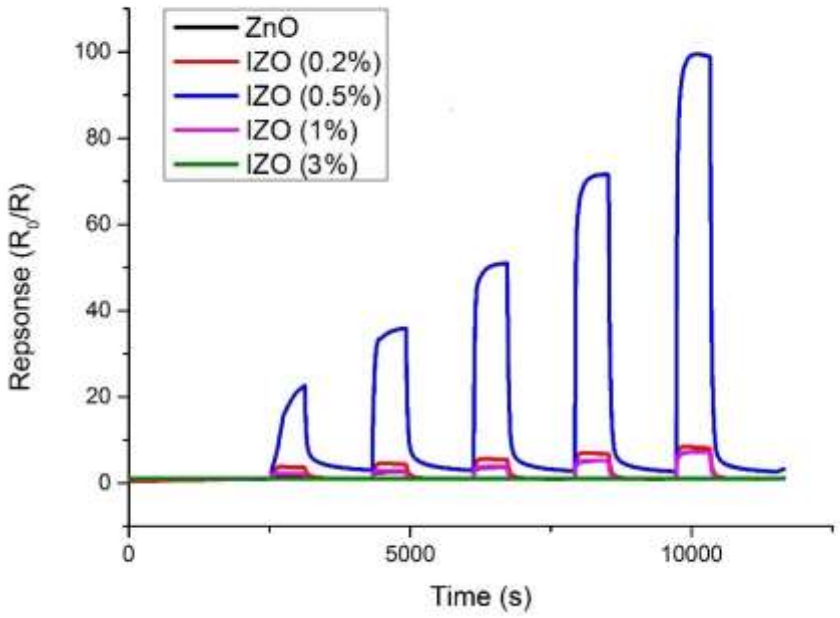

Figure 6.5. Response of ZnO and indium doped ZnO at 0.2, 0.5, 1 and 3 mol % to 600 second pulses of 5, 10, 20, 40 and 80 ppm ethanol at an operating temperature of 500°C.

At an operating temperature of 400°C (Fig 6.6) all sensors show a strong response to pulses of ethanol. Lower doped IZO (0.2-0.5%) sensors show enhancement over the ZnO sensor, while higher doped IZO (1-3%) are shown to be significantly less responsive. The 1 and 3% indium doped ZnO sensors show responses that are a similar order of magnitude, suggesting that above a certain doping level, the response to ethanol at this operating temperature is saturated and not affected further by increased doping.

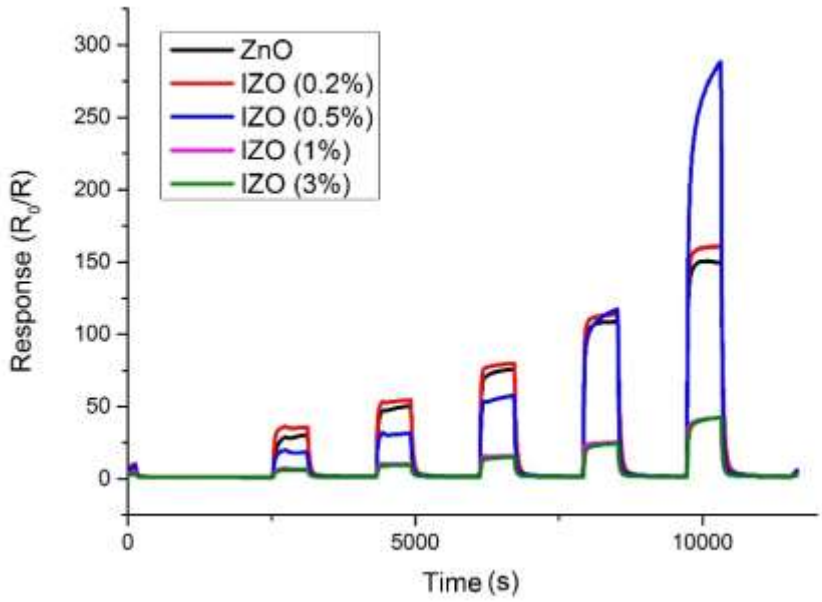

Figure 6.6. Response of ZnO and indium doped ZnO at 0.2, 0.5, 1 and 3 mol % to 600 second pulses of 5, 10, 20, 40 and 80 ppm ethanol at an operating temperature of 400°C.

At an operating temperature of 350°C (Fig 6.7) all sensors show significantly reduced magnitudes of response to pulses of ethanol gas. Samples doped with 0.2-0.5% indium were again found to be most responsive to ethanol with responses of $R_0/R = 29.2$ to 80 ppm ethanol for the 0.5% indium doped ZnO sensor. Higher doped ZnO (1-3%) are found to be slightly less responsive than the unmodified ZnO sensor, with the IZO (3%) sensor giving a response of $R_0/R = 21.1$ to 80 ppm of ethanol.

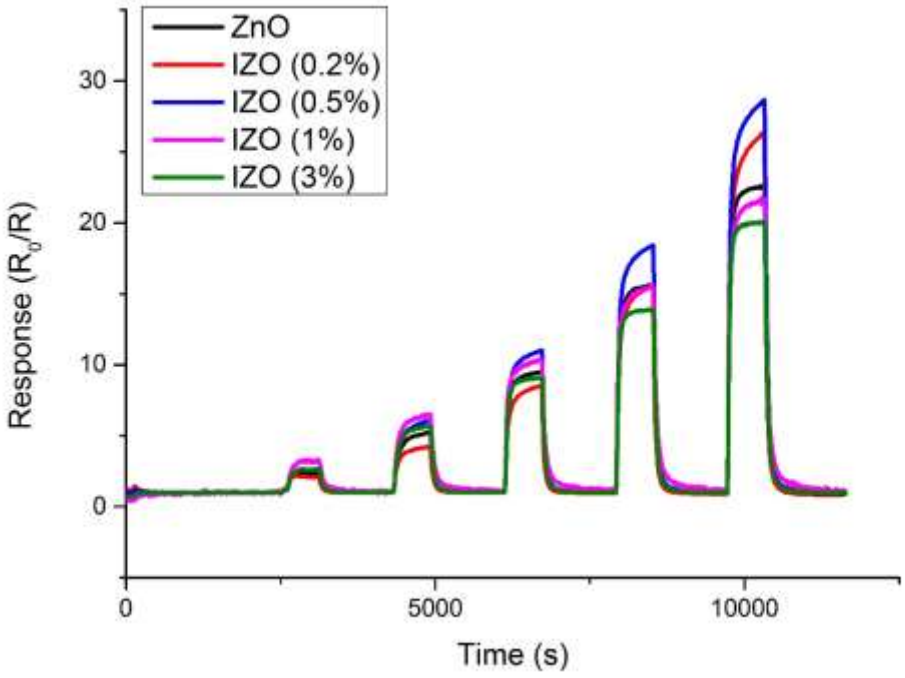

Figure 6.7. Response of ZnO and indium doped ZnO at 0.2, 0.5, 1 and 3 mol % to 600 second pulses of 5, 10, 20, 40 and 80 ppm ethanol at an operating temperature of 350°C.

Strong conductive responses (decreases in resistance) to ethanol vapour were found at all temperatures (Fig 6.8). Indium doped sensors show a larger magnitude of response as compared to the unmodified ZnO sensor. The magnitude of response in IZO sensors doped with 0.2 % and 0.5 % indium were significantly larger than unmodified ZnO with 0.5 % doping being the most responsive. IZO sensors with 1 and 3 % In doping showed much lower responses than both undoped ZnO and IZO materials with lower doping levels, likely as a result of their lower conductivity. All sensors showed a larger magnitude of conductive response, at higher gas concentrations, due to the increased availability of ethanol in the environment to react at the sensor surface.

Indium doped ZnO samples with low doping levels show a marked increase in their responsiveness to gases. It is commonly known that the sensing mechanism in MOS based sensors is surface controlled. The surface microstructure, grain size, oxygen adsorption and surface states all play a key role in the sensor performance. Responses in all sensors were shown to be of the highest magnitude at 400°C. Plots of the maximum

response to ethanol vapour against temperature are not linear, but show plateauing effects in most cases, suggesting that these sensors world be best suited to detection of concentrations of ethanol less than 100 ppm, as sensors may become saturated at higher concentrations. The exception to this is IZO (0.5%), which shows an almost exponential increase.

Interestingly, when the ethanol sensing properties of the zinc oxide sensor utilised in the studies contained within this chapter, was compared to the undoped zinc oxide sensor used in section 3.3.2, the zinc oxide that was synthesised (in this section) was found to be more responsive than the supplied zinc oxide (used in section 3.3.2). This may be due to increased impurities in the synthesised material, such as interstitial oxygen defects that may increase the n-type character of the material.

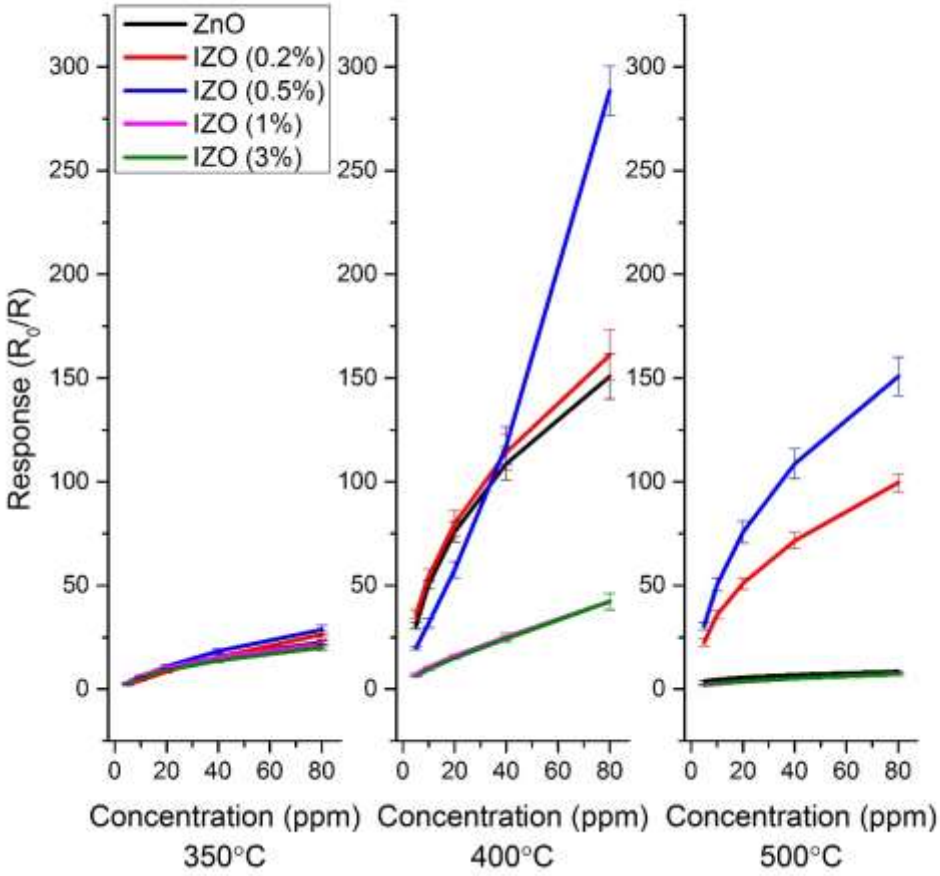

Figure 6.8. Responses (±1 SD) of ZnO and 0.2%, 0.5%, 1% and 3% indium doped ZnO to concentrations of ethanol 5-80 ppm at operating temperatures of 350°C, 400°C and 500°C.

All ZnO and IZO sensors were exposed to three successive pulses of 40-ppm ethanol. Results from this experiment (Fig. 6.9) show good repeatability between sensors, with the magnitude of response between these three pulses and a 40-ppm pulse in Fig. 6.7 in agreement. Additionally, the peak shape between all pulses is similar, as are the response and recovery times.

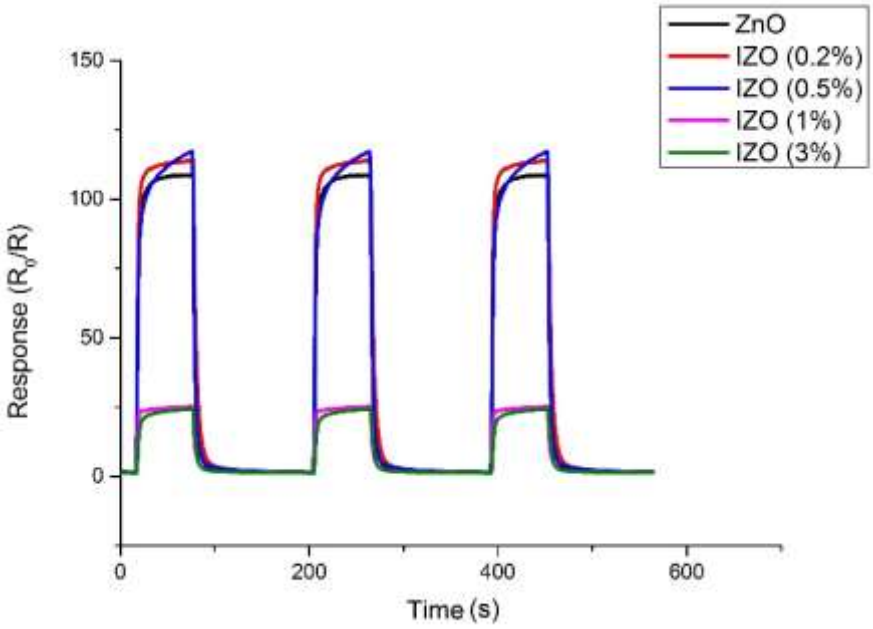

Figure 6.9. Response of ZnO and indium doped ZnO at 0.2, 0.5, 1 and 3-mol % to three 600 second pulses of 80 ppm ethanol.

The response time, T_{res}, the time taken for sensors to reach 90% of their maximum response is shown in table 6.5. As operating temperature increases, the response time decreases, this is due to the increased rate of reaction at the sensor surface. There is not a significant difference in response time between the undoped ZnO and the indium doped ZnO sensors.

Table 6.5. Response times to 80-ppm ethanol for ZnO and 0.2%, 0.5%, 1% and 3% indium doped ZnO sensors.

	Response time (s ±5)		
	350°C	**400°C**	**500°C**
ZnO	90	70	30
IZO (0.2%)	100	60	40
IZO (0.5%)	140	120	70
IZO (1%)	150	40	30
IZO (3%)	90	60	-

6.3.3. Exposure to Methanol

All ZnO and IZO sensors were exposed to 5, 10, 20, 40 and 80 ppm methanol at operating temperatures of 350°C, 400°C and 500°C. The results of this exposure at an operating temperature of 500°C (Fig. 6.10) indicates that all IZO doped sensors show enhanced responses compared to the undoped ZnO sensor. IZO (0.5%) is found to be the most responsive sensor, with response of R_0/R= 3.15 to 80 ppm. Other IZO sensors (0.2%, 1% and 3% indium) observed similar responses at all concentrations to methanol.

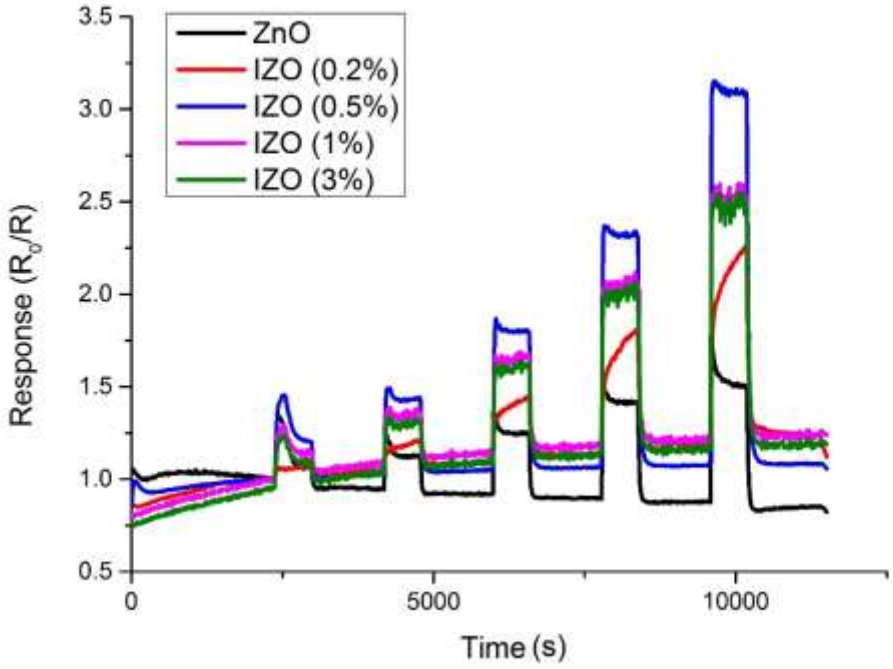

Figure 6.10. Response of ZnO and indium doped ZnO at 0.2, 0.5, 1 and 3 mol % to 600 second pulses of 5, 10, 20, 40 and 80 ppm of methanol at an operating temperature of 500°C.

The response of sensors to methanol at an operating temperature of 400°C (Fig 6.11) show unusual peak shapes, similar to some observed with zeolite modified sensors (section 3.3.5). Undoped ZnO and 0.5 and 1% indium doped ZnO show an initial spike in response, before a reduction, this may suggest that, at these doping concentrations, methanol is broken down into methyl and hydroxyl group which results in a slightly lower response. Lower doped IZO sensors (0.2-0.5%) show enhancements in the magnitude of response compared with unmodified ZnO. All sensors show a good recovery to baseline response, with the exception of IZO (0.2%), which has significant baseline drift and a poor recovery. The largest response observed comes from IZO (0.5%) at 400°C, with a response of R_0/R= 3.42.

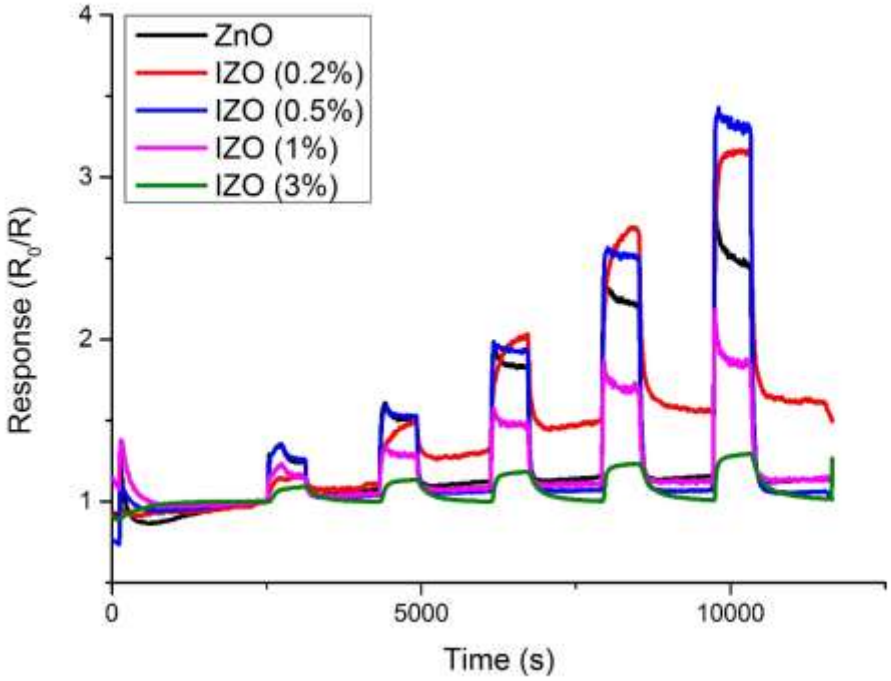

Figure 6.11. Response of ZnO and indium doped ZnO at 0.2, 0.5, 1 and 3 mol % to 600 second pulses of 5, 10, 20, 40 and 80 ppm of methanol at an operating temperature of 400°C.

At an operating temperature of 350°C (Fig 6.12) sensors again show poorer responses than those observed upon exposure to ethanol, all sensors show good response and recovery, however the response of IZO (0.5%) is found to be quite noisy compared to the other sensors. Only the IZO (0.5%) sample shows enhancement over the unmodified zinc oxide sensor.

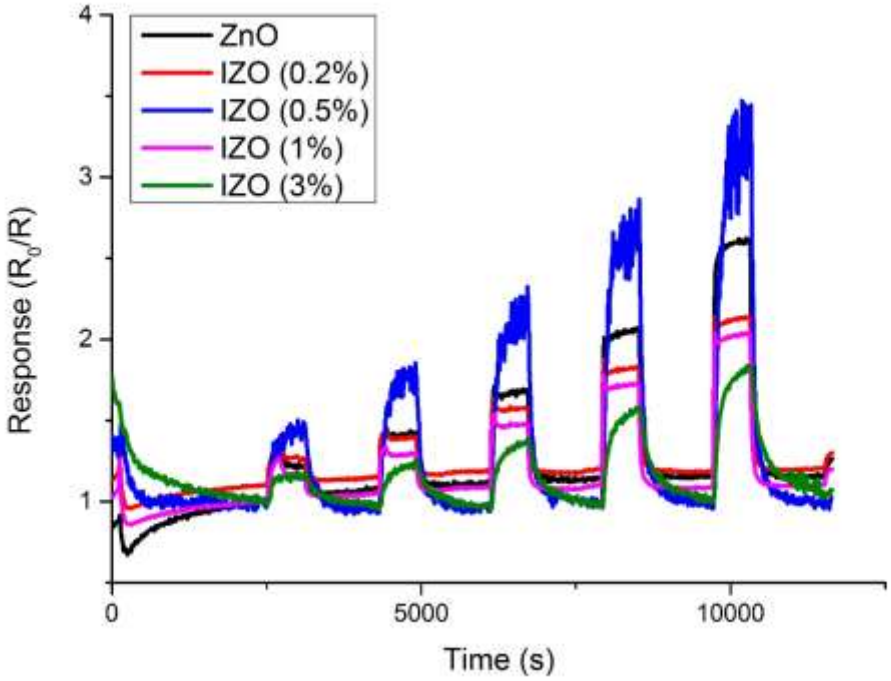

Figure 6.12. Response of ZnO and indium doped ZnO at 0.2, 0.5, 1 and 3 mol % to 600 second pulses of 5, 10, 20, 40 and 80 ppm of methanol at an operating temperature of 350°C.

Responses to methanol at all temperatures (Fig. 6.13) show the maximum responses of ZnO and IZO (0.2%) and IZO (0.5%) are at 400°C while higher doped IZO films (1% and 3%) demonstrate a maximum response at 500°C. The higher doped zinc oxide sensors are shown to be less responsive than the unmodified ZnO sensor, while lower doped samples (< 1% indium doping) are more responsive than undoped ZnO.

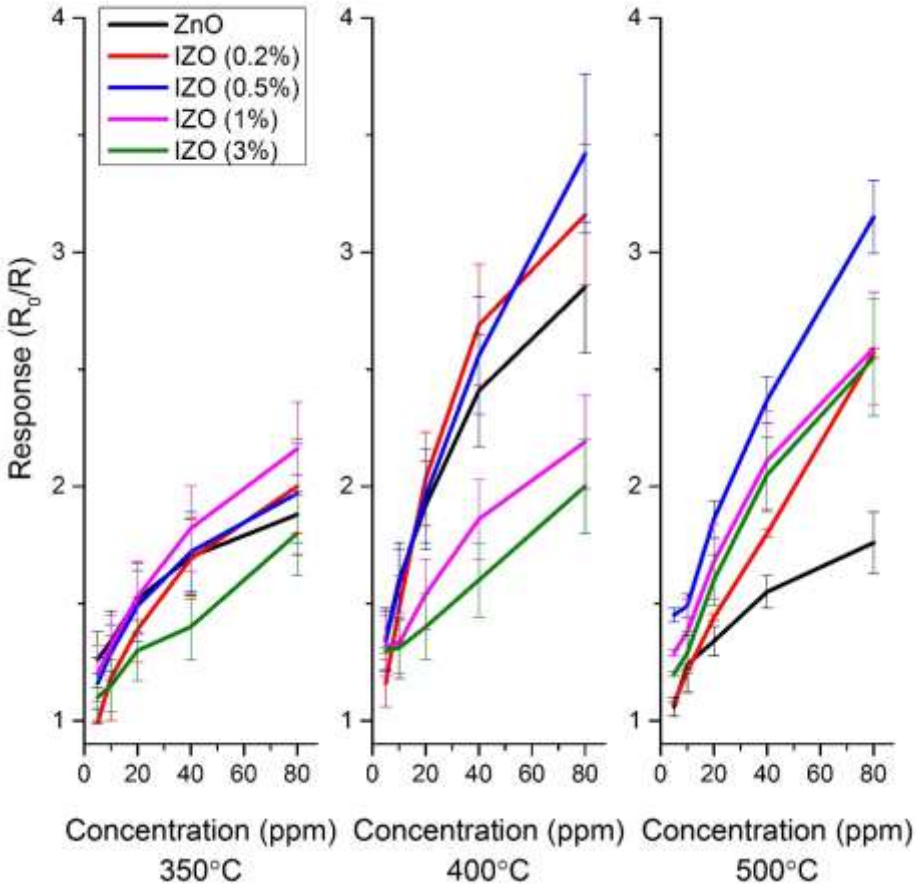

Figure 6.13. Responses (±1 SD) of ZnO and 0.2%, 0.5%, 1% and 3% indium doped ZnO to concentrations of methanol 5-80 ppm at operating temperatures of 350°C, 400°C and 500°C.

The response times to 80-ppm methanol (table 6.6) are all relatively low, with all times less than one minute. There is no significant difference between the response times of undoped ZnO and indium-doped materials.

Table 6.6. Response times to 80-ppm methanol for ZnO and 0.2%, 0.5%, 1% and 3% indium doped ZnO sensors.

	Response time (s ±5)		
	350°C	**400°C**	**500°C**
ZnO	40	40	30
IZO (0.2%)	50	50	20
IZO (0.5%)	40	30	20
IZO (1%)	40	30	30
IZO (3%)	40	40	30

6.3.4. Response to *n*-Butanol

All ZnO and IZO sensors were exposed to 5, 10, 20, 40 and 80 ppm *n*-butanol at operating temperatures of 350°C, 400°C and 500°C.

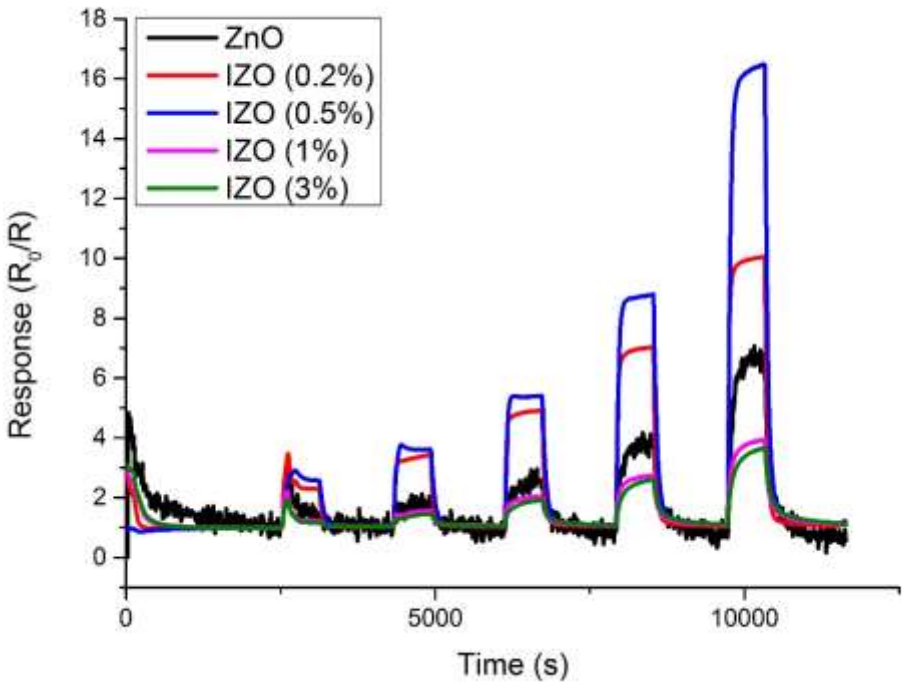

Figure 6.14. Response of ZnO and indium doped ZnO at 0.2, 0.5, 1 and 3 mol % to 600 second pulses of 5, 10, 20, 40 and 80 ppm of *n*-butanol at an operating temperature of 500°C.

The response of ZnO and IZO sensors at an operating temperature of 500°C (Fig 6.14) show good response and recovery of all sensors at all concentrations of *n*-butanol. The response of unmodified ZnO is slightly noisy, however there is a good signal to noise ratio. The response of 0.5% doped ZnO is found to be the largest in magnitude with a response of R_0/R = 16.9 to 80 ppm of *n*-butanol. Sensors with high doping levels of indium (1 and 3%) show similar responses to all pulses of *n*-butanol with the largest response being R_0/R = 4 to 80 ppm.

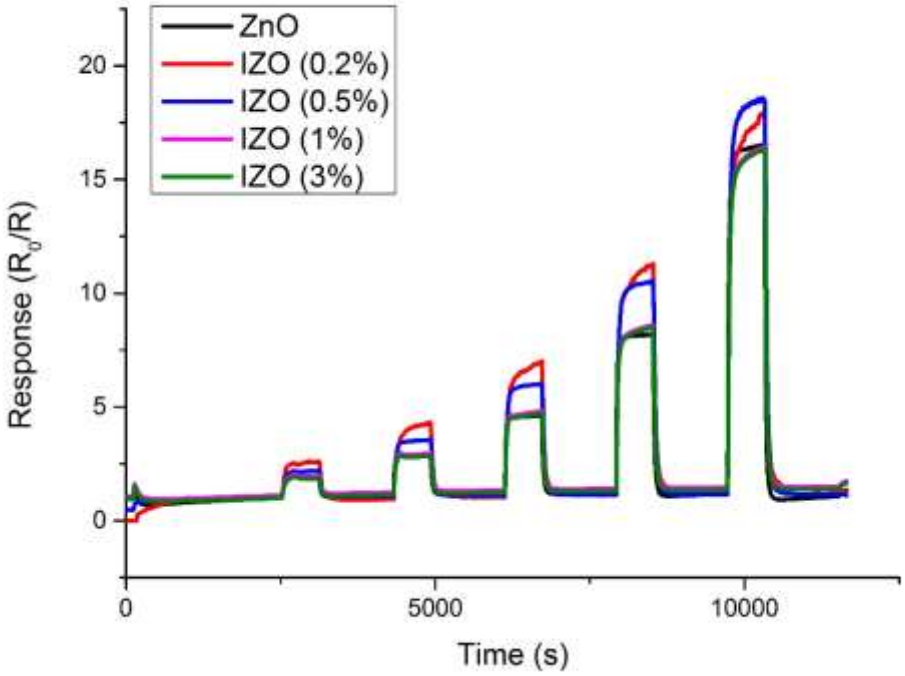

Figure 6.15. Response of ZnO and indium doped ZnO at 0.2, 0.5, 1 and 3 mol % to 600 second pulses of 5, 10, 20, 40 and 80 ppm of *n*-butanol at an operating temperature of 400°C.

At an operating temperature of 400°C, all ZnO and IZO sensors show similar responses to *n*-butanol. At all concentrations, unmodified ZnO, IZO (1%) and IZO (3%) show very similar responses, with $R_0/R \approx 17$ to 80 ppm of *n*-butanol. Lower doped IZO sensors (0.2% and 0.5%) were found to be slightly more responsive with the response of IZO (0.5%) being R_0/R= 19.2 to 80 ppm of *n*-butanol. All sensors show a good response and a fast recovery back to baseline following each gas pulse.

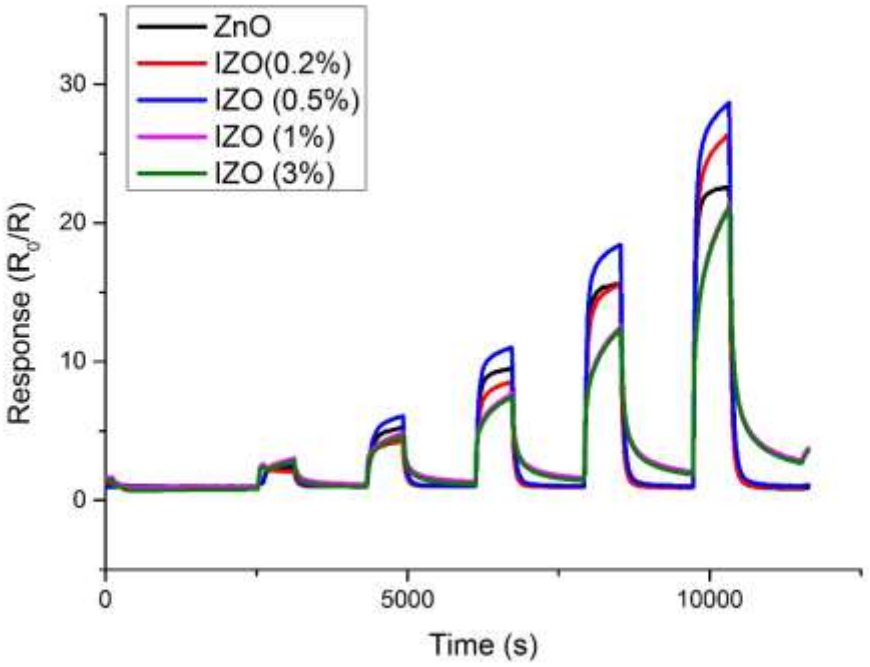

Figure 6.16. Response of ZnO and indium doped ZnO at 0.2, 0.5, 1 and 3 mol % to 600 second pulses of 5, 10, 20, 40 and 80 ppm of *n*-butanol at an operating temperature of 350°C.

Responses at an operating temperature of 350°C (Fig 6.16) show that low doped ZnO sensors (with indium doping levels of 0.2 and 0.5%) show enhancements in the responsiveness to *n*-butanol, compared to undoped ZnO. Higher doped IZO sensors (1% and 3%) are shown to be less responsive to the undoped ZnO sensor. Undoped ZnO and lowed doped IZO sensors show good response and recovery to *n*-butanol at all concentrations, while IZO (1%) and IZO (3%) show much slower recovery following gas pulses.

Responses at all temperatures (Fig 6.17) show that ZnO and IZO sensor responsiveness to *n*-butanol increase with decreasing temperature. Zinc oxide sensors with low doping levels (0.2% and 0.5%) show enhancements in response compared to the undoped ZnO, while the sensors with higher indium doping levels (1% and 3%) are found to be less responsive than the pure ZnO sensor. The largest magnitude of response is observed at an operating temperature of 350°C with the IZO (0.5%) sensor, this was a response of R_0/R= 28.7 to 80 ppm *n*-butanol.

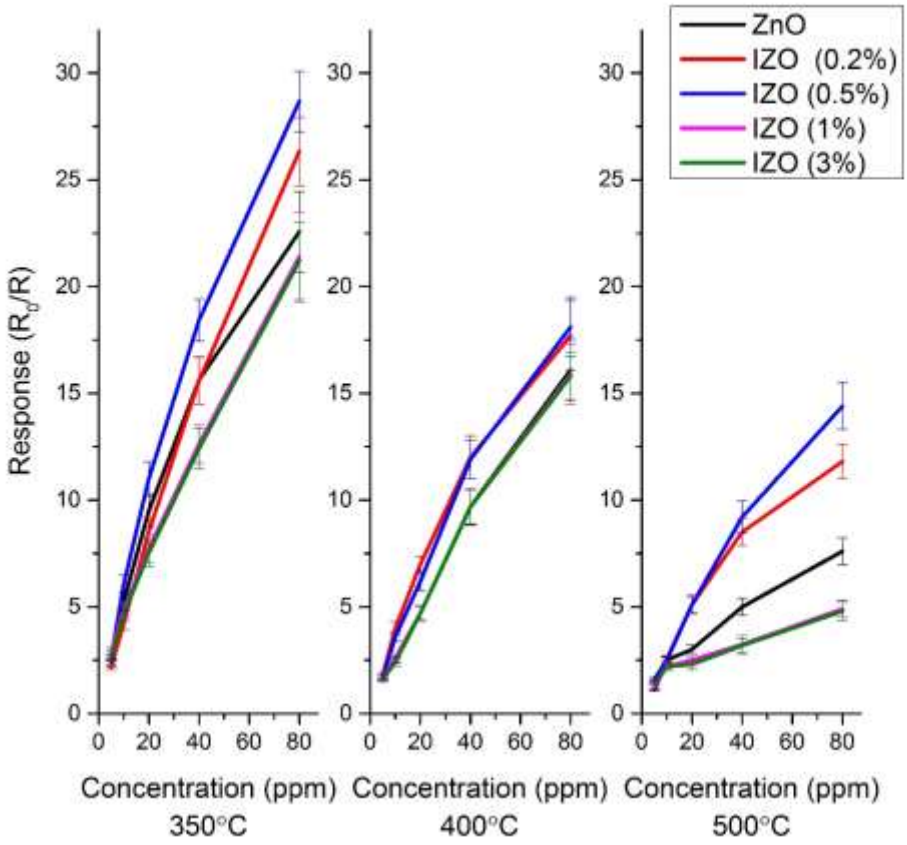

Figure 6.17. Responses (±1 SD) of ZnO and 0.2%, 0.5%, 1% and 3% indium doped ZnO to concentrations of *n*-butanol 5-80 ppm at operating temperatures of 350°C, 400°C and 500°C.

The response times to 80-ppm *n*-butanol for ZnO and all IZO sensors (Table 6.7) shows little difference between the undoped ZnO and IZO sensors. At lower temperatures, IZO (1%) and IZO (3%) show slightly longer response times (~70 s) than the undoped material and lower doped IZO sensors. Response times are considerably smaller at 500°C, than at 350°C (70-80% smaller at 500°C).

Table 6.7. Response times to 80-ppm *n*-butanol for ZnO and 0.2%, 0.5%, 1% and 3% indium doped ZnO sensors.

	Response time (s ±5)		
	350°C	**400°C**	**500°C**
ZnO	120	70	40
IZO (0.2%)	140	70	30
IZO (0.5%)	130	80	40
IZO (1%)	180	70	50
IZO (3%)	190	90	40

6.3.5. Response to Acetone

All ZnO and IZO sensors were exposed to 5, 10, 20, 40 and 80 ppm of acetone. All results, apart from 3-mol % doped ZnO (IZO 3%); show strong responses to all concentrations of acetone.

At an operating temperature of 500°C (Fig 6.18) all sensors show fast responses to acetone. Unmodified ZnO and IZO (1%) and IZO (3%) sensors reach a steady state within the 600-second gas pulse, sensors with a lower levels of indium doping (0.2% and 0.5%) do not reach a steady state response during the gas pulse. Except for IZO (0.5%), all sensors exhibited a fast recovery back to baseline response. The largest magnitude of response was found to be IZO (0.5%) with a response of R_0/R = 14.8 to 80 ppm of acetone. All sensors, except for IZO (3%), show enhancements in response to acetone when compared with undoped ZnO, which shows good response and recovery times, but a poor magnitude of response to all concentrations of acetone, the largest being R_0/R = 1.8 to 80 ppm.

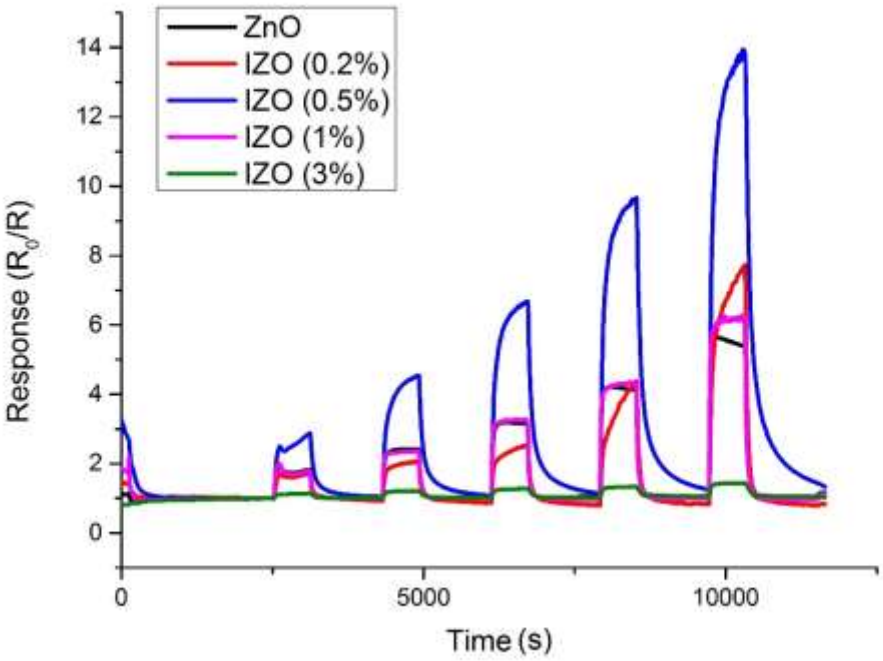

Figure 6.18. Response of ZnO and indium doped ZnO at 0.2, 0.5, 1 and 3 mol % to 600 second pulses of 5, 10, 20, 40 and 80 ppm acetone at an operating temperature of 500°C.

Upon exposure to all concentrations of acetone at 400°C, IZO (0.5%) and IZO (0.2%) show the largest responses (80 ppm acetone - R_0/R = 39.5 and R_0/R = 32.4 respectively). The IZO (3%) sensor shows very poor response at an operating temperature of 400°C, with a response of R_0/R=1.4 to 80 ppm acetone. During the 600-second gas pulse, no sensor reaches a steady state response. The IZO (0.2%) sensor re-establishes a baseline response slightly above R_0/R = 1 following each gas pulse, this suggests that not all acetone desorbs from the sensor surface following a gas pulse, but reaches equilibrium with the environment, demonstrated by the establishment of a steady baseline.

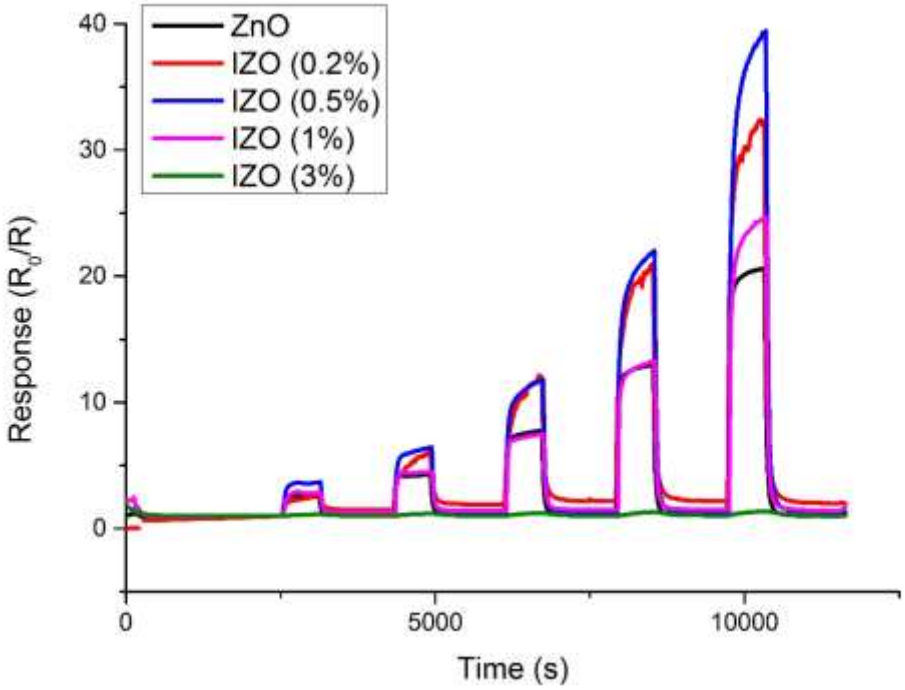

Figure 6.19. Response of ZnO and indium doped ZnO at 0.2, 0.5, 1 and 3 mol % to 600 second pulses of 5, 10, 20, 40 and 80 ppm acetone at an operating temperature of 400°C.

At an operating temperature of 350°C (Fig. 6.20), the IZO (3%) sensors show no response to acetone, it does however maintain a stable response with no drift during the entire experiment. All other indium doped sensors show enhancement in response when compared to the undoped ZnO. Once again, IZO (0.5%) is found to be the most responsive sensor with a response of R_0/R = 46.9 to 80 ppm acetone. During the 600-second gas pulse, only undoped ZnO reached a steady state response. Following each gas pulse, all sensors (except for 3% doped ZnO) demonstrated a fast recovery to baseline.

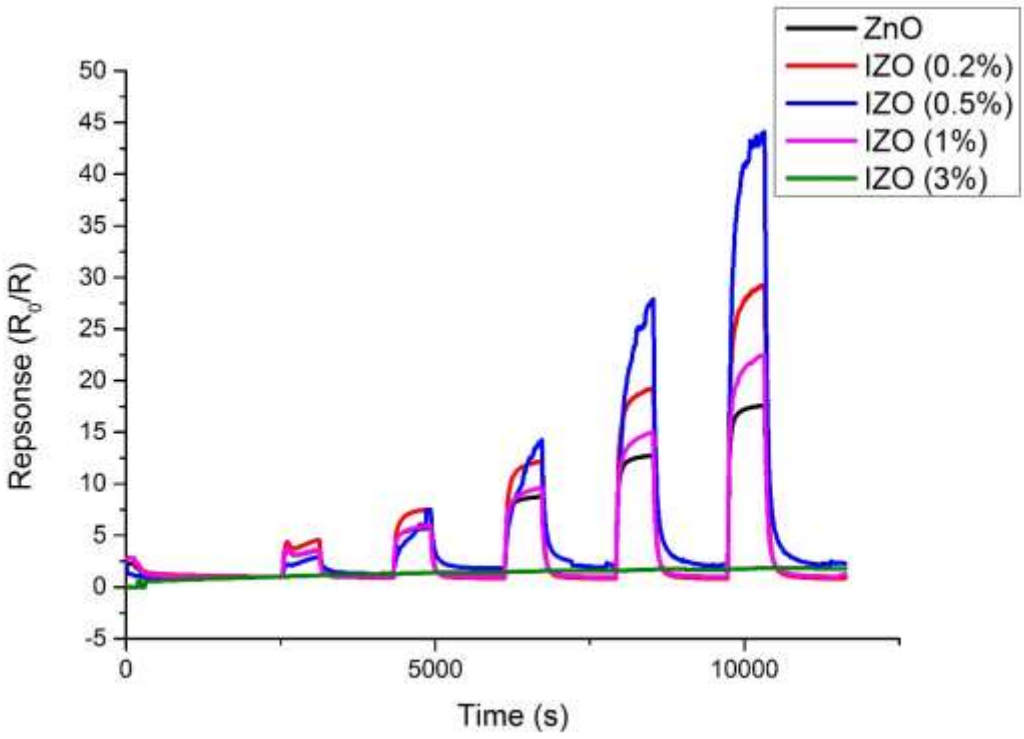

Figure 6.20. Response of ZnO and indium doped ZnO at 0.2, 0.5, 1 and 3 mol % to 600 second pulses of 5, 10, 20, 40 and 80 ppm acetone at an operating temperature of 350°C.

Sensor responsiveness to acetone increases with decreasing temperature and all sensors, with the exception of IZO (3%), show enhancements in the responsiveness over the unmodified ZnO sensor. The largest magnitude of response is observed with IZO (0.5%) at an operating temperature of 500°C, with a response of R_0/R = 44.1 to 80 ppm acetone.

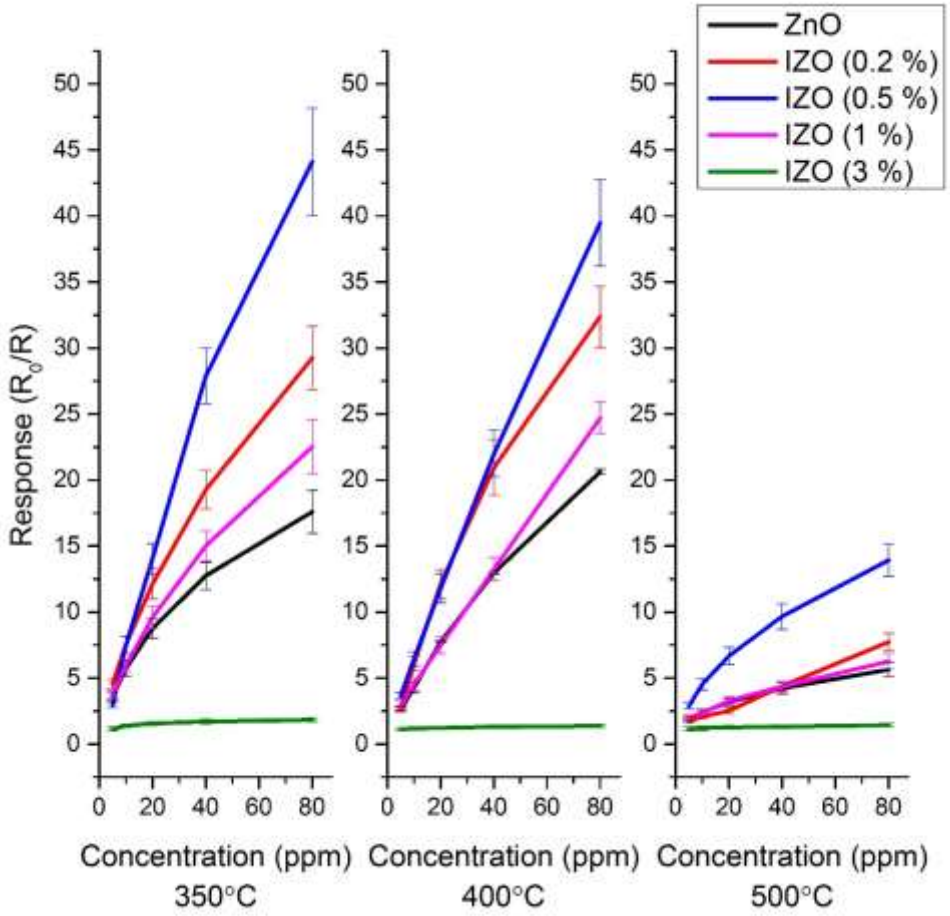

Figure 6.21. Responses (±1 SD) of ZnO and 0.2%, 0.5%, 1% and 3% indium doped ZnO to concentrations of acetone 5-80 ppm at operating temperatures of 350°C, 400°C and 500°C.

The response times of all sensors to 80-ppm acetone (Table 6.8) show that the longest response times observed are with IZO (0.2%) and IZO (0.5%). As temperature increases, response time decreases, a result of faster rate of reaction at the sensor surface at higher temperatures.

Table 6.8. Response times of ZnO and indium doped ZnO (IZO) sensors to 80-ppm acetone. The response time of IZO (3%) is left blank at 350°C, as there was no response to this concentration of acetone at an operating temperature of 350°C.

	Response time (s ±5)		
	350°C	**400°C**	**500°C**
ZnO	120	80	30
IZO (0.2%)	190	190	140
IZO (0.5%)	190	190	160
IZO (1%)	160	140	50
IZO (3%)	-	90	30

6.4. Discussion

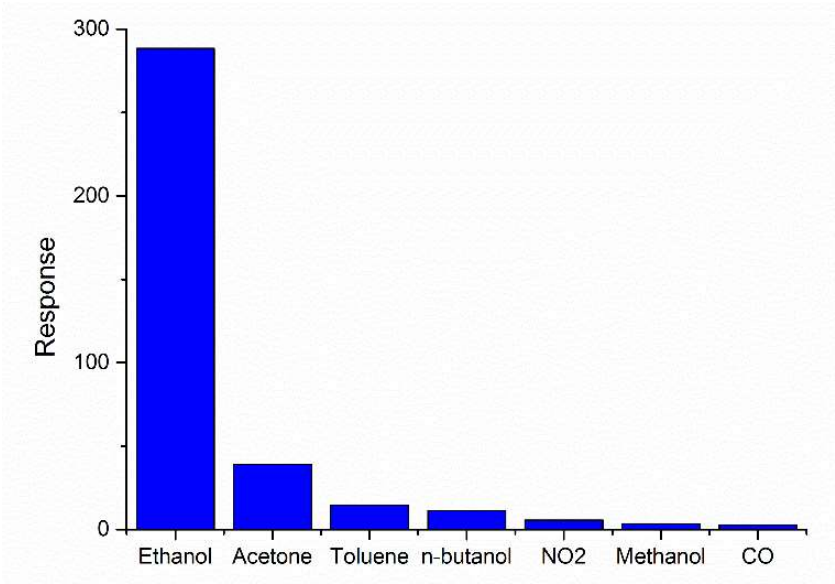

Figure 6.22. Maximum response to IZO (0.5%) to 80 ppm of a 600-second pulse of a range of gases at a concentration of 80 ppm and an operating temperature of 400°C.

The indium doped sensors response to ethanol is far superior to the responses displayed upon exposure to several other gases at the same operating temperature and concentrations (Fig. 6.22). Considering these results, it appears, indium doped ZnO, with 0.5 % indium shows great promise for inclusion into gas sensing array with the purpose of detecting ethanol.

Undoped ZnO responses are consistent with reported literature values to similar concentrations of test gases[258,259]. Indium doped ZnO of 0.5% was found to be the most responsive sensor, with a response of R_0/R = 288.4 to 80 ppm of ethanol. Low doping levels of Indium in ZnO materials show larger responses to similar concentrations of ethanol than SnO_2[260], Fe_2O_3[261] and WO_3[262].

The gas sensing mechanism of doped metal oxides is well defined. Initially, at elevated temperatures, oxygen species are adsorbed onto the surface, forming $O_{(ads)}^-$ species and removing electrons from the material, this leads to the formation of a depletion region. In the presence of a reducing gas (R), oxygen is removed from the surface, reintroducing trapped electrons into the material, decreasing the size of the depletion region and increasing the conductivity. This can be generally described as:

$$O_{2(g)} + 2e^- \rightarrow 2O^-_{(ads)}$$

$$R_{(g)} + O^-_{(ads)} \rightarrow RO_{(g)} + e^-$$

Doping In^{3+} in place of Zn^{2+} increases the conductivity of the material, by increasing the electron density of the doped material. Therefore, indium doping facilitates the creation of $O^-_{(ads)}$ species, as electrons are more readily available at the sensor surface. It is well known that the responsiveness of gas sensors relates directly to the number of $O^-_{(ads)}$ species at the sensor surface[263]. With increased conductivity in indium-doped materials, more $O^-_{(ads)}$ species are formed; consequently, a larger change in magnitude is possible as there are more positions for reducing gases to react at the sensor surface.

However, too much doping will lead to the screening effect observed here, which is caused by surface doped ion aggregation, which is unfavourable for gas diffusion into the sensing films, leading a decrease in the responsiveness of sensors[264].

Different magnitudes of response are observed at different operating temperatures. There are many reasons for this; the adsorption and desorption of oxygen and analyte gases, which control the baseline resistance and magnitude of gas response, are greatly

affected by the surface temperature of the sensor. Residence time on the sensor surface is partly determined by the temperature and reactions at the surface occurring too fast or slow can lead to detrimental effects on the sensor response. Physical properties of the material such as; Debye length, work function and charge carrier concentration are also affected by the temperature. These sensors show good levels of reproducibility, with all results showing less than 10% variation in identical tests.

In response to all gases tested, IZO samples with 1 and 3% doping show poor results, this is attributed to the formation of an In_2O_3 phase above 0.5% doping.

When compared to zeolite modified sensors (Sections 3.3, 4.3 and 5.3) indium doped ZnO sensors demonstrated faster response and recovery times. In almost all cases, the sensors recover fully back to baseline and show considerably less noise than zeolite-modified sensors. The reason for this is potentially that in indium doped sensors, without the secondary zeolite phase, there is only one type of surface that analyte molecules can adsorb to, whereas in zeolite modified sensors, gas molecules can adsorb onto both the gas sensitive material and the zeolite, resulting in the molecules becoming 'trapped' and leading to inconsistent adsorption and desorption of gas molecules. This means that doped metal oxide sensors therefore show greater potential than some zeolite modified metal oxide sensors for use in an electronic nose, as they do not suffer from the poor recovery and signal-to-noise issues that are commonly associated with zeolite modified sensors.

6.5. Conclusion

A series of ZnO and indium doped ZnO sensors were synthesised and manufactured. This is, to our knowledge, the first example of thick films IZO materials being used for ethanol vapour detection. Low doping levels of indium in zinc oxide showed an increase in the responsiveness to ethanol (from $R_0/R = 150$ to $R_0/R = 288$) and acetone (from $R_0/R = 17.5$ to $R_0/R = 44.1$). The ease of production of materials and sensors, combined with the low cost of synthesis materials and sensor electronics mean that these materials show great potential for low cost, highly sensitive ethanol sensors.

The IZO sensors, and in particular the IZO (0.5%) sensor shows great potential for inclusion in an electronic nose. The sensors meet the main criteria for sensors that can be utilised in electronic noses.

- Sensors are highly responsive to low levels of a variety of gases.
- The IZO (0.5%) sensors show excellent selectivity towards ethanol.
- Sensors have faster response and recovery times then zeolite modified materials.
- The IZO sensors demonstrate reproducible responses of the signal over multiple exposures to the test gas and power cycling.

7. Machine Learning Implementation

This chapter illustrates the implementation and application of four-machine learning techniques to assess the selectivity of all of the sensors utilised throughout this investigation. Machine-learning techniques were applied to sensor data from chapters 3, 4 and 5 and outputs were used to classify the gases used in this investigation. The aim of this process was to correctly identify the class of gas (the gas that the sensors had been exposed to). The machine learning techniques used were: a support vector machine, logistic regression, a J48 decision tree and a random forest. Sensors were then exposed two gas pulses outside of the test set to determine the ability of the machine learning algorithms to identify individual gas classes based on data not part of the training set. Sensors were analysed individually, as well as in groups based on sensor material.

7.1. Introduction

No sensor is 100% selective to a single gas; this is mainly due to the similar nature of the reactions occurring at the sensor surface, especially between volatile organic compounds. Electronic noses are a means to overcome this selectivity problem. An electronic nose consists of several sensors, whose data is analysed by some form of classifying algorithm. Sensors within an individual electronic nose are varied by material, auxiliary elements or operating temperature. Data acquired from each sensor, such as the change in resistance, the speed of response, or functions thereof (for example linear combinations), can be used to create a fingerprint of an individual analyte[265]. The data collected can be processed with classifying techniques, such as neural networks and support vector machines (SVMs).

Machine learning is a method of data analysis that allows software to accurately predict outcomes without being explicitly programmed. Machine learning relies on algorithms to analyse large datasets by receiving input data and using statistical analysis to predict an output value within an acceptable range. Machine learning techniques have been

utilised to provide predictive classification of sensor data along with other applications, including image recognition, predictive maintenance, resource scheduling and fraud detection.

7.2. Classification Techniques

Four classification techniques were applied to individual sensors and subsets of all zeolite modified sensors to obtain an accurate data set for the identification of a target gas. All methods used were examples of supervised learning techniques, whereby example data (a training set) are utilised to "train" the algorithm, in order to correctly predict the correct response when exposed to new examples. The classification techniques are discussed in more detail below.

7.2.1. Support Vector Machine

First proposed by Boser *et.al.*[266], a support vector machine is a method of maximum marginal classification based on statistical learning theory. This method uses a training data set to derive an algorithm to linearly separate classes of data. Not all data can be separated linearly in its basic form (its input space). To overcome this, a function maps the data in a higher dimensional space (a feature space) and a separating hyperplane is applied (Fig 7.1).

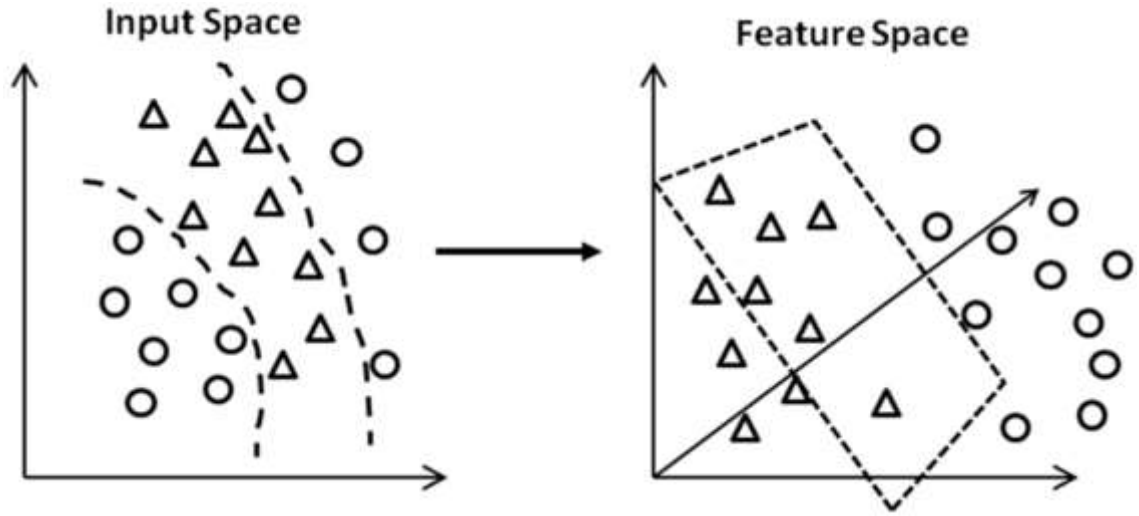

Figure 7.1. Schematic demonstration of the difference between input space and feature space. The data in its input space format is not linearly separable. When the data is extended, incorporating higher dimensional features so that the data can be separated by a hyperplane, and therefore be classified in a binary fashion. Figure adapted from images by Pei *et.al.*[267].

The position of the hyperplane is dependant on a number of features. In a 2D case, the hyperplane, or decision boundary, is a simple straight line separating the two classes of data. If the line is too close to any data points, the algorithm will be noise sensitive and this will lead to an increase in misclassification, therefore the optimal hyperplane will be as far away from all data points as possible. The distance between the nearest data points of each class is known as the margin. The optimal hyperplane is at the position where the margin is at a maximum (Fig 7.2)[268].

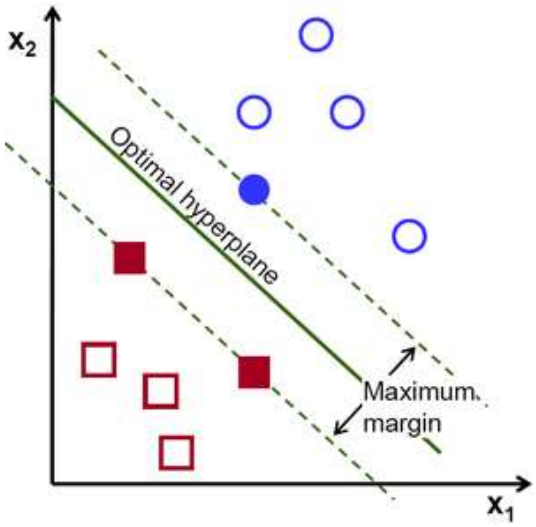

Figure 7.2. Two classes of data (circles and squares) separated by a hyperplane demonstrating the maximum margin between the two sets of data. Figure adapted from images by OpenCV[268].

Support vector machines are binary classifiers; in many cases however, data sets are not binary (including in this study, where one of five gases should be determined). There are two methods to separate multiple classes of data: one is to separate an individual class from all other classes (a one against all technique), i.e. separating gas data out as ethanol and not ethanol. The second method is to train a classifier for every pair of classes, in this instance to classify a piece of data, a number of votes is allocated to each class based on pairwise comparisons. The class is then assigned based on the greatest number of votes (a one against one technique).

Support vector machines are popular with data scientists for a variety of applications due to a wide range of characteristics including:

- Robust handling of noisy data and outliers
- Ability to handle data sets with more than one variable
- Effective handling of large data sets (up to ~10,000 training examples)
- Automatic detection of non-linearity in data
- A comprehensive array of techniques for binary and multiclass classification, regression and detection of anonymous or novel data.

7.2.2. Logistic Regression

Logistic regression is a binary logistic model, used to estimate the probability of a binary response based on one or more predictors (or independent) variable features. Logistic regression, like other forms of regression analysis, uses one or more predictor variables that are either continuous or categorical. Unlike linear regression, logistic regression is used to predict dependent variables that belong to one of a limited number of categories (such as one of five gas classes) as opposed to a continuous outcome. As a result of this difference, the assumptions applied to linear regression are violated; the residuals cannot be normally distributed.

Regression models predict a value of the unknown variable (in this case, the class of gas) given known values of the known variables (sensor responses). Prediction within the range of values in the dataset used for model-fitting is known informally as interpolation. Prediction outside this range of the data is known as extrapolation. Performing extrapolation relies strongly on the regression assumptions. The further the extrapolation goes outside the data, the more room there is for the model to fail due to differences between the assumptions and the sample data or the true values.

In logistic regression, the dependent variable is categorical. Logistic regression can be binomial (0 or 1) or Multinomial, which deals with situations that can have three or more outcomes, e.g. gas A, B or C, which are not ordered. This multiclass regression uses a one against may strategy.

Logistic regression does not perform well when feature space becomes too large (> more than 15,000 individual vectors), nor does it handle many variables well.

7.2.3. Decision Trees

A decision tree is a decision support tool that uses a tree like graphical representation to separate data into mutually exclusive regions, which are assigned a label. A decision

tree is therefore comprised of internal and external nodes, connected by branches (Figure 7.3). Each internal node is associated with a decision on which branch to proceed, while external nodes, known as terminal, or leaf nodes, indicate a given output vector.

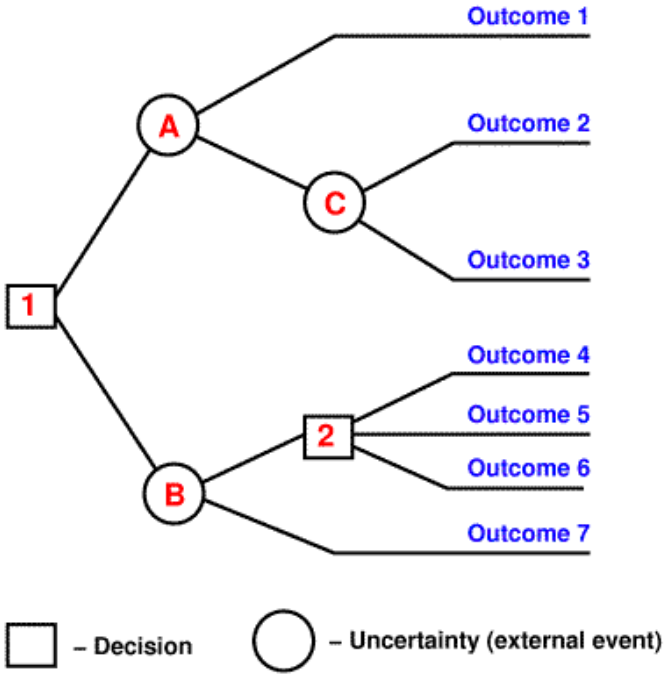

Figure 7.3. Classic decision tree consisting of seven separate outcomes. Figure adapted from images from time management guide[269].

The most common form of decision tree algorithm is the C4.5 method, proposed by Quinlan[270]; this method uses the concept of information gain. Information gain relies on the formula for informative entropy, this is a generalised formula that describes the expected value from the information contained in a message.

$$\text{entropy} = \sum -p_i \log_2 p_i$$

In this formula, p is the probability of a class. The decision tree algorithm detects a feature that can split the dataset into two partitions when the average informative entropy diminishes to a number less that the theoretical maximum of 1 on that feature.

At each node of the tree, the algorithm chooses an attribute from the training data that successfully splits its samples into subsets that are enriched for one particular class. The splitting criterion is the normalised information gain (the difference in entropy). The attribute with the highest normalised information gain is chosen to make the decision. This process is then repeated on smaller subsets until a final decision on classification can be reached and becomes a terminal node.

Following the formation of a decision tree, the tree is "pruned". This reduces the size of the tree by removing sections that provide higher redundancy in classification. Pruning reduces the complexity of the system and therefore reduces the potential for over fitting of the data.

Decision trees have many advantages over other classification methods, they are easy to understand and interpret, require very little data preparation, are robust, able to handle numerical and categorical data and use a white box model, meaning decisions are viewable at any point on the tree. Their output is easily translated into rules and therefore easily understood by humans. However, decision trees can produce over complex trees that will not classify well away from the training data sets. This leads to over fitting of data and provides little use for real world implementation of the algorithm. Additionally, when using categorical data with multiple layers, information gain can become biased in favor of those with more layers.

Decision trees have been used in a number of classification studies using gas sensor information[271,272].

7.2.4. Random Forests

While single decision trees have a number of advantages, the resulting models have a wide range of variances, a way to overcome this is to build multiple decision trees and compare and average their results. Random forests, first proposed by Brieman[273], use an ensemble of unpruned decision trees to classify data into discreet classes.

In this method, each decision tree is grown independently, in parallel, using a random subset of data, and randomly selected features, this introduces variation between individual trees within the forest.

The prediction power of random forests over the simple decision tree is mainly in the bootstrap sampling (sampling with replacement) used to grow each tree. In a bootstrapped sample, it is possible to find the same example repeated multiple times. Sampling repetition not only removes some noise, but also creates more variation in the ensemble of decision trees.

Random forests have many benefits, including:

- They can fit complex target functions.
- Are easy to tune as they have only one hyper-parameter, the number of subsampled features.
- The algorithm is able to select the features it needs automatically (through random subsampling of features in branch splitting).

The forest's error rate is dependent on two things, the correlation between any two trees in the forest, a higher correlation will result in a larger error, and the strength of each individual tree, a tree with a lower error rate is a good classifier. Increasing the strength of individual trees decreases the error rate of the forest.

Reducing the number of variables (m) reduces both the correlation and the strength of the forest, increasing m will increase both. For this reason, an optimal (usually quite wide) range of m is chosen.

Many of the advantages of random forest classification are similar to that of decision trees, a large amount of data can be handled easily, categorical and numerical data can be handled in tandem and random forests correct for decision trees habit of over fitting data. Random forest calculations are however, computationally expensive, as many trees are being grown in parallel.

Random forest and decision tree methods are 'white box techniques' while SVM is a 'black box technique'. A white box technique is one in which the acquired knowledge can be expressed in a readable form, one can view every branch of a decision tree and the attributes used to make a final classification, whereas black box techniques are not easily interpretable.

7.3. Data

A subset of data comprising 3375 vectors was compiled, consisting of the operating temperature, sensors type and response (In R_0/R and R/R_0 form) recorded every 100 seconds during each gas pulse as well as the maximum response.

All analysis was performed using the data-mining package, WEKA[274]. Support vector machine analysis was performed using a 10-fold cross validation, logistic regression was performed using 10-fold classification and random forest classification was performed using a 10 tree, 10-fold classification method.

7.4. Individual Sensor Performance

Table 7.1 demonstrates each sensor's ability to classify which of the tested gases is present in any single gas pulse. This information shows that no sensor is 100% selective to all gases used in the study.

Zinc oxide sensors were generally poor at predicting gas class (i.e. whether ethanol, acetone, nitrogen dioxide or ammonia) using SVM, with all sensors achieving less than 54% accuracy. Prediction using logistic regression showed greater accuracy, with up to 80% of gas classes correctly classified. Decision tree methods found accuracies between 53-78% for the zinc oxide sensors.

The accuracy in classifying the gas present with a CTO based sensor varied greatly using SVM methods. The most accurate CTO based sensor was found to be zeolite beta modified CTO, while the least accurate was ZSM5 modified CTO, which has an accuracy

of 38.6%. The poor accuracy of ZSM5 modified CTO under SVM is not reflected in other classification methods; regression analysis found an accuracy of 84.0%, a single decision tree, 73.3% and random forest analysis was shown to be 81.3%. Other sensors were generally higher in accuracy than their ZnO based counterparts.

Table 7.1. Classification accuracy and root mean square error (RMSE) of 15 different ZnO, CTO and V_2O_5 based sensors, consisting of an unmodified sensor and zeolite beta, Y, mordenite and ZSM5 modified sensors of each material.

	SVM		Logistic Regression		J48 decision tree		Random forest	
Sensor	**(%)**	**RMSE**	**(%)**	**RMSE**	**(%)**	**RMSE**	**(%)**	**RMSE**
ZnO	53.4	0.36	80.8	0.23	78.1	0.28	76.7	0.25
ZnO/B	41.3	0.38	72.0	0.28	66.6	0.34	66.6	0.29
ZnO/Y	45.3	0.38	64.3	0.29	66.6	0.33	66.6	0.29
ZnO/MOR	49.3	0.37	70.3	0.28	78.6	0.27	85.3	0.22
ZnO/ZSM5	45.9	0.37	58.6	0.31	58.6	0.36	53.6	0.34
CTO	53.5	0.35	88.8	0.19	55.6	0.39	73.3	0.27
CTO/B	72.0	0.34	82.7	0.23	68.0	0.3	68.0	0.29
CTO/Y	53.3	0.35	73.3	0.28	76.0	0.3	66.7	0.29
CTO/MOR	50.7	0.36	89.3	0.20	65.3	0.35	66.6	0.30
CTO/ZSM5	38.6	0.37	84.0	0.23	73.3	0.31	81.3	0.24
V_2O_5	79.7	0.33	78.5	0.24	72.0	0.3	82.4	0.24
V_2O_5/B	89.33	0.33	80.0	0.28	81.3	0.26	81.3	0.29
V_2O_5/Y	93.3	0.32	93.4	0.16	77.3	0.28	69.3	0.29
V_2O_5/MOR	94.7	0.32	92.0	0.18	77.3	0.29	88.0	0.19
V_2O_5/ZSM5	94.6	0.32	90.7	0.19	92.0	0.17	85.3	0.20

The most accurate sensors when determining class of gas were vanadium pentoxide based materials, vanadium pentoxide based sensors were the least responsive to all gases. Despite this, mordenite modified vanadium pentoxide was able to achieve 94.7% accuracy in predicting the class of gas with an SVM the most accurate of any sensor using this classification technique. This high accuracy is also observed with regression analysis (92.0%) and in decision tree methods (77.3 and 88.0%). Under SVM analysis, all vanadium pentoxide sensors could predict the class of gas with better accuracy than the equivalent zinc oxide and chromium titanate sensors.

7.5. Total Classification

A larger magnitude of classification accuracy can be obtained if sensors are grouped together, for example by sensor or zeolite material. When all 15 control and zeolite modified sensors (ZnO, CTO and V_2O_5 based sensors) were used as 15-sensor array, classification of the class of gas was relatively accurate, with all classification methods obtaining accuracies of greater than 80%.

The accuracy of SVM analysis (Table 7.2) shows an accuracy of 83.3%, with perfect classification of acetone and NO_2 exposure. There was some confusion between ammonia, ethanol and toluene, due to their similar responses and response times.

Table 7.2. Results of support vector machine classification of ZnO, CTO and V_2O_5 and zeolite beta, Y, mordenite and ZSM5 modified gas sensors. The true class is defined vertically, with the output classification across the output horizontal. Correctly classified results are shown in bold. An accuracy of 83.3% was achieved.

	Output Classification				
	Acetone	**Ammonia**	**Ethanol**	**NO_2**	**Toluene**
Acetone	**117**	0	0	0	0
Ammonia	0	**93**	3	0	21
Ethanol	0	76	**76**	0	28
NO_2	0	0	0	**117**	0
Toluene	0	12	21	0	**84**

Logistic regression analysis (Table 7.3) achieved a classification accuracy that was slightly lower than that of a support vector machine, with 81.9% of instances correctly classified. Again, acetone and NO_2 were correctly classified in all instances in this subset.

Table 7.3. Confusion matrix-demonstrating results of logistic regression classification of ZnO, CTO and V_2O_5 and zeolite beta, Y, mordenite and ZSM5 modified gas sensors. The true class is defined vertically, with the output classification across the output horizontal. Correctly classified results are shown in bold. An accuracy of 81.8% was achieved.

	Output Classification				
	Acetone	**Ammonia**	**Ethanol**	**NO_2**	**Toluene**
Acetone	**117**	0	0	0	0
Ammonia	0	**90**	9	0	18
Ethanol	0	15	**78**	0	24
NO_2	0	0	0	**117**	0
Toluene	0	17	20	0	**77**

A single decisions tree classification (Table 7.4) found a classification accuracy of 91.8%, once again with 100% accuracy to acetone and NO_2.

Table 7.4. Confusion matrix-demonstrating results of a J48 decision tree classification of ZnO, CTO and V_2O_5 and zeolite beta, Y, mordenite and ZSM5 modified gas sensors. The true class is defined vertically, with the output classification across the output horizontal. Correctly classified results are shown in bold. An accuracy of 91.8% was achieved.

	Output Classification				
	Acetone	**Ammonia**	**Ethanol**	**NO_2**	**Toluene**
Acetone	**117**	0	0	0	0
Ammonia	0	**102**	4	0	11
Ethanol	0	5	**98**	0	14
NO_2	0	0	0	**117**	0
Toluene	0	3	11	0	**103**

The most accurate classification is found with a 10-fold random forest (Table 7.5). This achieved an accuracy of 92.3%. Although no gas was perfectly classified, all classes of gas achieved a relatively accurate classification. While this 15-sensor array achieves a good level of accuracy, the power required to heat and operate 15 separate gas sensors would require an incredibly large power supply (>1W), limiting the portability of an electronic nose of this type.

Table 7.5. Confusion matrix-demonstrating results of a 10-tree random forest analysis of ZnO, CTO and V_2O_5 sensors and zeolite beta, Y, mordenite and ZSM5 modified gas sensors. The true class is defined vertically, with the output classification across the output horizontal. Correctly classified results are shown in bold. An accuracy of 92.3% was achieved.

	Output Classification				
	Acetone	**Ammonia**	**Ethanol**	**NO_2**	**Toluene**
Acetone	**116**	0	0	1	0
Ammonia	0	**107**	2	0	8
Ethanol	0	7	**99**	0	11
NO_2	1	0	0	**116**	0
Toluene	0	8	7	0	**102**

7.6. Zinc Oxide classification

Unmodified zinc oxide, zeolite beta, Y, mordenite and ZSM5 modified ZnO sensors were analysed to assess the ability of the ZnO series to identify the gas present. When the series of sensors is combined, the accuracy of all four methods is found to be greater than the individual accuracies of individual sensors. The greatest accuracy was towards nitrogen dioxide; this was classified correctly in 222/225 cases in this subset. This is due to the opposite observed response, i.e. NO_2 exposure causes an increase in sensor response, while all other gases induce a decrease in resistance.

Table 7.6. Results of support vector machine classification of ZnO and zeolite beta, Y, mordenite and ZSM5 modified ZnO gas sensors. The true class is defined vertically, with the output classification across the output horizontal. Correctly classified results are shown in bold. An accuracy of 86.1% was achieved.

	Output Classification				
	Acetone	**Ammonia**	**Ethanol**	**NO_2**	**Toluene**
Acetone	**204**	3	12	0	6
Ammonia	15	**198**	9	0	3
Ethanol	24	42	**150**	0	9
NO_2	3	0	0	**222**	0
Toluene	21	3	6	0	**195**

Table 7.7. Confusion matrix-demonstrating results of logistic regression of ZnO and zeolite beta, Y, mordenite and ZSM5 modified ZnO gas sensors. The true class is defined vertically, with the output classification across the output horizontal. Correctly classified results are shown in bold. An accuracy of 84.5% was achieved.

	Output Classification				
	Acetone	**Ammonia**	**Ethanol**	**NO_2**	**Toluene**
Acetone	**180**	12	15	6	12
Ammonia	17	**197**	9	0	0
Ethanol	7	10	**54**	0	12
NO_2	2	8	0	**215**	0
Toluene	17	0	6	0	**202**

Table 7.8. Confusion matrix-demonstrating results of a J48 decision tree of ZnO and zeolite beta, Y, mordenite and ZSM5 modified ZnO gas sensors. The true class is defined vertically, with the output classification across the output horizontal. Correctly classified results are shown in bold. An accuracy of 85.1% was achieved.

	Output Classification				
	Acetone	**Ammonia**	**Ethanol**	**NO_2**	**Toluene**
Acetone	**202**	5	12	7	9
Ammonia	5	**181**	3	0	7
Ethanol	9	45	**171**	0	0
NO_2	11	0	0	**214**	0
Toluene	6	8	0	4	**207**

Table 7.9. Confusion matrix-demonstrating results of a 10-tree random forest analysis of ZnO and zeolite beta, Y, mordenite and ZSM5 modified ZnO gas sensors. The true class is defined vertically, with the output classification across the output horizontal. Correctly classified results are shown in bold. An accuracy of 81.4% was achieved.

	Output Classification				
	Acetone	**Ammonia**	**Ethanol**	**NO_2**	**Toluene**
Acetone	**210**	5	2	0	6
Ammonia	4	**192**	23	0	6
Ethanol	8	24	**189**	0	4
NO_2	2	1	0	**223**	0
Toluene	2	4	3	0	**216**

All five zinc oxide sensors (ZnO and zeolite beta, Y, mordenite and ZSM5 modified ZnO gas sensors) were exposed to two pulses of gas that had not been included in the training set to assess the arrays ability to detect the presence of an unknown gas. All sensors were exposed to two separate pulses of ethanol and ammonia at 80 ppm at an operating temperature of 350°C. The results of this classification are shown in table 7.10, in all cases, the machine learning techniques correctly classified pulses of ethanol and ammonia. These results are in agreement with those observed in Table 7.6-7.9.

Table 7.10. Results of a classification algorithm performed on exposure of ZnO based sensors (ZnO and zeolite beta, Y, mordenite and ZSM5 modified ZnO gas sensors) to two unknown pulses of gas at an operating temperature of 350°C. Upon exposure to the gases, the sensors were able to correctly classify the gas that was interacting with the sensor surface in all cases, using four different classification techniques.

Classification method	Classified as	
	80 ppm ethanol	**80 ppm ammonia**
SVM	Ethanol	Ammonia
Logistic Regression	Ethanol	Ammonia
Decision Tree	Ethanol	Ammonia
Random Forest	Ethanol	Ammonia

7.7. Chromium Titanate Classification

Much like the observed response of ZnO sensors, the accuracy in determining class of gas is increased when several sensors are combined, compared to the accuracy of individual sensors. An accuracy of 100% is achieved using a random forest method, this is likely to be an over fit, where the algorithm 'memorises' the training data, rather than 'learning' to generalise from the trend. Once again, nitrogen dioxide is found to be most accurately classified, with 100% of cases classified correctly using logistic regression, decision tree and random forest methods. When logistic regression, decision trees and random forest methods are applied, the accuracies are very high (> 85%). The cases that are classified incorrectly are because of some confusion between toluene and ethanol pulses; this is demonstrated in the logistic regression (Table 7.12) and decision tree (Table 7.13) models. The magnitude of response on exposure to both ethanol and toluene are of a similar order and have similar response times. Ammonia is classified well, with 100% of classes accurately attributed using three methods.

Table 7.11. Confusion matrix-demonstrating results of a support vector machine analysis of CTO and zeolite beta, Y, mordenite and ZSM5 modified CTO gas sensors. The true class is defined vertically, with the output classification across the output horizontal. Correctly classified results are shown in bold. An accuracy of 75.6% was achieved.

	Output Classification				
	Acetone	**Ammonia**	**Ethanol**	**NO_2**	**Toluene**
Acetone	**204**	0	0	4	17
Ammonia	8	**189**	0	28	0
Ethanol	36	0	**156**	0	33
NO_2	57	6	0	**162**	0
Toluene	33	0	51	0	**141**

Table 7.12. Confusion matrix-demonstrating results of a logistic regression analysis of CTO and zeolite beta, Y, mordenite and ZSM5 modified CTO gas sensors. The true class is defined vertically, with the output classification across the output horizontal. Correctly classified results are shown in bold. An accuracy of 85.9% was achieved.

	Output Classification				
	Acetone	**Ammonia**	**Ethanol**	**NO_2**	**Toluene**
Acetone	**219**	0	2	0	4
Ammonia	0	**225**	0	0	0
Ethanol	14	0	**156**	0	55
NO_2	0	0	0	**225**	0
Toluene	23	0	52	0	**156**

Table 7.13. Confusion matrix-demonstrating results of a J48 Decision tree forest analysis of CTO and zeolite beta, Y, mordenite and ZSM5 modified CTO gas sensors. The true class is defined vertically, with the output classification across the output horizontal. Correctly classified results are shown in bold. An accuracy of 99.4% was achieved.

	Output Classification				
	Acetone	**Ammonia**	**Ethanol**	**NO_2**	**Toluene**
Acetone	**223**	0	1	0	1
Ammonia	0	**225**	0	0	0
Ethanol	0	0	**220**	0	5
NO_2	0	0	0	**225**	0
Toluene	0	0	0	0	**225**

Table 7.14. Confusion matrix-demonstrating results of a 10-tree random forest analysis of CTO and zeolite beta, Y, mordenite and ZSM5 modified CTO gas sensors. The true class is defined vertically, with the output classification across the output horizontal. Correctly classified results are shown in bold. An accuracy of 100% was achieved.

	Output Classification				
	Acetone	**Ammonia**	**Ethanol**	**NO_2**	**Toluene**
Acetone	**225**	0	0	0	0
Ammonia	0	**225**	0	0	0
Ethanol	0	0	**225**	0	0
NO_2	0	0	0	**225**	0
Toluene	0	0	0	0	**225**

All five chromium titanate sensors (CTO and zeolite beta, Y, mordenite and ZSM5 modified CTO gas sensors) were exposed to two pulses of gas previously unseen in the training set. The five CTO based sensors were exposed to two separate pulses of ethanol and ammonia, at concentrations of 80 ppm (Table 7.15). All four-classification methods could accurately classify pulses of ethanol and ammonia. This is in agreement with the results of the confusion matrices in Tables 7.11-7.14.

Table 7.15. Results of a classification algorithm performed on exposure of CTO based sensors (CTO and zeolite beta, Y, mordenite and ZSM5 modified CTO gas sensors) to two unknown pulses of gas at an operating temperature of 350°C. Upon exposure to the gases, the sensors were able to correctly classify the gas that was interacting with the sensor surface in all cases, using four different classification techniques.

Classification method	Classified as	
	80 ppm ethanol	**80 ppm ammonia**
SVM	Ethanol	Ammonia
Logistic Regression	Ethanol	Ammonia
Decision Tree	Ethanol	Ammonia
Random Forest	Ethanol	Ammonia

7.8. Vanadium Pentoxide Classification

Despite the strong performance of individual sensors (with accuracies around 90%), when all vanadium pentoxide sensors are combined, the accuracy of the array in predicting the class of gas present is far lower than their individual accuracies. A support vector machine is able to accurately classify the gas in only 52.4% of cases; this is the lowest classification of any materials used in this investigation. When ZnO and CTO arrays are exposed to a gas, usually at least one of the sensors has a response significantly distinctive in magnitude compared to other modified sensors. Vanadium pentoxide sensors generally have responses between one and three; this significantly smaller magnitude of response means there is a lot of overlap between responses and consequently a large number of cases are incorrectly classified.

Table 7.16. Confusion matrix-demonstrating results of a support vector machine analysis of V_2O_5 and zeolite beta, Y, mordenite and ZSM5 modified V_2O_5 gas sensors. The true class is defined vertically, with the output classification across the output horizontal. Correctly classified results are shown in bold. An accuracy of 52.4% was achieved.

	Output Classification				
	Acetone	**Ammonia**	**Ethanol**	**NO_2**	**Toluene**
Acetone	**138**	0	0	67	21
Ammonia	32	**81**	3	13	0
Ethanol	72	36	**69**	21	24
NO_2	19	0	0	**168**	0
Toluene	17	8	3	3	**132**

Table 7.17. Confusion matrix-demonstrating results of a logistic regression analysis of V_2O_5 and zeolite beta, Y, mordenite and ZSM5 modified V_2O_5 gas sensors. The true class is defined vertically, with the output classification across the output horizontal. Correctly classified results are shown in bold. An accuracy of 73.5% was achieved.

	Output Classification				
	Acetone	**Ammonia**	**Ethanol**	**NO_2**	**Toluene**
Acetone	**165**	19	23	0	18
Ammonia	22	**171**	13	0	18
Ethanol	45	20	**150**	0	10
NO_2	0	0	0	**225**	0
Toluene	51	42	0	0	**132**

Table 7.18. Confusion matrix-demonstrating results of a J48 decision tree analysis of V_2O_5 and zeolite beta, Y, mordenite and ZSM5 modified V_2O_5 gas sensors. The true class is defined vertically, with the output classification across the output horizontal. Correctly classified results are shown in bold. An accuracy of 83.7% was achieved.

	Output Classification				
	Acetone	**Ammonia**	**Ethanol**	**NO_2**	**Toluene**
Acetone	**212**	8	0	0	5
Ammonia	9	**168**	26	4	18
Ethanol	0	48	**162**	0	144
NO_2	3	0	0	**222**	0
Toluene	5	14	25	0	**181**

Table 7.19. Confusion matrix-demonstrating results of 10-tree random forest analysis of V_2O_5 and zeolite beta, Y, mordenite and ZSM5 modified V_2O_5 gas sensors. The true class is defined vertically, with the output classification across the output horizontal. Correctly classified results are shown in bold. An accuracy of 81.8 % was achieved.

	Output Classification				
	Acetone	**Ammonia**	**Ethanol**	**NO_2**	**Toluene**
Acetone	**165**	9	20	0	17
Ammonia	19	**188**	12	0	6
Ethanol	46	17	**133**	0	29
NO_2	0	0	0	**225**	0
Toluene	34	42	0	0	**132**

Five vanadium pentoxide based sensors (vanadium pentoxide and zeolite beta, Y, mordenite and ZSM5 modified V_2O_5 gas sensors) were exposed to two pulses of gas whose data was unseen in the training set. The four classification techniques were used to determine the gas present in an unknown sample (Table 7.20). The logistic regression and random forest methods were able to accurately classify an ethanol pulse and an ammonia pulse. When SVM and decision tree classification techniques were applied, the ethanol pulses were wrongly classified as acetone. The wrong classifications as well as the generally poorer classification accuracies observed with vanadium pentoxide

sensors is likely due to the poor responsiveness and inadequate signal-to-noise ratios observed on exposure to some gases, in particular; ammonia.

Table 7.20. Results of a classification algorithm performed on exposure of V_2O_5 based sensors (V_2O_5 and zeolite beta, Y, mordenite and ZSM5 modified V_2O_5 gas sensors) to two unknown pulses of gas at an operating temperature of 350°C. Upon exposure to the gases, the sensors were able to correctly classify the gas that was interacting with the sensor surface in all cases, using four different classification techniques.

Classification method	Classified as	
	80 ppm ethanol	80 ppm ammonia
SVM	Acetone	Ammonia
Logistic Regression	Ethanol	Ammonia
Decision Tree	Acetone	Ammonia
Random Forest	Ethanol	Ammonia

7.9. Discussion

Of the five gases that all four classification techniques seek to identify, the presence of nitrogen dioxide is correctly classified in almost 100% of cases. The gas sensing responses of modified and unmodified sensors (sections 3.3.3, 4.3.2 and 5.3.3) show very different response peak shapes than the expected 'shark-fin' type response when exposed to nitrogen dioxide. The change in resistivity is the opposite of that seen with other gases, a result of the oxidising nature of nitrogen dioxide. An initial reducing response also occurs in all cases, this is likely to be the result of imperfections in the gas sensing apparatus, meaning some reducing gas may be caught in the instrumentation. This combination of factors results in a completely different gas sensing response to those observed with reducing gases, making the presence of a pulse of nitrogen dioxide easily identifiable.

Pulses of the four reducing gases (acetone, ammonia, ethanol and toluene) are frequently misclassified, with pulses of acetone, ethanol and toluene often misclassified interchangeably. At low concentrations poor responses are observed, with notable responses to these gases only observed at the highest 2 concentrations. The similarity

in peak size and shape in many cases at lower concentrations may have resulted in the misclassification of the analyte gas present. At higher concentrations, for example exposure to 80 ppm of toluene to zeolite modified ZnO at 500°C (section 3.3.5), the peak shapes observed are different, as a result of acid-catalysed break down at the zeolite surface (section 3.6). In such cases, it is much more likely that these instances are correctly classified, due to the unique peak shapes observed on exposure to the gas.

The chromium titanate series was found to be capable of the most accurate classifications, with an average accuracy of 90.2 %, whereas zinc oxide sensors had an average accuracy of 84.3 % and vanadium pentoxide of 73.9 %. The likely reason for the higher accuracy in determining class of gas is the range of magnitudes of response that the CTO sensors demonstrate. For example, when exposed to 80 ppm ethanol, at an operating temperature of 250 °C, the range (highest value – lowest value) of responses is 474.4, whereas for vanadium pentoxide sensors the range is 2.8.

The magnitudes of response for several sensors to a single gas create a chemical fingerprint for that analyte; this can be used to classify a gas. The classification accuracy of an array is found to be more accurate when magnitudes of response are varied between different sensors. For example, for the CTO based sensor array, the range with 80-ppm ethanol is 474.4, while for 40-ppm toluene the range is 32.1 and for ammonia exposure (40-ppm), the range is 6.1, this covers three orders of magnitude. For all vanadium pentoxide sensors, the range of responses is between the 0.2 and 2.8 for all gasses, therefore with vanadium pentoxide sensors, the likelihood of misclassification is much higher.

While individually, vanadium pentoxde sensors all demonstrated relatively strong classification ability, when combined into a five sensors array, the ability of the electronic nose to classify gases was poor with all techniques. Classification accuracy of the five gasses to vanadium pentoxide and zeolite modified vanadium pentoxide (section 7.8) was poor, with no classification technique able to achieve more than 84% accuracy in identifying the analyte gas present. In addition to the poor classification from a test set, the machine learning techniques also misclassified pulses of acetone as

ethanol upon exposure to the five-sensor (Table 7.20). The reason for this poor classification is likely to be due to the poor responses and poor signal to noise ratios observed on exposure to all gases (section 5.3). While individually, it is identifiable which peaks respond to each gas, when combined with data from four other sensors, all demonstrating similar peak shapes and magnitudes of response, there may be some misclassification of data.

Tree based classifiers (J48 and random forest) are found to be significantly more accurate than regression and SVM based methods in a number of cases. While support vector machines are much less prone to over fitting than tree based models[275], many researches have shown that tree based algorithms, such as J48 trees and random forest methods are able to demonstrate the best performance, on average, across several different metrics[276], with better predictions made using these methods.

A good model should not only fit the training data, but also accurately classify instances that the algorithm has not previously seen. Overdeveloped trees can lead to overfitting, where they show a good classification accuracy for the examples used in this study, but an unknown or untrained instance (e.g. a 72-ppm ethanol pulse) would likely result in a misclassification. This issue can be overcome by pruning the decision tree where data splits are not statistically significant ($p < 0.05$).

The classification accuracies achieved to sensing arrays, especially to ZnO and CTO based sensing arrays, is high (up to 94% accuracy) however, these accuracies are still not suitable for a security device as a high likelihood of false positives can still cause errors, ideally classification accuracy should exceed 99%. Further testing is required to determine the optimum number of sensors for an electronic nose and the sensors that would be most suited to this task.

For an ideal electronic nose, the sensors used should show the least similarity, in order to maximise the classification potential and accuracy as well as keeping power requirements low. The optimum number of sensors required for an electronic nose should also be determined, fewer sensors in an array are advantageous for both power

consumption and form factor reasons, but also may provide better accuracy than a sensor array with a larger number of sensors. An array of four zinc oxide based sensors (unmodified zinc oxide and zeolite beta, Y and mordenite modified ZnO) was able to accurately classify four gases (accuracy = 92%) using an SVM implementation[258]. While a five-sensor array (Table 7.6) was able to classify five gases with 86% accuracy. This reduction in sensor data may have led to an improvement in classification accuracy.

When combined into five sensor arrays, based on their material type, the sensors studied in this investigation can present a degree of selectivity that is not achievable without machine learning applications. These methods show that there is potential for these materials (zeolite modified ZnO, CTO and V_2O_5) to become part of a fully selective electronic nose, when used in combination as part of an array.

8 Discussion and Future Work

8.1. Introduction

All of the sensors discussed in the previous chapters were fabricated, characterised and tested for their gas sensing properties against five gases; acetone, ammonia, ethanol, nitrogen dioxide and toluene, prior to undergoing machine-learning techniques to assess their classification potential. Here an overview of the gas sensing properties of each of these sensors and the potential mechanisms that may underlie their responses is discussed.

The metal oxide semiconducting sensors created throughout this study were based upon 3 different materials, zinc oxide, chromium titanate and vanadium pentoxide; all of these sensors show differing responses when exposed specific gasses at varying temperatures. Four different mechanisms likely perpetuate these responses. The mechanism will depend on both the type of sensor material and the redox behaviour of the analyte gas, for example at temperatures between 200-500°C, oxygen molecules from the atmosphere adsorb onto the metal oxide surface of metal, forming ions such as O^-, O^{2-} and O_2^-. The formation of such ions requires the removal of electrons from the semiconducting material, giving the metal oxide sensor a baseline resistance at these temperatures. The mechanism for such a reaction is illustrated below.

$$O_{2(g)} + 2e^- \rightarrow 2O^-_{(ads)}$$

In general, at surface temperatures <150 °C, O_2^- ions are predominantly formed, whereas at temperatures >150°C and <400°C the principal ion formed is likely O^-, and above these temperatures O_2^- ions dominate[277]. The movement of electrons from the material leads to either an electron depletion layer (EDL, in n-type materials) or a hole accumulation layer (HAL, in p-type materials) (Fig. 8.1)[278].

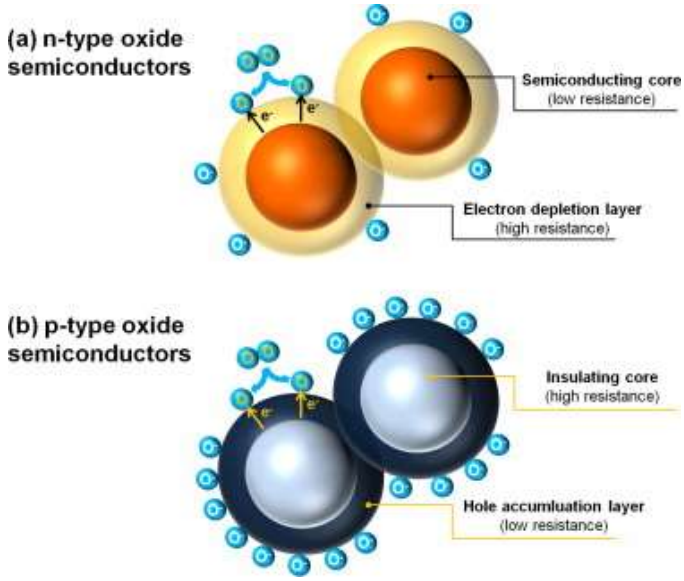

Figure 8.1. Metal oxide grain surfaces at elevated temperatures with adsorbed oxygen at the surface, demonstrating the formation of a high resistance electron depletion layer in an n-type semiconductor (a) and the formation of a low resistance hole accumulation layer in a p-type material (b). Figure adapted from Kim *et.al.* (2014)[278].

At suitable operating temperatures (>150°C) reducing gases react at the semiconductor surface, where the analyte species is thought to undergo a redox reaction to remove the adsorbed oxygen. In n-type sensors, this reintroduces electrons to the bulk material, decreasing the size of the depletion layer, leading to an increase in charge carrier concentration and conductivity and a concurrent decrease in resistivity via the mechanism illustrated below.

$$O^-_{(ads)} + R_{(g)} \rightarrow RO + e^-$$

In p-type materials however, when electrons are reintroduced into the material, the hole density in the material decreases leading to an increase in the resistance due to the smaller charge carrier concentration.

Many gases can undergo multiple sequential redox reactions at the sensor surface, producing a variety of compounds, for example, primary alcohols undergo oxidation to produce an aldehyde, which can be subsequently be oxidised to a carboxylic acid.

Products of such redox reactions can themselves interact with adsorbed oxygen at the sensor surface and can thereby contribute to the sensor response.

8.2. Operating Temperature

When operating an electronic nose, it is advantageous to operate the sensors at as low a temperature as possible, as heating the sensors uses a lot of power and restricts the ability for a sensor to be truly mobile.

Chromium titanate and vanadium pentoxide sensors were operated at temperatures between 250°C and 350°C, while zinc oxide and indium zinc oxide based sensors were operated at temperatures between 350°C and 500°C. The large band gap of zinc oxide, indium zinc oxide and zeolite modified zinc oxide sensors is likely to be responsible for their diminished responses at temperatures below 350°C. Zinc oxide has a band gap of 3.4 eV, while vanadium pentoxide has a band gap of 2.2 eV and chromium titanate 1.8 eV. The larger band gaps, require more energy to promote an electron from the valance band to the conduction band and induce a current in the material. Zinc oxide therefore requires more energy for conductivity and the formation of an electron depletion layer at the sensor surface than materials with a lower band gap, such as chromium titanate and vanadium pentoxide.

When assessing operating temperatures, one must also consider the redox properties of the material, as this will vary with temperature[279]. In addition, the adsorption and desorption properties of analytes at the sensor surface are temperature dependent and the residence time of an analyte is therefore also affected by temperature.

An optimum temperature, resulting in maximum responsiveness, is apparent for the reaction of each analyte gas at a sensor surface. Below this optimum temperature, the rate of reaction is too slow to give a peak response, whilst above the optimum temperature the redox reaction will proceed so rapidly that the concentration of the analyte becomes diffusion limited and the concentration 'seen' by the sensor

approaches zero, here the reaction takes place at the sensor surface without producing a noticeable electric charge in the material[280].

8.3. Incorporation of Zeolites

In many cases, zeolite modification improves the responsiveness of the sensor material, compared to the unmodified sensor. This improved response is a result of several properties of the zeolite material.

The large surface area of zeolite materials, leads to a concurrent increase in the surface area of the sensing material compared to the unmodified material. This can lead to a more open microstructure with larger pores, examples of which are shown in SEM images of sensor surfaces shown in sections 3.2, 4.2 and 5.2. This larger surface area and more open microstructure allow oxygen species and target gases to penetrate deeper into the material and access areas of the porous structure that were previously not accessible in the unmodified material. Zeolite modification can, therefore, allow a greater area for oxygen species to adsorb and for electron transfer to occur, increasing the responsiveness of the sensor material.

Zeolites are well known for their adsorption properties, and there are many reports of gases used in this study adsorbing well and reacting at the surface of the zeolites incorporated into the sensors[281]. The strong adsorption of target gases by the incorporated zeolites means that gases can be 'held' close to the sensor surface ensuring that there are many analyte molecules available to adsorb and react at the sensor surface. This is demonstrated by the increased recovery times of zeolite-modified sensors, compared to the unmodified sensors.

As all zeolites contain an H^+ counter ion, they are able to act as acid catalysts. The zeolite molecules facilitate the dehydration and breakdown of target gasses leading to the formation of a greater number of analyte molecules, as well as more reactive species at the sensor surface (as noted in section 3.7). These reactions contribute towards the

larger magnitudes of response observed in the zeolite modified sensors compared to their unmodified counterparts.

Simultaneous response pulses to multiple gases (section 3.6.1 and 4.4.8) show that zeolite catalysed reactions play a role in the individual response pulses. Varying concentrations of two different gases leads to different response and recovery times and varying peak shapes, this is likely due to reactions resulting in new chemical species that arise from reactions between the two analyte gases either in the gaseous phase or at the zeolite surface. These newly formed chemical species can subsequently react with adsorbed oxygen species and contribute to the gas sensing responses observed.

Zeolites are insulating materials; as such, the inclusion of these materials into a semiconductor environment is thought to restrict the percolation of charge carriers through the material. This may result in an increase in resistance, such as that observed in zinc oxide sensors with NO_2. In this capacity, the zeolite materials, may act as capacitors, storing charge carriers; consequently, when sensors are exposed to a gas pulse, and the charge carrier concentration begins to change, all charge carriers are released simultaneously leading to a sudden increase in conductivity. This theory may explain the unusual peak shape observed with some zeolite modified sensors upon exposure to ammonia (section 4.3.6).

Whilst in the majority of cases, the response of the zeolite-modified sensors are larger in magnitude than their unmodified counterpart, the magnitude of response does not determine the length of response time. Measurement of response times to pulses of gases used in this study showed that all zeolite modified sensors take significantly longer to reach 90% of their maximum response. These long response times may be due to the breakdown of gases and a slow rate of reaction between adsorbed oxygen at the sensor surface and target gases occurring at more locations on the sensor surface. In addition, due to the more open, porous morphology reactions may take place in areas of the sensor that are not necessarily accessible in the unmodified sensor, leading to a further increase in the observed response times.

The responses of zeolite modified zinc oxide and chromium titanate sensors were found to generally be of a similar order of magnitude, with some exceptions, for example upon exposure to ethanol. The responses of zeolite-modified vanadium pentoxide were, however, significantly lower than the other materials utilised in this investigation. Vanadium pentoxide sensors were found to have similar surface areas to other zeolite modified sensors, therefore access to the sensor surface for analyte gases is presumed to be similar, however the resistance of the vanadium pentoxide materials in air is consistently lower than the comparative chromium titanate and zinc oxide sensors. This implies that the vanadium pentoxide material contains far more charge carriers per unit volume than the other sensor materials (as detailed in section 5.5). The size of the space charge region is inversely proportional to the charge carrier density and therefore when a material has a significantly larger density there will be a smaller electron depletion layer leading to a lower magnitude of response.

8.4. Responses to Nitrogen Dioxide

Three types of sensor (zeolite modified zinc oxide, chromium titanate and vanadium pentoxide) were exposed to concentrations of 50-800 ppb nitrogen dioxide at their respective operating temperatures. Of note, was the considerable enhancements in the responsiveness of the zeolite-modified sensors compared to their unmodified counterparts. This enhancement was most notable in zeolite Y and mordenite modified sensors and the largest observed magnitude of response was noted with zinc oxide based sensors.

The increase in response is likely a result of nitrogen dioxide's ability to react directly with the sensor surface, whereas other gases utilised in this study react with oxygen ions adsorbed at the senor surface. The reactions at the sensor surface, as proposed by Wetchakun *et.al*.[282] are likely:

$$NO_{2(g)} + 3e^- \rightarrow NO^{2-}_{(ads)} + O^-_{(ads)}$$

$$NO^{2-}_{(ads)} + O^-_{(ads)} + e^- \rightarrow NO_{(g)} + 2O^{2-}_{(ads)}$$

These reactions remove electrons from the material. In n-type sensors, this increases the resistance in the material, whilst in p-type materials; the removal of electrons increases the hole density, thereby decreasing the resistance in the sensor material.
Upon exposure to nitrogen dioxide, responses were significantly enhanced in mordenite and zeolite Y modified sensors compared to other sensors. The large response of mordenite-modified sensors can be attributed to its mono dimensional pore structure. While other sensors have multiple channels, operating across different axis, allowing for collisions between gas particles travelling in different directions, the one-dimensional channel structure of mordenite increases the likelihood of nitrogen dioxide molecules reaching the gas sensitive surface.

The increased responsiveness of zeolite Y modified sensors is likely due to the significantly large pore diameter of zeolite Y compared to other zeolites (11.24 Å)[283]. This large pore diameter allows more analyte gas to travel through the zeolite channels, with a smaller likelihood of collisions with the pore walls or other gas particles, enabling more analyte gas to reach and react at the gas sensitive surface, thereby increasing the response.

The responses of zeolite beta and ZSM5 modified sensors to nitrogen dioxide at all concentrations are of a similar magnitude. Both zeolite beta and ZSM5 are three-dimensional zeolites with similar pore diameters, which may account for the similar response of these sensors to nitrogen dioxide.

8.5. Responses to Ammonia

Three types of sensor (zeolite modified zinc oxide, chromium titanate and vanadium pentoxide) were exposed to ammonia at concentrations between 2.5-40 ppm at their respective operating temperatures. The response of all tested sensors to ammonia was generally quite poor, with no particular sensor demonstrating excellent responsiveness. The recovery of the sensors is also quite poor, with sensors taking as long as 20 minutes to fully recover following a gas pulse. This long recovery time indicates that that the adsorption of ammonia on the metal oxide and zeolite surfaces is relatively strong

compared to other analyte gases used in this study. The reactions that proceed at the sensor surface are not thermodynamically favourable, and any reactions that do occur, liberate few electrons back into the bulk material. An example of such a reaction is illustrated below.

$$2NH_3 + 3O^-_{(ads)} \rightarrow N_2 + 3H_2O + 3e^-$$

This shows that only 1.5 electrons are liberated for each ammonia molecule adsorbed at the sensor surface, which is considerably less than other analyte gasses (6 electrons per ethanol molecule and 8 electrons per acetone molecule).

At higher operating temperatures, zeolite modified zinc oxide sensors show stronger responsiveness to ammonia, while at lower temperatures (300°C and 250°C), zeolite modified chromium titanate sensors show strong responsiveness (R/R_0 = 22 to 40 ppm). The largest magnitudes of response in both cases are observed with ZSM5 modified sensors, while zeolite beta modified sensors are found to be the least responsive. Vanadium pentoxide sensors show very poor responses at all operating temperatures, with no response larger than R_0/R =1.45 to 40 ppm of ammonia.

Enhancements in response may be due to the formation of hydrogen molecules at the zeolite surface, ammonia can breakdown at the zeolite surface under the following reaction:

$$2NH_3 \rightarrow N_2 + 3H_2$$

Nitrogen is an unreactive noble gas and so will play no further part in the sensor response, however hydrogen is able to react at the sensor surface to form water, a favourable reaction that may lead to an enhancement in responsiveness at the sensor surface.

$$H_2 + O^- \rightarrow H_2O + e^-$$

8.6. Response to Toluene

Zeolite modified; zinc oxide, chromium titanate and vanadium pentoxide sensors were exposed to toluene at their respective operating temperatures, at concentrations between 2.5-40 ppm. ZSM5 and mordenite modified sensors showed the strongest responses upon exposure to toluene across all sensor materials. Strong responses to toluene were found with zinc oxide sensors at an operating temperature of 500°C and with chromium titanate sensors at an operating temperature of 300°C.

Analysis of exhaust gases showed that toluene undergoes catalytically activated breakdown to constituent hydrocarbon molecules, including benzene, pentadiene and butadiene, at the zeolite surface. These reactions involve breaking σ and π bonds between carbon atoms to produce a greater number of molecules (for example a single toluene molecule may break down into a benzene molecule and a methane molecule) enabling an increased number of reactants at the sensor surface. In these reactions the zeolites act as acid catalysts.

$$C_7H_8 \rightarrow C_6H_5^+ + CH_3^+ + 2e^-$$

The ZSM5 modified sensors consistently shows a longer response time than all other sensors, with response times of up to 420 seconds (7 minutes), this implies that a large amount of the target gas is adsorbed into the zeolite, which may then undergo acid catalysed breakdown to smaller species.

8.7. Response to Acetone

Sensors (zeolite modified zinc oxide, chromium titanate and vanadium pentoxide) were exposed to acetone at concentrations between 0.5-8 ppm at their respective operating temperatures. At an operating temperature of 500°C, zeolite modification produced no enhancement in the responsiveness of sensors, in fact the magnitudes of response in zeolite modified zinc oxide sensors are approximately half that of that observed for the unmodified zinc oxide sensors. At lower temperatures, zeolite modification leads to

enhancements in the responsiveness to acetone. At 350-400°C, zeolite Y and ZSM5 modified sensors show the largest enhancements upon exposure acetone compared to their unmodified counterparts. Below 350°C, zeolite beta - modification was found to produce the most responsive sensor. The variation in most responsive sensor can be attributed to the adsorption properties of the various zeolites at different operating temperatures, for example at higher operating temperatures, ZSM5 adsorbs acetone better, however its adsorption ability is reduced as temperature decreases.

At the zeolite surface, acetone molecules may be dehydrated to form water and an allene molecule; both of these products are less reactive than the acetone molecule itself and would therefore induce a weaker response (as observed at 500°C in section 3.3.4). The formula to represent this reaction is indicated below:

$$C_3H_6O \rightarrow C_3H_4 + H_2O$$

At lower operating temperatures, zeolite modified sensors are found to give enhanced responses compared to the unmodified sensor. This may be due to incomplete dehydration leading to the formation of carbocation molecules that are able to react with the adsorbed oxygen molecules, inducing strong responses at the sensor surface via reactions such as that illustrated below.

$$C_3H_6O \rightarrow C_3H_5^+ + OH^-$$

Zeolite modification of sensors following exposure to acetone induces longer recovery times, suggesting that the adsorbed analyte materials at the zeolite surface continue to make a contribution at the gas sensitive surface after the end of the gas pulse.

In all materials, zeolite beta modified sensors were found to have the longest response times, this is likely because the capacity for adsorption of acetone on zeolite beta is greater than with other zeolites, slowing the flow of acetone to the surface. In many cases, the zeolite beta modified sensor is not the most responsive sensor in the series.

Zeolite modified zinc oxide sensors were found to be most responsive upon exposure to acetone, these responses were considerably larger in magnitude than chromium titanate and vanadium pentoxide sensors, with responses around R_0/R = 5-10.

8.8. Response to Ethanol

Indium doped zinc oxide as well as zeolite modified zinc oxide, chromium titanate and vanadium pentoxide sensors were exposed to ethanol at concentrations between 5-80 ppm. All sensors demonstrated relatively strong responses when exposed to ethanol compared to other test gases utilised throughout this work. Zeolite modification of chromium titanate and vanadium pentoxide sensors leads to enhancements in the responsiveness at all operating temperatures, with the largest magnitude of response in this study recorded with ZSM5 modified chromium titanate. Zeolite modification of zinc oxide sensors leads to enhancements in the responsiveness upon exposure to ethanol, however at an operating temperature of 400°C the zeolite modified sensors show a smaller magnitude of response to the unmodified samples.

Indium-zinc oxide sensor responses to ethanol are large; indium-zinc oxide (0.5%) was shown to not only to be extremely responsive to ethanol but this increased response appeared to be specific for this alcohol species as it was significantly larger than that recorded upon exposure to a large number of other chemicals, including methanol and *n*-butanol.

As demonstrated previously, the formation of a space charge region involves electrons from the material becoming trapped to form a chemisorbed oxygen species ($O^-_{(ads)}$)[80]. Oxygen is available in abundance from the atmosphere; therefore the rate of formation of $O^-_{(ads)}$ is determined by the electron density in the material. Introduction of a more electron dense material, by for example replacing Zn^{2+} with In^{3+}, increases the conductivity and therefore electron density of the material. This increase in electron density allows the formation of more chemisorbed oxygen sites and therefore provides

more sites for surface reactions to take place, consequently leading to larger magnitudes of responses.

In general the large responses to ethanol are likely as a result of the reactive nature of ethanol, which is primarily due its hydroxyl group. Ethanol is well known to undergo dehydration reactions, leading to the formation of ethane and water at zeolite surfaces[284,285,286]. At high operating temperatures (> 400°C), under acidic conditions, ethanol is fully dehydrated at the zeolite surface, leading to the formation of ethene and water, two unreactive species (see the reaction below). At lower operating temperatures, the incomplete dehydration of ethanol, can lead to the formation of carbocations and other charged species that will lead to an enhanced response due to the favourable reaction between positively charged ions and the negatively charged adsorbed oxygen ions at the sensor surface.

$$C_2H_5OH + H^+ \rightarrow C_2H_5^+ + H_2O$$

The adsorption at the zeolite-modified surface is therefore strong and ethanol is 'held' in close proximity to the metal oxide sensor, increasing the likelihood of collisions with the sensor material, and thereby forcing a change in the resistance of the sensor. A second consequence of this strong adsorption is that the recovery times (the time taken for the sensor to return to within 10% of its original baseline resistance, following a gas pulse) of zeolite modified sensors are far longer than that of unmodified sensors, due to the slow desorption rate from the sensor.

Zeolite modified chromium titanate sensors were found to be the most responsive to ethanol, with responses of $R/R_0 > 450$ to 80 ppm. Zeolite modified vanadium pentoxide sensors were found to be the least responsive, likely due to poor space charge region formation.

8.9. Further Work

This thesis illustrates work undertaken in laboratory conditions to validate the production of an electronic nose responsive to gases commonly found in clandestine chemistry locations. In order for this work to be translated in to the development of a useful device, field tests of true to life scenarios are required.

Firstly, a final gas sensing array must be selected by analysing the materials developed in this thesis, alongside other common gas sensing materials (SnO_2, NiO, etc) to select a suitable number of sensors to provide selectivity to a range of gases. This selectivity of this array should be determined using machine learning techniques to identify a similarity measure across all the sensors. This will specify how similar the responses of sensors are when exposed to a predetermined set of gases and will be used to ensure there is no redundancy within the array as the optimisation will based on the separability of target gases and the similarity of sensor responses. The advantage of the proposed method lies in its performance being independent of the choice of the pattern recognition engine[287].

This final array will require the testing in a larger sensing chamber, the size of an average room (15-20 m^3) and using vapours of target gases created by various reactions similar to those observed in the production of methamphetamine, as opposed to predetermined pulses of one or two analytical standard gases at set concentrations.

To further validate the use of these sensors in a “real life” electronic nose device additional considerations must also be addressed, these are discussed briefly below.

8.9.1. Investigation into Humidity

The sensors utilised in chapters 3, 4 and 5 show some humidity dependent alteration in response. This is because water molecules chemisorbed at the sensor surface and may disassociate to form surface hydroxyls at the designated operating temperatures.

Further water molecules are also able to physisorb to the surface by hydrogen bonding to the surface hydroxyl group as well as to other water molecules. Chemisorbed hydroxyl groups remove electrons, forming an electron depletion layer, however large numbers of water molecules close to the sensor surface can prevent target gas molecules from reacting at the sensor surface and therefore the response to many test gases is lower in a humid environment.

In order to correctly calculate the concentration of a gas, the humidity of the environment must be taken into account. One may wish to incorporate a humidity meter into the electronic nose array and apply an algorithm to correct for the level of humidity in the sensing chamber to accurately calculate the analyte concentration. It may also be possible to include a hygroscopic material, such as a cellulose fibre, calcium chloride or potassium hydroxide, into the sensing unit, as a filter over the entrance of the sensing chamber to adsorb any moisture in the air and reduce the humidity with the chamber itself. A filter or adsorbent material would however, require regular replacement to prevent the material becoming saturated and allowing the introduction of water to the environment.

8.9.2. Batch to Batch Variability.

In order for the sensors presented in this thesis to become commercially viable entities, more work must be undertaken to assess the batch-to-batch variability as the largest contribution to sensor-to-sensor variability is inconsistency in the film thickness. There are large differences in sensor response based on the number of layers of metal oxide suspension printed onto sensor substrates. The average thickness of sensors in this study was 75 µM, however this varied between 71-78 µM. In order for sensors to be mass-produced and sold as commercial units, methods to ensure that consistent film thickness is achieved between batches must be implemented. Perceived variability in sensor thickness can also arise from discrepancies in the location of the measured sensor within the sensor strip, with sensors in the middle of the strip often thicker than those at the ends. In this study a sensor from the same position within the strip was utilised for all experiments to ensure as close an accurate representation of thickness

and uniformity as possible between sensors. This method would waste more than 90% of sensors printed and could therefore not be translated to the production of sensors on a larger commercial scale.

8.9.3. Implementation of a Wireless Network

In addition to testing the sensing array in a more real-life situation, the ability to read sensor data remotely would be required to analyse results away from the immediate environment. The development of a wireless sensor network would therefore be required.

There are many examples of wireless sensor networks being deployed in hotels[288], train stations[289], stadiums[290] and even on volcanoes[291]. A sensor network consists of a number of nodes, which include the sensor array, a processor, memory, a power supply, a radio and an actuator[292]. The actuator is used to control different parts of the node, adjust sensing parameters and monitor the power within the node. All of the nodes in the vicinity report data, though the radio component, to a base station, and a computer or tablet device displays data for an end user to observe.

There are two types of wireless sensor network: structured and unstructured. An unstructured sensor network consists of a dense collection of sensor nodes, placed throughout the sensing area in an ad-hoc manner. Once this system is deployed, the sensor nodes are left unattended to monitor and report on the local area. Maintenance of the network and managing connectivity between the nodes and a base station is often difficult, because nodes may be located in difficult to access locations.

A structured network consists of a number of networks in a pre-planned spatial arrangement at fixed locations. Structured networks are placed at specific locations to obtain maximum coverage, while unstructured networks have more potential to contain black spots.

When detecting clandestine activity, a structured network would serve as a better detection network. This would allow specific areas to be analysed and alert appropriate parties. Although structured networks can also lead to black spots, as long as these locations are kept as small as possible, a large area can be monitored using a sensor network containing metal oxide sensors.

8.9.4. Power Consumption

Electronic noses containing metal oxide gas sensors have a high-power requirement (~100 mW), methods to reduce this and therefore the operating cost for the sensor would be required before the sensor array could become commercially viable. The majority of the power is required for heating the sensors and keeping them at a constant operating temperature. Ideally to reduce the power consumption, the sensors would be maintained at a temperature close to room temperature and heated to the appropriate operating temperature for a brief period only, for example 10 minutes every hour. The heating time and temperature would depend on the toxicity of the gases being analysed, as more toxic gases will need to be detected sooner in order to alert any bystanders in a timely manner. Sensors use considerably less power at lower operating temperatures, therefore spending more time at lower temperatures (and therefore not actively sensing) means that the unit will use less power and consequently cost the user less, making the units more commercially viable. A balance between frequency of measurement and power consumption must therefore be found.

8.10 Conclusions

The work presented in this thesis represents the novel development of a sensor device for the practical monitoring of potential locations of clandestine chemistry. The potential for different classes of modified sensors to be incorporated into an electronic nose device for the successful identification of sites of clandestine activity has been demonstrated.

This work has incorporated the modification of metal oxides with zeolites and metal ion doping techniques to achieve sensor selectivity. Modification of sensor materials alters the morphology, particle size and capacitance of the materials to change the gas sensing properties of the materials, and present a degree of selectivity for otherwise unresponsive and unselective candidates for electronic noses.

Analysis of exhaust gases following sensor exposure, using mass spectrometry, demonstrated the catalytic capabilities of the zeolite auxiliary elements in breaking down analyte gas molecules through acid catalysed reactions at the surface. These reactions lead to enhancements (or in some cases reduction) in the sensor responsivity to a range of analyte gases.

Doping of zinc oxide with low levels of indium increased the conductivity within the material significantly. This enhancement in conductivity led to large enhancements in response for samples of zinc oxide doped with 0.2 and 0.5% indium, compared with pure zinc oxide. Additionally, indium doped zinc oxide at 0.5% demonstrated selectivity to ethanol, showing responses over 10 times greater than that of other gases at the same concentration.

When sensor data was combined to form a unique chemical fingerprint to a gas, machine-learning techniques were applied to successfully predict the gas present.

This work demonstrates for the first time, a mechanism by which zeolite admixture materials enhance the responses of gas sensors. By breaking down analyte species into their constituent parts for easier reaction at the sensor surface, reactions are able to take place at a faster rate, leading to a larger transfer of electrons at the sensor surface. The exact reactions will vary based on the analyte gas, zeolite and operating temperature.

This thesis also demonstrates for the first time, the high level of selectivity that is obtained towards ethanol through indium doped zinc oxide gas sensors, thought to be due to the enhanced conductivity and microstructure of the material.

Finally, this study demonstrates the use of several different methods of machine learning to correctly identify gases present using an array of chemical sensors. These methods can be used in combination with a range of sensors to produce an electronic nose capable of correctly identifying locations of clandestine chemistry.

[1] Parkes, J. D., & Fenton, G. W. (1973). Levo (−) amphetamine and dextro (+) amphetamine in the treatment of narcolepsy. *Journal of Neurology, Neurosurgery & Psychiatry*, *36*(6), 1076-1081.

[2] Griffiths, P., Mravcik, V., Lopez, D., & Griffiths, P. (2008). Quite a lot of smoke but very limited fire—the use of methamphetamine in Europe. *Drug and alcohol review*, *27*(3), 236-242.

[3] King L.A. "Forensic Chemistry of Substance Misuse: A Guide to Drug Control" RSC Publishing, Cambridge, 2009

[4] McKetin, R., McLaren, J., Kelly, E., & Chalmers, J. (2009). The market for crystalline methamphetamine in Sydney, Australia. *Global Crime*, *10*(1-2), 113-123.

[5] Great Britain. Misuse of Drugs Act 1971: Elizabeth II Chapter 38 (1971) London: The Stationary Office

[6] Snow, O. (1998) *Amphetamine Syntheses: Overview & Reference Guide for Professionals*. Thoth Press, London.

[7] Burgess, J. L., Barnhart, S., & Checkoway, H. (1996). Investigating clandestine drug laboratories: adverse medical effects in law enforcement personnel. *American Journal of Industrial Medicine*, *30*(4), 488-494.

[8] Martyny, J. W., Arbuckle, S. L., McCammon, C. S., Esswein, E. J., Erb, N., & Van Dyke, M. (2007). Chemical concentrations and contamination associated with clandestine methamphetamine laboratories. *Journal of Chemical Health and Safety*, *14*(4), 40-52.

[9] Shukla, R. K., Crump, J. L., & Chrisco, E. S. (2012). An evolving problem: Methamphetamine production and trafficking in the United States. *International Journal of Drug Policy*, *23*(6), 426-435.

[10] Allen, A. C., & Kiser, W. O. (1987). Methamphetamine from ephedrine: I. Chloroephedrines and aziridines. *Journal of Forensic Science*, *32*(4), 953-962.

[11] Sexton, R. L., Carlson, R. G., Leukefeld, C. G., & Booth, B. M. (2006). Patterns of illicit methamphetamine production ("cooking") and associated risks in the rural South: An ethnographic exploration. *Journal of Drug Issues*, *36*(4), 853-876.

[12] Martyny, J. W., Van Dyke, M., McCammon, C. S., Erb, N., & Arbuckle, S. L. (2005). Chemical exposures associated with clandestine methamphetamine laboratories using the hypophosphorous and phosphorous flake method of production. *National Jewish Medical Research Center http://www. njc. org/pdf/meth-hypo-cook. pdf (Accessed 9 July 2016)*.

[13] Crass, M. F. (1941). A history of the match industry. *Journal of Chemical Education*, *18*(6), 277.

[14] Dauvergne, M. (2009). Trends in police-reported drug offences in Canada. *Juristat: Canadian Centre for Justice Statistics*, *29*(2), 1C.

[15] Kulish, N. Europe Fears That Meth Foothold Is Expanding. *New York: New York Times A*, (2007) *1*.

[16] Hunt, D. E. (2006). Methamphetamine abuse: Challenges for law enforcement and communities. *NIJ Journal*, *254*(1), 24-28.

[17] Mitka, M. (2005) Meth lab fires put heat on burn centers. *JAMA: the journal of the American Medical Association*, *294*(16), 2009-2010.

[18] Bratcher, L., Clayton, E. W., & Greeley, C. (2007). Children in methamphetamine homes: a survey of physicians practicing in southeast Tennessee. *Pediatric emergency care*, *23*(10), 696-702.

[19] Wayne, P. B. (2003). Life after meth: proactive property management is critical to preventing on-site meth labs. *Journal of Property Management*, 68(3), 62-67.

[20] Ramos, F. "Two killed, homes flattened in south Indianapolis explosion" WTHR News http://www.wthr.com/story/20064503/homes-flattened-in-south-indianapolis-explosion (Accessed 12/06/16)

[21] Dobkin, C., & Nicosia, N. (2009). The war on drugs: methamphetamine, public health, and crime. *The American economic review*, *99*(1), 324-349.

[22]Allen N "'15' feared dead after explosion at Texas fertiliser plant" *The Daily Telegraph* 18th April 2013

[23] Fernandez M and Schwartz (2013) Plant explosion tears at the heart of a Texas Town The New York Times 18 April http://www.nytimes.com/2013/04/19/us/huge-blast-at-texas-fertilizer-plant.html?pagewanted=all&_r=0 (accessed 18/05/16)

[24] Broeders, A. P. A. (2006). Of earprints, fingerprints, scent dogs, cot deaths and cognitive contamination—a brief look at the present state of play in the forensic arena. *Forensic Science International*, *159*(2), 148-157.

[25] Cornu, J. N., Cancel-Tassin, G., Ondet, V., Girardet, C., & Cussenot, O. (2011). Olfactory detection of prostate cancer by dogs sniffing urine: a step forward in early diagnosis. *European urology*, *59*(2), 197-201.

[26] Reindl-Thompson, S. A., Shivik, J. A., Whitelaw, A., Hurt, A., & Higgins, K. F. (2006). Efficacy of Scent Dogs in Detecting Black-Footed Ferrets at a Reintroduction Site in South Dakota. *Wildlife Society Bulletin*, *34*(5), 1435-1439.

[27] Wells, D. L., Lawson, S. W., & Siriwardena, A. N. (2008). Canine responses to hypoglycemia in patients with type 1 diabetes. *The Journal of Alternative and Complementary Medicine*, *14*(10), 1235-1241.

[28] Bromenshenk, J. J., Henderson, C. B., Seccomb, R. A., Welch, P. M., Debnam, S. E., & Firth, D. R. (2015). Bees as biosensors: chemosensory ability, honey bee monitoring systems, and emergent sensor technologies derived from the pollinator syndrome. *Biosensors*, 5(4), 678-711.

[29] S. Sielemann, J.I. Baumbach, H. Schmidt, P. Pilzecker, (2000) Quantitative analysis of benzene, toluene, and m-xylene with the use of a UV-ion mobility spectrometer, *Field Analytical Chemistry & Technology* 4(4) 157–169.

[30] Hill, H. H., & Simpson, G. (1997). Capabilities and limitations of ion mobility spectrometry for field screening applications. *Field Analytical Chemistry & Technology*, *1*(3), 119-134.

[31] Smiths Detection, SABRE 4000, CENTURION II, HGVI, Watford, Herts, UK.

[32] Ewing, R. G., Atkinson, D. A., Eiceman, G. A., & Ewing, G. J. (2001). A critical review of ion mobility spectrometry for the detection of explosives and explosive related compounds. *Talanta*, *54*(3), 515-529.

[33] Murray, G. M., & Southard, G. E. (2002). Sensors for chemical weapons detection. *IEEE instrumentation & measurement magazine*, *5*(4), 12-21.

[34] Keller, T., Miki, A., Regenscheit, P., Dirnhofer, R., Schneider, A., & Tsuchihashi, H. (1998). Detection of designer drugs in human hair by ion mobility spectrometry (IMS). *Forensic science international*, *94*(1), 55-63.

[35] Liaud, C., Nguyen, N. T., Nasreddine, R., & Le Calvé, S. (2014). Experimental performances study of a transportable GC-PID and two thermo-desorption based methods coupled to FID and MS detection to assess BTEX exposure at sub-ppb level in air. *Talanta*, *127*(7), 33-42.

[36] Kessel, R. (1997). *U.S. Patent No. 5,654,498*. Washington, DC: U.S. Patent and Trademark Office.

[37] Rismanchian, M., Golbabaei, F., Mortazavi, Y., Pourtaghi, G., & Foroushani, A. R. (2012). Evaluation of photoionisation detector performance in photocatalytic studies for removing volatile organic compounds. *International Journal of Environmental Health Engineering*, *1*(1), 42.

[38] Pert, A. D., Baron, M. G., & Birkett, J. W. (2006). Review of analytical techniques for arson residues. *Journal of forensic sciences*, *51*(5), 1033-1049.

[39] Chao, C. Y. H., & Hu, J. S. (2004). Development of a dual-mode demand control ventilation strategy for indoor air quality control and energy saving. *Building and Environment*, *39*(4), 385-397.

[40] Wang, Q. G., Lee, T. H., Fung, H. W., Bi, Q., & Zhang, Y. (1999). PID tuning for improved performance. *IEEE Transactions on control systems technology*, *7*(4), 457-465.

[41] Wolfbeis, O. S. (2004). Fiber-optic chemical sensors and biosensors. *Analytical chemistry*, *76*(12), 3269-3284.

[42] McDonagh, C., Burke, C. S., & MacCraith, B. D. (2008) Optical chemical sensors. *Chemical reviews*, *108*(2), 400-422.

[43] Firooz, A. R., Movahedi, M., & Ensafi, A. A. (2012). Selective and sensitive optical chemical sensor for the determination of Hg (II) ions based on tetrathia-12-crown-4 and chromoionophore I. *Sensors and Actuators B: Chemical*, *171*(3), 492-498.

[44] Deng, S., Doherty, W., McAuliffe, M. A., Salaj-Kosla, U., Lewis, L., & Huyet, G. (2016) A low-cost, portable optical sensing system with wireless communication compatible of real-time and remote detection of dissolved ammonia. *Photonic Sensors*, *6*(2), 107-114.

[45] Satyanarayana, S., Surface stress and capacitive MEMS sensor arrays for chemical and biological sensing, Ph.D. thesis, University of California, Berkeley, 2005.

[46] Basabe-Desmonts, L., Reinhoudt, D. N., & Crego-Calama, M. (2007). Design of fluorescent materials for chemical sensing. *Chemical Society Reviews*, *36*(6), 993-1017.

[47] Domanský, K., Baldwin, D. L., Grate, J. W., Hall, T. B., Li, J., Josowicz, M., & Janata, J. (1998). Development and calibration of field-effect transistor-based sensor array for measurement of hydrogen and ammonia gas mixtures in humid air. *Analytical chemistry*, *70*(3), 473-481.

[48] Covington, J. A., Gardner, J. W., Bartlett, P. N., & Toh, C. S. (2004). Conductive polymer gate FET devices for vapour sensing. *IEE Proceedings-Circuits, Devices and Systems*, *151*(4), 326-334.

[49] Sasahara, T., Kato, H., Saito, A., Nishimura, M., & Egashira, M. (2007). Development of a ppb-level sensor based on catalytic combustion for total volatile organic compounds in indoor air. *Sensors and Actuators B: Chemical*, *126*(2), 536-543.

[50] Schreiter, M., Gabl, R., Lerchner, J., Hohlfeld, C., Delan, A., Wolf, G., & Pompe, W. (2006). Functionalized pyroelectric sensors for gas detection. *Sensors and Actuators B: Chemical*, *119*(1), 255-261.

[51] e2V technologies, VQ41TSB, VQ547TS, Chelmsford, Essex, UK.

[52] Sierra Monitor, Model 4100 Series, Milpitas, CA, USA.

[53] Duan, B. K., Zhang, J., & Bohn, P. W. (2011). Conductance-based chemical sensing in metallic nanowires and metal-semiconductor nanostructures. *Analytical chemistry*, *84*(1), 2-8.

[54] Man, G., Stoeber, B., & Walus, K. (2009). An assessment of sensing technologies for the detection of clandestine methamphetamine drug laboratories. *Forensic science international*, *189*(1), 1-13.

[55] Gentry, S. J., & Jones, T. A. (1986). The role of catalysis in solid-state gas sensors. *Sensors and Actuators*, *10*(1-2), 141-163.

[56] Sommer, V., R. Rongen, P. Tobias, and D. Kohl. (1992) Detection of methane/butane mixtures in air by a set of two microcalorimetric sensors. *Sensors and Actuators B: Chemical* 6(1) 262-265.

[57] Taguchi, N. (1962). A metal oxide gas sensor. *Japanese Patent*, (45-38200).

[58] Sun Sky Home Security Gas Sensor http://www.sunskyonline.com/view/269814/Home+Security+Gas+Sensor+Detector+Alarm.htm (Accessed 10/6/16)

[59] SGX Sensortech http://www.sgxsensortech.com/site/sgx-sensortech-products-services/gas-sensors-environmental-monitoring/ (accessed 10/6/16)

[60] Patra, M. K., Manzoor, K., Manoth, M., Negi, S. C., Vadera, S. R., & Kumar, N. (2008). Nanotechnology applications for chemical and biological sensors. *Defence Science Journal*, *58*(5), 636.

[61] Atkins, P., T. Overton, J. Rourke, M. Weller, and F. Armstrong (2006). *Inorganic Chemistry* 4th Ed, Oxford University Press 103

[62] Mahato, N., Ansari, M. O., & Cho, M. H. (2015). Production of Utilizable Energy from Renewable Resources: Mechanism, Machinery and Effect on Environment. *Advanced Materials Research,* 1116, 1-32.

[63] Reitzig, M. (2003). What determines patent value?: Insights from the semiconductor industry. *Research Policy*, 32(1), 13-26.

[64] R Turton Chapter 5: Semiconductors *in* The Physics of Solids 2000 Oxford University Press Inc, New York, USA. 117-148

[65] Semiconductors (electrical properties of materials) Retrieved from http://what-when-how.com/electronic-properties-of-materials/semiconductors-electrical-properties-of-materials-part-2/

[66] Korotcenkov, G. (2007). Metal oxides for solid-state gas sensors: What determines our choice? *Materials Science and Engineering: B*, *139*(1), 1-23.

[67] Sun, Y. F., Liu, S. B., Meng, F. L., Liu, J. Y., Jin, Z., Kong, L. T., & Liu, J. H. (2012). Metal oxide nanostructures and their gas sensing properties: a review. *Sensors*, *12*(3), 2610-2631.

[68] Yamazoe, N. (2005). Toward innovations of gas sensor technology. *Sensors and Actuators B: Chemical*, *108*(1), 2-14.

[69] Koirala, R., Pratsinis, S. E., & Baiker, A. (2016). Synthesis of catalytic materials in flames: opportunities and challenges. *Chemical Society Reviews*, *45*(11), 3053-3068.

[70] Briand, D., Labeau, M., Currie, J. F., & Delabouglise, G. (1998). Pd-doped SnO 2 thin films deposited by assisted ultrasonic spraying CVD for gas sensing:

selectivity and effect of annealing. *Sensors and Actuators B: Chemical*, *48*(1), 395-402.

[71] Ansari, S. G., Ansari, Z. A., Seo, H. K., Kim, G. S., Kim, Y. S., Khang, G., & Shin, H. S. (2008). Urea sensor based on tin oxide thin films prepared by modified plasma enhanced CVD. *Sensors and Actuators B: Chemical*, *132*(1), 265-271.

[72] Sberveglieri, G., Faglia, G., Groppelli, S., Nelli, P., & Taroni, A. (1992). A novel PVD technique for the preparation of SnO 2 thin films as C_2H_5OH sensors. *Sensors and Actuators B: Chemical*, *7*(1), 721-726.

[73] Qu, W., & Wlodarski, W. (2000). A thin-film sensing element for ozone, humidity and temperature. *Sensors and Actuators B: Chemical*, *64*(1), 42-48.

[74] Barsan, N., Huebner, M., & Weimar, U., Conducting mechanism in semiconducting metal oxide sensing films: impact and transduction *in* Jaaniso, R., & Tan, O. K. (Eds.). (2013). *Semiconductor gas sensors*. Elsevier.

[75] Lee, S. W., Tsai, P. P., & Chen, H. (2000). Comparison study of SnO 2 thin-and thick-film gas sensors. *Sensors and Actuators B: Chemical*, *67*(1), 122-127.

[76]Lee, S. P. (2013). Electrode materials and electrode-oxide interfaces in semiconductor gas sensors. *Semiconductor Gas Sensors*, Elsevier.

[77] Afonja, O. A. (2012) Use of zeolites to effect discrimination in metal oxide semiconductor gas sensors, Ph.D. thesis, University College London.

[78] Williams, D. E. (1987). Conduction and gas response of semiconductor gas sensors. *Solid state gas sensors*, 71.

[79] Xu, C., Tamaki, J., Miura, N., & Yamazoe, N. (1991). Grain size effects on gas sensitivity of porous SnO2-based elements. *Sensors and Actuators B: Chemical*, *3*(2), 147-155

[80] Naisbitt, S. C., Pratt, K. F. E., Williams, D. E., & Parkin, I. P. (2006). A microstructural model of semiconducting gas sensor response: The effects of sintering temperature on the response of chromium titanate (CTO) to carbon monoxide. *Sensors and Actuators B: Chemical*, *114*(2), 969-977.

[81] Barsan, N., Simion, C., Heine, T., Pokhrel, S., & Weimar, U. (2010). Modeling of sensing and transduction for p-type semiconducting metal oxide based gas sensors. *Journal of Electroceramics*, *25*(1), 11-19.

[82] Chou, J. (2000). *Hazardous gas monitors: a practical guide to selection, operation and applications*. McGraw-Hill Professional Publishing.

[83] Chowdhury, S. S., Tudu, B., Bandyopadhyay, R., & Bhattacharyya, N. (2008, December). Portable electronic nose system for aroma classification of black tea. In *Industrial and Information Systems, 2008. ICIIS 2008. IEEE Region 10 and the Third international Conference on* (pp. 1-5). IEEE.

[84] Ghasemi-Varnamkhasti, M., S. S. Mohtasebi, M. L. Rodriguez-Mendez, J. Lozano, S. H. Razavi, and H. Ahmadi. Potential application of electronic nose technology in brewery. *Trends in Food Science & Technology* 22, no. 4 (2011): 165-174.

[85] El Barbri, N., Llobet, E., El Bari, N., Correig, X., & Bouchikhi, B. (2008). Electronic nose based on metal oxide semiconductor sensors as an alternative technique for the spoilage classification of red meat. *Sensors*, *8*(1), 142-156.

[86] Wilson, A.D. (2013). Diverse Applications of Electronic-Nose Technologies in Agriculture and Forestry. *Sensors* 13(2) 2295-2348.

[87] McAleer, Jerome F., Patrick T. Moseley, John OW Norris, David E. Williams, and Bruce C. Tofield. (1988). Tin dioxide gas sensors. Part 2. The role of surface additives. *J. Chem. Soc., Faraday Trans. 1* 84(2) 441-457.

[88] Moseley, P. T. (1991) New trends and future prospects of thick-and thin-film gas sensors. *Sensors and Actuators B: Chemical* 3, no. 3: 167-174.

[89] Leite, E. R., I. T. Weber, E. Longo, and J. A. Varela. (2000): A new method to control particle size and particle size distribution of SnO_2 nanoparticles for gas sensor applications. *Advanced materials* 12(13) 965-968.

[90] Nayral, Céline, Teyeb Ould-Ely, Andre Maisonnat, Bruno Chaudret, Pierre Fau, Lionel Lescouzeres, and Andre Peyre-Lavigne. (1999) A novel mechanism for the synthesis of tin/tin oxide nanoparticles of low size dispersion and of nanostructured SnO_2 for the sensitive layers of gas sensors. *Advanced Materials* 11(1) 61-63.

[91] Leite, E. R., I. T. Weber, E. Longo, and J. A. Varela. (2000) A new method to control particle size and particle size distribution of SnO_2 nanoparticles for gas sensor applications."*Advanced materials* 12(13): 965-968.

[92] Star, A., Joshi, V., Skarupo, S., Thomas, D., & Gabriel, J. C. P. (2006). Gas sensor array based on metal-decorated carbon nanotubes. *The Journal of Physical Chemistry B*, *110*(42), 21014-21020.

[93] Chopra, S., McGuire, K., Gothard, N., Rao, A. M., & Pham, A. (2003). Selective gas detection using a carbon nanotube sensor. *Applied Physics Letters*, *83*(11), 2280-2282.

[94] Liang, Y. X., Chen, Y. J., & Wang, T. H. (2004). Low-resistance gas sensors fabricated from multiwalled carbon nanotubes coated with a thin tin oxide layer. *Applied Physics Letters*, *85*(4), 666-668.

[95] Zhou, J., Li, P., Zhang, S., Long, Y., Zhou, F., Huang, Y., & Bao, M. (2003). Zeolite-modified microcantilever gas sensor for indoor air quality control. *Sensors and Actuators B: Chemical*, *94*(3), 337-342.

[96] Vilaseca, M., J. Coronas, A. Cirera, A. Cornet, J. R. Morante, and J. Santamarıa. (2003) Use of zeolite films to improve the selectivity of reactive gas sensors. *Catalysis today* 82(1): 179-185.

[97] Chakraborty, S., Sen, A., & Maiti, H. S. (2006). Selective detection of methane and butane by temperature modulation in iron doped tin oxide sensors. *Sensors and Actuators B: Chemical*, *115*(2), 610-613.

[98] Yoon, J. W., Kim, H. J., Kim, I. D., & Lee, J. H. (2013). Electronic sensitization of the response to C2H5OH of p-type NiO nanofibers by Fe doping. *Nanotechnology*, *24*(44), 444005

[99] Simon, U., & Franke, M. E. (2000). Electrical properties of nanoscaled host/guest compounds. *Microporous and Mesoporous Materials*, *41*(1), 1-36.

[100] Kelemen, G., & Schön, G. (1992). Ionic conductivity in dehydrated zeolites. *Journal of materials science*, *27*(22), 6036-6040.

[101] Krogh Andersen, E., Krogh Andersen, I., & Skou E. Proton conduction in zeolites *in* Colomban, P. (Ed.) (1992). *Proton Conductors: Solids, membranes and gels-materials and devices* (Vol. 2). Cambridge University Press. p.210

[102] Jacobs, P. A., & Leuven, K. U. (1982). Acid zeolites: An attempt to develop unifying concepts (PH Emmett award address, 1981). *Catalysis Reviews Science and Engineering*, *24*(3), 415-440.

[103] Bruch, I., Fritsche, J., Bänninger, D., Alewell, U., Sendelov, M., Hürlimann, H., & Alewell, C. (2011). Improving the treatment efficiency of constructed wetlands with zeolite-containing filter sands. *Bioresource technology*, *102*(2), 937-941..

[104] Binions, R., Davis, H., Afonja, A., Dungey, S., Lewis, D.W., Williams, D.E., & Parkin, I.P. (2008). Zeolite Modified Discriminating Gas Sensors. *ECS Transactions*, *16*(11), 275-286.

[105] Meier, B., Werner, T., Klimant, I., & Wolfbeis, O. S. (1995). Novel oxygen sensor material based on a ruthenium bipyridyl complex encapsulated in zeolite Y: dramatic differences in the efficiency of luminescence quenching by oxygen on going from surface-adsorbed to zeolite-encapsulated fluorophores. *Sensors and Actuators B: Chemical*, *29*(1), 240-245.

[106] Peveler, W. J., Binions, R., Hailes, S. M., & Parkin, I. P. (2013). Detection of explosive markers using zeolite modified gas sensors. *Journal of Materials Chemistry A*, *1*(7), 2613-2620.

[107] Moos, R., Müller, R., Plog, C., Knezevic, A., Leye, H., Irion, E., ... & Binder, K. (2002). Selective ammonia exhaust gas sensor for automotive applications. *Sensors and Actuators B: Chemical*, *83*(1), 181-189.

[108] Franke, M. E., Simon, U., Moos, R., Knezevic, A., Müller, R., & Plog, C. (2003). Development and working principle of an ammonia gas sensor based on a refined model for solvate supported proton transport in zeolites. *Physical Chemistry Chemical Physics*, *5*(23), 5195-5198.

[109] Hagen, G., Dubbe, A., Rettig, F., Jerger, A., Birkhofer, T., Müller, R., & Moos, R. (2006). Selective impedance based gas sensors for hydrocarbons using ZSM-5 zeolite films with chromium (III) oxide interface. *Sensors and Actuators B: Chemical*, *119*(2), 441-448.

[110] Hagen, G., Dubbe, A., Rettig, F., Jerger, A., Birkhofer, T., Müller, R., & Moos, R. (2006). Selective impedance based gas sensors for hydrocarbons using ZSM-5 zeolite films with chromium (III) oxide interface. *Sensors and Actuators B: Chemical*, *119*(2), 441-448..

[111] Bordiga, S., Lamberti, C., Geobaldo, F., Zecchina, A., Palomino, G. T., & Areán, C. O. (1995). Fourier-transform infrared study of CO adsorbed at 77 K on H-mordenite and alkali-metal-exchanged mordenites. *Langmuir*, *11*(2), 527-533.

[112] Yang, Jiun-Chan, and Prabir K. Dutta. (2007) High temperature amperometric total NO_X sensors with platinum-loaded zeolite Y electrodes. *Sensors and Actuators B: Chemical* 123(2) 929-936.

[113] Szabo, Nicholas F., Hongbin Du, Sheikh A. Akbar, Ahmed Soliman, and Prabir K. Dutta. (2002) "Microporous zeolite modified yttria stabilized zirconia (YSZ) sensors for nitric oxide (NO) determination in harsh environments." *Sensors and Actuators B: Chemical* 82(2) 142-149.

[114] Coronas, J., and J. Santamaria. (2004) The use of zeolite films in small-scale and micro-scale applications. *Chemical engineering science* 59(22) 4879-4885.

[115] Fukui, Kiyoshi, and Sachiko Nishida. (1997) CO gas sensor based on Au–La_2O_3 added SnO_2 ceramics with siliceous zeolite coat. *Sensors and Actuators B: Chemical* 45(2) 101-106.

[116] Lutz, W. (2014). Zeolite Y: synthesis, modification, and properties—A case revisited. *Advances in Materials Science and Engineering*, *2014*.

[117] Zeolites for Cleaner Technologies. (Eds.: M. Guisnet, J.-P. Gilson). Imperial College Press, London, 2002.

[118] Zeolites: Science and Technology. (Eds.: F. R. Ribeiro, A. E. Rodrigues, L. D. Rollmann, C. Naccache), Martinus Nijhoff Publishers, the Hague, 1984.

[119] Das, J., Bhat, Y. S., & Halgeri, A. B. (1994). Transalkylation and disproportionation of toluene and C9 aromatics over zeolite beta. *Catalysis letters*, *23*(1-2), 161-168..

[120] Martens, J. A., Perez-Pariente, J., Jacobs, P. A., & Selton, R. (1986). Chemical Reactions in Organic and Inorganic Constrained Systems, NATO ASI Ser.

[121] Tsai, Tseng-Chang, and Ikai Wang. (1991) "Cumene disproportionation over zeolite β: II. stability enhancement with silica deposition and steam pretreatment." *Applied catalysis* 77(2) 209-222.

[122] Hugon, O., M. Sauvan, P. Benech, Christophe Pijolat, and F. Lefebvre. (2000) "Gas separation with a zeolite filter, application to the selectivity enhancement of chemical sensors." *Sensors and Actuators B: Chemical* 67, (3) 235-243.

[123] Fukui, Kiyoshi, and Sachiko Nishida. (1997) "CO gas sensor based on Au–La_2O_3 added SnO_2 ceramics with siliceous zeolite coat." *Sensors and Actuators B: Chemical* 45(2) 101-106.

[124] Argauer, R. J., & Landolt, G. R. (1972). *U.S. Patent No. 3,702,886*. Washington, DC: U.S. Patent and Trademark Office.

[125] Modeling of Structure and Reactivity in Zeolites (1992). Ed: C.R.A. Catlow. Academic Press, Ltd.: London. ISBN 0-12-164140-6

[126] Martens, J. A., Parton, R., Uytterhoeven, L., Jacobs, P. A., & Froment, G. F. (1991). Selective conversion of decane into branched isomers: A comparison of platinum/ZSM-22, platinum/ZSM-5 and platinum/USY zeolite catalysts. *Applied catalysis*, *76*(1), 95-116.

[127] Young, L. B., Butter, S. A., & Kaeding, W. W. (1982). Shape selective reactions with zeolite catalysts: III. Selectivity in xylene isomerization, toluene-methanol alkylation, and toluene disproportionation over ZSM-5 zeolite catalysts. *Journal of Catalysis*, *76*(2), 418-432.

[128] Weisheit, R. A., & Wells, L. E. (2010). Methamphetamine laboratories: The geography of drug production. *W. Criminology Rev.*, *11*, 9.

[129] Verweij, A. M. (1989). Impurities in illicit drug preparations: amphetamine and methamphetamine. *Forensic Science Rev*iew *1*(1), 1-11.

[130] Abdullaha, A. F. L., & Miskellyb, G. (2010). Residues at clandestine methamphetamine laboratories and their health effects. *Health and the Environment Journal*, *1*(1), 21-29.

[131] Kane, L. E., Dombroske, R., & Alarie, Y. (1980). Evaluation of sensory irritation from some common industrial solvents. *The American Industrial Hygiene Association Journal*, *41*(6), 451-455.

[132] Qiao, Y., Gao, Z., Liu, Y., Cheng, Y., Yu, M., Zhao, L., ... & Liu, Y. (2014). Breath ketone testing: a new biomarker for diagnosis and therapeutic monitoring of diabetic ketosis. *BioMed research international*, *2014*.

[133] Hughart, Joseph L. (2000): "Chemical hazards related to clandestine drug laboratories." *Arhiv za Higijenu Rada I Toksikologiju/Archives of Industrial Hygiene and Toxicology* 51(3) 305-310.

[134] Knops, L. A., Northrop, D. M., & Person, E. C. (2006). Capillary electrophoretic analysis of phosphorus species in clandestine methamphetamine laboratory samples. *Journal of forensic sciences*, *51*(1), 82-86.

[135] Ramazan, K. A., Wingen, L. M., Miller, Y., Chaban, G. M., Gerber, R. B., Xantheas, S. S., & Finlayson-Pitts, B. J. (2006). New experimental and theoretical approach to the heterogeneous hydrolysis of NO_2: Key role of molecular nitric acid and its complexes. *The Journal of Physical Chemistry A*, *110*(21), 6886-6897.

[136] Janni, J., Gilbert, B. D., Field, R. W., & Steinfeld, J. I. (1997). Infrared absorption of explosive molecule vapors. *Spectrochimica Acta Part A: Molecular and Biomolecular Spectroscopy*, *53*(9), 1375-1381.

[137] Liu, Z. P., Jenkins, S. J., & King, D. A. (2004). Car exhaust catalysis from first principles: selective NO reduction under excess O2 conditions on Ir. *Journal of the American Chemical Society*, *126*(34), 10746-10756.

[138] US Dept. of Health and Human Services, Public Health Service, Agency for Toxic Substances and Disease Registry, Division of Toxicology. April 2002

[139] Esplugues, A., Ballester, F., Estarlich, M., Llop, S., Fuentes, V., Mantilla, E., & Iñiguez, C. (2010). Indoor and outdoor concentrations and determinants of NO_2 in a cohort of 1-year-old children in Valencia, Spain. *Indoor air*, *20*(3), 213-223.

[140] Rasmussen, T. R., Kjaergaard, S. K., Tarp, U., & Pedersen, O. F. (1992). Delayed effects of NO2 exposure on alveolar permeability and glutathione peroxidase in healthy humans. *American Review of Respiratory Disease*, *146*(3), 654-659.

[141] Speizer, F. E., Ferris Jr, B., Bishop, Y. M., & Spengler, J. (1980). Respiratory Disease Rates and Pulmonary Function in Children Associated with NO_2 Exposure 1–4. *American Review of Respiratory Disease*, *121*(1), 3-10..

[142] Heather Walton, David Dajnak, Sean Beevers, Martin Williams, Paul Watkiss and Alistair Hunt Understanding the Health Impacts of Air Pollution in London https://www.scribd.com/doc/271641490/King-s-College-London-report-on-mortality-burden-of-NO2-and-PM2-5-in-London (Accessed 25/05/16)

[143] Garett R (2013) How a common fertilizer became a meth magnet *Modern Farmer*, 24 May

[144] McKenzie, L. B., Ahir, N., Stolz, U., & Nelson, N. G. (2010). Household cleaning product-related injuries treated in US emergency departments in 1990–2006. *Pediatrics*, *126*(3), 509-516.

[145]Zamfirescu, C., & Dincer, I. (2009). Ammonia as a green fuel and hydrogen source for vehicular applications. *Fuel processing technology*, *90*(5), 729-737.

[146] Włochowicz, A., & Stelmasiak, E. (1983). Change in thermal properties of wool after treatment with liquid ammonia. *Journal of Thermal Analysis and Calorimetry*, *26*(1), 17-22.

[147] Loerting, T. (2007). *U.S. Patent Application No. 12/306,187*.

[148] Niemeyer, D., Williams, D. E., Smith, P., Pratt, K. F., Slater, B., Catlow, C. R. A., & Stoneham, A. M. (2002). Experimental and computational study of the gas-sensor behaviour and surface chemistry of the solid-solution Cr 2− x Ti x O 3 (x≤ 0.5). *Journal of Materials Chemistry*, *12*(3), 667-675.

[149] Chamberlin, R. R., & Hill, J. E. (1964). *U.S. Patent No. 3,148,084*. Washington, DC: U.S. Patent and Trademark Office.

[150] Estrada-Izquierdo, I., Sánchez-Espindola, E., Uribe-Hernández, R., & Ramón-Gallegos, E. (2012, October). Analysis of the impregnation of ZnO: Mn 2+ nanoparticles on cigarette filters for trapping polycyclic aromatic hydrocarbons (PAHs). In F. E. T. Zamudio, M. E. Brandan, I. Gamboa-deBuen, G. Herrera-Corral, & L. A. Medina-Velázquez (Eds.), *AIP conference proceedings* (Vol. 1494, No. 1, pp. 140-142). AIP.

[151] Housecroft, C. E., & Constable, E. C. (2010). *Chemistry: An introduction to organic, inorganic and physical chemistry*. Pearson education.

[152] Xu, J., Pan, Q., & Tian, Z. (2000). Grain size control and gas sensing properties of ZnO gas sensor. *Sensors and Actuators B: Chemical*, *66*(1), 277-279.

[153] Siyama, T., & Kato, A. (1962). A new detector for gaseous components using semiconductor thin film. *Analytical Chem*istry *34*(11), 1502-1503.

[154] Yu, J.H., & Choi, G. M., (1999) Electrical and CO Gas-Sensing Properties of ZnO/SnO_2 Hetero-Contact, *Sensors and Actuators B 61*(4), 59–67

[155] Bott, B., Jones, T. A., & Mann, B. (1984). The detection and measurement of CO using ZnO single crystals. *Sensors and Actuators*, *5*(1), 65-73.

[156] Egashira, M., Kanehara, N., Shimizu, Y., & Iwanaga, H. (1989). Gas-sensing characteristics of Li+-doped and undoped ZnO whiskers. *Sensors and Actuators*, *18*(3), 349-360.

[157] Saito, S., Miyayama, M., Koumoto, K., & Yanagida, H. (1985). Gas sensing characteristics of porous ZnO and Pt/ZnO ceramics. *Journal of the American Ceramic Society*, *68*(1), 40-43.

[158] Lambrich, R., Hagen, W., & Lagois, J. (1983, September). Metal oxide films as selective gas sensors. In *Proceedings of the International Meeting on Chemical Sensors, Fukuoka, Japan*.

[159] Romppainen, P., Lantto, V., & Leppävuori, S. (1990). Effect of water vapour on the CO response behaviour of tin dioxide sensors in constant temperature and temperature-pulsed modes of operation. *Sensors and Actuators B: Chemical*, *1*(1-6), 73-78.

[160] C. N. R. Rao, A. R. Raju, and K. Vijayamohanan, Gas-Sensor Materials, in New Materials (S. K. Joshi, T. Tsuruta, C. N. R. Rao, and S. Nagakura, Eds., Narosa, New Delhi, 1992, and the references therein).

[161] Williams, G., & Coles, G. S. (1999). The semistor: a new concept in selective methane detection. *Sensors and Actuators B: Chemical*, *57*(1), 108-114.

[162] de Lacy Costello, B. P. J., Ewen, R. J., Ratcliffe, N. M., & Sivanand, P. S. (2003). Thick film organic vapour sensors based on binary mixtures of metal oxides. *Sensors and Actuators B: Chemical*, *92*(1), 159-166.

[163] Raju, A. R., & Rao, C. N. R. (1991). Gas-sensing characteristics of ZnO and copper-impregnated ZnO. *Sensors and Actuators B: Chemical*, *3*(4), 305-310.

[164] de Lacy Costello, B. P. J., Ewen, R. J., Guernion, N., & Ratcliffe, N. M. (2002). Highly sensitive mixed oxide sensors for the detection of ethanol. *Sensors and Actuators B: Chemical*, *87*(1), 207-210.

[165] Egashira, M., Shimizu, Y., & Takao, Y. (1990). Trimethylamine sensor based on semiconductive metal oxides for detection of fish freshness. *Sensors and Actuators B: Chemical*, *1*(1-6), 108-112.

[166] Nanto, H., Minami, T., & Takata, S. (1986). Zinc-oxide thin-film ammonia gas sensors with high sensitivity and excellent selectivity. *Journal of Applied Physics*, *60*(2), 482-484.

[167] Wagh, M. S., Jain, G. H., Patil, D. R., Patil, S. A., & Patil, L. A. (2006). Modified zinc oxide thick film resistors as NH 3 gas sensor. *Sensors and Actuators B: Chemical*, *115*(1), 128-133.

[168] de Lacy Costello, B. P. J., Ewen, R. J., Jones, P. R. H., Ratcliffe, N. M., & Wat, R. K. M. (1999). A study of the catalytic and vapour-sensing properties of zinc oxide

and tin dioxide in relation to 1-butanol and dimethyldisulphide. *Sensors and Actuators B: Chemical*, *61*(1), 199-207.

[169] Lou, X., Shen, H. S., & Shen, Y. S. (1991). Development of ZnO series ceramic semiconductor gas sensors. *J. Sens. Trans. Technol*, *3*(1), 1-5.

[170] Cheng, X. L., H. Zhao, L. H. Huo, S. Gao, and J. G. Zhao. (2006) "ZnO nanoparticulate thin film: preparation, characterization and gas-sensing property." *Sensors and Actuators B: Chemical* 102(2), 248-252.

[171] Takahara, I., Saito, M., Matsuhashi, H., Inaba, M., & Murata, K. (2007). Increase in the number of acid sites of a H-ZSM5 zeolite during the dehydration of ethanol. *Catalysis letters*, *113*(3-4), 82-85.

[172] Phillips, C. B., & Datta, R. (1997). Production of ethylene from hydrous ethanol on H-ZSM-5 under mild conditions. *Industrial & engineering chemistry research*, *36*(11), 4466-4475.

[173] Sun, H., Lu, L., Chen, X., & Jiang, Z. (2008). Surface-modified zeolite-filled chitosan membranes for pervaporation dehydration of ethanol. *Applied Surface Science*, *254*(17), 5367-5374.

[174] Aronson, M. T., Gorte, R. J., & Farneth, W. E. (1986). The influence of oxonium ion and carbenium ion stabilities on the Alcohol/H-ZSM-5 interaction. *Journal of Catalysis*, *98*(2), 434-443.

[175] Zhang, K., Lively, R. P., Noel, J. D., Dose, M. E., McCool, B. A., Chance, R. R., & Koros, W. J. (2012) Adsorption of water and ethanol in MFI-type zeolites. *Langmuir*, *28*, 8664-8673.

[176] Watson, J., Ihokura, K., & Coles, G. S. (1993). The tin dioxide gas sensor. *Measurement Science and Technology*, *4*(7), 711.

[177] Besson, M., & Gallezot, P. (2000). Selective oxidation of alcohols and aldehydes on metal catalysts. *Catalysis Today*, *57*(1), 127-141.

[178] Jinkawa, T., Sakai, G., Tamaki, J., Miura, N., & Yamazoe, N. (2000). Relationship between ethanol gas sensitivity and surface catalytic property of tin oxide sensors modified with acidic or basic oxides. *Journal of Molecular Catalysis A: Chemical*, *155*(1), 193-200.

[179] Zhabrova, G. M., & Egorov, E. V. (1961). Sorption and ion exchange on amphoteric oxides and hydroxides. *Russian Chemical Reviews*, *30*(6), 338-346.

[180] Yamazoe, N., Sakai, G., & Shimanoe, K. (2003). Oxide semiconductor gas sensors. *Catalysis Surveys from Asia*, *7*(1), 63-75.

[181] Jinkawa, T., Sakai, G., Tamaki, J., Miura, N., & Yamazoe, N. (2000). Relationship between ethanol gas sensitivity and surface catalytic property of tin oxide sensors modified with acidic or basic oxides. *Journal of Molecular Catalysis A: Chemical*, *155*(1), 193-200.

[182] Ryabtsev, S. V., Shaposhnick, A. V., Lukin, A. N., & Domashevskaya, E. P. (1999). Application of semiconductor gas sensors for medical diagnostics. *Sensors and Actuators B: Chemical*, *59*(1), 26-29.

[183] Kim, K. S., Baek, W. H., Kim, J. M., Yoon, T. S., Lee, H. H., Kang, C. J., & Kim, Y. S. (2010). A nanopore structured high performance toluene gas sensor made by nanoimprinting method. *Sensors*, *10*(1), 765-774.

[184] Sagade, A. A., & Sharma, R. (2008). Copper sulphide (Cu_xS) as an ammonia gas sensor working at room temperature. *Sensors and Actuators B: Chemical*, *133*(1), 135-143.

[185] Spetz, A., Armgarth, M., & Lundström, I. (1988). Hydrogen and ammonia response of metal-silicon dioxide-silicon structures with thin platinum gates. *Journal of applied physics*, *64*(3), 1274-1283.

[186] Blasse, G., De Korte, P. H. M., & Mackor, A. (1981). The colouration of titanates by transition-metal ions in view of solar energy applications. *Journal of Inorganic and Nuclear Chemistry*, *43*(7), 1499-1503.

[187] Abdel-Latif, A. I. (1994). *U.S. Patent No. 5,310,422*. Washington, DC: U.S. Patent and Trademark Office.

[188] Crystal tutorial project http://www.theochem.unito.it/crystal_tuto/mssc2008_cd/tutorials/surfaces/surfaces_tut.html (Accessed 22/08/14)

[189] Niemeyer, D., Williams, D. E., Smith, P., Pratt, K. F., Slater, B., Catlow, C. R. A., & Stoneham, A. M.. (2002) Experimental and computational study of the gas-sensor behaviour and surface chemistry of the solid-solution $Cr_{2-x}Ti_xO_3$ ($x \leq 0.5$). *Journal of Materials Chemistry*, *12*(3), 667-675.

[190] Naisbitt, S. C., Pratt, K. F. E., Williams, D. E., & Parkin, I. P. (2006). A microstructural model of semiconducting gas sensor response: The effects of

sintering temperature on the response of chromium titanate (CTO) to carbon monoxide. *Sensors and Actuators B: Chemical*, *114*(2), 969-977.

[191] Dawson, D. H., Henshaw, G. S., & Williams, D. E. (1995) Description and characterization of a hydrogen sulfide gas sensor based on $Cr_{2-y}Ti_yO_{3+x}$. *Sensors and Actuators B: Chemical*, *26*(1-3), 76-80.

[192] Moseley, P. T., & Williams, D. E. (1990). A selective ammonia sensor. *Sensors and Actuators B: Chemical*, *1*(1-6), 113-115.

[193] Jayaraman, V., Gnanasekar, K. I., Prabhu, E., Gnanasekaran, T., & Periaswami, G. (1999) Preparation and characterisation of $Cr_{2-x}Ti_xO_3+\delta$ and its sensor properties. *Sensors and Actuators B: Chemical*, *55*(2), 175-179.

[194] Afonja, A., Binions, R., Dungey, S., Parkin, I. P., Lewis, D. W., & Williams, D. E. (2010). Zeolites as transformation elements in discriminating semiconductor metal oxide sensors. *Procedia Engineering*, *5*, 103-106.

[195] Arenamnart, S., & Trakarnpruk, W. (2006). Ethanol conversion to ethylene using metal-mordenite catalysts. *International Journal of Applied Science and Engineering*, *4*(1), 21-32.

[196] Phillips, C. B., & Datta, R. (1997). Production of ethylene from hydrous ethanol on H-ZSM-5 under mild conditions. *Industrial & engineering chemistry research*, *36*(11), 4466-4475.

[197] Chica, A., Strohmaier, K. G., & Iglesia, E. (2005). Effects of zeolite structure and aluminum content on thiophene adsorption, desorption, and surface reactions. *Applied Catalysis B: Environmental*, *60*(3), 223-232.

[198] Pope, C. G. (1986). Sorption of benzene, toluene and p-xylene on silicalite and H-ZSM-5. *The Journal of Physical Chemistry*, *90*(5), 835-837.

[199] Chen, N. Y., Kaeding, W. W., & Dwyer, F. G. (1979). Para-directed aromatic reactions over shape-selective molecular sieve zeolite catalysts. *Journal of the American Chemical Society*, *101*(22), 6783-6784.

[200] Van der Gaag, F. J., Louter, F., Oudejans, J. C., & Van Bekkum, H. (1986). Reaction of ethanol and ammonia to pyridines over zeolite ZSM-5. *Applied catalysis*, *26*, 191-201.

[201] Takahara, I., Saito, M., Inaba, M., & Murata, K. (2005). Dehydration of ethanol into ethylene over solid acid catalysts. *Catalysis Letters*, *105*(3), 249-252.

[202] Kondo, J. N., Ito, K., Yoda, E., Wakabayashi, F., & Domen, K. (2005). An ethoxy intermediate in ethanol dehydration on Brønsted acid sites in zeolite. *The Journal of Physical Chemistry B*, *109*(21), 10969-10972.

[203] Beck, L. W., & Haw, J. F. (1995). Multinuclear NMR-studies reveal a complex acid function for zeolite-Beta. *Journal of Physical Chemistry*, *99*(4), 1076-1079.

[204] Hutchings, G. J., Johnston, P., Lee, D. F., & Williams, C. D. (1993). Acetone conversion to isobutene in high selectivity using zeolite β catalyst. *Catalysis letters*, *21*(1), 49-53.

[205] Chabanis, C., Parkin, I.P., Williams, D.E. (2001) Microspheres of the gas sensor material Cr2á− áxTixO3 prepared by the sol–emulsion–gel route. *Journal of Materials Chemistry*, *11*(6), 1651-1655.

[206] Shaw, G. A., Pratt, K. F., Parkin, I. P., & Williams, D. E. (2005) Gas sensing properties of thin film (≤ 3µm) $Cr_{2-x}Ti_xO_3$ (CTO) prepared by atmospheric pressure chemical vapour deposition (APCVD), compared with that prepared by thick film screen-printing. *Sensors and Actuators B: Chemical*, *104*(1), 151-162.

[207] Wang, L., Kalyanasundaram, K., Stanacevic, M., & Gouma, P. (2010). Nanosensor device for breath acetone detection. *Sensor Letters*, *8*(5), 709-712.

[208] Dirksen, J. A., Duval, K., & Ring, T. A. (2001). NiO thin-film formaldehyde gas sensor. *Sensors and Actuators B: Chemical*, *80*(2), 106-115.

[209] Kim, K. S., Baek, W. H., Kim, J. M., Yoon, T. S., Lee, H. H., Kang, C. J., & Kim, Y. S. (2010). A nanopore structured high performance toluene gas sensor made by nanoimprinting method. *Sensors*, *10*(1), 765-774.

[210] Kanda, K., & Maekawa, T. (2005). Development of a WO 3 thick-film-based sensor for the detection of VOC. *Sensors and Actuators B: Chemical*, *108*(1), 97-101.

[211] Makhija, K. K., Ray, A., Patel, R. M., Trivedi, U. B., & Kapse, A. H. (2005). Indium oxide thin film based ammonia gas and ethanol vapour sensor. *Bulletin of Materials Science*, *28*(1), 9-17.

[212] Süli, A., Török, M. I., & Hevesi, I. (1986) On the capacitance of nV_2O_5/p-Si heterojunctions. *Thin Solid Films*, *139,* 233-246.

[213] Bullett, D. W. (1980) The energy band structure of V_2O_5: a simpler theoretical approach. *Journal of Physics C: Solid State Physics*, *13*, L595.

[214] Murphy, D. W., Christian, P. A., DiSalvo, F. J., & Waszczak, J. V. (1979) Lithium incorporation by vanadium pentoxide. *Inorganic Chemistry*, *18*, 2800-2803.

[215] Julien, C., Guesdon, J. P., Gorenstein, A., Khelfa, A., & Ivanov, I. (1995), The influence of the substrate material on the growth of V_2O_5 flash-evaporated films. *Applied surface science*, *90* 389-391.

[216] J. Muster, G.T. Kim, V. Krstic, J.G. Park, Y.W. Park, S. Roth, M. Burghard (2000), Electrical transport through individual vanadium pentoxide nanowires *Advanced Materials,* 12 420–424

[217] Raible, I., Burghard, M., Schlecht, U., Yasuda, A., & Vossmeyer, T. (2005) V_2O_5 nanofibres: novel gas sensors with extremely high sensitivity and selectivity to amines. *Sensors and Actuators B: Chemical*, *106*, 730-735.

[218] Raj, A. D., Pazhanivel, T., Kumar, P. S., Mangalaraj, D., Nataraj, D., & Ponpandian, N. (2010) Self assembled V_2O_5 nanorods for gas sensors. *Current Applied Physics*, *10*, 531-537.

[219] Liu, J. F., Wang, X., Peng, Q., & Li, Yadong (2005). Vanadium pentoxide nanobelts: highly selective and stable ethanol sensor materials. *Advanced Materials*, *17*(6), 764-767.

[220] Chen, D., Hou, X., Wen, H., Wang, Y., Wang, H., Li, X., ... & Sun, J. (2009). The enhanced alcohol-sensing response of ultrathin WO3 nanoplates. *Nanotechnology*, *21*(3), 035501.

[221] Lou, Z., Wang, L., Wang, R., Fei, T., & Zhang, T. (2012). Synthesis and ethanol sensing properties of SnO 2 nanosheets via a simple hydrothermal route. *Solid-State Electronics*, *76*, 91-94.

[222] Abdeen, F. R., Mel, M., Al-Khatib, M., & Azmi, A. S. . Dehydration of Ethanol on Zeolite Based Media Using Adsorption Process. *Proceedings of the 3rd (2011) CUTSE International Conference*

[223] Bezoukhanova, C. P., & Kalvachev, Y. A. (1994) Alcohol reactivity on zeolites and molecular sieves. *Catalysis Reviews—Science and Engineering*, *36*, 125-143.

[224] Koda, S., Yoshikawa, K., Okada, J., & Akita, K. (1985). Reaction kinetics of nitrogen dioxide with methanol in the gas phase. *Environmental science & technology*, *19*(3), 262-264.

[225] Merényi, G., Lind, J., Goldstein, S., & Czapski, G. (1998) Peroxynitrous acid homolyzes into OH and NO_2 radicals. *Chemical research in toxicology*, *11*, 712-713.

[226] Wetchakun, K., Samerjai, T., Tamaekong, N., Liewhiran, C., Siriwong, C., Kruefu, V & Phanichphant, S. (2011) Semiconducting metal oxides as sensors for environmentally hazardous gases. *Sensors and Actuators B: Chemical*, *160*, 580-591.

[227] Korotcenkov, G., Brinzari, V., Golovanov, V., Cerneavschi, A., Matolin, V., & Tadd, A. (2004) Acceptor-like behavior of reducing gases on the surface of n-type In_2O_3. *Applied surface science*, *227*, 122-131.

[228] Chen, N. Y. (1976) Hydrophobic properties of zeolites. *The Journal of Physical Chemistry*, *80*, 60-64.

[229] Bartolomeu, R., Henriques, C., da Costa, P., & Ribeiro, F. (2011) deNO_x over Ag/H-ZSM5: Study of NO_2 interaction with ethanol. *Catalysis Today*, *176,* 81-87.

[230] Liu, J. F., Wang, X., Peng, Q., & Li, Y. (2005) Vanadium pentoxide nanobelts: highly selective and stable ethanol sensor materials. *Advanced Materials*, *17*, 764-767.

[231] Ishihara, T., Shiokawa, K., Eguchi, K., & Arai, H. (1989) The mixed oxide Al_2O_3-V_2O_5 as a semiconductor gas sensor for NO and NO_2. *Sensors and Actuators*, *19*, 259-265.

[232] Aslam, M., Chaudhary, V. A., Mulla, I. S., Sainkar, S. R., Mandale, A. B., Belhekar, A. A., & Vijayamohanan, K. (1989) A highly selective ammonia gas sensor using surface-ruthenated zinc oxide. *Sensors and Actuators A: Physical*, *75*, 162-167.

[233] Karunagaran, B., Uthirakumar, P., Chung, S. J., Velumani, S., & Suh, E. K. (2007) TiO_2 thin film gas sensor for monitoring ammonia. *Materials Characterization*, *58,* 680-684.

[234] Inoue, T., Ohtsuka, K., Yoshida, Y., Matsuura, Y., & Kajiyama, Y. (1995) Metal oxide semiconductor NO_2 sensor. *Sensors and Actuators B: Chemical*, *25,* 388-391.

[235] Penza, M., Martucci, C., & Cassano, G. NO_x gas sensing characteristics of WO_3 thin films activated by noble metals (Pd, Pt, Au) layers. (1998) *Sensors and Actuators B: Chemical*, *50*, 52-59.

[236] Luthra, V., Singh, A., Pugh, D. C., & Parkin, I. P. (2016) Ethanol sensing characteristics of $Zn_{0.99}M_{0.01}O$ (M= Al/Ni) nanopowders. *physica status solidi (a)*, *213*(1), 203-209.

[237] Yu, X., Ma, J., Ji, F., Wang, Y., Cheng, C., & Ma, H. (2005). Thickness dependence of properties of ZnO: Ga films deposited by rf magnetron sputtering. *Applied Surface Science*, *245*(1), 310-315.

[238] Kumar, P. R., Kartha, C. S., Vijayakumar, K. P., Abe, T., Kashiwaba, Y., Singh, F., & Avasthi, D. K. (2004). On the properties of indium doped ZnO thin films. *Semiconductor science and technology*, *20*(2), 120.

[239] Gong, H., Hu, J. Q., Wang, J. H., Ong, C. H., & Zhu, F. R. (2006). Nano-crystalline Cu-doped ZnO thin film gas sensor for CO. *Sensors and Actuators B: Chemical*, *115*(1), 247-251.

[240] Xue, X., Xing, L., Chen, Y., Shi, S., Wang, Y., & Wang, T. (2008). Synthesis and H2S sensing properties of CuO−SnO_2 core/shell pn-junction nanorods. *The Journal of Physical Chemistry C*, *112*(32), 12157-12160.

[241] Dimitrov, I. G., Dikovska, A. O., Atanasov, P. A., Stoyanchov, T. R., & Vasilev, T. (2008). Al doped ZnO thin films for gas sensor application. In *Journal of Physics: Conference Series* (Vol. 113, No. 1, p. 012044). IOP Publishing.

[242] M. H. Shahrokh Abadi, R. Wagiran, M. N. Hamidon, A. H. Shaari, N. Adbullah, N. Misron and M. Malekzadeh, (2009) *International Journal of Engineering Technology*, 6(1), 34-40

[243] Luthra, V. (2014). Tweaking electrical and magnetic properties of Al–Ni co-doped ZnO nanopowders. *Ceramics International*, *40*(9), 14927-14932.

[244] Miki-Yoshida, M., Morales, J., & Solis, J. (2000). Influence of Al, In, Cu, Fe and Sn dopants on the response of thin film ZnO gas sensor to ethanol vapour. *Thin Solid Films*, *373*(1), 137-140.

[245] Lupan, O., Shishiyanu, S., Chow, L., & Shishiyanu, T. (2008). Nanostructured zinc oxide gas sensors by successive ionic layer adsorption and reaction method and rapid photothermal processing. *Thin solid films*, *516*(10), 3338-3345.

[246] Cheng, X. L., Zhao, H., Huo, L. H., Gao, S., & Zhao, J. G. (2004). ZnO nanoparticulate thin film: preparation, characterization and gas-sensing property. *Sensors and Actuators B: chemical*, *102*(2), 248-252.

[247] Ning, Z. Y., Cheng, S. H., Ge, S. B., Chao, Y., Gang, Z. Q., Zhang, Y. X., & Liu, Z. G. (1997). Preparation and characterization of ZnO: Al films by pulsed laser deposition. *Thin Solid Films*, *307*(1-2), 50-53.

[248] Postava, K., Sueki, H., Aoyama, M., Yamaguchi, T., Murakami, K., & Igasaki, Y. (2001). Doping effects on optical properties of epitaxial ZnO layers determined by spectroscopic ellipsometry. *Applied surface science*, *175*, 543-548.

[249] Meng, F., Yin, J., Duan, Y. Q., Yuan, Z. H., & Bie, L. J. (2011). Co-precipitation synthesis and gas-sensing properties of ZnO hollow sphere with porous shell. *Sensors and Actuators B: Chemical*, *156*(2), 703-708.

[250] Xiangfeng, C. (2003). High sensitivity chlorine gas sensors using CdIn 2 O 4 thick film prepared by co-precipitation method. *Materials research bulletin*, *38*(13), 1705-1711.

[251] Van Heerden, J. L., & Swanepoel, R. (1997). XRD analysis of ZnO thin films prepared by spray pyrolysis. *Thin Solid Films*, *299*(1), 72-77.

[252] Qi, J., Zhang, H., Lu, S., Li, X., Xu, M., & Zhang, Y. (2015). High performance indium-doped ZnO gas sensor. *Journal of Nanomaterials*, *16*(1), 74.

[253] Ellmer, K., & Mientus, R. (2008). Carrier transport in polycrystalline transparent conductive oxides: A comparative study of zinc oxide and indium oxide. *Thin solid films*, *516*(14), 4620-4627.

[254] Phillips, J. M., Cava, R. J., Thomas, G. A., Carter, S. A., Kwo, J., Siegrist, T.,& Rapkine, D. H. (1995). Zinc-indium-oxide: a high conductivity transparent conducting oxide. *Applied Physics Letters*, *67*(15), 2246-2248.

[255] Luthra, V., Pratt, K. F., Palgrave, R. G., Williams, D. E., Tandon, R. P., & Parkin, I. P. (2010). Gas-sensing properties of $Fe_{2-x}TixO_{3+y}$ (x= 0–1.4). *Polyhedron*, *29*(4), 1225-1230.

[256] Ohashi, N., Terada, Y., Ohgaki, T., Tanaka, S., Tsurumi, T., Fukunaga, O., ... & Tanaka, J. (1999). Synthesis of ZnO bicrystals doped with Co or Mn and their electrical properties. *Japanese journal of applied physics*, *38*(9R), 5028.

[257] Oba, F., & Tanaka, I. (1999). Effect of oxidation on chemical bonding around 3d transition-metal impurities in ZnO. *Japanese journal of applied physics*, *38*(6R), 3569.

[258] Pugh, D. C., Newton, E. J., Naik, A. J. T., Hailes, S. M. V., & Parkin, I. P. (2014). The gas sensing properties of zeolite modified zinc oxide. *Journal of Materials Chemistry A*, *2*(13), 4758-4764.

[259] M. Kalyan Chakravarthi and B. Bharath, (20012) in Mechatronics and its Applications (ISMA), 2012 8th International Symposium, IEEE, 2012, p. 1. 50

[260] Jinkawa, T., Sakai, G., Tamaki, J., Miura, N., & Yamazoe, N. (2000). Relationship between ethanol gas sensitivity and surface catalytic property of tin oxide sensors modified with acidic or basic oxides. *Journal of Molecular Catalysis A: Chemical*, *155*(1), 193-200.

[261] Wang, Y., Cao, J., Wang, S., Guo, X., Zhang, J., Xia, H., ... & Wu, S. (2008). Facile synthesis of porous α-Fe2O3 nanorods and their application in ethanol sensors. *The Journal of Physical Chemistry C*, *112*(46), 17804-17808.

[262] Khadayate, R. S., Waghulde, R. B., Wankhede, M. G., Sali, J. V., & Patil, P. P. (2007). Ethanol vapour sensing properties of screen printed WO3 thick films. *Bulletin of Materials Science*, *30*(2), 129-134.

[263] Zakrzewska, K. (2004). Gas sensing mechanism of TiO 2-based thin films. *Vacuum*, *74*(2), 335-338.

[264] Ellmer, K., & Mientus, R. (2008). Carrier transport in polycrystalline transparent conductive oxides: A comparative study of zinc oxide and indium oxide. *Thin solid films*, *516*(14), 4620-4627.

[265] Röck, F., Barsan, N., & Weimar, U. (2009, May). Metal Oxide Gas Sensor Arrays: Geometrical Design and Selectivity. In M. Pardo, & G. Sberveglieri (Eds.), *AIP Conference Proceedings* (Vol. 1137, No. 1, pp. 140-143). AIP.

[266] Boser, B. E., Guyon, I. M., & Vapnik, V. N. (1992, July). A training algorithm for optimal margin classifiers. In *Proceedings of the fifth annual workshop on Computational learning theory* (pp. 144-152). ACM.

[267] Pei, L., Liu, J., Guinness, R., Chen, Y., Kuusniemi, H., & Chen, R. (2012). Using LS-SVM based motion recognition for smartphone indoor wireless positioning. Sensors, 12(5), 6155-6175.

[268] OpenCV (2014, June 6) Introduction to Support Vector Machines (Web Blog Post) Retrieved from http://docs.opencv.org/2.4/doc/tutorials/ml/introduction_to_svm/introduction_to_svm.html Accessed 13/09/16

[269] Time Management Guide (2005, June 21) Use a decision tree analysis to systematically arrive at your smartest choice. Retrieved from http://www.time-management-guide.com/decision-tree.html (Accessed 21 April 2016)

[270] Quinlan, J. R. (1986). Induction of decision trees. *Machine learning*, *1*(1), 81-106.

[271] Cho, J. H., & Kurup, P. U. (2011). Decision tree approach for classification and dimensionality reduction of electronic nose data. *Sensors and Actuators B: Chemical*, *160*(1), 542-548.

[272] Bermak, A., Belhouari, S. B., Shi, M., & Martinez, D. (2006). Pattern recognition techniques for odor discrimination in gas sensor array. *Encyclopedia of Sensors*, *10*, 1-17.

[273] Breiman, L. (2001). Random forests. *Machine learning*, *45*(1), 5-32.

[274] Hall, M., Frank, E., Holmes, G., Pfahringer, B., Reutemann, P., & Witten, I. H. (2009). The WEKA data mining software: an update. *ACM SIGKDD explorations newsletter*, 11(1), 10-18.

[275] Han, J., Pei, J., & Kamber, M. (2011). *Data mining: concepts and techniques*. Elsevier.

[276] Caruana, R., & Niculescu-Mizil, A. (2006, June). An empirical comparison of supervised learning algorithms. In *Proceedings of the 23rd international conference on Machine learning* (pp. 161-168). ACM.

[277] Barsan, N., & Weimar, U. (2001). Conduction model of metal oxide gas sensors. *Journal of electroceramics*, *7*(3), 143-167.

[278]Kim, H. J., & Lee, J. H. (2014). Highly sensitive and selective gas sensors using p-type oxide semiconductors: overview. *Sensors and Actuators B: Chemical*, *192*, 607-627.

[279] Corma, A., Nemeth, L. T., Renz, M., & Valencia, S. (2001). Sn-zeolite beta as a heterogeneous chemoselective catalyst for Baeyer–Villiger oxidations. *Nature*, *412*(6845), 423-425.

[280] Sun, Y. F., Liu, S. B., Meng, F. L., Liu, J. Y., Jin, Z., Kong, L. T., & Liu, J. H. (2012). Metal oxide nanostructures and their gas sensing properties: a review. *Sensors*, *12*(3), 2610-2631.

[281] Wernert, V., Schäf, O., Ghobarkar, H., & Denoyel, R. (2005). Adsorption properties of zeolites for artificial kidney applications. Microporous and mesoporous materials, 83(1), 101-113.

[282] Wetchakun, K., Samerjai, T., Tamaekong, N., Liewhiran, C., Siriwong, C., Kruefu, V., & Phanichphant, S. (2011). Semiconducting metal oxides as sensors for environmentally hazardous gases. *Sensors and Actuators B: Chemical*, *160*(1), 580-591.

[283] Janssen, A. H., Koster, A. J., & de Jong, K. P. (2001). Three-Dimensional Transmission Electron Microscopic Observations of Mesopores in Dealuminated Zeolite Y. *Angewandte Chemie*, *113*(6), 1136-1138.

[284] Derouane, E. G., Nagy, J. B., Dejaifve, P., van Hooff, J. H., Spekman, B. P., Védrine, J. C., & Naccache, C. (1978). Elucidation of the mechanism of conversion of methanol and ethanol to hydrocarbons on a new type of synthetic zeolite. *Journal of Catalysis*, *53*(1), 40-55.

[285] Vane, L. M., Namboodiri, V. V., & Bowen, T. C. (2008). Hydrophobic zeolite–silicone rubber mixed matrix membranes for ethanol–water separation: effect of zeolite and silicone component selection on pervaporation performance. *Journal of Membrane Science*, *308*(1), 230-241.

[286] L Le Van Mao, R., Levesque, P., McLaughlin, G., & Dao, L. H. (1987). Ethylene from ethanol over zeolite catalysts. *Applied catalysis*, *34*, 163-179.

[287] Sunil, T. T., Chaudhuri, S., & Mishra, V. (2015). Optimal selection of SAW sensors for E-Nose applications. *Sensors and Actuators B: Chemical*, 219, 238-244.

[288] Wheeler, A. (2007). Commercial applications of wireless sensor networks using ZigBee. *IEEE Communications Magazine*, *45*(4).

[289] Aboelela, E., Edberg, W., Papakonstantinou, C., & Vokkarane, V. (2006, April). Wireless sensor network based model for secure railway operations. In *Performance, Computing, and Communications Conference, 2006. IPCCC 2006. 25th IEEE International* (pp. 6-pp). IEEE.

Conference, 2006. IPCCC 2006. 25th IEEE International (6-12). IEEE.

[290] Pattath, A., Bue, B., Jang, Y., Ebert, D., Zhong, X., Ault, A., & Coyle, E. (2006, October). Interactive visualization and analysis of network and sensor data on mobile devices. In *Visual Analytics Science And Technology, 2006 IEEE Symposium On* (pp. 83-90). IEEE.

[291] Werner-Allen, G., Lorincz, K., Ruiz, M., Marcillo, O., Johnson, J., Lees, J., & Welsh, M. (2006). Deploying a wireless sensor network on an active volcano. *IEEE internet computing*, *10*(2), 18-25.

[292] Yick, J., Mukherjee, B., & Ghosal, D. (2008). Wireless sensor network survey. *Computer networks*, *52*(12), 2292-2330.